CIVIL ENGINEERING STUDIES
Illinois Center for Transportation Series No. 14-015
UILU-ENG-2014-2017
ISSN: 0197-9191

Concrete with Steel Furnace Slag and Fractionated Reclaimed Asphalt Pavement

Prepared By
Alexander S. Brand
Jeffery R. Roesler
University of Illinois at Urbana-Champaign

Research Report No. ICT-14-015

Illinois Center for Transportation

September, 2014

Technical Report Documentation Page

1. Report No.	2. Government Accession No.	3. Recipient's Catalog No.
ICT-14-015		

4. Title and Subtitle

Concrete with Steel Furnace Slag and Fractionated Reclaimed Asphalt Pavement

5. Report Date
September, 2014

6. Performing Organization Code

7. Author(s)
Alexander S. Brand and Jeffery R. Roesler

8. Performing Organization Report No.
ICT-14-015
UILU-ENG-2014-2015

9. Performing Organization Name and Address

Illinois Center for Transportation
Department of Civil and Environmental Engineering
University of Illinois at Urbana-Champaign
205 N. Mathews Ave, MC 250
Urbana, IL 61801

10. Work Unit (TRAIS)

11. Contractor Grant No.

12. Sponsoring Agency Name and Address

Illinois State Toll Highway Authority
2700 Ogden Ave
Downers Grove, IL 60515

National Slag Association
PO Box 1197
Pleasant Grove, Utah 84062

13. Type of Report and Period Covered

14. Sponsoring Agency Code

15. Supplementary Notes

16. Abstract

Steel furnace slag (SFS) is an industrial by-product material that can contain free calcium oxide (CaO) and free magnesium oxide (MgO), both of which can cause significant expansion when hydrated. SFS aggregates are therefore not commonly used in concrete, although SFS aggregates have been used as a high quality frictional aggregate for hot-mix asphalt (HMA) surface courses. The resultant fractionated reclaimed asphalt pavement (FRAP) when the HMA with SFS is removed has also seen little usage.

This study aims to continue the previous work by the authors that indicated that up to 50% dolomite FRAP can be used in concrete as a replacement of coarse aggregate. The objective of this work was to evaluate the effects of SFS FRAP at 20% and 50% replacements of the coarse aggregate in concrete. In addition, the chemical, mineralogical, physical, and expansive properties of three SFS FRAP sources were investigated along with investigations of three virgin SFS sources for comparison.

The chemical, mineralogical, and physical properties of the SFS FRAP and virgin SFS sources were similar to values presented in the literature. The estimated total free CaO content of the virgin SFS sources ranged from low (<0.1%) to high (3.4%), while the free CaO content of the SFS FRAP sources was estimated to be 1.0% to 1.5%. The free MgO content of the virgin SFS sources ranged from 0.2% to 2.2%. Autoclave expansion tests correlated well for the virgin SFS sources with regard to the free CaO content (i.e., high free CaO content resulted in high expansion), while the SFS FRAP with asphalt binder removed did expand, but not necessarily proportionally to the free CaO content. Autoclave expansion tests of the SFS FRAP with the asphalt binder resulted in contraction rather than expansion. The results validated the findings from other studies that have shown that SFS FRAP will not significantly expand because of the asphalt coating.

Concrete tests revealed that the strength, modulus, shrinkage, and fracture properties were similar between concretes with SFS FRAP and with dolomite FRAP. The modulus of elasticity was slightly higher for concrete with SFS FRAP compared with dolomite FRAP, possibly because of the presence of the stiffer SFS aggregate. The fracture properties were statistically similar for concrete with and without SFS FRAP aggregates. The freeze/thaw durability was reduced with higher SFS FRAP contents, possibly because of the asphalt coating on the FRAP rather than the SFS in the FRAP, because the mixes with 100% virgin SFS exhibited superior freeze/thaw durability.

Based on these findings, it is evident that SFS FRAP can retain free CaO and free MgO contents, despite years in service in a pavement layer and/or years being weathered in a stockpile. The presence of the asphalt coating hinders, but may not necessarily prevent, the hydration of the free CaO and free MgO in the SFS. Therefore, it is recommended that the SFS FRAP be tested for free CaO, free MgO, and asphalt contents and autoclave expansion potential prior to being utilized in a structural concrete layer. Immediate usage of SFS FRAP may not be detrimental for non-structural applications, such as temporary roads or shoulders. To ensure that future SFS FRAP can be used in concrete pavements, the SFS that is presently used in HMA should be weathered and have low free CaO contents and low expansion potential.

17. Key Words	18. Distribution Statement
Fractionated reclaimed asphalt pavement, FRAP, reclaimed asphalt pavement, RAP, steel furnace slag, SFS, electric arc furnace slag, EAF, basic oxygen furnace slag, BOF, expansion, autoclave, free lime, free CaO, ethylene glycol test, concrete durability, concrete fracture	No restrictions. This document is available to the public through the National Technical Information Service, Springfield, Virginia 22161.

19. Security Classif. (of this report)	20. Security Classif. (of this page)	21. No. of Pages	22. Price
Unclassified	Unclassified	170	

ACKNOWLEDGMENT

This study was funded by the Illinois State Toll Highway Authority (ISTHA) and the National Slag Association (NSA). Acknowledgment is given to Steve Gillen and Ross Bentsen (ISTHA), John Yzenas (Edw. C. Levy Co.), and Karen Kiggins (NSA). A special thanks to Abbas Kachwalla, Jeff LaHucik, and Jim Meister for all the assistance with testing, and to Tube City IMS, South Shore Slag, and Edw. C. Levy Co. for providing the steel furnace slag materials. The x-ray diffraction and thermogravimetric analysis was carried out in part in the Frederick Seitz Materials Research Laboratory Central Research Facilities, University of Illinois.

DISCLAIMER

EXECUTIVE SUMMARY

Previous studies have indicated that fractionated reclaimed asphalt pavement (FRAP) can be suitably utilized as a partial replacement of coarse aggregate in concrete for pavement applications. While previous research studied the use of FRAP containing dolomite coarse aggregate, this study investigates the potential of using FRAP sources containing steel furnace slag (SFS) aggregates. Because it is an industrial by-product, SFS aggregates have seen relatively few applications in concrete pavements and other bound applications, primarily because of the potential expansive nature of SFS. Depending on the type of SFS, the slag can contain significant quantities of unassimilated, or free, calcium oxide (CaO) and magnesium oxide (MgO), both of which expand when hydrated with water. This expansive property of SFS has limited its usage to unbound applications as well as an aggregate in asphalt pavement for improving abrasion resistance and maintaining surface friction.

A review of state construction specifications indicated that SFS is allowed in certain applications, such as asphalt pavements or unbound base courses, but no state currently permits its use in concrete or other cementitious-stabilized materials. A number of studies have been conducted on the use of SFS aggregate in concrete, and most results suggested that the concrete strength and durability could potentially be improved. With regard to the properties and performance of SFS FRAP, past literature results clearly indicate that the deleterious expansion of the SFS may be significantly reduced because of the asphalt coating.

The materials for this investigation included three (virgin) SFS sources and three SFS FRAP sources. The SFS samples were sourced from basic oxygen furnace (BOF) slag, electric arc furnace (EAF) slag, and EAF/ladle metallurgy furnace (LMF) slag stockpiles. The three SFS FRAP samples were obtained from Tollway projects around Chicago, Illinois, and approximately one-third of the total aggregate content consisted of BOF slag aggregates. All six sources had similar chemical and mineralogical compositions to SFS compositions reported in the literature. A complexometric titration with an ethylene glycol extraction technique was conducted in conjunction with thermogravimetric analysis to estimate the total free CaO content of the samples. The virgin SFS samples had high (3.4%) to low (<0.1%) free CaO contents, depending on the SFS type, and the SFS in the FRAP contained significant free CaO contents at around 2.9% to 4.2%, which corresponded to estimated total free CaO contents of 1.0% to 1.5% in the SFS FRAP. The free MgO content was also estimated to range from 0.2% to 2.2% for the virgin SFS sources.

In order to test the expansive characteristics of the virgin SFS and the SFS FRAP, compacted samples were subjected to an autoclave environment with steam pressure and temperature at 300 psi and 420°F, respectively, for three hours. As expected, the samples with high free CaO contents expanded the most. The virgin BOF slag sample with 3.4% free CaO expanded by 8.8% while the virgin EAF slag sample with <0.1% free CaO expanded by only 0.1%. The SFS FRAP samples expanded minimally or contracted, as some of the asphalt mobilized and filled the voids between particles and as the β-dicalcium silicate in the SFS converted to γ-dicalcium silicate, which resulted in particle disintegration and specimen contraction. When the SFS FRAP asphalt binder coating was removed, the samples expanded significantly (2.1% to 6.6%). Autoclave tests with unreactive dolomite FRAP also

contracted because of the asphalt mobilizing and filling voids. Overall, the expansion tests findings indicated that the asphalt coating appears to prevent or hinder the hydration of the free CaO and free MgO in the SFS FRAP. Thermal analysis of the post-autoclaved SFS materials indicated that both the free CaO and free MgO were being hydrated by the autoclave environment.

Concrete specimens with a ternary cementitious blend (65% Type I portland cement, 25% ground granulated blast furnace slag, and 10% Class C fly ash) were cast to test the effects of SFS FRAP at 20% and 50% volume replacement levels of the dolomitic coarse aggregate. The concrete with SFS FRAP behaved similar to concrete with dolomite FRAP, i.e., as the SFS FRAP content increased, the concrete strength and modulus decreased. The compressive and split tensile strengths were statistically similar between the concrete with SFS FRAP and dolomite FRAP, suggesting that the presence of the SFS in the FRAP did not impact the concrete strength. The flexural strength was statistically higher for concrete with SFS FRAP compared with dolomite FRAP. The static modulus of elasticity was statistically higher for concrete with SFS FRAP compared with dolomite FRAP as expected with a stiffer SFS aggregate. The concrete fracture properties were statistically similar between the mixes with and without SFS FRAP, with the exception of the critical crack tip opening displacement and initial fracture energy for the mix with 50% SFS FRAP. The concrete fracture properties for mixes with 100% coarse virgin SFS (BOF and EAF) were statistically greater than the control concrete fracture properties. The drying shrinkage was slightly higher for mixes with SFS FRAP relative to the control and statistically greater at later ages. For concrete with 100% coarse virgin SFS, greater shrinkage was obtained relative to concrete containing SFS FRAP. In all shrinkage mixtures (virgin, SFS, and SFS FRAP), the aggregate gradations were not the same and the SFS FRAP had higher asphalt content. Finally, the freeze/thaw durability testing indicated that concrete with SFS FRAP or virgin SFS can be freeze/thaw resistant. After 300 freeze/thaw cycles, the mix with 50% SFS FRAP had a net durability factor of 80%, which was the only mix that had a final durability factor less than 99%. Continuing the freeze/thaw cycles significantly compromised the durability of the mixes with SFS FRAP, resulting in net durability factors of 88% and 53% for the mixtures with 20% and 50% SFS FRAP, respectively. The reduction in freeze/thaw durability was likely caused by the asphalt coating on the FRAP particles rather than the SFS in the FRAP.

Autoclave expansion testing of the SFS aggregate (extracted or virgin) correlated strongly with the free CaO contents. The Tollway can use the autoclave test and free CaO and post-autoclave MgO tests to determine the best application for SFS (asphalt, unbound, or concrete). SFS FRAP did not necessarily show any significant net expansion in the autoclave, but this can be misleading because of the asphalt filling the voids and dicalcium silicate phase conversion. Over time, it is possible that moisture ingress could react with some free CaO or free MgO, resulting in deleterious expansion in concrete. Therefore, any SFS FRAP with significant amounts of free CaO and MgO should not be used in paving concrete. If SFS (in FRAP or virgin) was found to be chemically innocuous, then concrete with virgin SFS or SFS FRAP was shown to exhibit suitable strength and durability properties. SFS FRAP or SFS aggregates with potential deleterious expansion in stabilized materials should be further tested to determine its suitability for unbound applications.

TABLE OF CONTENTS

CHAPTER 1 INTRODUCTION

The previous work at the University of Illinois at Urbana-Champaign has clearly demonstrated that fractionated reclaimed asphalt pavement (FRAP) can be appropriate for usage in concrete pavements at coarse aggregate replacement levels up to 50% (Brand et al. 2012; Brand and Roesler 2014). Additional studies by the authors have also demonstrated that, while coarse FRAP reduces the concrete strength, the concrete slab capacity can be similar if not greater than virgin concrete, mainly because of the similar fracture properties (Brand et al. 2013, 2014). Both of the previous studies only considered coarse FRAP that had conventional virgin coarse aggregates (i.e. dolomite and quartz). With the possibility of some of the Tollway's FRAP millings containing some percentage of steel furnace slag (SFS), the concrete results from the previous study need to be validated or updated to consider this new source type.

Aggregates produced from SFS are of high quality, durable, and have good frictional quality, and, as a result, SFS aggregates have found usage in flexible pavement applications for its skid resistance, stripping resistance, stability, and resistance to rutting (FHWA 1998). The 2012 world output of SFS was on the order of 150 to 230 million tons, while in the United States the amount of iron and steel-making slag was around 17 to 22 million tons (van Oss 2013). The hard and abrasion resistant properties of SFS aggregate have made it a good candidate for usage in hot-mix asphalt (HMA) pavement, as fill or embankment material, as railroad ballast, and for snow and ice control (Collins and Ciesielski 1994). After adequate weathering, Dunster (2002) reported that SFS could be used for roadway bases or subbases, surface wearing courses, armour stones, and as aggregates in specific dense concrete applications (such as sea defense barriers, although adequate weathering of the SFS is critical).

1.1 THE USE OF SFS AGGREGATES IN PAVEMENTS

Few states presently allow the usage of SFS in highway applications, but a number of states have been reported to have conducted studies on applications of SFS aggregates. It was reported in 1976 that Alabama was routinely using SFS for highway bases or subbases while California, Missouri, and Pennsylvania were conducting field experiments with steel slag in asphalt pavements (Collins 1976). NCHRP 166 (Miller and Collins 1976) reported that California and Missouri were conducting field studies with SFS in asphalt pavements and Pennsylvania was conducing field studies with open hearth slag (a type of SFS) in cement-treated bases and in asphalt wearing courses, while Ohio was using SFS in asphalt and concrete highway pavement applications and Alabama was using open hearth slag in highway base courses. In 1991, there were nine states that allowed the use of SFS in highway construction, four of which allowed its application in wearing courses (Ahmed 1991; Ahmed and Lovell 1992). As of 1994, at least 11 states used SFS aggregates in asphalt pavement (Alabama, California, Illinois, Indiana, Kentucky, Louisiana, Michigan, Missouri, Pennsylvania, South Carolina, and West Virginia); another two states were using SFS as a subbase or embankment material (Maryland and New York); 16 states had specifications for use of SFS aggregate in asphalt pavements (Alabama, California, Colorado, Illinois, Indiana, Kansas, Kentucky, Michigan, Minnesota, Missouri, Pennsylvania, South Carolina, Tennessee, Texas, Virginia, and West Virginia); and no states had specifications for SFS aggregate in concrete (Collins and Ciesielski 1994). As of 2009, there were 13 states in the US that permitted the use of SFS in HMA, while other

allowable applications are very limited: four states allowed the use in non-structural pavement surface treatments, three states allowed use as an embankment material, and two states allowed use in concrete pavements (NCHRP 2013). Figure 1 depicts the number of applications allowed by states for SFS. Indiana rated “good” general performance of SFS in concrete pavements, and Colorado was the only state to rate “poor” general performance of steel slag in asphalt pavements (NCHRP 2013). The only advantage of using SFS in asphalt pavements was reported as friction by Iowa, while the disadvantages were reported as material property issues by Iowa, poor experience by Colorado, and not cost effective and construction difficulties by Virginia (NCHRP 2013). One report concluded that the utilization of SFS in roadways has low potential for use in cement-bound layers and no potential for use as aggregate in concrete and that the best potential was in asphalt-bound layers or surface dressings (Collins and Sherwood 1995).

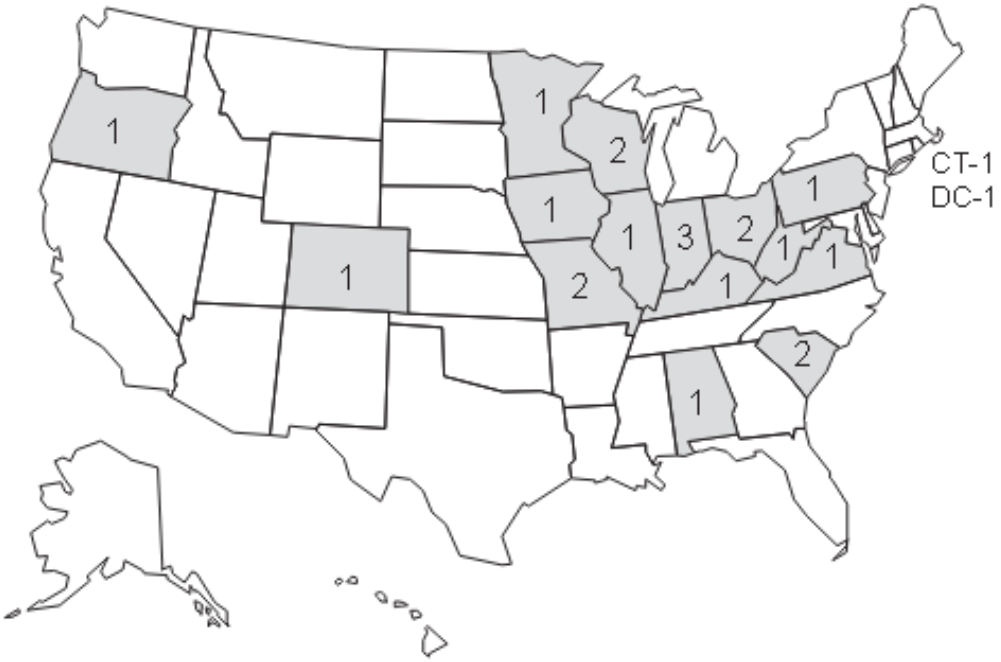

Figure 1. Results of a 2009 survey indicating the number of applications a given state allows for SFS. Source: NCHRP (2013)

In a survey of the state construction specifications conducted by this project, it was found that a number of states allow the use of SFS, typically in asphalt pavements. Some states, however, specify the use of slag, but do not further define the allowable types of slags (i.e., SFS, blast furnace slag, etc.). Of the states that allow the use of SFS aggregates, only a few further specify an expansion limit requirement. A summary of the review is as follows:

- Illinois allows the use of SFS aggregate as a fine or coarse aggregate in HMA (IDOT 2012, Sections 1003.03 and 1004.03).
- Indiana permits the use of SFS in certain HMA applications if the deleterious content is less than 4.0% by Indiana Test Method (ITM) 219 (INDOT 2014, Section 904.01). Indiana also has provisions for the use of reclaimed asphalt pavement with SFS aggregate.

- Pennsylvania requires that the SFS be weathered for at least 6 months in wet stockpiles, and the material cannot be used until the expansion is less than 0.50% by Pennsylvania Test Method (PTM) 130 (PennDOT 2011a, Sections 703.1 and 703.2). The specification states: “Fine aggregate manufactured from steel slag may not be used in cement concrete or mortar mixtures” and “Aggregate manufactured from steel slag is not acceptable for pipe or structure backfill or in cement concrete. Steel slag may be used for subbase, selected granular material, shoulders, selected material surfacing, and in bituminous surface courses” (PennDOT 2011a, Sections 703.1 and 703.2).
- Ohio lists ASTM D4792 as an optional test for SFS fine aggregates with a guide limit of 1.5% expansion, although the SFS can be used as the coarse or fine aggregate in asphalt base or asphalt intermediate courses (ODOT Supplement 1071 2008; ODOT 2013, Section 401.03). An autoclave disruption test is also listed as an optional test method in ODOT Supplement 1071. Section 703.14 includes extensive details for other non-pavement uses of SFS, in both confined and unconfined applications.
- West Virginia requires that the SFS be weathered for at least 6 months in wet stockpiles, and the material cannot be used until the expansion is less than 0.50% by ASTM D4792 (WVDOH 2010, Section 703.3.1). However, if the SFS is used in HMA, the expansion requirement is waived, and if the SFS is not confined, then the expansion requirement could be waived. The specification also states that: “Steel slag shall not be used in any item where expansion might be detrimental. Such items include, but not necessarily limited to, the following: aggregate for Portland Cement concrete, backfill around drainage structures, piers, abutments, walls, etc.” (WVDOH 2010, Section 703.3.1).
- New Jersey permits the use of up to 30% SFS aggregate in soils, provided that the expansion is 0.50% by ASTM D4792 (NJDOT 2007, Section 901.11).
- Kansas allows the use of crushed SFS in HMA (KDOT 2007, Section 1103.2). There is no mention of an expansion requirement, although it is stated that the crushed SFS is to be from electric arc furnace slag.
- Minnesota requires that the SFS be tested by ASTM D4792 and that the expansion be less than 0.50% before it can be used in asphalt mixtures (Mn/DOT 2014, Section 3139.2).
- Missouri requires that the SFS be aged at least three months after crushing and screening before the material can be used as a coarse aggregate in asphalt pavements (MoDOT 2011, Section 1002).
- In the 2006 Standard Special Provisions, California allowed the use of SFS for certain applications, such as an aggregate in HMA, as a special provision but also required that the SFS be aged at least three months (Caltrans 2006, SSP S8-M25). SFS aggregates are not allowed for use in concrete pavements.
- South Carolina allows the use of “crushed slag” in concrete as a coarse aggregate, provided that the slag does not contain “free lime in deleterious quantities” (SCDOT 2007, Section 701.2.10.2). Specifically for use in HMA, the South Carolina specification requires that the slag be stockpiled and meet an expansion requirement of less than 0.50% by ASTM D4792 (SCDOT 2007, Section 401.2.2.4).
- Alabama allows the use of “crushed slag” in asphalt wearing courses, subject to a limit on the amount of glassy particles in the slag (ALDOT 2012, Section 801.05).

- Colorado states that “crushed slag” may be used for aggregate bases and as an aggregate in HMA (CDOT 2011, Sections 703.03 and 703.04). However, the “crushed slag” is further specified in cover coat materials to be air-cooled blast furnace slag aggregate (Section 703.05).
- Arkansas permits SFS aggregates in asphalt surface treatments and as coarse aggregates in HMA and slurry seals, subject to limits on the aggregate durability (AHTD 2014, Sections 403.01, 409.01, 418.02).

The state construction specifications revealed that there was no specific mention of using SFS as an aggregate in concrete despite a Pennsylvania Department of Transportation survey reporting that California and Nebraska use or had used SFS in concrete pavements (PennDOT 2011b). In another document there was a mention of a concrete pavement in Texas with SFS aggregates, possibly constructed in the 1960s (TxDOT 1999).

Internationally, other countries have limits and allowances on the use of SFS aggregates. Typical limits on the maximum free lime content are at 4.5-5.0% in order to use SFS aggregates in an unbound pavement application (Smith and Collis 2001). In Germany, SFS can be used as an unbound layer if the free lime content is less than 7% and can be used in an asphalt layer if the free lime content is less than 4% (Motz and Geiseler 2000). In Brazil, SFS can be used in pavements (base and subbase) when the expansion by PTM 130 is less than 3.0% (da Silveira et al. 2005). A Federal Highway Administration report stated that the Netherlands and Belgium limit the free lime content of SFS aggregates to 4.5% before it can be used in granular bases and that the material must be weathered for at least one year prior to use (FHWA 1998). The British standard requires that SFS aggregates be weathered prior to usage in unbound pavement applications (Smith and Collis 2001), and Maw (1991) reported that weathered SFS with free CaO contents as high as 4.5% have been successfully used in the United Kingdom in asphalt pavements. In Japan, the free CaO content is limited to 0.5% to be used as a construction material (Kim et al. 2014).

ASTM D5106 (2013) is the specification for SFS aggregates to be used in asphalt pavements. For expansion, the D5106 standard specifies that ASTM D4792 should be used to evaluate the expansion potential for dense-graded materials, and that “aggregates that contain components subject to hydration, such as free lime (CaO), shall be obtained from sources approved by the purchaser on the basis of either satisfactory performance record, aging, or other treatment known to reduce potential expansion to a satisfactory level” (ASTM D5106 2013).

1.2 SCOPE OF THE REPORT

As with the previous FRAP sources, the Illinois Tollway has produced excess stockpiles of SFS FRAP from maintenance and rehabilitation activities. The main limitation to using SFS aggregates in concrete is the presence of free calcium oxide (CaO) and free magnesium oxide (MgO), both of which expand when reacted with water, which can cause cracking and accelerated deterioration. With the SFS aggregate already being in service in the asphalt concrete, the main question is whether free oxides are still present and will have deleterious expansion potential if utilized in concrete pavement. The scope of this study is to investigate the expansion potential of SFS FRAP and to ascertain if the SFS in the FRAP will deleteriously impact the concrete performance.

CHAPTER 2 LITERATURE REVIEW

2.1 SFS AGGREGATE PRODUCTION AND COMPOSITION

Modern SFS is the by-product produced by one of two methods: in a basic oxygen furnace (BOF), where iron is converted to steel, or in an electric arc furnace (EAF), where steel is produced by melting scrap steel (Shi 2004). BOF slag is also sometimes called Linz-Donawitz (LD) or LD-converter slag. Though now obsolete and very uncommon, another type of SFS is known as open hearth furnace (OHF) slag. The BOF process involves a furnace being charged with hot liquid metal (sourced from the blast furnace), scrap, and fluxes (lime and dolomitic lime), which is then injected with pressurized oxygen; the purpose of oxygen injection is to combine with the impurities to form the SFS (Shi 2004). The EAF process does not use hot liquid metal but instead cold metal scrap that is melted by the heat generated from electric arcs that pass from graphite electrodes (Shi 2004); as with BOF, oxygen is injected in the EAF process to produce the SFS. Once the molten metal and slag are separated, the steel is transferred to a ladle for additional refining, which involves the production of additional slag, known as ladle furnace slag, which has different properties than the SFS. The molten SFS can then be cooled in a number of methods, including cooling in air, spraying with water, quenching with air or water, and shallow box chilling (Shi 2004).

Chemically, SFS is mainly composed of calcium oxide (CaO), iron (II) oxide (FeO), silica (SiO_2), and magnesium oxide (MgO), as can be seen in Table 1, which also depicts the variability in composition between BOF and EAF slags. Typically, steel slags have iron oxide contents greater than 20% by weight, a lime-to-silica ratio greater than 7:3, and low (<0.2%) sulfur contents (Barnes and Strong 1980). In general, air-cooled SFS can contain the minerals merwinite ($3CaO\text{-}MgO\text{-}2SiO_2$), tricalcium silicate ($3CaO\text{-}SiO_2$), dicalcium silicate ($2CaO\text{-}SiO_2$), rankinite ($3CaO\text{-}2SiO_2$), wollastonite ($CaO\text{-}SiO_2$), diopside ($CaO\text{-}MgO\text{-}2SiO_2$), monticellite ($CaO\text{-}MgO\text{-}SiO_2$), calcium aluminate ($CaO\text{-}Al_2O_3$), calcium ferrite ($CaO\text{-}Fe_2O_3$), magnesium silicate ($2MgO\text{-}SiO_2$), various sulfides (CaS, MnS, FeS), lime (CaO), periclase (MgO), iron oxides (FeO, Fe_2O_3), and a solid solution phase FeO-MnO-CaO-MgO (Shi 2004). Motz and Geiseler (2000) reported that the main phases for both BOF and EAF slags are dicalcium silicate ($2CaO\text{-}SiO_2$), dicalcium ferrite ($2CaO\text{-}Fe_2O_3$), and wüstite (FeO). Similarly, Maw (1991) stated that the dicalcium silicate, wüstite, and ferrite phases are the most prevalent phases in SFS. In BOF slags, the wüstite forms as a calciowüstite unless there is a higher magnesium content in the slag, in which case a magnesiowüstite forms, and in EAF slags, the wüstite forms as magnesiowüstite (Geiseler 1995). Tricalcium silicate is often only found in steel slags with high CaO/SiO_2 ratios (Robinson 2002).

By weight, BOF slags consist mainly of 30-60% dicalcium silicate ($2CaO\text{-}SiO_2$), 0-30% tricalcium silicate ($3CaO\text{-}SiO_2$), 0-10% free CaO, 10-40% wüstite (FeO), and 5-20% dicalcium ferrite ($2CaO\text{-}Fe_2O_3$) (Balcázar et al. 1999). Around 35-85% of the total volume of the SFS may consist of the silicate phase (Maw 1991). Another reference reported that, by weight, calcic steel slags consist of 30-60% dicalcium silicate ($2CaO\text{-}SiO_2$), 0-20% tricalcium silicate ($3CaO\text{-}SiO_2$), 0-10% other silicate phases, 15-30% magnesiocalciowustite (RO-phase, a solid solution of (Fe,Mn,Mg,Ca)O), 10-25% dicalcium ferrite ($Ca_2(Fe,Al,Ti)_2O_5$), 0-5% magnetite-type phase ($(Fe,Mn,Mg)_3O_4$), 0-15% lime phase ((Ca,Fe)O), 0-5% periclase phase ((Mg,Fe)O), and 0-1%

fluorite (CaF_2) (Goldring and Juckes 1997). About 1% of the composition of SFS may also be free metal (Robinson 2002).

Sourced from steel plants in Indiana, Yildirim and Prezzi (2011) found that BOF slags contained major phases of portlandite ($Ca(OH)_2$), srebrodolskite ($Ca_2Fe_2O_5$), and merwinite ($Ca_3Mg(SiO_4)_2$) and minor phases of larnite (Ca_2SiO_4), manganoan calcite ($(Ca,Mn)CO_3$), lime (CaO), and dolomite ($CaMg(CO_3)_2$, and the EAF slags contained major phases of portlandite ($Ca(OH)_2$) and mayenite ($Ca_{12}Al_{14}O_{33}$) and minor phases of larnite (Ca_2SiO_4), lime (CaO), uvavorite ($Ca_3Cr_2(SiO_4)_3$), wollastonite ($(Ca,Fe)SiO_3$), and periclase (MgO).

Overall, the mineralogical compositions of SFS can be variable, particularly between different sources, and contain various other compounds, as shown in Table 2. In addition, there is some evidence to support that the composition of SFS aggregates is not uniform in that the interior may have a different composition than the exterior (Coomarasamy and Walzak 1995).

The composition of SFS changes over time, such as with weathering. One study found that BOF slag aggregates weathered outside for three months had developed a white powder on the surface, and further analysis revealed that the powder consisted of calcite ($CaCO_3$), calcium silicate hydrate, and calcium carboaluminate hydrate (Kawamura et al. 1983). The presence of $CaCO_3$ has also been found on the surface and in fine cracks in LD-slag samples (Thomas 1983). Another study also found that weathered BOF slag had higher calcite and calcium hydroxide contents (Belhadj et al. 2012). Tufa, a porous calcium carbonate precipitate, was found to form and clog bases and subbases with BOF slag aggregates, and it was concluded that calcium oxide, magnesium oxide, calcium hydroxide, and calcium carbonate have the potential to precipitate tufa (Gupta et al. 1994). However, even though weathering does reduce the content of free CaO, the reduction may not necessarily be sufficient enough to prevent tufa formation (Gupta et al. 1994). In another study, samples of EAF slag aggregates were obtained from a 10-year old asphalt pavement and precipitates of gypsum ($CaSO_4$-$2H_2O$), melanterite ($FeSO_4$-$7H_2O$), and calcium silicates were found on the slag particle surface (Suer et al. 2009).

High alloy steel EAF slags mainly consist of dicalcium silicates with no stabilizing components, so they often disintegrate into a fine powder (Balcázar et al. 1999) and are therefore unfit for civil engineering applications. In other steel slags, the dicalcium silicates are stabilized by the phosphorous pentoxide (P_2O_5) in the slag (Motz and Geiseler 2000). The dicalcium silicate that is present in SFS is in the β form, which is potentially metastable, although it is inactive in SFS (Emery 1982).

Table 1. Percent Chemical Composition Ranges for BOF and EAF Slags

Compound	BOF Slag	EAF Slag (carbon steel)	EAF Slag (alloy steel)	BOF Slag	EAF Slag (carbon steel)	EAF Slag (alloy steel)	BOF Slag (United Kingdom)	EAF Slag (United Kingdom)	BOF (South Africa)
Silica (SiO_2)	8-20	9-20	24-32	11-18	8-18	28-40	9-19	11-24	10-16
Alumina (Al_2O_3)	1-6	2-9	3-7.5	1-5	3-10	2-8	0.5-3	5-18	--
Iron (II) Oxide (FeO)	10-35	15-30	1-6	--	--	--	--	--	--
Total Iron (Fe)	--	--	--	14-22	20-30	0.4-3	24-45	5-30	17-23
Calcium Oxide (CaO)	30-55	35-60	39-45	45-54	25-35	34-48	33-51	31-50	50-60
Free CaO	--	--	--	1-10	0-4	--	--	--	--
Magnesium Oxide (MgO)	5-15	5-15	8-15	1-6	2-9	7-13	0.5-4	2-8	2-3
Manganese (II) Oxide (MnO)	2-8	3-8	0.4-2	--	--	1.3-2.0	--	--	~4
Manganese (III) Oxide (Mn_2O_3)	--	--	--	--	--	--	3-10	6-22	--
Total Mn	--	--	--	1-5	2-8	--	--	--	--
Titanium Dioxide (TiO_2)	0.4-2	--	--	--	--	--	0.5-1	0.3-1	~3
Sulfur (S)	0.05-0.15	0.08-0.2	0.1-0.3	--	--	--	0.05-0.15	0.04-0.4	--
Sulfite (SO_3)							0.05-0.4	0.04-0.9	--
Phosphorus (P)	0.2-2	0.01-0.25	0.01-0.07	--	--	--	--	--	--
Phosphorus Pentoxide (P_2O_5)	--	--	--	--	--	--	0.8-1.8	0.03-1.8	--
Fluoride (F)	--	--	--	--	--	--	0.02-0.5	0.1-2.6	--
Sodium Oxide (Na_2O)	--	--	--	--	--	--	0.05-0.1	0.05-0.3	--
Potassium Oxide (K_2O)	--	--	--	--	--	--	0.02-0.1	0.04-0.4	--
Chromium (Cr)	0.1-0.5	0.1-1	0.1-2.0	0.1-0.3	0.5-2.2	--	--	--	--
Chromium (III) Oxide (Cr_2O_3)	--	--	--	--	--	1-10	--	--	--
CaO/SiO_2 Ratio				2.8-4.4	1.7-4.0	1.3-1.6			
Reference	*Shi (2004)*			*Balcázar et al. (1999)*			*Gutt and Nixon (1979)*		

Table 2. Mineralogical Compositions of SFS from Various Studies

Mineral	EAF	BOF and LD
Silicates		
Larnite, belite, β-dicalcium silicate (β-Ca_2SiO_4)	Abu-Eishah et al. (2012); Diener (2006); Ducman and Mladenovič (2011); Iacobescu et al. (2011); Luxán et al. (2000); Manso et al. (2004); Pellegrino et al. (2013); Pellegrino and Faleschini (2013); Rojas and de Rojas (2004); San-José et al. (2013); Tsakiridis et al. (2008); Yildirim and Prezzi (2011); Vázquezramonich and Barra (2001)	Belhadj et al. (2012); Gupta et al. (1994); Kawamura et al. (1983); Mahieux et al. (2009, 2014); Poh et al. (2006); Vlcek et al. (2013); Wachsmuth et al. (1981); Waligora et al. (2010); Wang (1992); Xue et al. (2006); Yildirim and Prezzi (2011)
Calcio-Olivine, γ-dicalcium silicate (γ-Ca_2SiO_4)		Gupta et al. (1994); Poh et al. (2006)
α'-dicalcium silicate (α'-Ca_2SiO_4)		Gumieri et al. (2004)
Alite, tricalcium silicate (Ca_3SiO_5)	Manso et al. (2004); Tsakiridis et al. (2008);	Gumieri et al. (2004); Mahieux et al. (2009, 2014); Poh et al. (2006); Wachsmuth et al. (1981); Wang (1992); Xue et al. (2006)
Wollastonite ($CaSiO_3$)		Yildirim and Prezzi (2011)**
Ferroan wollastonite ($(Ca,Fe)SiO_3$)	Yildirim and Prezzi (2011)	
Monticellite ($CaMgSiO_4$)	Diener (2006)	Yildirim and Prezzi (2011)**
Merwinite ($Ca_3Mg(SiO_4)_2$)	Diener (2006); Iacobescu et al. (2011); Qian et al. (2002); Rojas and de Rojas (2004); Yildirim and Prezzi (2011)**; Vázquezramonich and Barra (2001)	Yildirim and Prezzi (2011)
Akermanite ($Ca_2MgSi_2O_7$)		Poh et al. (2006)
Bredigite ($Ca_7Mg(SiO_4)_4$)	Abu-Eishah et al. (2012); Luxán et al. (2000); Rojas and de Rojas (2004); Vázquezramonich and Barra (2001)	
Kirschsteinite ($Ca(Mg,Fe)SiO_4$)	Qian et al. (2002); San-José et al. (2013)	
Nagelschmidite ($2Ca_2SiO_4$-$Ca_3(PO_4)_2$)		Gupta et al. (1994)
Glaucochroite ($(Ca,Mn)_2SiO_4$)		Gupta et al. (1994)*
Manganese calcium silicate ($Mn_{0.8}Ca_{0.2}SiO_3$)		Gumieri et al. (2004)
Gehlenite ($Ca_2Al_2SiO_7$)	Ducman and Mladenovič (2011); Iacobescu et al. (2011); Luxán et al. (2000); Rojas and de Rojas (2004); San-José et al. (2013); Tsakiridis et al. (2008); Vázquezramonich and Barra (2001)	
Hydrogrossular ($Ca_3Al_2(SiO_4,CO_3(OH)_3)$)		Gupta et al. (1994)
Goosecreekite ($CaAl_2SiO_6$-$5H_2O$)		Gupta et al. (1994)
Uvavorite ($Ca_3Cr_2(SiO_4)_3$)	Yildirim and Prezzi (2011)	
Clinoenstatite ($MgSiO_3$)	Diener (2006); Vázquezramonich and Barra (2001)	
Wadsleyite ($(Mg,Fe)_2SiO_4$)		Gupta et al. (1994)
Iscorite (Fe_7SiO_{10})	Nicolae et al. (2007);	
Slinoferrosilite ($FeSiO_3$)		Gupta et al. (1994)
Fayalite (Fe_2SiO_4)	Nicolae et al. (2007)	Wang (1992)
Magnesium Fayalite ($(Fe,Mg)_2SiO_4$)		Gupta et al. (1994)
Quartz (SiO_2)	Tsakiridis et al. (2008)	Belhadj et al. (2012); Gupta et al. (1994)

*Trace mineral; **probable mineral phase

Table 2 (continued). Mineralogical Compositions of SFS from Various Studies

Mineral	EAF	BOF and LD
Oxides		
Wüstite (FeO)	Abu-Eishah et al. (2012); Ducman and Mladenovič (2011); Iacobescu et al. (2011); Manso et al. (2004); Pellegrino et al. (2013); Pellegrino and Faleschini (2013); Rojas and de Rojas (2004); San-José et al. (2013); Tsakiridis et al. (2008); Vázquezramonich and Barra (2001)	Belhadj et al. (2012); Gupta et al. (1994); Kawamura et al. (1983); Vlcek et al. (2013); Wachsmuth et al. (1981); Waligora et al. (2010)
Hematite (Fe_2O_3)	Pellegrino et al. (2013); Pellegrino and Faleschini (2013); Rojas and de Rojas (2004); Vázquezramonich and Barra (2001)	Kawamura et al. (1983); Yildirim and Prezzi (2011)**
Magnetite (Fe_3O_4)	Abu-Eishah et al. (2012); Iacobescu et al. (2011); Luxán et al. (2000); Rojas and de Rojas (2004); San-José et al. (2013); Tsakiridis et al. (2008); Vázquezramonich and Barra (2001)	Gupta et al. (1994)*; Mahieux et al. (2009)
Lime, calcium oxide (CaO)	Manso et al. (2004); Yildirim and Prezzi (2011)	Belhadj et al. (2012); Kawamura et al. (1983); Mahieux et al. (2009, 2014); Vlcek et al. (2013); Wachsmuth et al. (1981); Waligora et al. (2010); Yildirim and Prezzi (2011)
Srebrodolskite ($Ca_2Fe_2O_5$); dicalcium ferrite (2CaO-Fe_2O_3)	Manso et al. (2004); San-José et al. (2013)	Belhadj et al. (2012); Gumieri et al. (2004); Gupta et al. (1994); Kawamura et al. (1983); Mahieux et al. (2009); Poh et al. (2006); Wachsmuth et al. (1981); Wang (1992); Waligora et al. (2010); Yildirim and Prezzi (2011)
Mayenite ($Ca_{12}Al_{14}O_{33}$)	Iacobescu et al. (2011); Pellegrino et al. (2013); Pellegrino and Faleschini (2013); Tsakiridis et al. (2008); Yildirim and Prezzi (2011)	
Brownmillerite, ferrite ($Ca_2(Al,Fe)_2O_5$)	Ducman and Mladenovič (2011); Iacobescu et al. (2011); Pellegrino et al. (2013); Pellegrino and Faleschini (2013); Tsakiridis et al. (2008);	Mahieux et al. (2014); Poh et al. (2006); Vlcek et al. (2013)
Periclase, magnesium oxide (MgO)	Pellegrino et al. (2013); Pellegrino and Faleschini (2013); Tsakiridis et al. (2008); Yildirim and Prezzi (2011)	Belhadj et al. (2012); Gupta et al. (1994); Yildirim and Prezzi (2011)**
Magnesioferrite ($MgFe_2O_4$)	Luxán et al. (2000); Rojas and de Rojas (2004)	Gupta et al. (1994)
Magnesium iron oxide ($Mg_{1-x}Fe_xO$)		Gumieri et al. (2004)
Calcium magnesium iron oxide ($Ca_2MgFe_2O_6$)		Gumieri et al. (2004)
Spinel ($MgAl_2O_4$)	Diener (2006); Iacobescu et al. (2011);	Gupta et al. (1994)
Hausmannite ($(Mn,Mg)(Mn,Fe)_2O_4$)		Gupta et al. (1994)
Chromite ($FeCr_2O_4$)	Ducman and Mladenovič (2011);	
Manganese oxides	Luxán et al. (2000); Nicolae et al. (2007); Rojas and de Rojas (2004)	
Magnesium iron oxide ($(MgO)_{0.239}(FeO)_{0.761}$)		Mahieux et al. (2009)
Magnesium iron oxide ($(MgO)_{0.432}(FeO)_{0.568}$)		Mahieux et al. (2014)
Aluminum oxide (Al_2O_3)	Abu-Eishah et al. (2012);	
RO Phase (FeO-MnO-MgO solid solution)	Qian et al. (2002)	Xue et al. (2006)

*Trace mineral; **probable mineral phase

Table 2 (continued). Mineralogical Compositions of SFS from Various Studies

Mineral	EAF	BOF and LD
Hydroxides		
Portlandite, calcium hydroxide ($Ca(OH)_2$)	Yildirim and Prezzi (2011); Vázquezramonich and Barra (2001)	Belhadj et al. (2012); Gupta et al. (1994); Kawamura et al. (1983); Mahieux et al. (2009); Poh et al. (2006); Yildirim and Prezzi (2011)
Vernadite (Mn(OH))		Gupta et al. (1994)
Pyrochoite ($Mn(OH)_2$)		Gupta et al. (1994)
Carbonates		
Calcite, calcium carbonate ($CaCO_3$)	Yildirim and Prezzi (2011)**; Vázquezramonich and Barra (2001)	Belhadj et al. (2012); Gupta et al. (1994); Kawamura et al. (1983); Mahieux et al. (2009);
Magnesite ($MgCO_3$)		Gupta et al. (1994); Yildirim and Prezzi (2011)**
Dolomite ($CaMg(CO_3)_2$)		Gupta et al. (1994)*; Yildirim and Prezzi (2011)
Ferroan dolomite ($Ca(Fe_{0.33},Mg_{0.67})(CO_3)_2$)		Gupta et al. (1994)*
Manganoan calcite ($(Ca,Mn)CO_3$)		Yildirim and Prezzi (2011)
Ankerite ($Ca(Fe,Mg)(CO_3)_2$)		Gupta et al. (1994)*
Sulfides and Sulfates		
Alabandite (MnS)		Gupta et al. (1994)*
Pyrite (FeS_2)		Gupta et al. (1994)*
Marcasite (FeS_2)		Gupta et al. (1994)
Pentahydrite ($MgSO_4$-$5H_2O$)		Yildirim and Prezzi (2011)**
Phosphates		
Berlinite ($AlPO_4$)		Gupta et al. (1994)
Other		
Iron (Fe)	Diener (2006)	Gumieri et al. (2004); Waligora et al. (2010)

*Trace mineral; **probable mineral phase

The trace element content is not very high in SFS, with the exception of chromium, as can be seen in Table 3. The chromium content of the slag is related to the type of the steel produced, so high alloyed steel will result in higher chromium contents in the slag (Balcázar et al. 1999). In general, though, leachates are not a critical issue with SFS (Emery 1982). The leaching of heavy metals from SFS is not very high, possibly because of the elements being bound in other phases; for example, in BOF slag, chromium and vanadium have been found to be in stable ferrous phases, though vanadium can also exist in the more reactive calcium silicate phases (Legret et al. 2010). Further study has suggested that chromium is present in BOF slag in the trivalent oxidation state, which is the less toxic and less mobile oxidation state and does not change oxidative forms upon leaching, whereas the vanadium is in a tetravalent

oxidation state in the BOF slag but oxidizes to the most toxic pentavalent state upon leaching (Chaurand et al. 2007).

Table 3. Trace Element Contents (in mg/kg) for Steel Slags. Source: Balcázar et al. (1999)

	BOF Slag	EAF Slag (carbon steel)	EAF Slag (alloy steel)
Arsenic (As)	< 1	< 15	3
Cadmium (Cd)	< 1	< 30	< 1
Total Chromium (Cr)	1000-3000	5000-22000	--
Copper (Cu)	< 50	< 300	< 100
Mercury (Hg)	< 0.5	< 0.5	<0.5
Nickel (Ni)	<10	< 70	< 200
Lead (Pb)	< 10	< 90	< 30
Zinc (Zn)	< 150	< 900	< 30

Free CaO in the slag can exist as a residual from the flux material and/or as a precipitated product from the molten slag (Shi 2004). While cooling, the tricalcium silicates present in the slag can decompose into dicalcium silicate and free CaO, but this free CaO is distributed in the matrix and does not react to cause volume expansion (Balcázar et al. 1999). The problematic free CaO forms that cause volume expansion are the coarser particles of excess CaO and unassimilated CaO (Balcázar et al. 1999); this free CaO was not able to dissolve completely into the matrix mainly because a given amount of lime needs to be added to the flux in order to meet the metallurgical objectives of the steel and to keep the phosphorus content low (Geiseler 1995). One study found that more than 90% of the total free CaO in an LD-slag was from CaO that was not fully assimilated in the matrix (Thomas 1983). Free MgO in the slag can be from dolomitic fluxes and/or the lining of the steel furnace (Shi 2004), and using dolomitic fluxes instead of lime fluxes results in a higher MgO content in the slag (Geiseler 1996). Longer melting times for EAF slag compared with BOF slag results in higher magnesium contents, mainly from being leached from the furnace lining (Geiseler 1995). Thus, free CaO is a concern for both BOF and EAF slags, but free MgO is more likely to exist in EAF slags.

Rojas and de Rojas (2004) assessed the composition of two EAF steel slags and found that the composition did not change significantly between aggregate sizes (0-6, 6-13, 13-23, and 23-50 mm). The EAF slags were found to be very crystalline. The pozzolanic activity of the EAF steel slag was also evaluated and it was found that the CaO content was essentially unreactive up to 90 days. Overall, the free CaO and free MgO contents, measured by chemical and leaching tests, were estimated to be relatively low at <0.1% and <1%, respectively.

2.2 SFS AGGREGATE EXPANSION

The deleterious components of SFS are primarily free lime (CaO) and free magnesium oxide (MgO), both of which react with water to form expansive compounds. Free lime forms strained calcium hydroxide $Ca(OH)_2$, otherwise known as epizet, and magnesium oxide forms magnesium hydroxide $Mg(OH)_2$. The increases in solid volumes in the reaction are 91.7% for $Ca(OH)_2$ and 119.6% for $Mg(OH)_2$ (Erlin and Jana 2003). These reactions are known as topochemical, which means that the reaction occurs on the surface of the oxide compound and then the hydroxide compounds form outward, thereby causing stress concentrations that can lead to microcracking (Erlin and Jana 2003). Hydration of LD-slag samples was mainly

attributed to unassimilated CaO and CaO solid solution, and partially to unassimilated MgO, dicalcium silicate, and dicalcium ferrite (Okamoto et al. 1981). The MgO in SFS can exist in a chemically combined state (such as in a mineral phase), a free state, or a solid solution state, and the MgO is reactive when it is in the free state or when the MgO content is high relative to the other phases in the solid solution, in particular if the ratio of MgO/(FeO+MnO) is greater than 1.0 (Luo 1980). Weathered SFS with low free CaO (<1%) has been found to be non-expansive (Mathur et al. 1999), and similarly, rapidly-cooled steel slag with very low free CaO (0.15%) has been found to undergo minimal expansion (Kim et al. 2014). With sufficient free expansive oxide phases, the expansion of unbound SFS aggregates can be upwards of 10% (Emery 1982).

Based on the theoretical versus actual measurements of density variation, Verhasselt and Choquet (1989) found that the expansion of an LD slag was due to more than just the hydration of fine particles (< 0.5 or 0.1 mm) of free CaO. For coarser particles (0 to 4 mm), the change in density can be approximated based on the hydration of free CaO. Therefore, the authors argued that, for finer particles, where the reactions are accelerated, reactions other than the hydration of free CaO are occurring, such as the hydrolysis of calcium silicates or iron oxides, which can then be carbonated. Though the authors did not conduct further analysis, they concluded that free CaO was not the only source of expansion in BOF slags. There is evidence of this for BOF slags of similar initial free CaO contents (<3.5%), but produce significantly different expansions, up to a factor of 2 to 3 or greater. The final recommendations by the authors were that BOF slag aggregates can be used as an unbound base or subbase material if: (1) the initial free CaO content is <4.5%, (2) the slag is weathered outside for at least one year, and (3) the volumetric stability of the source material is tested. However, the authors also state that BOF slags should not be used in rigid bound layers because of the potential for severe expansion.

A study by Wang (2010) attempted to measure the expansive force of BOF slag aggregates. Confined BOF slag aggregates were submerged in water and a load cell measured the force daily. It was found that the three different BOF slag aggregates exhibited final expansive forces that corresponded to estimated surface tension stresses ranging from 0.6 to 1.3 MPa (87 to 189 psi). Only the BOF slag source that produced the highest expansion force resulted in some slight concrete deterioration under autoclave conditions. While this study aimed to quantify the expansive capability of SFS slag, it is limited in that: (1) the test was stopped after less than four weeks, so any free MgO may not have fully hydrated and (2) the free CaO and free MgO contents were not reported, so it is unknown why the different BOF slag sources resulted in different expansive pressures.

2.3 CONCRETE WITH SFS AGGREGATES (LABORATORY STUDIES)

A number of laboratory studies have investigated the usage of SFS aggregates in concrete. The literature review is summarized in Table 4 (strength and modulus properties) and Table 5 (shrinkage, fracture, and durability properties). This literature review only summarizes the studies that incorporated BOF, EAF, LD, or otherwise labeled steel slag aggregates in concrete. Overall, SFS aggregates in concrete can increase the concrete strength and modulus relative to virgin aggregate concrete, although there is insufficient information to definitively conclude the effect on other concrete properties (i.e. shrinkage, durability, fracture). However,

from the studies that investigated potential expansion because of CaO and/or MgO hydration, it is evident that the expanded products may have a detrimental effect on the concrete properties.

Abu-Eishah et al. (2012) tested the mechanical and durability properties of concrete made with EAF slag aggregate replacing about 70% of the coarse aggregate. No virgin aggregate concrete was tested for comparison in this study. Relative to conventional concrete, the fresh and hardened concrete unit weight was greater with the addition of slag aggregates. The authors found that the compressive strength of the concrete could be further increased with the use of Class F fly ash and silica fume. The ratio of split tensile strength to compressive strength was in the range of 2.3% to 4.4%, which is less than the typical ratio of 10% for conventional concrete. While rapid chloride penetration tests were conducted, it was concluded by the authors that the test was not valid because the steel in the aggregate could have affected the electric current used in the test procedure. The inclusion of fly ash and silica fume also reduced the water absorptivity of the concrete.

Adégoloyé et al. (2013) investigated the effects of EAF and stabilized argon oxygen decarburization (AOD) stainless steel slags as coarse aggregate replacements in concrete. Partial (50%) and full (100%) replacements of virgin coarse aggregate with the EAF and AOD slag aggregates increased the compressive strength and dynamic modulus relative to the control concrete. However, the concrete porosity and gas permeability were higher for concrete with stainless steel slags, although the permeability was still lower than the maximum recommended value for building construction. The concrete expansion was measured on prismatic samples stored in water, and it was found that concrete with EAF slag had similar expansions to the control, but the AOD slag concrete expanded more, which was likely due to a higher MgO content. The expansion amounts for all concretes were still below the maximum allowable limit.

By replacing either the coarse or fine aggregate with 100% steel slag aggregate, Akinmusuru (1991) found that the compressive strength was greater than conventional crushed stone aggregate concrete. The water absorption was also less for the concrete with coarse or fine steel slag aggregates, and the concrete water absorption was reduced by a greater extent by using fine steel slag aggregates compared with coarse steel slag aggregates.

Al-Negheimish et al. (1997) utilized EAF slag aggregate at 0 and 100% replacements of coarse aggregate in concrete. The concrete unit weight increased with the addition of the EAF slag aggregate. The compressive strength of concrete with EAF slag aggregate was similar to concrete with gravel aggregates, even under different curing conditions. The concrete flexural and split tensile strengths and modulus of elasticity increased with the use of EAF slag aggregates. Drying shrinkage strains appeared to be reduced with the use of EAF slag aggregates.

Table 4. Effect of SFS Aggregates on Concrete Strength Relative to Conventional Concrete

Property	Effect Relative to Virgin Concrete	Reference
Compressive Strength	Increase	Sersale et al. (1986a); Wang (1988); Akinmusuru (1991); Montgomery and Wang (1991); Wang (1992); Madej et al. (1996); Vázquezramonich and Barra (2001); De Schutter et al. (2002); Alizadeh et al. (2003); Beshr et al. (2003); Maslehuddin et al. (2003); Almusallam et al. (2004); Mohammed et al. (2009); Pellegrino and Gaddo (2009); Qasrawi et al. (2009)[1]; Coppola et al. (2010); Etxeberria et al. (2010)[3]; Papayianni and Anastasiou (2010a, 2011); Liu et al. (2011); Qasrawi (2012, 2014); Adégoloyé et al. (2013);Pellegrino and Faleschini (2013); Pellegrino et al. (2013); San-José et al. (2013); Anastasiou et al. (2014); Tarawneh et al. (2014)
	Decrease	Kawamura et al. (1982); Manso et al. (2004); Netinger et al. (2011); Ameri et al. (2012); Mathew et al. (2013)
	Similar	Al-Negheimish et al. (1997); Maslehuddin et al. (1999); Manso et al. (2006)[2]; Obratil et al. (2009); Tomasiello and Felitti (2010); González-Ortega et al. (2014)
Split Tensile Strength	Increase	Montgomery and Wang (1991); Al-Negheimish et al. (1997); De Schutter et al. (2002); Ali (2003); Alizadeh et al. (2003)[3]; Beshr et al. (2003); Almusallam et al. (2004); Pellegrino and Gaddo (2009); Coppola et al. (2010); Papayianni and Anastasiou (2010a, 2011); Qasrawi (2012); Pellegrino and Faleschini (2013); Pellegrino et al. (2013); Anastasiou et al. (2014)
	Similar	Alizadeh et al. (2003)[4]; Obratil et al. (2009); San-José et al. (2013)
	Decrease	Maslehuddin et al. (2003); Etxeberria et al. (2010)[5]; Mathew et al. (2013)
Flexural Strength	Increase	Wang (1988); Montgomery and Wang (1991); Al-Negheimish et al. (1997); De Schutter et al. (2002); Alizadeh et al. (2003); Mohammed et al. (2009); Qasrawi et al. (2009); Coppola et al. (2010); Papayianni and Anastasiou (2010a, 2011); Ameri et al. (2012); Anastasiou et al. (2014); Qasrawi (2014)
	Decrease	Maslehuddin et al. (1999, 2003); Liu et al. (2011); Netinger et al. (2011); Mathew et al. (2013)
	Similar	Obratil et al. (2009)
Modulus of Elasticity	Increase	Montgomery and Wang (1991); Al-Negheimish et al. (1997); Alizadeh et al. (2003); Beshr et al. (2003); Almusallam et al. (2004); Pellegrino and Gaddo (2009); Coppola et al. (2010); Papayianni and Anastasiou (2011); Pellegrino and Faleschini (2013); Pellegrino et al. (2013); Anastasiou et al. (2014); González-Ortega et al. (2014); Qasrawi (2014)
	Similar	Etxeberria et al. (2010)[5]; San-José et al. (2013)
	Decrease	Netinger et al. (2011)
Dynamic Modulus	Increase	Madej et al. (1996); Adégoloyé et al. (2013)

[1]With material passing #100 sieve removed; [2]at later ages; [3]high strength concrete; [4]normal strength concrete; [5]with a cement content of 350 kg/m^3 and a water-to-cement ratio of 0.50

Table 5. Effect of SFS Aggregates on Concrete Shrinkage, Fracture, and Durability Properties Relative to Conventional Concrete

Property	Effect Relative to Virgin Concrete	Reference
Stress Intensity Factor	Increase	Montgomery and Wang (1992)
Total Fracture Energy	Increase	Papayianni and Anastasiou (2010a)
Brittleness Index	Decrease	Montgomery and Wang (1992)
Bond Strength	Increase	Montgomery and Wang (1991)
Drying Shrinkage	Increase	Coppola et al. (2010)
	Similar	Netinger et al. (2011)
	Decrease	Madej et al. (1996); Al-Negheimish et al. (1997); Liu et al. (2011)
Water Absorption	Decrease	Akinmusuru (1991); Maslehuddin et al. (1999, 2003); Mohammed et al. (2009)
	Increase	Manso et al. (2004, 2006)
	No change	Anastasiou et al. (2014)
Sorptivity	Variable	Etxeberria et al. (2010)
Freeze/Thaw Durability	Acceptable	Obratil et al. (2009); Papayianni and Anastasiou (2010a)
	Decrease in Strength	Manso et al. (2006); Pellegrino and Gaddo (2009)
	Increase in Strength	Pellegrino et al. (2013)
Wetting/Drying Durability	Decrease in Strength	Manso et al. (2006); Pellegrino and Gaddo (2009); Pacheco et al. (2010)
	Decrease or Increase in Strength	Pellegrino et al. (2013)
Abrasion Resistance	Improved	Sersale et al. (1986a); Papayianni and Anastasiou (2003, 2010a, 2011)
High-Temperature Resistance	Decrease in Strength	Sersale et al. (1986a); Netinger et al. (2010, 2012)
Water Penetration	Increase	Manso et al. (2004, 2006); Anastasiou et al. (2014)
	Similar	Papayianni and Anastasiou (2010a)
	Decrease	Pacheco et al. (2010); San-José et al. (2013)
Sulfate Attack Resistance	Similar	De Schutter et al. (2002); Ali et al. (2011)
Alkali-Aggregate Reactivity	Low Reactivity	De Schutter et al. (2002); Manso et al. (2006)
Chloride Diffusion	Increase	Pacheco et al. (2010)
Chloride Diffusion Coefficient	Similar	Ali (2003)
Chloride Penetration Resistance	Increase	Anastasiou et al. (2014)
Porosity	Increase	Manso et al. (2004, 2006); Adégoloyé et al. (2013); San-José et al. (2013); Anastasiou et al. (2014)
	Similar	Pacheco et al. (2010); Papayianni and Anastasiou (2010a)
Gas Permeability	Increase	Adégoloyé et al. (2013)
Volume of Permeable Pores	Decrease	Maslehuddin et al. (2003)
Pulse Velocity	Increase	Maslehuddin et al. (2003)
	Similar	González-Ortega et al. (2014)
Time to Corrosion Initiation	Increase	Maslehuddin et al. (1999, 2003); Ali (2003)
Time to Cracking (Corrosion)	Increase	Maslehuddin et al. (1999, 2003); Ali (2003)
Corrosion Current Density	Decrease	Ali (2003)
Corrosion Susceptibility (Concrete pH)	No change	Netinger et al. (2011)

Ali (2003) investigated the effect of aggregates on the corrosion potential of steel reinforcement in concrete and compared the results from concretes made with 100% limestone and 100% steel slag as coarse aggregate. The split tensile strength of concrete increased with the use of steel slag aggregates. Also, the time to initiation of corrosion increased, the time to initiation of concrete corrosion cracking increased, and the corrosion current density decreased when steel slag aggregates were used in the concrete. The chloride diffusion coefficient was not very different between the concretes with different coarse aggregates. After thermal cycling, the concrete with steel slag aggregates still had the highest split tensile strength, and the reduction in strength with increasing thermal cycles was greater for the concretes with limestone aggregates.

Ali et al. (2011) examined the use of EAF slag aggregate as 0, 10, 50 and 100% replacements of coarse aggregate in concrete. After 28 days of curing, the concrete specimens were exposed to a sulfate solution for 20 weeks. There was minimal volumetric change for all concrete mixes, demonstrating that concrete with EAF slag aggregates is as resistant to sulfate attack as concrete with granite aggregate.

Normal and high strength concrete with coarse EAF slag aggregate was investigated by Alizadeh et al. (2003), and in both concrete types the inclusion of EAF slag aggregates increased the compressive and flexural strengths and modulus of elasticity relative to the control concrete. The split tensile strength increased with the inclusion of the EAF slag aggregate for the high strength concrete, but there was no change for the normal strength concrete.

Ameri et al. (2012) investigated different replacements (0, 25, 50, 75, and 100%) of virgin aggregate with BOF slag aggregate. The authors found that 25% BOF slag increased the compressive strength relative to the control (100% virgin aggregate) while the other replacement ratios decreased the strength. Not all replacement levels were tested for flexural strength, but in general, the inclusion of BOF slag aggregate increased the flexural strength of concrete.

Anastasiou et al. (2014) tested mortar and concrete with combined coarse EAF slag aggregates, fine construction and demolition waste (CDW), and high calcium fly ash. With 100% coarse EAF aggregate, the compressive, split tensile, and flexural strengths and the modulus of elasticity increased relative to the control. When CDW fine aggregates were used, the addition of coarse EAF slag aggregates did not significantly improve the properties. The high calcium fly ash further improved the hardened properties of the concrete with 100% coarse EAF slag aggregates, but only at later ages (>1 year). The use of coarse EAF slag aggregates did not appear to increase the water absorption, but the concrete porosity was slightly increased; the use of CDW with and without EAF slag aggregates increased the porosity and water absorption. Under pressure, the water penetration increased when EAF slag and/or CDW aggregates were used. The chloride penetration resistance slightly improved with EAF slag aggregates and decreased with CDW.

Bäverman and Aran Aran (1997) examined a concrete with 0 and 100% replacements of natural fine aggregates with EAF slag aggregate. The use of the EAF slag aggregate increased the concrete unit weight. The compressive strength was similar for both concretes, being classified as a medium-strength concrete, although the concrete with EAF slag aggregate was reported as being “more brittle.” A leaching test revealed that the leachates were similar between the two concretes except for the chromium content, although the chromium

concentration leached from the concrete with EAF slag aggregate was a minimum around a pH of 12.5.

Beshr et al. (2003) compared concretes made with four different coarse aggregate types: three limestone (calcareous, dolomitic, and quartzitic) and one steel slag. Relative to the other limestone aggregates, the steel slag aggregate resulted in higher compressive and split tensile strengths and a higher modulus of elasticity. Additional work by the authors considered the effects of adding silica fume to the same concrete mixtures (Almusallam et al. 2004), which revealed that the compressive and split tensile strengths increased. At all silica fume dosages, the concrete with steel slag aggregate had higher compressive strengths than the limestone aggregate concretes. With 0 and 15% silica fume, the concrete with steel slag aggregate had higher split tensile strengths than the limestone aggregate concretes, while with 10% silica fume the concrete with steel slag aggregate had similar split tensile strengths to the quartzitic limestone aggregate concrete and higher strengths than the calcareous and dolomitic limestone aggregate concretes. With 0 and 15% silica fume, the concrete with steel slag aggregate had a higher elastic modulus than the limestone aggregate concretes, while with 10% silica fume, the concrete with steel slag aggregate had a lower elastic modulus than the quartzitic limestone aggregate concrete and a higher elastic modulus than the calcareous and dolomitic limestone aggregate concretes.

Coppola et al. (2010) studied partial replacements (0, 10, 15, 20, and 25%) of the total (coarse, intermediate, and fine) aggregates in concrete with EAF slag aggregate. As the percentage of EAF slag aggregate increased, the slump loss rate increased, the modulus of elasticity increased, and the compressive, split tensile, and flexural strengths increased. Increasing contents of EAF slag aggregates drastically increased the drying shrinkage strain in the concrete with 25% EAF slag aggregate increasing the shrinkage strain by 30% at later ages.

De Schutter et al. (2002) investigated using LD-slag as partial and full replacements (0, 20, 40, and 100%) of aggregate in concrete blocks for maritime structures. The mixes with 20% and 40% LD-slag used steam-weathered slag while the mix with 100% LD-slag had untreated slag. The concrete unit weight increased with increasing LD-slag contents, although the addition of the LD-slag reduced the concrete slump. The addition of the LD-slag was found to increase the compressive strength and slightly increase the flexural and split tensile strengths of the concrete. No damage was found in any of the concrete cube specimens after 14 freeze/thaw cycles. After 13 weeks in sodium sulfate solution, only the mix with 100% untreated LD-slag showed some swelling and cracking damage. A test for alkali-silica reaction (ASR) yielded some swelling in the mixes with treated LD-slag, which the authors concluded was not likely due to ASR but rather due to the expansion of unhydrated products in the LD-slag.

Ducman and Mladenovič (2011) studied the use of fine EAF slag aggregate (0-4 mm size) as partial and full replacements of a cement mortar with bauxite aggregates (0-6 mm size) for refractory applications. It was found that EAF steel slag was not suitable for high-temperature applications because of a phase transformation (wüstite to magnetite) around 700-800°C which led to expansion, cracking, and reduced mechanical properties. However, the transformation is irreversible, so if the EAF slag aggregate is heated to 1000°C and then added to the concrete, then the concrete remains stable in high-temperature applications.

Among other industrial by-product materials, Etxeberria et al. (2010) investigated the use of 0, 25, 50, and 100% coarse EAF slag aggregates replacements of natural aggregates. With a

cement content of 300 kg/m^3 and a water-to-cement ratio of 0.55, it was found that only 25% EAF slag aggregate increased the compressive and split tensile strengths and modulus of elasticity relative to concrete with natural aggregates. With a cement content of 350 kg/m^3 and a water-to-cement ratio of 0.50, at all EAF slag aggregate contents, the compressive strength was higher, the split tensile strength was lower, and the modulus of elasticity was lower but similar to the control concrete. By submerging the concrete samples in water, the length change of the concrete with EAF slag aggregates was similar or lower than the control concrete. Only the concrete with 100% EAF slag aggregate had a lower sorptivity than the control concrete. After exposing the concrete to 800°C for 4 hours, the concrete with EAF slag aggregates had a greater residual strength than the control concrete. Testing the same concrete with 0, 20, and 100% EAF slag aggregates, Pacheco et al. (2010) found that the concrete porosity was similar with and without EAF slag aggregates. Conducting a wetting/drying test, all concretes experienced a reduction in strength, although the reductions were less severe for the concretes with EAF slag aggregates. Concrete with EAF slag aggregates demonstrated better resistance against water penetration. In a chloride diffusion test, the surface concentration of chlorides and the unsteady apparent diffusion coefficient were higher for the concrete with EAF slag aggregates, and, in addition, the rate of chloride penetration was higher than the control for the mix with 100% EAF slag aggregate. It is possible that the chloride contents were higher in the concrete with EAF slag aggregate because of chlorides binding to the slag.

Fujii et al. (2007) examined a concrete that contained SFS as the aggregate and used combinations of cement, ground granulated blast furnace slag, and fly ash as the cementitious binder. The results indicated that the compressive strength can be similar to conventional concrete. The concretes produced typically failed before the freeze/thaw durability limit of 300 cycles. The results indicated that SFS aggregates with lower absorption capacity was more freeze/thaw durable compared with SFS aggregates with higher absorption capacity, especially if an air-entraining admixture was used. The authors theorized that the SFS aggregates leached calcium hydroxide, which reacted with the air-entraining agent, causing large bubbles to form and lowering the freeze/thaw durability of the concrete. The authors recommended the use of fly ash to reduce the calcium hydroxide content.

George and Sorrentino (1982) made mortars using a BOF slag aggregate created by adding an “aluminous slagging agent” to the converter during production, which reportedly reduced the free lime content. It was found that the steel slag aggregate increased the flexural and compressive strengths of the mortar relative to a siliceous aggregate mortar. The authors speculated that the improved flexural strength with steel slag aggregates was caused by mechanical and chemical influences. Electron micrographs showed that the fracture for siliceous aggregates occurred near the paste-aggregate interface, while for steel slag aggregates, the fracture occurred through the paste and the aggregate.

González-Ortega et al. (2014) studied the mechanical and radiological properties of concrete with weathered non-expansive coarse and fine EAF slag aggregates. The concrete containing EAF slag aggregates could have similar compressive strengths to limestone aggregate concrete. The static modulus of elasticity was upwards of 10% greater for concrete with EAF slag aggregates. The ultrasonic pulse velocity of the concrete was similar for the virgin aggregate concrete and the concrete with EAF slag aggregates. The attenuation of gamma rays was 11% greater for concrete with EAF slag aggregates, relative to limestone aggregate

concrete, indicating that concrete with EAF slag aggregates may provide better radiation shielding.

Kawamura et al. (1982) evaluated two BOF slag aggregate sources as full replacements of fine and/or coarse aggregates in concrete. Concretes were produced with BOF slag aggregates that had been weathered outside for 0, 1, and 3 months. The BOF slag aggregate properties changed with weathering. In general, as the amount of weathering increased, the slag specific gravity and unit weight decreased while the absorption capacity increased. The concrete slump increased when the weathered BOF slag aggregates were used. Overall, the compressive strength of the concrete at 28 days was reduced when BOF slag aggregates were used as fine aggregates, coarse aggregates, or both. The compressive strength further decreased when weathered slag aggregates were used. After concretes made with 3-month-weathered slag aggregates were submerged in 20°C water for 17 weeks, the concrete with slag aggregates expanded more than the virgin aggregate concrete despite the lack of visual signs of cracks or pop-outs.

Khan and Shinde (2013) examined 0, 20, 40, 60, 80 and 100% replacements of natural fine aggregate with steel slag fine aggregate in concrete. The results indicated that the compressive, split tensile, and flexural strengths increased and then decreased with increasing fine steel slag aggregate content. The results indicated that the 60% fine steel slag aggregate maximized the concrete strength.

Liu et al. (2011) investigated the use of EAF slag aggregates as replacements of both fine and coarse aggregates in concrete. By replacing 100% coarse and fine aggregate with EAF slag aggregate, the compressive strength increased while the flexural strength slightly decreased relative to the control concrete. The drying shrinkage decreased with the use of EAF slag aggregates.

Lun et al. (2008) investigated various methods to reduce the free CaO content in BOF steel slag fine aggregate for use in concrete. The treatment methods were by steam for 8 and 12 hours and by autoclaving for 3 hours, all of which reduced the free CaO content. By soaking mortar bars in hot water, the steam-treated steel slag aggregates delayed the onset of, but did not prevent, deleterious expansion while the autoclave-treated steel slag did not undergo deleterious expansion. Initial results, without deleterious expansion, showed that the treated slag aggregate mortars had higher compressive and flexural strengths than the control with untreated slag aggregate. After the mortar was hot water cured and the aggregates expanded, the compressive and flexural strengths decreased, although the strengths were relatively consistent for the autoclaved slag aggregate mortar.

Madej et al. (1996) examined two different slags from EAF iron alloy production: a high carbon ferro chromium (FeCrC) slag and a ferro silico manganese (FeSiMn) slag. In an autoclave unsoundness test, the steel alloy slag aggregates did not undergo significant expansion, around of 0.10%, compared with an LD-slag with a high free CaO content that expanded up to 13%. Compared with a dolomite concrete with a similar water-to-cement ratio, the concretes with the steel alloy slag exhibited greater magnitudes of unit weight, compressive strength, and dynamic modulus. In addition, the drying shrinkage was less for the concretes with steel alloy slag. An investigation of the cement-aggregate interface using scanning electron microscopy with the FeCrC slag aggregate revealed little calcium silicate hydrate (C-S-H), but large crystals of oriented calcium hydroxide were observed.

Manso et al. (2004) made mortar and concrete with EAF slag aggregates that had been weathered outside for 90 days in wetted stockpiles that were periodically turned. Mortar samples were created with blends (33, 50, and 67%) of EAF slag fine aggregate and limestone filler and compared with a control mortar with limestone sand. The mortar compressive strengths were similar to the control although the mix with 67% EAF slag aggregate was slightly lower than the control. Concrete was made with replacements up to 100% of the total (fine, intermediate, and coarse) aggregate with EAF slag aggregate. Relative to the limestone aggregate control mix, mixes with EAF slag aggregate resulted in higher water absorption, increased water penetration, higher porosity, and reduced compressive strength; these detrimental effects were reduced once limestone fine aggregate was used instead of EAF slag fine aggregate. The use of a limestone filler partly mitigated some of the negative effects that the slag aggregate had on the concrete properties. An accelerated aging test was performed by curing the concrete samples in warm water and then weathering the samples outdoors, but there did not appear to be a negative effect on compressive strength. A sulfate solution soundness test revealed that the mixes with slag aggregate and limestone filler had a greater reduction in compressive strength and greater expansion compared with the control mix, although the expansion was less than the allowable maximum limit. A leaching test on the concrete with steel slag aggregate and plain steel slag showed that the leachates were below the maximum allowable limits for sulfates, fluorides, and total chromium. A continuation of the study by Manso et al. (2006) revealed reductions in compressive strengths at early ages (7, 28 days) relative to the control when replacing coarse and fine aggregate with EAF slag, although the compressive strengths were similar to the control at later ages (90 days, 1 year). The results also indicated that the water absorption, water penetration, and porosity increased with increasing steel slag aggregate content. Concrete samples were autoclaved and then weathered outdoors for 90 days, which demonstrated that there was a reduction in the compressive strength although the EAF slag aggregate concrete had less significant reductions in strength. An accelerated aging test was also conducted by curing samples in warm water and then weathering outdoors, and this accelerated aging scheme did not have a negative impact on compressive strength. A test for alkali-aggregate reactivity revealed that the expansion was lower than the critical limit. After 25 freeze/thaw cycles, all mixes experienced reductions in compressive strength, but the reductions were more severe for the mixes with EAF slag aggregates. Additionally, after 30 wetting/drying cycles, all mixes experienced a reduction in compressive strength, but the mixes with EAF slag aggregate resulted in greater reductions in strength. Another leaching test was performed and, again, the leachates were below the maximum allowable limits for sulfates, fluorides, and total chromium. Additional research by the Manso et al. (2011) demonstrated that precast concrete can be made with both coarse and fine EAF slag aggregates in conjunction with ladle furnace slag (as a partial replacement of cement) and limestone filler (as a partial replacement of fine aggregate). Additional work showed that ladle furnace slag could be used in conjunction with EAF slag aggregates (Polanco et al. 2011), although at high contents of ladle furnace slag, the expansion caused by MgO hydration can be detrimental.

Maslehuddin et al. (1999) investigated the use of 0 and 100% replacements of coarse aggregate with steel slag aggregate at different coarse to total aggregate ratios. At the same coarse aggregate ratio, the compressive and flexural strengths were similar for the concretes

with and without steel slag aggregate, i.e., there was a 3.8% reduction in flexural strength with the steel slag aggregate. Concrete with steel slag aggregate was found to be less permeable based on the reduction in total water absorbed. The shrinkage of mortar samples with steel slag aggregate was lower than mortar with sand. Testing for steel corrosion susceptibility, the concrete with steel slag aggregate increased the time to corrosion initiation as well as the time to cracking. Additional work by the authors (Maslehuddin et al. 2003) replaced 100% of the coarse aggregate with EAF slag aggregate and compared it with limestone aggregate concrete. For the same coarse aggregate ratio, the compressive strength was higher, the flexural and split tensile strengths were slightly lower, the concrete absorption was lower, the volume of permeable pores was lower, and the pulse velocity was higher for the concrete with steel slag aggregates versus virgin aggregate concrete. Exposed to thermal cycles, the concrete strength, pulse velocity, and absorption decreased, but the compressive strength and pulse velocity were higher and the absorption was lower for the slag aggregate versus the limestone aggregate concrete. The drying shrinkage was lower for slag aggregate mortar, and after exposing mortar to a moist environment for 110 days, the slag aggregate mortar had experienced expansion while the limestone mortar did not. Testing for steel reinforcement corrosion, the steel slag aggregate concrete had a longer time to initiation of corrosion as well as a longer time to cracking.

Mathew et al. (2013) replaced crushed granite coarse aggregate with 0, 20, 40, 60, 80, and 100% steel slag aggregate. The concrete slump increased with increasing steel slag aggregate content. As the slag aggregate content increased, the compressive, split tensile, and flexural strengths decreased. However, the target flexural strength for concrete pavements was achieved by all steel slag aggregate concretes.

Matsunaga et al. (2004) investigated a material called “steel slag hydrated matrix,” which was a cementitious material for marine structures made with steel slag aggregate (maximum sizes of 20 or 40 mm) mixed with water, ground granulated blast furnace slag, fly ash, and calcium hydroxide. Compared with conventional concrete, the steel slag hydrated matrix had a lower modulus of elasticity, better abrasion resistance, and could have similar compressive, tensile, and flexural strengths. This “steel slag hydrated matrix” has been also researched as a material for seaweed growth to deter sea desertification (Nakagawa et al. 2010).

Mohammed et al. (2009) studied concrete specimens with 0, 25, 50, and 60% replacements of natural aggregates with steel slag aggregates. The compressive and flexural strengths increased with increasing slag aggregate content. The water absorption of the concrete decreased with increasing slag aggregate content.

Montgomery and Wang (1991) examined the use of instant-chilled steel slag, also known as shallow box chilled steel slag, at 0, 20, 40, 60, 80, and 100% (by volume) replacements of coarse limestone aggregate. An increase in the split tensile strength of the concrete with steel slag aggregate content was found, but the interfacial bond strength (using a split tension test) was greater between a steel slag surface and mortar versus a limestone surface and mortar. With increasing steel slag aggregate content, the compressive and flexural strengths and the elastic modulus also increased. Microhardness test results suggested that the steel slag aggregate may have a harder interfacial transition zone. Additional work by the authors (Montgomery and Wang 1992) using notched compact compression fracture specimens revealed that the stress intensity factor is greater by about 10% and the brittleness factor is

lower for concrete with 100% coarse steel slag aggregates relative to concrete with limestone aggregates.

Moon et al. (2002) examined both EAF and converter steel slag aggregates as well as different processing methods to mitigate the deleterious expansion, including air aging for one month, hot water aging at 80°C for one and three days, and steam aging at 100°C and 1 atm for three days. An immersed expansion test of the slag aggregate revealed that all aging methods were successful at reducing the expansion, although the hot water (three days) and steam aging methods were most effective, particularly with the converter steel slag. Dehydration tests revealed that the hot water and the steam aging methods were the most successful at converting free CaO to $Ca(OH)_2$. The aging methods affected the compressive strength of concrete somewhat, and the results suggested that the degree of expansion (amount of free lime) affected the compressive strength.

Moosberg-Bustnes (2004) created mortars with AOD steel slag fine aggregate as filler material (<45 μm) by partially replacing (10, 20, and 30%) cement. The steel slag mortar resulted in higher compressive strengths than the reference at all replacement levels and resulted in higher flexural strengths for only the 10 and 20% replacement levels. The author speculated that the increase in strength was possibly due to the filler effect and/or due to the hydration of the silicate phases in the steel slag. An additional part of the study used EAF and AOD steel slags as filler that had been wet-ground in order to increase the activity (i.e. reactivity) of the slag. The slags were then added as partial (0, 20, and 40%) replacements of cement. The results indicated that the compressive strength was reduced when using either of the steel slags as filler material, although at later ages the strength was higher for the mixes with 20% steel slag (either EAF or AOD) relative to the mix with 20% quartz filler. The shrinkage was not significantly affected by the presence of the steel slag filler material.

Netinger et al. (2010) investigated the effects of temperature on concretes with dolomite fine aggregates and either steel slag or dolomite coarse aggregates. The cured concretes were treated at temperatures of 100°, 200°, 400°, 600°, and 800°C. The high-temperature treatments reduced the compressive and flexural strengths and the elastic moduli of all concretes. Concrete with steel slag aggregates had similar residual compressive strength to dolomite concrete at temperature treatments 100°, 200°, 400°, and 600°C, and at 800°C, the dolomite concrete had better residual compressive strength. Similar behavior was noted for the flexural strength, although one of the steel slag aggregate concrete mixes had significantly reduced strength after the 600°C, and none of the mixes had any residual flexural strength after the 800°C treatment. The elastic modulus behavior was similar for all concretes up to temperatures of 400°C; the steel slag aggregate concrete mixtures had lower relative elastic moduli to the dolomite concrete after high-temperature treatments (600° and 800°C). The weight loss was similar for all concretes except for the dolomite concrete at 800°C, which experienced greater mass loss than the steel slag aggregate concretes. Measurement of the ultrasonic pulse velocity through the concrete specimens indicated that the microcracking was more severe in the concretes with steel slag aggregates, especially after higher temperature treatments (600° and 800°C). Additional concrete mixtures were tested by Netinger et al. (2012), which confirmed the previous findings. The significant damage to the concrete at elevated temperatures was due to the expansive phase transition that steel slag undergoes after 550°C.

An additional study by Netinger et al. (2011) tested two EAF slag aggregates sources for potential full replacement of coarse aggregate in concrete. Fresh concrete with slag aggregate had a higher unit weight, higher air content, and the same slump relative to virgin aggregate (dolomite) concrete. The addition of slag aggregates reduced the compressive and flexural strengths and the elastic modulus compared with the virgin aggregate concrete. The inclusion of slag aggregates did not affect the pH of the concrete pore solution, indicating that it would not affect the corrosion susceptibility of steel reinforcement. The drying shrinkage of the concrete was similar between virgin and steel slag aggregates.

Researchers at Cleveland State University (Bosela et al. 2008; Obratil et al. 2008) investigated three different BOF aggregates at varying replacements of coarse and fine aggregates up to 100% levels in concrete. For concrete fresh properties, the steel slag aggregate reduced workability, increased unit weight, and had variable effects on the air content. The compressive strength was similar for all concrete mixtures, with SFS aggregate contents ranging from 10% to 100%. The effect of steel slag on the concrete split tensile strength was variable. Although the authors did not compare the hardened properties with a control mix with virgin natural aggregates, the hardened properties of concrete with slag aggregates were suitable for paving concrete. Additional work by Obratil et al. (2009) studied a SFS aggregate source as partial and full replacements of virgin aggregate for paving concrete. The SFS aggregates reduced workability and increased unit weight. The air content appeared to be suitably controlled by the amount of air-entraining admixture dosed. The compressive strength was reportedly not adversely affected by the slag aggregate and therefore it met the required strength level at 28 days. The split tensile and flexural strengths were additionally not greatly affected by the steel slag aggregate. Concrete length change measurements of concrete in lime water were inconclusive regarding the expansive potential of the steel slag aggregate. In addition, the freeze/thaw durability of concretes with steel slag aggregates was acceptable after 300 cycles.

Ozeki (1997) reported that studies were carried out in Japan on the use of EAF slag aggregates in concrete. No additional details were provided and it was simply stated that the concrete strength and durability properties were similar between EAF and natural aggregates.

Ozkul (1996) created concrete mixtures with 100% EAF coarse aggregate and with natural sand or ladle furnace slag as the fine aggregate. The compressive and flexural strengths were similar for the two concretes, although the mix with natural sand had slightly higher compressive strengths, and, at later ages (at 28 days and 180 days), the concrete with ladle furnace slag fine aggregates had higher flexural strengths. The abrasion resistance of the concrete was improved with the slag fine aggregates. After 20 wetting/drying cycles, both concretes had about a 3% reduction in dynamic modulus. The volume expansion of the concretes after being stored in water for 180 days was similar to virgin aggregate concrete.

Papayianni and Anastasiou (2003) studied the effect of using steel slag aggregates as 100% replacements of coarse and/or fine aggregates in concrete, in combination with 30-60% replacements of cement with high calcium fly ash and 0-30% replacements of cement with ground granulated steel slag. The authors investigated the strength (compression, split tension, and flexure), modulus (static and dynamic), abrasion resistance, wet/dry durability, and outdoor exposure durability properties. However, because the w/cm ratio was not held constant for all concrete mixtures, it is difficult to definitively conclude the effects of the steel slag, although the

concrete abrasion resistance improved with the inclusion of steel slag aggregates. The heavy metals present in the steel slag aggregate were not as susceptible to leaching once they were incorporated into the concrete.

Papayianni and Anastasiou (2005) utilized steel slag aggregates as coarse aggregates in a heavy-weight concrete application for radiation shielding. While the authors did not compare the findings with those of conventional concrete with virgin (natural) aggregates, they tested the effect of steel slag coarse aggregates on the concrete strength (compression, split tension, and flexure), modulus (static and dynamic), and fracture (Hillerborg's total fracture energy and impact fracture) properties. In testing for radiation shielding properties compared with conventional concrete, steel slag aggregate concretes had similar gamma ray attenuation in the energy region of ~1 MeV and better gamma ray attenuation in the energy region of 0.1 MeV, but had an increased secondary gamma ray production.

Papayianni and Anastasiou (2010a) examined the feasibility of using 100% coarse and 50% fine EAF slag aggregate in concrete with partial replacements of cement with either 30% ladle furnace slag or 50% high calcium fly ash. The concrete unit weight increased with the use of EAF slag aggregate. For concrete mixes with cement and with and without high calcium fly ash, the mixes with coarse EAF slag aggregate and with coarse and fine EAF slag aggregate had higher compressive, split tensile, and flexural strengths compared with the control mix with limestone aggregates. The mix with coarse EAF slag aggregate and ladle furnace slag had similar strengths to the control mix. For concrete with plain cement, the mixes with coarse EAF slag aggregate and with coarse and fine EAF slag aggregate resulted in up to 27% higher total fracture energies compared with virgin aggregate concrete. Abrasion resistance improved with EAF slag aggregates, and the freeze/thaw durability was acceptable for all mixes except for those with the high calcium fly ash. The depth of water penetration under pressure was good for all mixes, indicating good impermeability, as was additionally evidenced by the low porosity of the concretes.

Papayianni and Anastasiou (2011) studied concrete with full replacements of coarse aggregate and partial replacements of fine aggregate with EAF slag aggregate in addition to 60% replacement of cement with high calcium fly ash. The EAF slag aggregates increased the unit weight of the concrete. Replacing only the coarse aggregate with EAF slag aggregates resulted in higher compression, split tension, and flexural strengths versus the virgin aggregate control mixes, both with and without fly ash. With coarse and fine EAF slag aggregates, the concrete resulted in slightly higher compression, split tension, and flexural strengths than the virgin aggregate control mix with fly ash. The elastic modulus was higher for the concrete with EAF slag aggregates compared with the virgin mixes with and without fly ash. The concrete with coarse EAF slag aggregate and fly ash showed improved abrasion resistance compared with the control concrete with limestone aggregate and no fly ash. A leaching test revealed that the leachate from the concrete with coarse EAF slag aggregate and fly ash was minimal and was categorized as "inactive waste."

Pellegrino and Gaddo (2009) investigated EAF slag as a potential aggregate in concrete. A leaching test found that the potential toxic chemicals from the slag were lower than the allowable limits. For the concrete mixture design, an ideal grading curve was developed and all aggregates ≥2 mm in size consisted of EAF slag aggregates while all aggregates <2 mm in size were natural aggregates. The concrete with EAF slag aggregates had higher unit weights,

compressive and split tensile strengths, and elastic moduli compared with the natural aggregate concrete. In an attempt to accelerate the hydration of free CaO and free MgO in the slag, concrete cylinders were placed in a 70°C water bath for 32 days, after which the compressive strength of the concrete with EAF slag aggregates decreased by 5.6% while the concrete with natural aggregates experienced a 9.1% increase in strength. An additional set of concrete cylinders were placed in a 70°C water bath for 32 days and then weathered outdoors for 90 days, after which the compressive strength of the concrete with EAF slag aggregates decreased by 2.4% while the concrete with natural aggregates experienced an 8.3% increase in strength. In another aging test, the cylinders were subjected to 25 freeze/thaw cycles, after which the compressive strength of the concrete with EAF slag aggregates decreased by 7.3% while the concrete with natural aggregates experienced an 11.5% increase in strength. In a final aging test, the cylinders were subjected to 30 wetting/drying cycles, after which the compressive strength of the concrete with EAF slag aggregates decreased by 26.5% while the concrete with natural aggregates experienced a 5.7% decrease in strength.

Building on the previous work, Pellegrino et al. (2013) examined 0, 50, and 100% replacements of coarse and fine aggregate with EAF slag aggregate in concrete. The addition of EAF slag aggregates could have higher unit weights, compressive and split tensile strengths, and elastic moduli relative to natural aggregate concrete, however, it is difficult to draw definitive conclusions because the water-to-cement ratio was not constant for all of the mixes. Additional aging tests were carried out by submerging the concrete cylinders in a 70°C water bath for 32 days and then weathering them outdoors for 90 days. Before and after the 90 days of outdoor weathering, all concretes experienced an increase in compressive strength, with the greatest increase typically occurring for the natural aggregate concrete. After 25 days of freeze/thaw cycles, all concrete mixtures experienced an increase in compressive strength. Additionally, after 30 wetting/drying cycles, all concretes experienced a decrease in compressive strength, with some of the mixes with EAF slag aggregates experiencing a greater decrease while others experienced a lesser decrease in compressive strength relative to natural aggregate concrete. There is some microstructural evidence to support that air-entrained concrete with 100% coarse and fine EAF slag aggregates may develop fewer and smaller air bubbles. Chemical and mineralogical studies on the concrete before and after durability testing did not reveal a significant difference.

Qasrawi et al. (2009) investigated using 0, 15, 30, 50, and 100% fine aggregate replacements with low calcium (0.4% CaO) high iron (97% Fe_2O_3) steel slag aggregate. As the fine slag aggregate content increased, the concrete workability decreased and the unit weight increased. Particularly at later ages, the concrete compressive strength for mixtures with 15, 30, and 50% fine steel slag aggregate was higher than the control (0% slag aggregate) while the mix with 100% steel slag aggregate was lower than the control. The flexural strength was higher than the control for concretes with fine steel slag aggregates at all replacement levels, and the strength increased with increasing slag aggregate content up to 50%. However, when the steel slag aggregate was sieved to remove all material passing the #100 sieve (0.15 mm), the compressive strength continued to increase as the fine steel slag aggregate content increased from 0% to 100%. The researchers concluded that a high amount of fines may adversely affect the concrete results because more cement is needed to effectively coat the particles.

Qasrawi (2012) investigated concrete with a SFS coarse aggregate that had an iron content of 37%. The higher iron content of this SFS aggregate reduced the concrete workability, but the compressive and split tensile strengths were found to increase with increasing SFS aggregate contents. In addition, the author did not find any indication of concrete staining from corrosion of the iron in the SFS aggregate after aging from 1 to 10 months.

Qasrawi (2014) tested concrete with 0, 25, 50, 75, and 100% by volume replacements of the virgin coarse aggregate with coarse SFS aggregate. Tests were then additionally conducted to determine the optimum replacement of virgin coarse aggregate with a combination of SFS and recycled concrete aggregate (RCA). The workability decreased while the air content increased with increasing SFS aggregate contents. The concrete compressive strength increased by as much as 20% when SFS aggregates were utilized. The use of RCA reduced the compressive strength, but with a blend of 67% SFS and 33% RCA, the compressive strength was relatively unaffected, even up to 100% replacement of virgin coarse aggregate. Similar behavior was noted in the concrete flexural strength. The use of SFS aggregates increased the modulus of elasticity upwards of 17%, but a combination of 67% SFS and 33% RCA reduced the modulus by <10%.

Rainová et al. (2012) studied fiber-reinforced concrete with either BOF or blast furnace slag aggregates and compared the results with those of other concretes with recycled aggregates from the literature. The results indicated that the concrete with BOF slag aggregate attained higher compressive and split tensile strengths compared with the concrete with blast furnace slag aggregates, although both mixtures had strengths less than those cited in the literature with EAF slag aggregates.

San-José et al. (2013) tested concrete with two different sources of EAF slag aggregates. The total aggregate consisted of mainly EAF slag coarse and fine aggregates (92-93% by weight) with some limestone filler added. The water-to-cement ratio was not constant between all mixtures, which may have skewed the interpretation of the results. Relative to a control concrete with limestone aggregates, the concretes with EAF slag aggregates resulted in similar split tensile strengths and moduli of elasticity but higher compressive strengths. The concrete porosity increased slightly for the concretes with EAF slag aggregates relative to the control. The depth of water penetration was below the allowable limit for all mixtures, although the concretes with EAF slag aggregates exhibited slightly lower depths of penetration than the control.

A number of different EAF slag samples were characterized by Sánchez Fransesch and Soria Tonda (2010) for use in cement mortars at contents of 0, 20, 30, 40, 50, and 100%. The overall findings suggested that SFS aggregate contents of 30 and 40% were the most promising for mortar performance. In addition, not all types of fine aggregate were suitable for use in conjunction with SFS aggregates in mortar, and variable results were found for a given SFS aggregate source once different cement sources were tested. Based on the SFS test results, the authors determined that the material exhibits potential for use in embankments, as fillers for drainage materials, as aggregates for HMA, as aggregates for mortar, as aggregates for concrete, as gravel, and as a raw material in cement clinker manufacture.

Sersale et al. (1986a) used LD slag aggregate as 0 and 100% replacements of coarse aggregate in concrete. Concrete with LD slag aggregate had higher compressive strengths than similar concretes produced with limestone or basalt coarse aggregates, particularly at later ages

(7 and 28 days). The abrasion resistance of the concrete also improved with the use of LD-slag aggregates. Treating the concrete at 200°C for 24 hours reduced the compressive strength of the concrete with steel slag aggregates by more than 50% relative to the limestone and basalt concretes.

Tarawneh et al. (2014) investigated by weight replacements of fine, intermediate, and coarse limestone in concrete with 10, 20, 30, 40, 50, 60, 70, 80, 90, and 100% SFS aggregates. The general trend indicated an increase in compressive strength with increasing SFS content.

Tomasiello and Felitti (2010) studied self-compacting concrete (SCC) with EAF slag aggregate as a partial replacement of the coarse aggregate. Fly ash and limestone filler were also examined as partial replacements of cement. Suitable workability was obtained for the SCC with EAF slag aggregates. The concretes with either fly ash or limestone filler resulted in similar compressive strengths for the mixes with and without EAF slag aggregate.

Vázquezramonich and Barra (2001) created various concrete mixtures with different EAF slag aggregate sources, replacing the total aggregate content by 0, 20, 35, and 100%. The concretes with EAF slag aggregates had a higher compressive strength than the mix with limestone aggregates, and the mixes with 100% EAF slag coarse and fine aggregates resulted in the highest strengths. Concrete specimens were then subjected to various aging conditions: curing room with ≥95% relative humidity at 20°C for 2 months, accelerated aging with 90% relative humidity at 70°C for two months, and autoclave accelerated aging at 0.2 MPa and 132°C for 4, 8, and 24 hours. Because the EAF slag sources were different, the dimensional changes for the various concretes was different as well; some concretes experienced similar dimensional changes to the reference concrete with limestone aggregates while other concretes experienced dimensional changes more than 2.5 times the reference concrete. Distresses (cracks, pop-outs) began to form in the concretes with EAF slag aggregates after 11 months for the specimens cured at ≥95% relative humidity and 20°C, after 2 weeks for the specimens cured at 90% relative humidity and 70°C, and after 4 hours, though more significantly after 8 and 24 hours, for the autoclaved specimens.

Wang (1988) utilized steel slag aggregates as partial and full replacements of fine aggregate in mortar and concrete samples. Mortar samples yielded higher compressive and flexural strengths with 100% steel slag aggregates compared with virgin sand. Additionally, concrete samples with partial and full replacements of fine aggregate with steel slag resulted in higher compressive and flexural strengths versus the control. The abrasion resistance of the concrete was reduced with increasing steel slag fine aggregate contents, although it is not clear if the test was performed on mortar or concrete samples. There is some evidence to support that the cement-aggregate bond is improved with the addition of steel slag fine aggregate, based on microhardness results and a finding that there is a greater amount of hydration products within 50 μm of the interface between steel slag aggregate and cement versus limestone aggregate and cement. Using scanning electron microscopy, it was found that the interface within 20 μm of the paste-aggregate interface contained finer calcium hydroxide crystals and was denser for the steel slag aggregate compared with the limestone aggregate. The author postulated that the improved characteristics of the paste-aggregate interfacial zone were because of the reaction of the cement hydration products with ions from the mineral phases in the steel slag aggregate.

Wang (1992) examined 100% coarse aggregate replacements with BOF slag aggregate. Microhardness tests revealed that the interfacial transition zone, about 25 μm away from the paste-aggregate interface, was harder for concrete with BOF aggregates compared with basalt aggregates, possibly because of the reaction of the BOF slag with cement. The compressive strength was higher for mixes with BOF coarse aggregate compared with basalt aggregate. The expansion of the samples soaked in water was the same for both BOF and basalt aggregates. Concrete samples were also subjected to a 100-minute autoclave test, which revealed that the samples remained volumetrically stable after the test.

Reinforced concrete structures have also been investigated incorporating EAF slag aggregates. Kim et al. (2012) found that the flexural performance of concrete with EAF slag aggregates was similar to concrete with natural aggregates. Additional work has also been conducted on spirally reinforced confined concrete columns with EAF slag aggregates (Kim et al. 2013). Work by Pellegrino and Faleschini (2013) showed similar behavior with increases in compressive and split tensile strength and elastic modulus when EAF slag aggregate was used, and in reinforced concrete beams, concrete with EAF slag aggregate yielded higher ultimate flexural and shear capacities versus concrete with natural aggregates.

2.4 CONCRETE WITH SFS AGGREGATES (FIELD STUDIES)

A number of concrete projects have been completed utilizing SFS aggregates. The performance results have not all been satisfactory, with a number of projects demonstrating significant failures and others performing satisfactorily. There have not been many documented concrete pavement applications with SFS aggregates, although it has been shown that, in Austria, through careful material evaluation, certain SFS aggregate sources can be used in concrete for road construction and for concrete floors (Geiseler 1996).

One report examined states that produce steel slag or are near other states that produce steel slag (Ohio, Indiana, West Virginia, Pennsylvania, Michigan, and Illinois), and in general found that these state departments of transportation do not permit the use of steel slag aggregates in concrete (Fronek et al. 2012). Primarily, the research on the use of steel slag aggregates in concrete has been done outside of the United States, namely in Spain, Germany, Canada, Italy, India, and Saudi Arabia (Fronek et al. 2012).

In the United States, early failures of projects with SFS aggregates essentially halted its usage in concrete pavements. In the early 1980s, a concrete pavement section of I-75 near Tampa, Florida, was constructed with expansive steel slag aggregates in a 6-inch econocrete base layer topped with an unbonded 9-inch concrete surface layer. Within 6 months, pavement distresses consisting of longitudinal cracks of 100 feet long and crack openings up to 2 inches wide were visually noted (Armaghani et al. 1988). In the late 1970s or early 1980s, a 16-inch concrete pavement runway was constructed on a 6-inch econocrete base with EAF slag aggregates at the Tampa International Airport in Florida; the expansion of the EAF slag in the econocrete resulted in shear failures in the asphalt shoulders and the doweled centerline joint opened several inches (Bosela et al. 2012; W. Charles Greer Jr., personal communication, April 2014).

In Gregg County, Texas, a concrete pavement with SFS aggregates may have been constructed on IH-20 in the 1960s (TxDOT 1999), but no additional information was located on the performance of this pavement.

Pennsylvania conducted a field experiment with OHF slag in a cement-treated base and subbase on Route 82 in Chester County. The slag was not sufficiently weathered and resulted in significant surface displacements. The horizontal and vertical surface displacements were on the order of four to six inches (Miller and Collins 1976).

Internationally, steel slag aggregates have been successfully used in construction projects in Spain, Greece, and Belgium. Between 2008 and 2010, the Labein-Tecnalia Kubik Building in Madrid, Spain, was constructed with EAF slag aggregates. The basement walls and floor slab utilized 100% coarse and fine EAF slag aggregate while up to 75% of the total aggregate was EAF slag aggregate for the foundation walls and slab (Arribas et al. 2010; Bosela et al. 2012) without distresses reported (Bosela et al. 2012). A base course test section has also been constructed in Spain which contained EAF and ladle slag aggregates stabilized with cement (Vázquez et al. 2010).

In Greece, a concrete pavement test section with EAF slag aggregates and high calcium fly ash was surveyed after 10 years of service (trafficked by trucks at a ready-mix concrete plant). Cores demonstrated that the compressive and split tensile strengths of the concrete were still superior to conventional concrete. Microscopic analysis of samples showed that the concrete had suitable air content (6-8%) and demonstrated strong paste-aggregate bonding (Papayianni and Anastasiou 2010b). There has also been field application of self-consolidating concrete with EAF slag fines as filler material (Lykoudis and Liapis 2010).

A low traffic rural road was constructed in Belgium with roller-compacted concrete that had stainless steel EAF slag aggregates as 85% of the total aggregate (De Bock and Van den Bergh 2004). Field cores taken 90 days after placement showed compressive strengths ranging from 24 to 53 MPa from four locations with a fifth location revealing compressive strengths as low as 7 MPa. Another site in Belgium utilized stainless steel EAF slag aggregates in a cement-treated road base. The base contained 78% steel slag aggregate by total weight of the dry materials. The 28-day unconfined compressive strength of the field-molded specimens ranged from 4.3 to 9.5 MPa. The base was constructed in three layers, and a nuclear density gauge confirmed that the compacted base reached 94% to 99% of the reference density. No additional details were provided on the performance of these field sections.

In the United Kingdom, Dunster (2002) reported that BOF slag aggregates had been used for coarse and fine aggregates in armour stones as sea defense barriers. After 18 months of wetting and drying cycles, visual inspections revealed no evidence of cracking or spalling.

An investigation into the mechanism of pop-outs in a concrete wall in South Korea one year after construction revealed that the cause was due to fine EAF slag aggregates. The hydration of free CaO and free MgO caused stress concentrations which led to the pop-out formation. Finite element analysis revealed that EAF particle sizes ≤5 mm can cause a pop-out up to 23 mm deep (Lee and Lee 2009).

2.4.1 SFS in Pavement Support Layers

Steel slag has been used in roadway applications other than in concrete. In Australia, steel slag aggregates are used in asphalt concrete or as a base or subbase material and can be used up to 100% in certain applications (CCAA 2008, 2013). Australian pavement test sections with BOF aggregates as a base material did not show any signs of deleterious expansion after two years (Heaton 1989). Australians have also used SFS aggregates as a road surfacing

material and as a compacted, unbound road shoulder material (Jones 1982). Heaton et al. (1996) and Heaton (1993,1996) discuss Australian test sections that used SFS aggregates and granulated blast furnace slag as a binder; the hypothesis was that the free CaO in the SFS aggregates would activate the granulated blast furnace slag. Heaton et al. (1996) and Heaton (1996) also argue that in a weathered SFS aggregate, the available free CaO has hydrated to form $Ca(OH)_2$, thus reducing the expansive potential of the SFS as well as providing the $Ca(OH)_2$ that may activate the hydration in a mix with fly ash and/or granulated blast furnace slag. A number of test sections in the United Kingdom showed promising performance with both weathered and virgin LD slag base materials (Thomas 1983). Test sections were built in Germany in the early 1990s using LD slag as base materials (Motz and Geiseler 2000). In Germany, steel slag aggregates can be used in bases and subbases as well as in asphalt surface layers. Certain regulations are in place in Germany for volume stability of the steel slag aggregates, and provided that the regulations are met, the aggregates have remained stable throughout the life of the pavement. The German experience has shown leaching is not an issue either.

A case study reported by Crawford and Burn (1969, 1971) involved steel slag aggregates in a backfill that ultimately expanded and caused building damage. A building located in Sault Ste. Marie, Ontario, Canada, was constructed in 1961-1962 in which a steel slag aggregate was used as backfill material before the concrete floor slabs were poured. Cracking in the building was originally noted in early 1963, and an excavation in 1965 revealed that the floor had been raised 1/2 inch, which then exceeded 1 inch in 1967. The vertical movement by the end of 1967 was indicative of a 9% expansion of the steel slag. The expansion continued and was reported to indicate an 18% expansion of the steel slag at the end of 1970.

In Brazil, an LD slag fill had to be removed to prevent the collapse of a building (da Silveira et al. 2005). Used as a backfill, SFS has been reported to cause issues with heaving building floor slabs in a number of cases (Bailey and Reitz 1970; Gnaedinger and Gnaedinger 1970; Gray and Salver 1970; Ritchie 1970; Spanovich and Fewell 1970; Gnaedinger 1987). In one instance, the concrete floor slab was reported to have heaved by 11 inches (Gnaedinger 1987). In one occurrence, the vertical heave of the concrete slab was 8.3% relative to the thickness of the SFS backfill (Gray and Salver 1970). Failures have also been reported in parking lots, where the surface course was replaced as a result of the expansion of the OHF slag base (Spanovich and Fewell 1970; Gnaedinger 1987) with surface heaves reported to be up to 15 inches.

Glass (2003) presented a case in South Africa where a mixture of steel slag and ferricrete was used as a backfill material at a steel mill. Over time, the expansion of the steel slag aggregate caused movements of the floors and walls of various buildings at the site. The floor movements were on the order of 100-250 mm. The steel slag expansion was estimated to be around 5%.

2.5 SFS FRAP AGGREGATES

To date, no studies have investigated the use of SFS FRAP aggregates in either concrete or asphalt mixtures. However, the expansive characteristics of reclaimed asphalt pavement (RAP) materials with SFS aggregates have been studied (Senior et al. 1994; Deniz et al. 2010; Dayioglu et al. 2014).

Deniz et al. (2010) studied the expansive characteristics of various recycled aggregates–such as RAP, SFS RAP, virgin SFS, virgin blast furnace slag, and virgin dolomite aggregates–in a highly alkaline (pH = 12) solution at 70°C to ascertain the applicability of the materials for unbound base or subbase applications. The expansion was monitored up to 60 days. The authors found that the total expansion of SFS FRAP aggregates was less than that of virgin SFS aggregates (Figure 2). The degree of expansion was 6.2% and 5.8% for virgin nonporous steel slag, 4.1% for a virgin porous steel slag, 1.7% for a RAP that contained about 92% steel slag aggregates, 1.5% and 1.1% for steel slag aggregate RAP, 0.9% for a stone mastic asphalt (SMA) RAP, 0.2% for a surface binder course RAP that contained about 60% steel slag aggregates, and 0.3% for a virgin steel slag aggregate, and nearly 0% for air-cooled blast furnace slag and virgin dolomite. While the authors did not conduct a chemical analysis, it is possible that the lower degree of expansion for the SFS FRAP was because of already hydrated and expanded free CaO and free MgO. Additionally, the virgin steel slag aggregates that did not expand significantly likely did not have high contents of free CaO and free MgO.

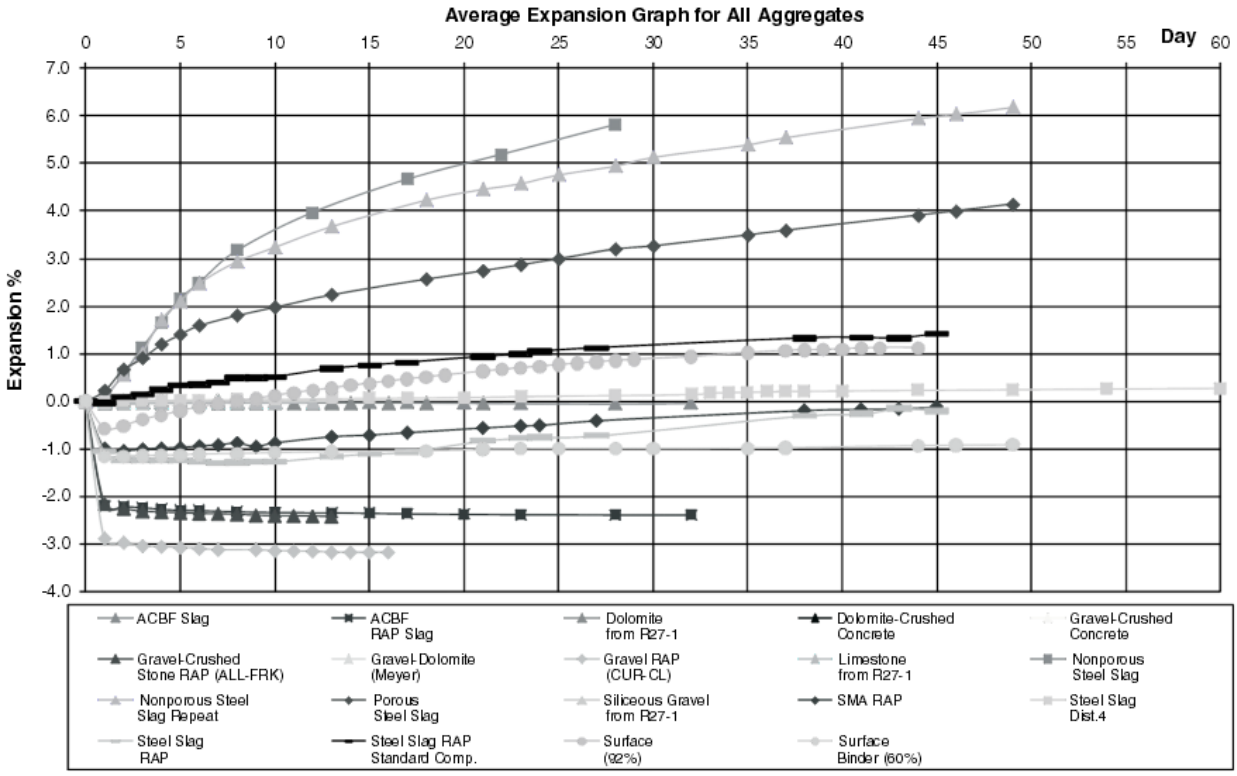

Figure 2. Expansion results for various aggregates, including virgin slags, SFS RAP, RAP, and natural aggregates. Source: Deniz et al. (2010).

Dayioglu et al. (2014) attempted to reduce the swelling potential (tested by ASTM D4792, conducted in water at 70°C) of SFS aggregates by coating the aggregates with asphalt binder (PG 64-22). As expected, the greatest expansion occurred with the uncoated SFS aggregate. With a coating of 7% by weight of asphalt, the SFS aggregate did not expand (Figure 3). Samples with lower contents of asphalt experienced swelling, but with a coating of 4% by weight of asphalt, the SFS aggregate expanded 70% less than the uncoated SFS aggregate sample. The swelling of the SFS aggregate was also reduced by mixing water treatment residual (WTR) with the aggregates.

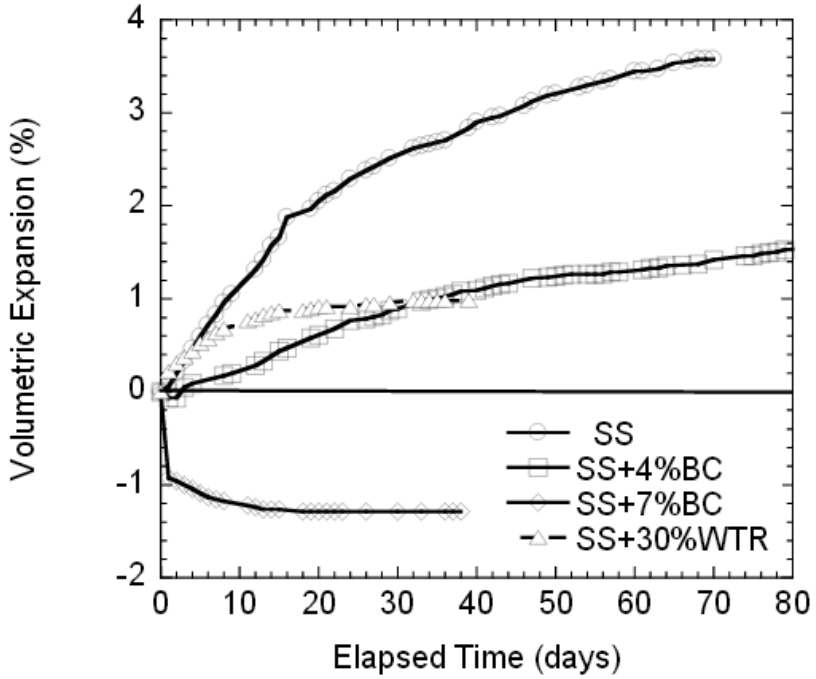

Figure 3. ASTM D4792 expansion results for virgin steel slag (SS) and with 4% and 7% bitumen contents (BC). Additional tests were conducted by adding water treatment residual (WTR). Source: Dayioglu et al. (2014).

Senior et al. (1994) examined the expansion potential of a 10-year-old SFS RAP by ASTM D4792. A blend of SFS RAP with granular material resulted in a low expansion (<1%) after 7 days while, at the same time, the virgin SFS aggregates (BOF and EAF) had high expansion (3-6%). Specifically, the expansion of the blended materials after 7 days was as follows: 15/85 SFS RAP/granular 0.44%, 30/70 SFS RAP/granular 0.61%, 40/60 SFS RAP/granular 0.61%, and 50/50 SFS RAP/granular 0.65%. An additional test with 100% SFS RAP resulted in very low expansion (0.03%), which was attributed to a delayed reaction. A RAP with trap rock underwent zero expansion as did a blend of virgin sand and gravel. At later ages, the expansion was similar between the samples with 100% SFS RAP and 30% SFS RAP, as can be seen in Figure 4. The virgin SFS aggregates underwent significant expansion, even at later ages. These findings led to the recommendations that a blend with a maximum of 30% SFS RAP is allowed for certain granular base and subbase applications in Ontario and that 100% SFS RAP is allowed for use as material for unpaved shoulders.

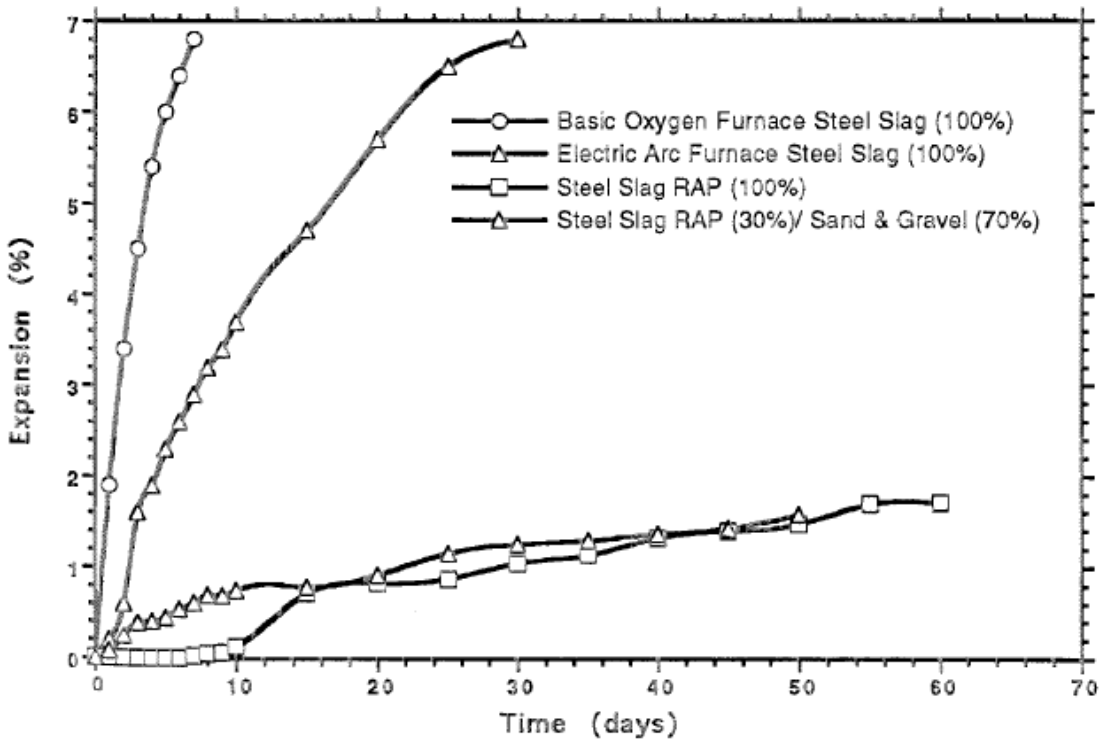

Figure 4. ASTM D4792 expansion results for virgin SFS and SFS RAP aggregates. Source: Senior et al. (1994).

There are very few specifications or recommendations that mention the allowable use of SFS RAP or SFS FRAP. The Indiana Department of Transportation (INDOT) allows the use of SFS RAP in asphalt pavements, provided that the existing specifications for RAP are still met (INDOT 2014). The Ministry of Transportation of Ontario (MTO) allows the use of some SFS RAP materials for unpaved gravel shoulders, but SFS RAP aggregates are not allowed in HMA pavements (MTO 2013).

2.5.1 Performance and Expansion of Hot-Mix Asphalt with SFS Aggregates

In the United Kingdom, asphalt-based construction has utilized steel slag starting in the 1920s (Thomas 1983). In Ontario, Canada, steel slag aggregates were allowed in HMA mixes until they were banned in 1991. However, a review of various projects in Ontario revealed that HMA with SFS aggregates can perform better than HMA with natural aggregates (Piché 2003).

Coomarasamy and Walzak (1995) examined field cores of asphalt pavements with SFS aggregates that were exhibiting “good” and “poor” performance. The “good” pavement revealed a uniform SFS aggregate-asphalt interface with good coverage and adhesion. The cracked and “poor” performing pavement showed white calcium-rich deposits, mainly calcium carbonate ($CaCO_3$), that were accumulating at the SFS aggregate-asphalt interface. When exposed to humidity, core cross-sections of the “good” and “poor” performing pavements showed some reactivity of the exposed SFS aggregate. This indicates that, in the field, the free CaO and MgO may or may not hydrate if the SFS aggregate is covered with asphalt although the potential for expansion still exists.

Kandhal and Hoffman (1997) found that HMA samples with SFS fine aggregates submerged in 150°F water or samples subjected to freeze/thaw cycles did not expand to an amount that correlated to the expansion potential of the SFS fine aggregates, even though one of the SFS sources produced very high expansions. This suggests that SFS aggregates coated with asphalt are impermeable to water ingress, so expansion cannot occur. HMA samples with higher asphalt contents experienced less expansion because of freeze/thaw. These results suggest that the SFS FRAP with higher asphalt contents may experience less volume expansion or may not expand at all if the asphalt coating prevents moisture ingress.

A scanning electron microscopy investigation revealed that the rough texture of BOF slag aggregate allowed for a strong bond strength and adhesion with asphalt (Shen et al. 2009). This may be the reason why other studies found that the HMA with SFS did not expand significantly and performed well under freeze/thaw cycling.

When immersed in water, an SMA mixture with steel slag aggregates expanded by less than 1% over 7 days (Wu et al. 2007). However, it is questionable whether or not all of the available free CaO and free MgO would have expanded in 7 days, so it is likely that much longer immersion times would have yielded more reliable results.

2.6 TESTING OF SFS AGGREGATES

Given that the composition and performance of SFS aggregates differ from conventional virgin aggregates, additional tests may be appropriate. Farrand and Emery (1995) suggested that performance testing of SFS is appropriate, particularly petrographic examination, expansion measurements after a 1-hour autoclaving, and expansion measurements after a 7-day water immersion (after ASTM D4792). However, chemical composition is also of critical importance, particularly in the form of free lime content determination.

2.6.1 Free CaO Content Determination

The total free CaO of the SFS is of critical importance, as the hydration of the CaO to form $Ca(OH)_2$ is the initial expansive reaction of the aggregate. Heaton et al. (1996) argued that the expansion of SFS aggregates is affected by the morphology and distribution of the free CaO in the SFS particle, so the estimated total free CaO content is not the only indicator of the expansion potential. A number of studies have investigated methods to measure free CaO content, and other studies have attempted to refine the measurement to provide a more accurate estimation. The most prevalent methods involve a chemical extraction technique.

The European Standard EN 1744-1:2009+A1 (2013) lists a number of testing methods for the free CaO content of SFS aggregates, including complexometry (complexometric titration), conductometry, and acidimetry. The SFS aggregate is ground and then free CaO is extracted by the sample using ethylene glycol. The calcium ion content can then be determined through complexometric titration or conductance measurements with the concentration of the calcium ions assumed to be only from the free CaO. Alternatively, in the acidimetry method, the free CaO can be extracted with ethyl acetoacetate and titrated with hydrochloric acid.

Ministry of Transportation of Ontario (MTO 1996) also specifies a test method for the free CaO content of SFS aggregates through complexometric titration. In this method, the sample is mixed with ethylene glycol and methyl alcohol and heated to dissolve the free CaO.

After filtering, the filtrate is titrated with hydrochloric acid after a bromothymol blue indicator is added.

A number of rapid test methods by complexometric titration have been developed to determine the free CaO content of cement and clinker, which were summarized in ASTM STP 985 (Gebhardt 1988). The four described methods involved dissolving the free CaO in hot ethylene glycol, which was at temperatures of 230°C, 80-100°C, 80-90°C, or 110°C, depending on the method. Three of the methods then specified using a phenolphthalein indicator and titration with hydrochloric acid while the other method specified a chrome blue-black indicator and titration with ethylenediaminetetraacetate (EDTA).

Thermogravimetric analysis (TGA) has also been used to refine the estimated total free CaO content of SFS aggregates (Kneller et al. 1994). The free CaO content was determined using ethylene glycol, phenolphthalein indicator, and titration with hydrochloric acid. Assuming that the CaO in the SFS aggregate can be hydrated to form calcium hydroxide or carbonated to form calcium carbonate, TGA was used to determine these contents knowing the decomposition temperatures of both calcium hydroxide and calcium carbonate. The total initial free CaO was assumed to be the sum of the free CaO (determined from complexometric titration) and the CaO contents from calcium hydroxide and calcium carbonate (determined from TGA).

Belhadj et al. (2012) extracted the calcium ions with glucose and then titrated with hydrochloric acid. The authors then used TGA and differential thermal analysis to determine the calcium hydroxide and calcium carbonate amounts in the sample in order to accurately determine (i.e. refine) the free CaO content. Similarly, Lun et al. (2008) and Gumieri et al. (2004) used an ethylene glycol method to determine the free CaO and calcium hydroxide content of the SFS and then used TGA to determine the calcium hydroxide content, whereas Papayianni and Anastasiou (2011) used the “sugar test” from ASTM C25 and TGA-DTA to fully quantify the free CaO content. Okamoto et al. (1981) also used TGA-DTA to estimate the contents of $Ca(OH)_2$, $Mg(OH)_2$, and $CaCO_3$.

Other studies have specified free CaO determination: extraction by ethylene glycol and methanol with titration (Coomarasamy and Walzak 1995), an ethylene glycol method (Thomas 1983; Motz and Geiseler 2000; Faraone et al. 2009), extraction by warm ethylene glycol with titration by hydrochloric acid with phenolphthalein indicator (Gupta et al. 1994), extraction by a sugar solution with titration by sulfuric acid with a phenolphthalein indicator (Waligora et al. 2010), the EN 1744-1 acidimetry method (Mahieux et al. 2009, 2014), the EN 1744-1 standard (Manso et al. 2006), the EN 1744-1 complexometric method (Netinger et al. 2011), the Spanish standard UNE 80-216-91 (Vázquezramonich and Barra 2001), an ethylene glycol method by the Brazilian standard NBR 7227 (Gumieri et al. 2004), chemical analysis and microscopy methods (Wachsmuth et al. 1981), a tribromophenol-glycerol extraction (Okamoto et al. 1981), and extraction with heated glycerol and titration with benzoic acid with phenolphthalein indicator (Wang 1992). A number of other studies reported a free CaO content, but did not describe the method in which the value(s) was determined.

A number of methods have been developed and used to determine the free CaO content of SFS, the most prominent of which appears to be ethylene glycol extraction with complexometric titration. One complication with the ethylene glycol extraction is that it also extracts the calcium ions from other phases, such as calcium hydroxide (MacPherson and Forbrich 1937). A number of researchers have therefore used thermal analysis in conjunction

with complexometric titration techniques to more accurately quantify and refine the free CaO content of SFS.

2.6.1.1 Free MgO Content Determination

No test method has yet been proposed to accurately determine the free MgO content of SFS aggregates. The European Standard EN 1744-1:2009+A1 (2013) states: “The total MgO content is used as a measure of free MgO, in the absence, at present of a reliable method of determining the content of free MgO.” Some researchers, however, have attempted to study the free MgO content by other methods. Rojas and de Rojas (2004) used a leaching method to estimate the free MgO content of EAF slags.

2.6.2 Mineralogical and Chemical Composition

The simplest and most common method for determining the mineralogical composition of a crystalline sample is by x-ray diffraction (XRD), in particular powder XRD. The European Standard EN 1744-1:2009+A1 (2013) provides some methodology for distinguishing CaO from $Ca(OH)_2$ in powdered SFS samples. All crystalline materials have a periodic spacing of atoms, the electrons of which scatter x-rays along certain crystallographic “planes” and the particular angles of scattering is more or less specific to a given crystalline compound (Kvick 2010). Therefore, XRD can be used to identify the mineralogical composition of SFS aggregates, as was exampled previously in Table 2. Quantitative XRD is possible, although accuracy levels of about 2-3% (by weight) are common, using internal/external standards, matrix flushing, the relative intensity ratio method, or the Rietveld method (Artioli 2010).

The chemical composition of SFS aggregates has been determined through numerous techniques, mainly x-ray fluorescence (XRF) and energy dispersive x-ray spectroscopy (EDX) (Gupta et al. 1994; Coomarasamy and Walzak 1995; Gumieri et al. 2004; Lun et al. 2008; Etxeberria et al. 2010; Iacobescu et al. 2011; Yildirim and Prezzi 2011; Belhadj et al. 2012; Qasrawi 2012; Mahieux et al. 2014; Pellegrino et al. 2013; Pellegrino and Faleschini 2013; San-José et al. (2013); Vlcek et al. 2013; Kim et al. 2014), but other studies have also used other methods, such as inductively coupled plasma atomic emission spectroscopy (Luxán et al. 2000; Rojas and de Rojas 2004; Xue et al. 2006; Faraone et al. 2009; Shen et al. 2009; Suer et al. 2009; Legret et al. 2010; Waligora et al. 2010), using an electron microprobe analyzer (Coomarasamy and Walzak 1995), and atomic absorption spectroscopy (Sersale et al. 1986b). While a number of other studies report the chemical composition of the tested SFS, description of the testing method for composition was not discussed.

The concept of XRF is that as photons are incident on a given atom, an electron from an inner orbital shell can be ejected, and in order for the atom to become stable again, an outer orbital electron is transferred to the vacancy in the inner orbital. Because there is an energy difference between the two shells, energy must be released, which is in the form of a photon, and this photon energy level, known as a characteristic x-ray, is specific to a given atom and shell transfer (Kramar 1999). This method can be used quantitatively because the peak intensity of a given characteristic energy is related to the concentration of that element. One type of XRF is known as energy dispersive x-ray spectroscopy (EDX), which refers to the method in which the energy dispersion and intensity is detected. An EDX system can commonly be found on

scanning electron microscopes (SEM), where characteristic x-rays are emitted by a sample as a result of the incident photon beam of high-energy electrons.

In atomic emission spectroscopy (AES), the elements in a given sample are excited by a plasma source, such as inductively coupled plasma (ICP). The excited atoms or ions emit light, which can then be detected to produce an emission spectrum. The wavelength of the emitted light is characteristic to a given element (Bonchin et al. 2010).

An electron probe analyzer works similarly to the previously discussed concepts. In this method, a focused beam of electrons is used to locally probe the surface of a sample to excite the atoms and obtain characteristic x-ray data. With this technique, regions as small as a few micrometers (or less) can be studied (Lifshin 2001).

With atomic absorption spectroscopy (AAS), a sample is atomized and a specific wavelength of light is introduced. Atoms will absorb the light in an amount proportional to the concentration of those atoms in the sample (Hill and Fisher 2010). However, AAS is only rapid when a few elements need to be determined, so it is perhaps not the best option for studying SFS.

2.6.3 Expansion Testing

Given the expansive nature of SFS, a number of test methods have been developed to further quantify the expansion potential. Because the expansion of SFS can be upwards of 10% (Emery 1982), it is very important to characterize the expansion of SFS as well as SFS FRAP.

European Standard EN 1744-1:2009+A1 (2013) provides a test method for the expansion of steel slag aggregates. In this method, the expansion of a compacted SFS sample subjected to 100°C steam is measured for either 24 or 168 hours, depending on the MgO content.

Pennsylvania Test Method (PTM) 130, which has since been redeveloped into ASTM D4792, specifies a test for the volumetric expansion of steel slag aggregates by submerging a compacted sample in water at 160°F for one week. Kandhal and Hoffman (1997) tested 10 steel slag aggregate sources for expansion by PTM 130 and found that sources that had been weathered outdoors for at least 6 months had negligible expansion (0.0-0.3%) while raw sources that had not been weathered had high expansions (1.1-2.8%). The results also indicated that coarser aggregates expand more than finer (passing #4 sieve) aggregates. Wang (1992) also tested compacted SFS samples in water at 165°F for upwards of 30 days but found that the expansion does not have a unique correlation with the SFS particle size. Wang et al. (2010) derived a theoretical expansion of SFS aggregates based on the specific gravity and free CaO content of the SFS, which was found to correlate well with the large expansion within the first 1-2 weeks of testing by ASTM D4792. A similar test method was proposed by Emery (1974), where a compacted sample was submerged in water at 180°F until the sample stopped swelling. The results indicated that typically one week was sufficient for the testing interval, because the expansion in 180°F water after 7 days was twice as much as the long-term expansion in 68°F water after 475 days (Emery 1977). However, gradation was found to have a significant impact on the expansion behavior (Emery 1974, 1977), so, for comparative testing, it was recommended that the gradation be controlled, although the gradation used for the aggregate application should also be tested (Emery 1974).

Cylindrical mortar specimens with OHF slag aggregates were measured for expansion by Crawford and Burn (1969). The results indicated that at 100°C and 100% relative humidity, the mortar with OHF linearly expanded rapidly to 3 to 5% elongation and then stopped after about 2 months. In contrast, mortar specimens with OHF slag aggregates cured at 15°C and 90% relative humidity continued expanding after 5 months at rates upwards of 3.5% per year.

Subjecting a sample to pressure and temperature, known as autoclaving, has also been used to characterize the expansion potential of SFS. Wang (1992) autoclaved loose aggregates at 357 kPa and 137°C for 50 minutes to check for unsoundness (i.e. disintegration, cracking). The Ohio Department of Transportation Supplement 1071 (ODOT 2008) lists that an autoclave disruption test is optional for SFS quality control requirements. Qian et al. (2002) also used an autoclave treatment at 2 and 5 MPa to observe the changes in mineralogy of finely powdered SFS and to measure the linear expansion of bars made with SFS and oil well cement. An autoclave test of mortar with SFS aggregate was conducted by Vázquezramonich and Barra (2001), but the authors concluded that the dimension of the mortar bar limited the maximum aggregate size too much to cause significant expansion. Mortar bars containing OHF slag were autoclaved (215°C and 300 psi for 3 hours) in a study by Crawford and Burn (1969), who found that some samples expanded linearly by around 10% while other specimens disintegrated.

Okamoto et al. (1981) autoclaved LD slag particles at different pressures and times to determine the degree of hydration, amount of disintegration, and percent volume expansion. The degree of hydration of the free CaO increased with increasing autoclaving times, increasing pressures, and decreasing particle size. The degree of disintegration varied with particle size, but there was no discernible trend. The reacted compounds of MgO and CaO, namely $Ca(OH)_2$, $Mg(OH)_2$, and $CaCO_3$, were all found to increase in increasing autoclaving pressures and times. The authors found that measuring the degree of hydration, amount of disintegration, or percent volume expansion were all useful in quantifying the expansion potential of LD slag, although the percent volume expansion measurement was the most sensitive. The findings also suggested that the hydration of MgO was slower than CaO. In one LD slag source, the CaO appeared to fully hydrate to $Ca(OH)_2$ after 24 hours under 43 psi and the MgO appeared to fully hydrate to $Mg(OH)_2$ after 24 hours under 426 psi. A regression analysis of 150 tests showed that the degree of hydration of the sample, based on the dry sample weight before and after autoclaving, was proportional to the pressure, treatment time, and free CaO content and inversely proportional to the particle size.

Autoclaving has also been performed on concrete samples (Vázquezramonich and Barra 2001), and it was found that some concretes with EAF slag aggregates expanded by more than double that of the reference control concrete while other EAF slag aggregate sources produced similar expansions to the reference. Wang (1992) autoclaved saw-cut discs of concrete with BOF aggregate for 100 minutes and found no distresses or disruptions. Kim et al. (2014) autoclaved mortar prisms and found that the mixture with rapidly cooled steel slag aggregate underwent less length change (i.e. expansion) than the mixture with natural sand.

Disintegration tests have also been used to characterize the expansion potential of SFS. The Indiana Test Method (ITM) 219 (ITM 2008) determines a content of deleterious material in SFS by heating a sample in an autoclave at 295 psi for 3 hours, and the deleterious content is defined as the ratio of the weight passing the #4 sieve after autoclaving to the weight retained on the #4 sieve before autoclaving. Heaton et al. (1996) described tests where the SFS particles

are placed in trays submerged in room-temperature water to observe the disintegration over time and found that the particle degradation is complete after 3 to 4 weeks, particularly for smaller particle sizes.

2.6.4 Permeability Testing

The volume stability of SFS has been found to be a function of the free CaO content and the porosity (Wachsmuth et al. 1981). Mercury porosimetry has been used to test the porosity of BOF slag aggregates (Okamoto et al. 1981; Wachsmuth et al. 1981; Xue et al. 2006), which were found to be more porous than limestone and basalt (Xue et al. 2006). A study of a blend of BOF and ladle furnace (LF) slags by nitrogen absorption-desorption revealed that there was an absence of microporosity in the slags, but that macropores were present, which were further investigated by mercury intrusion porosimetry (Navarro et al. 2010). The findings by Okamoto et al. (1981) suggest that the open pore volume of LD slag aggregates is related to the degree of hydration of free CaO. The porosity of RCA, which contained different aggregate types including blast furnace slag and limestone, has also been investigated using a helium pycnometer and an envelope density analyzer as well as image analysis (Deshpande and Hiller 2012).

The pore volume of aggregates can be thought of as two components: (1) the pores that are accessible from the surface and (2) the pores that are isolated from the surface by the surrounding solid (Winslow 1994). The aggregate properties that relate to porosity, such as water absorption capacity, are related to those pores that are accessible from the surface and are not a function of the isolated pores. The permeability of a porous medium is a function of the porosity and the pore volume of the medium, as related by the Kozeny equation.

2.7 CONCRETE WITH RAP/FRAP

A number of studies have investigated the properties and performance of concrete with RAP/FRAP as a partial replacement of virgin aggregate. In these studies, however, the base aggregate has been an inert or unreactive aggregate, such as limestone or river gravel. No study has reported the use of SFS FRAP in concrete.

Brand et al. (2012) recently summarized the findings from the studies of RAP/FRAP in concrete. The general trends of using concrete with RAP/FRAP are shown in Table 6. Overall, the literature findings suggest that the presence of RAP/FRAP in concrete will reduce the strength and stiffness of the concrete, although the durability and fracture properties may not be greatly affected.

Concrete pavements with RAP or FRAP have been constructed in the field. In France, roller-compacted concretes (RCC) with RAP have been tested, which have demonstrated favorable performance with accelerated pavement test sections (Bilodeau et al. 2011, 2012; Nguyen et al. 2012). Additional studies have shown that RCC with RAP can have suitable fracture properties (Sachet et al. 2011; Ferrebee et al. 2014). Two-lift concrete pavements have also been constructed with RAP in the bottom lift in Kansas (Wojakowski 1998) and Illinois (Gillen et al. 2012; Bentsen et al. 2013). Other two-lift test sections have contained a blend of both RAP and RCA in the bottom lift, which have been constructed in Iowa (Bergren and Britson 1977) and Austria (Sommer 1994).

Table 6. Effect of RAP/FRAP Aggregates on Concrete Properties Relative to Conventional Concrete (Updated from Brand et al. 2012)

Concrete Property	Effect on Property	References
Compressive strength	Decrease	Patankar and Williams 1970; Kolias 1996a; Delwar et al. 1997; Li et al. 1998; Sommer and Bohrn 1998; Dumitru et al. 1999; Hassan et al. 2000; Mathias et al. 2004; B. Huang et al. 2005, 2006; Katsakou and Kolias 2007; Hossiney et al. 2008, 2010; Al-Oraimi et al. 2009; Okafor 2010; Bilodeau et al. 2011; Bly and Weiss 2012; Berry et al. 2013; Brand and Roesler 2014; Brand et al. 2014; Erdem and Blankson 2014; Ibrahim et al. 2014; Su et al. 2014
Split tensile strength	Decrease	Patankar and Williams 1970; Kolias 1996a; Sommer and Bohrn 1998; Mathias et al. 2004; Katsakou and Kolias 2007; Hossiney et al. 2008, 2010; B. Huang et al. 2005, 2006; Bilodeau et al. 2011; Brand and Roesler 2014; Brand et al. 2014; Ibrahim et al. 2014; Su et al. 2014
Flexural strength	Decrease	Patankar and Williams 1970; Sommer 1994; Kolias 1996a; Li et al. 1998; Sommer and Bohrn 1998; Dumitru et al. 1999; Hassan et al. 2000; Katsakou and Kolias 2007; Hossiney et al. 2008, 2010; Al-Oraimi et al. 2009; Okafor 2010; Bly and Weiss 2012; Berry et al. 2013; Brand and Roesler 2014; Brand et al. 2014; Erdem and Blankson 2014
Direct tensile strength	Decrease	Patankar and Williams 1970; Katsakou and Kolias 2007
Indirect tensile strength	Decrease	Su et al. 2014
Modulus of elasticity	Decrease	Patankar and Williams 1970; Kolias 1996a, 1996b; Delwar et al. 1997; Sommer and Bohrn 1998; Dumitru et al. 1999; Mathias et al. 2004; B. Huang et al. 2006; Katsakou and Kolias 2007; Hossiney et al. 2008, 2010; Al-Oraimi et al. 2009; Bilodeau et al. 2011; Berry et al. 2013; Brand and Roesler 2014; Brand et al. 2014; Erdem and Blankson 2014; Su et al. 2014
Complex stiffness modulus	Decrease	Kolias 1996b; Bilodeau et al. 2011; Brand and Roesler 2014
Resilient modulus	Decrease	Li et al. 1998
Free shrinkage	Increase	Dumitru et al. 1999
	Decrease	Hossiney et al. 2008
	Variable*	Hossiney et al. 2010; Ibrahim et al. 2014
	No Effect	Sommer 1994; Brand and Roesler 2014
Creep strains	Increase	Kolias 1996a
Coefficient of thermal expansion	Variable*	Hossiney et al. 2008, 2010
Toughness	Increase	B. Huang et al. 2005, 2006; Su et al. 2014
Fatigue properties	Reduce	Mathias et al. 2004
	Improve	Li et al. 1998
Fracture properties	Similar	Brand and Roesler 2014; Brand et al. 2014
Porosity	Increase	Hassan et al. 2000
Oxygen permeability	Increase	Hassan et al. 2000
Surface absorption	No Effect	Al-Oraimi et al. 2009
Frost resistance	Decrease	Sommer 1994; Sommer and Bohrn 1998
Freeze/Thaw durability	Suitable	Brand and Roesler 2014
Rapid chloride penetrability	Similar	Brand and Roesler 2014
Poisson Ratio	Variable*	Su et al. 2014

*Variable = no clear trend

CHAPTER 3 AGGREGATE PROPERTIES OF SFS AND SFS FRAP

In this study, three SFS FRAP and three virgin SFS aggregate sources were evaluated for comparison of the properties and chemical and mineralogical composition. Only one of the SFS FRAP sources was then evaluated for its effect on numerous concrete properties, but all SFS FRAP sources were tested for strength. Two of the virgin SFS sources were also tested for their effect on the concrete properties.

Details of the three SFS FRAP sources can be found in Table 7. All three of the SFS FRAP aggregates were sourced from asphalt concrete pavements that had total aggregate contents roughly consisting of one-third SFS aggregate, one-third dolomitic coarse aggregate, and one-third crushed stone fine aggregate. The SFS aggregates in these pavements were sourced from plants in northwest Indiana, and all three sources were likely BOF slag. The original performance grade (PG) of the asphalt for all three mixes was PG 76-22.

Table 7. SFS FRAP Sources and Testing Regimen

	SFS FRAP 1	SFS FRAP 2	SFS FRAP 3
SFS FRAP Production Source	Curran Contracting (DeKalb, IL)	Geneva Construction	Central Blacktop
Year of Placement	2001	1997	2001
Year of Milling	2012	2008*	2012
SFS Aggregate Source	Multiserv (East Chicago, Indiana)	Heckett-LTV (northwest Indiana)	Heritage Slag/ Beemsterboer Slag (Gary, Indiana)
Design Asphalt Content	5.6%	5.4%	5.4%
SFS Content in Original HMA Mix	33%	32-33%	35%

*Aggregate was stockpiled after milling

A total of three virgin SFS sources were evaluated. The sources of the virgin SFS aggregates are shown in Table 8. One of the sources is from a ladle metallurgy furnace (LMF) process, which is a modified EAF process. It was requested from Edw. C. Levy (Virgin SFS 2 and 3) that one source be of high expansion potential and the other low expansion.

Table 8. Virgin SFS Sources and Testing Regimen

	Virgin SFS 1	Virgin SFS 2	Virgin SFS 3
Virgin SFS Source	Beemsterboer Slag (Gary, IN)	Edw. C. Levy, Butler Mill Service (Butler, IN)	Edw. C. Levy, Charleston Mill Service (Huger, SC)
SFS Type	BOF	EAF	EAF/LMF
Product Specification	IDOT CM 13, CM 14	QA 11	Pea Gravel

3.1 AGGREGATE PHYSICAL PROPERTIES

The coarse aggregate physical properties that were tested for each of the three SFS FRAP and three virgin SFS sources and the corresponding standard are shown in Table 9. Three replicates of each test were performed per source, except for the asphalt content and characterization tests, in which only one or two replicates were performed.

Table 9. Coarse Aggregate Properties Tested

Test	Standard
Gradation	ASTM C136 (2006)
Unit Weight (Rodding Method)	ASTM C29 (2009)
Specific Gravity and Absorption	ASTM C127 (2007)
Asphalt Content and Characterization	AASHTO T164 (2011); AASHTO T313 (2010); AASHTO T315 (2010); ASTM D5404 (2011); ASTM D6847 (2002)

3.1.1 SFS FRAP Physical Properties

The results for the aggregate properties are shown in Table 10 (SFS FRAP 1), Table 11 (SFS FRAP 2), and Table 12 (SFS FRAP 3). Table 13 compares the SFS FRAP properties with previous FRAP studies with Figure 5 comparing the various FRAP sources gradations. SFS FRAP has slightly higher specific gravities and absorption relative to dolomite FRAP. The higher absorption capacity of the SFS FRAP aggregates is caused by the SFS aggregate, which can have a higher absorption capacity relative to dolomite. The original pavements only contained about one-third SFS aggregate, so the SFS FRAP aggregate should have slightly higher specific gravities with the presence of the SFS aggregate. From Table 13, the SFS FRAP sources still have a significant amount of material passing the #4 (4.75 mm) sieve. In particular, SFS FRAP 3 has a high amount passing the #4 sieve, which is probably why the bulk unit weight is higher than the other FRAP sources.

Table 10. SFS FRAP 1 (Curran Contracting) Aggregate Properties

		Test 1	Test 2	Test 3	Average
Relative SG (OD)		2.63	2.65	2.63	2.63
Relative SG (SSD)		2.68	2.70	2.68	2.69
Apparent SG		2.77	2.79	2.78	2.78
Absorption (%)		1.96	2.02	2.01	2.00
Bulk Unit Weight (lb/ft^3)		96.0	96.5	97.0	96.5
Asphalt Content (%)		3.5	3.6	--	3.6
Gradation					
Sieve Size		Cumulative Percent Passing			
3/4 in	19mm	100.0%	100.0%	100.0%	100.0%
5/8 in	16mm	100.0%	100.0%	100.0%	100.0%
1/2 in	12.5mm	99.8%	99.9%	99.8%	99.9%
3/8 in	9.5mm	83.1%	83.6%	84.3%	83.7%
1/4 in	6.35mm	37.9%	38.1%	38.8%	38.3%
#4	4.75mm	13.2%	13.5%	13.3%	13.3%
#8	2.36mm	4.1%	4.2%	3.5%	3.9%
#16	1.18mm	3.1%	3.1%	2.4%	2.8%
#30	0.6mm	2.7%	2.7%	2.1%	2.5%
#50	0.3mm	2.3%	2.3%	1.9%	2.2%
#100	0.15mm	1.7%	1.7%	1.6%	1.7%
#200	0.075mm	0.9%	0.7%	0.8%	0.8%

Table 11. SFS FRAP 2 (Geneva Construction) Aggregate Properties

		Test 1	Test 2	Test 3	Average
Relative SG (OD)		2.50	2.51	2.51	2.51
Relative SG (SSD)		2.59	2.59	2.60	2.59
Apparent SG		2.74	2.74	2.75	2.74
Absorption (%)		3.53	3.41	3.40	3.44
Bulk Unit Weight (lb/ft^3)		96.5	96.0	96.5	96.4
Asphalt Content (%)		3.5	4.1	--	3.8
Gradation					
Sieve Size		Cumulative Percent Passing			
3/4 in	19mm	100.0%	100.0%	100.0%	100.0%
5/8 in	16mm	99.9%	99.7%	99.9%	99.9%
1/2 in	12.5mm	97.6%	97.6%	98.4%	97.9%
3/8 in	9.5mm	83.5%	83.8%	83.0%	83.4%
1/4 in	6.35mm	40.6%	39.7%	39.1%	39.8%
#4	4.75mm	15.2%	14.4%	13.8%	14.5%
#8	2.36mm	7.5%	6.9%	6.4%	6.9%
#16	1.18mm	6.6%	6.1%	5.7%	6.1%
#30	0.6mm	6.1%	5.6%	5.3%	5.7%
#50	0.3mm	4.7%	4.4%	4.3%	4.4%
#100	0.15mm	2.8%	2.7%	2.7%	2.7%
#200	0.075mm	0.7%	0.6%	0.5%	0.6%

Table 12. SFS FRAP 3 (Central Blacktop) Aggregate Properties

		Test 1	Test 2	Test 3	Average
Relative SG (OD)		2.63	2.63	2.63	2.63
Relative SG (SSD)		2.70	2.70	2.70	2.70
Apparent SG		2.82	2.82	2.83	2.83
Absorption (%)		2.64	2.59	2.72	2.65
Bulk Unit Weight (lb/ft^3)		100.9	100.9	101.4	101.1
Asphalt Content (%)		3.8	3.9	--	3.9
Gradation					
Sieve Size		Cumulative Percent Passing			
3/4 in	19mm	100.0%	100.0%	100.0%	100.0%
5/8 in	16mm	100.0%	100.0%	100.0%	100.0%
1/2 in	12.5mm	99.5%	99.1%	99.1%	99.3%
3/8 in	9.5mm	89.4%	87.6%	87.9%	88.3%
1/4 in	6.35mm	59.2%	61.0%	60.3%	60.2%
#4	4.75mm	38.9%	40.2%	39.6%	39.6%
#8	2.36mm	12.2%	12.5%	12.0%	12.2%
#16	1.18mm	6.5%	6.7%	6.3%	6.5%
#30	0.6mm	5.2%	5.4%	5.0%	5.2%
#50	0.3mm	4.1%	4.4%	4.1%	4.2%
#100	0.15mm	2.2%	2.2%	2.3%	2.3%
#200	0.075mm	0.4%	0.4%	0.4%	0.4%

Table 13. Comparison of SFS FRAP and Dolomite FRAP Aggregate Properties

		SFS FRAP 1	SFS FRAP 2	SFS FRAP 3	Clean FRAP*	Unwashed Dirty FRAP*	Washed Dirty FRAP*	FRAP**
Relative SG (OD)		2.63	2.51	2.63	2.53	2.52	--	2.50
Relative SG (SSD)		2.69	2.59	2.70	2.59	2.56	--	2.54
Apparent SG		2.78	2.74	2.83	2.70	2.64	--	2.62
Absorption (%)		2.00	3.44	2.65	2.45	1.79	--	1.96
Bulk Unit Weight (lb/ft^3)		96.5	96.4	101.1	93.4	90.1	--	94.8
Asphalt Content (%)		3.6	3.8	3.9	2.14	3.26	--	3.76
Gradation (Cumulative Percent Passing)								
Sieve Size		SFS FRAP 1	SFS FRAP 2	SFS FRAP 3	Clean FRAP*	Unwashed Dirty FRAP*	Washed Dirty FRAP*	FRAP**
1 in	25mm	100.0%	100.0%	100.0%	100.0%	100.0%	100.0%	100.0%
3/4 in	19mm	100.0%	100.0%	100.0%	99.9%	100.0%	100.0%	100.0%
5/8 in	16mm	100.0%	99.9%	100.0%	--	--	--	100.0%
1/2 in	12.5mm	99.9%	97.9%	99.3%	78.4%	99.3%	99.4%	65.0%
3/8 in	9.5mm	83.7%	83.4%	88.3%	37.9%	86.3%	82.7%	25.2%
1/4 in	6.35mm	38.3%	39.8%	60.2%	--	--	--	14.5%
#4	4.75mm	13.3%	14.5%	39.6%	3.6%	21.9%	4.5%	8.3%
#8	2.36mm	3.9%	6.9%	12.2%	1.6%	5.5%	0.2%	3.0%
#16	1.18mm	2.8%	6.1%	6.5%	1.1%	2.8%	0.1%	1.5%
#30	0.6mm	2.5%	5.7%	5.2%	0.8%	1.9%	0.1%	1.0%
#50	0.3mm	2.2%	4.4%	4.2%	0.6%	1.3%	0.1%	0.7%
#100	0.15mm	1.7%	2.7%	2.3%	0.3%	0.7%	0.1%	0.3%
#200	0.075mm	0.8%	0.6%	0.4%	0.1%	0.3%	0.0%	0.1%

*Source: Brand et al. (2012); **source: Brand et al. (2013)

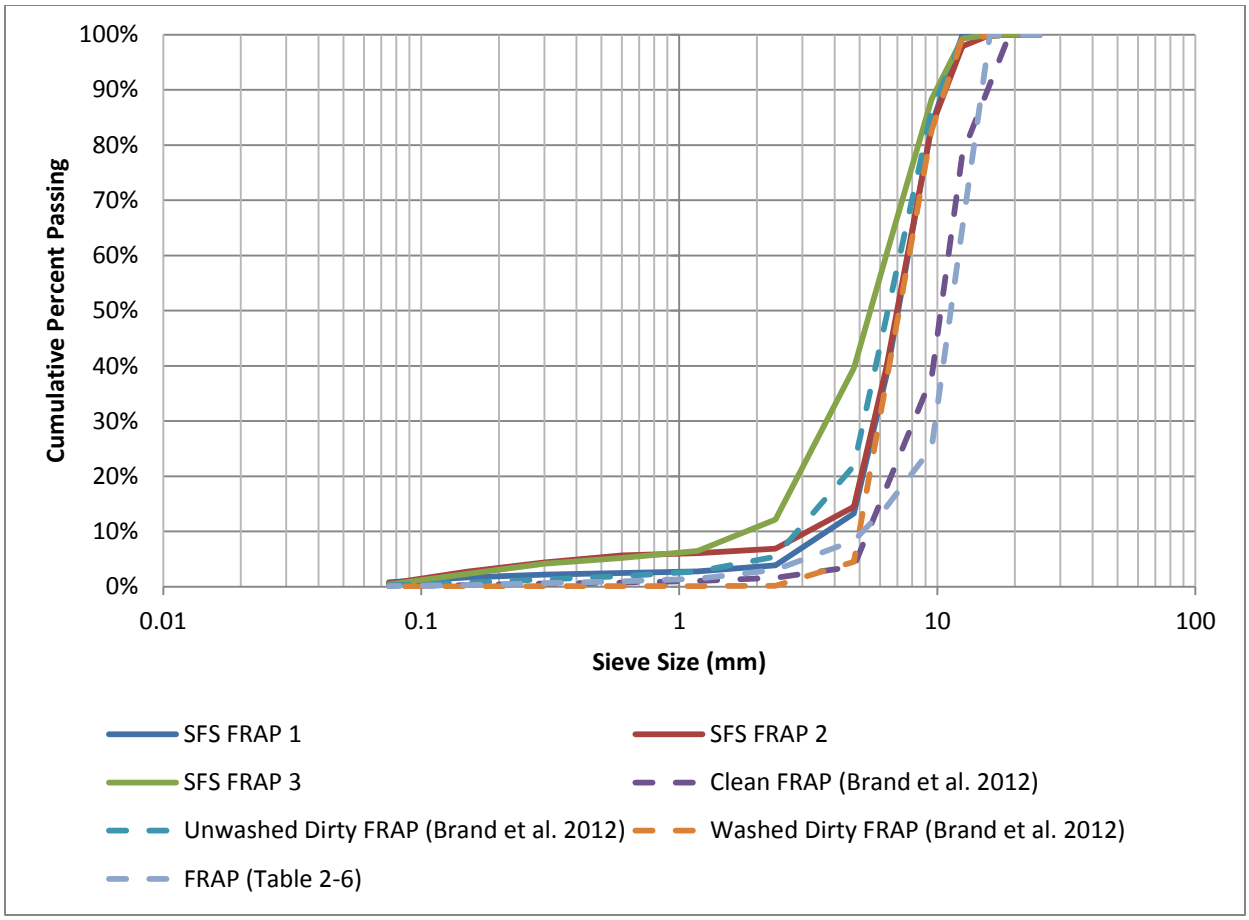

Figure 5. Gradation comparisons between various SFS and dolomite FRAP sources.

3.1.2 Virgin SFS Aggregate Physical Properties

For the virgin SFS aggregates, the unit weights, specific gravities, and gradations are shown in Table 14 (Virgin SFS 1), Table 15 (Virgin SFS 2), and Table 16 (Virgin SFS 3). As expected, the specific gravities are higher than virgin dolomite aggregates (Table 17), given the composition of SFS aggregates contains heavier elements, such as iron. In general, the specific gravity of SFS aggregates can be around 3.2 to 3.5 (Emery 1982). Overall, it appears that the BOF slag has a higher absorption but lower specific gravity than the two EAF slags.

Table 14. Virgin SFS 1 (BOF) Aggregate Properties

		Test 1	Test 2	Test 3	Average
Relative SG (OD)		3.27	3.25	3.26	3.26
Relative SG (SSD)		3.34	3.32	3.33	3.33
Apparent SG		3.53	3.52	3.52	3.52
Absorption (%)		2.32	2.36	2.26	2.31
Bulk Unit Weight (lb/ft^3)		127.7	128.2	127.7	127.9
Gradation					
Sieve Size		Cumulative Percent Passing			
3/4 in	19mm	100.0%	100.0%	100.0%	100.0%
5/8 in	16mm	100.0%	99.9%	99.9%	99.9%
1/2 in	12.5mm	89.5%	89.2%	89.3%	89.4%
3/8 in	9.5mm	52.8%	54.0%	49.9%	52.2%
1/4 in	6.35mm	10.8%	16.2%	8.9%	12.0%
#4	4.75mm	5.9%	10.9%	4.7%	7.2%
#8	2.36mm	4.3%	8.7%	3.4%	5.5%
#16	1.18mm	3.9%	7.7%	3.1%	4.9%
#30	0.6mm	3.6%	6.3%	2.8%	4.2%
#50	0.3mm	2.9%	4.5%	2.3%	3.2%
#100	0.15mm	1.9%	2.4%	1.7%	2.0%
#200	0.075mm	0.6%	0.7%	0.6%	0.6%

Table 15. Virgin SFS 2 (EAF) Aggregate Properties

		Test 1	Test 2	Test 3	Average
Relative SG (OD)		3.65	3.63	3.64	3.64
Relative SG (SSD)		3.72	3.70	3.70	3.70
Apparent SG		3.91	3.88	3.88	3.89
Absorption (%)		1.79	1.77	1.69	1.75
Bulk Unit Weight (lb/ft^3)		130.2	130.6	131.1	130.6
Gradation					
Sieve Size		Cumulative Percent Passing			
3/4 in	19mm	100.0%	100.0%	100.0%	100.0%
5/8 in	16mm	100.0%	100.0%	100.0%	100.0%
1/2 in	12.5mm	99.9%	99.8%	99.8%	99.9%
3/8 in	9.5mm	83.0%	83.3%	83.6%	83.3%
1/4 in	6.35mm	47.1%	43.8%	45.0%	45.3%
#4	4.75mm	25.0%	23.1%	24.2%	24.1%
#8	2.36mm	4.8%	4.5%	4.8%	4.7%
#16	1.18mm	2.3%	2.1%	2.2%	2.2%
#30	0.6mm	1.9%	1.8%	1.9%	1.9%
#50	0.3mm	1.7%	1.5%	1.6%	1.6%
#100	0.15mm	1.3%	1.2%	1.3%	1.3%
#200	0.075mm	0.9%	0.9%	0.9%	0.9%

Table 16. Virgin SFS 3 (EAF/LMF) Aggregate Properties

		Test 1	Test 2	Test 3	Average
Relative SG (OD)		3.47	3.43	3.46	3.45
Relative SG (SSD)		3.53	3.49	3.52	3.51
Apparent SG		3.69	3.66	3.67	3.68
Absorption (%)		1.71	1.86	1.65	1.74
Bulk Unit Weight (lb/ft^3)		123.8	123.3	123.3	123.5
Gradation					
Sieve Size		Cumulative Percent Passing			
3/4 in	19mm	100.0%	100.0%	100.0%	100.0%
5/8 in	16mm	100.0%	100.0%	100.0%	100.0%
1/2 in	12.5mm	96.5%	96.2%	96.4%	96.3%
3/8 in	9.5mm	73.6%	75.7%	72.1%	73.8%
1/4 in	6.35mm	30.7%	29.4%	24.3%	28.2%
#4	4.75mm	13.0%	11.4%	4.8%	9.7%
#8	2.36mm	3.1%	2.8%	3.6%	3.2%
#16	1.18mm	2.8%	2.5%	3.2%	2.9%
#30	0.6mm	2.7%	2.4%	3.1%	2.7%
#50	0.3mm	2.2%	1.9%	2.5%	2.2%
#100	0.15mm	1.4%	1.3%	1.5%	1.4%
#200	0.075mm	0.6%	0.6%	0.6%	0.6%

Table 17. Comparison of Virgin SFS with Virgin Dolomite and SFS FRAP Aggregate Properties

		Virgin SFS 1 (BOF)	Virgin SFS 2 (EAF)	Virgin SFS 3 (EAF/ LMF)	Virgin Dolomite*	SFS FRAP 1	SFS FRAP 2	SFS FRAP 3
Relative SG (OD)		3.26	3.64	3.45	2.67	2.63	2.51	2.63
Relative SG (SSD)		3.33	3.70	3.51	2.72	2.69	2.59	2.70
Apparent SG		3.52	3.89	3.68	2.81	2.78	2.74	2.83
Absorption (%)		2.31	1.75	1.74	1.80	2.00	3.44	2.65
Bulk Unit Weight (lb/ft^3)		127.9	130.6	123.5	96.9	96.5	96.4	101.1
Gradation (Cumulative Percent Passing)								
Sieve Size		Virgin SFS 1	Virgin SFS 2	Virgin SFS 3	Virgin Dolomite*	SFS FRAP 1	SFS FRAP 2	SFS FRAP 3
1 in	25mm	100.0%	100.0%	100.0%	100.0%	100.0%	100.0%	100.0%
3/4 in	19mm	100.0%	100.0%	100.0%	96.2%	100.0%	100.0%	100.0%
5/8 in	16mm	99.9%	100.0%	100.0%	--	100.0%	99.9%	100.0%
1/2 in	12.5mm	89.4%	99.9%	96.3%	36.5%	99.9%	97.9%	99.3%
3/8 in	9.5mm	52.2%	83.3%	73.8%	11.1%	83.7%	83.4%	88.3%
1/4 in	6.35mm	12.0%	45.3%	28.2%	--	38.3%	39.8%	60.2%
#4	4.75mm	7.2%	24.1%	9.7%	1.3%	13.3%	14.5%	39.6%
#8	2.36mm	5.5%	4.7%	3.2%	1.1%	3.9%	6.9%	12.2%
#16	1.18mm	4.9%	2.2%	2.9%	1.1%	2.8%	6.1%	6.5%
#30	0.6mm	4.2%	1.9%	2.7%	1.1%	2.5%	5.7%	5.2%
#50	0.3mm	3.2%	1.6%	2.2%	1.0%	2.2%	4.4%	4.2%
#100	0.15mm	2.0%	1.3%	1.4%	0.9%	1.7%	2.7%	2.3%
#200	0.075mm	0.6%	0.9%	0.6%	0.7%	0.8%	0.6%	0.4%

*Source: Brand and Roesler (2014)

3.2 SFS FRAP ASPHALT CHARACTERIZATION

To obtain a sufficient quantity of asphalt needed for characterization, only one test was conducted using a quantity of asphalt binder from numerous extractions. The original grade of the asphalt used in the pavement from which the SFS FRAP was obtained was PG 76-22. The grades of the extracted asphalt are shown in Table 18. Previous results suggested that the low temperature grade of the extracted FRAP does not change (Brand et al. 2012), so only the low temperature grade of SFS FRAP 3 was tested. In fact, only SFS FRAP 3 was the only FRAP source that experienced a change in the high-temperature performance grade, i.e., PG 82-22 versus the original PG 76-22.

Table 18. Performance Grade of the Extracted SFS FRAP Asphalt

Sample	Original Performance Grade	Performance Grade of the Extracted Asphalt*
SFS FRAP 1 (Curran)	PG 76-22	PG 76
SFS FRAP 2 (Geneva)	PG 76-22	PG 76
SFS FRAP 3 (Central Blacktop)	PG 76-22	PG 82-22

*Low temperature grade only determined for SFS FRAP 3

3.3 MINERALOGICAL COMPOSITION

The virgin SFS and SFS FRAP aggregates with binder removed were crushed (powdered) and the particles passing the #100 sieve (≤150 μm) and the #325 sieve (≤44 μm) were collected for powder XRD; this ensured that a representative mineralogical sample was obtained from the stockpile since all aggregate sizes were crushed. A Siemens-Bruker D5000 XRD was used, which utilizes copper (Cu) Kα radiation and has a graphite monochromator and a scintillation detector. The machine was operated at 40 kV and 30 mA. The sample size was 0.5 cm^3. The scan range was from 10° to 80° with an increment of 0.02° and a scan speed of 0.5 degrees per minute.

The identified phases for virgin SFS are summarized in Table 19 with individual scans shown in Figure 6 to Figure 12. Comparing the SFS compositions with those from other studies (previously shown in Table 2) generally suggests they are similar to other published SFS. However, many of the peaks of the identified phases overlap, which indicates that steel slag is a multi-phase material with numerous impure phases that can have interstitial elements, which skews the peak location and makes it difficult to definitively identify the phases. Wüstite and larnite were the most prevalently identified phases in the SFS. The other phases that were identified, while potentially present in the sample, were not as definitively identified by the analysis software.

Evidence of carbonation was noted in the first scan of the virgin SFS 1 (BOF) sample (Figure 6), so a second scan was performed (Figure 7), which indicated evidence of free CaO that was instead identified in the carbonated calcite form in the first scan. All phases identified for Virgin SFS 1 (BOF) were in agreement with previous literature, with the exception of the magnesioferrite phase, which is not a commonly-identified phase for BOF SFS. However, this phase appeared to fit the XRD pattern better than the other potential phases.

The phases identified for Virgin SFS 2 (EAF) matched rather well with the commonly identified phases in the literature for EAF SFS. Only three phases were identified for Virgin SFS 3 (EAF/LMF), which were commonly identified phases for EAF SFS. However, it can be noted that XRD patterns for Virgin SFS 3 (EAF/LMF) contain relatively fewer peaks and is less noisy than the XRD patterns for the other virgin SFS samples, so it is possible that virgin SFS 3 (EAF/LMF) does not have as many mineralogical phases.

The presence of CaO was only detected in Virgin SFS 1 (BOF), which is the free CaO in the slag. As shown later in Section 3.5, Virgin SFS 1 (BOF) had the highest measured free CaO content of the virgin SFS samples. The free CaO contents in the other SFS samples were likely too low to be detected by XRD. None of the virgin SFS samples had detectable periclase (MgO), which suggests the following: 1) the MgO in the samples is assimilated into other phases (i.e. magnesioferrite, bredigite) and is not in an unassimilated “free” state for reaction and/or 2) the “free” MgO amount is low enough that it is not detectable by XRD.

The identified phases for SFS FRAP (with asphalt binder removed) are summarized in Table 19 and shown in individual scans in Figure 13 to Figure 18. Dolomite was predominantly identified, with some additional evidence of calcite and quartz (likely from the virgin aggregates in the original aggregate blend) with wüstite potentially identified in the smaller peaks. The sample was mainly dolomite aggregate and therefore it was expected that XRD would mainly identify the dolomitic phases. In order to better identify the phases present in the SFS from the SFS FRAP, the samples were visually separated into the natural and SFS aggregate types and

then the SFS was crushed and scanned separately. The SFS particles were taken from the FRAP samples that were used to determine the asphalt content and/or from the methylene chloride extractions to prepare the autoclave samples. The identified phases were similar from all three FRAP samples, and the identified phases confirmed that the SFS in the FRAP was BOF slag, mainly because of the presence of srebrodolskite ($Ca_2Fe_2O_5$), which is predominantly found in BOF slag (see literature summary shown in Table 2). The free CaO content was apparently high enough to be identified in SFS FRAP 1 and 2 but not SFS FRAP 3.

Table 19. Identified Mineralogical Phases Present in the SFS FRAP and Virgin SFS Samples

Phase	SFS FRAP 1	SFS FRAP 2	SFS FRAP 3	Virgin SFS 1 (BOF)	Virgin SFS 2 (EAF)	Virgin SFS 3 (EAF/LMF)	Virgin Coarse Aggregate*	Virgin Fine Aggregate (Natural Sand)*
Dolomite ($CaMg(CO_3)_2$)	X	X	X				X	X
Quartz (SiO_2)	X	X	X					X
Larnite, Dicalcium Silicate (Ca_2SiO_4)	X	X	X	X	X	X		
Tricalcium Silicate (Ca_3SiO_5)				X				
Calcium Oxide (CaO)	X	X		X				
Calcite ($CaCO_3$)		X	X	X				
Wüstite (FeO)	X	X	X	X	X	X		
Magnetite (Fe_3O_4)					X			
Magnesioferrite ($MgFe_2O_4$)				X				
Bredigite ($Ca_7Mg(SiO_4)_4$)					X			
Srebrodolskite ($Ca_2Fe_2O_5$)	X	X	X	X				
Mayenite ($Ca_{12}Al_{14}O_{33}$)					X	X		

*Source: Brand et al. (2012)

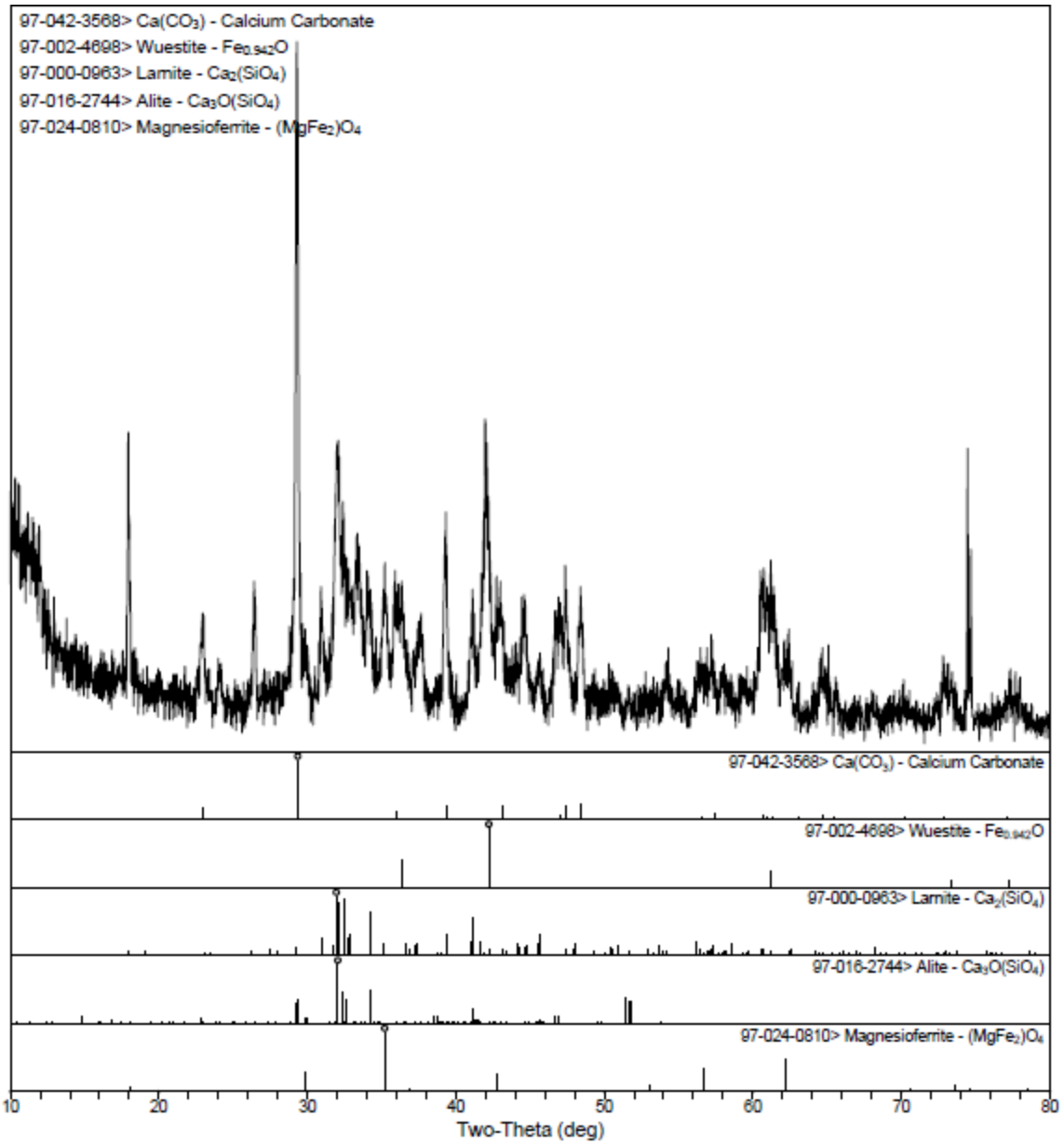

Figure 6. XRD scan and identified phases for Virgin SFS 1 (BOF), ≤150 µm particle size.

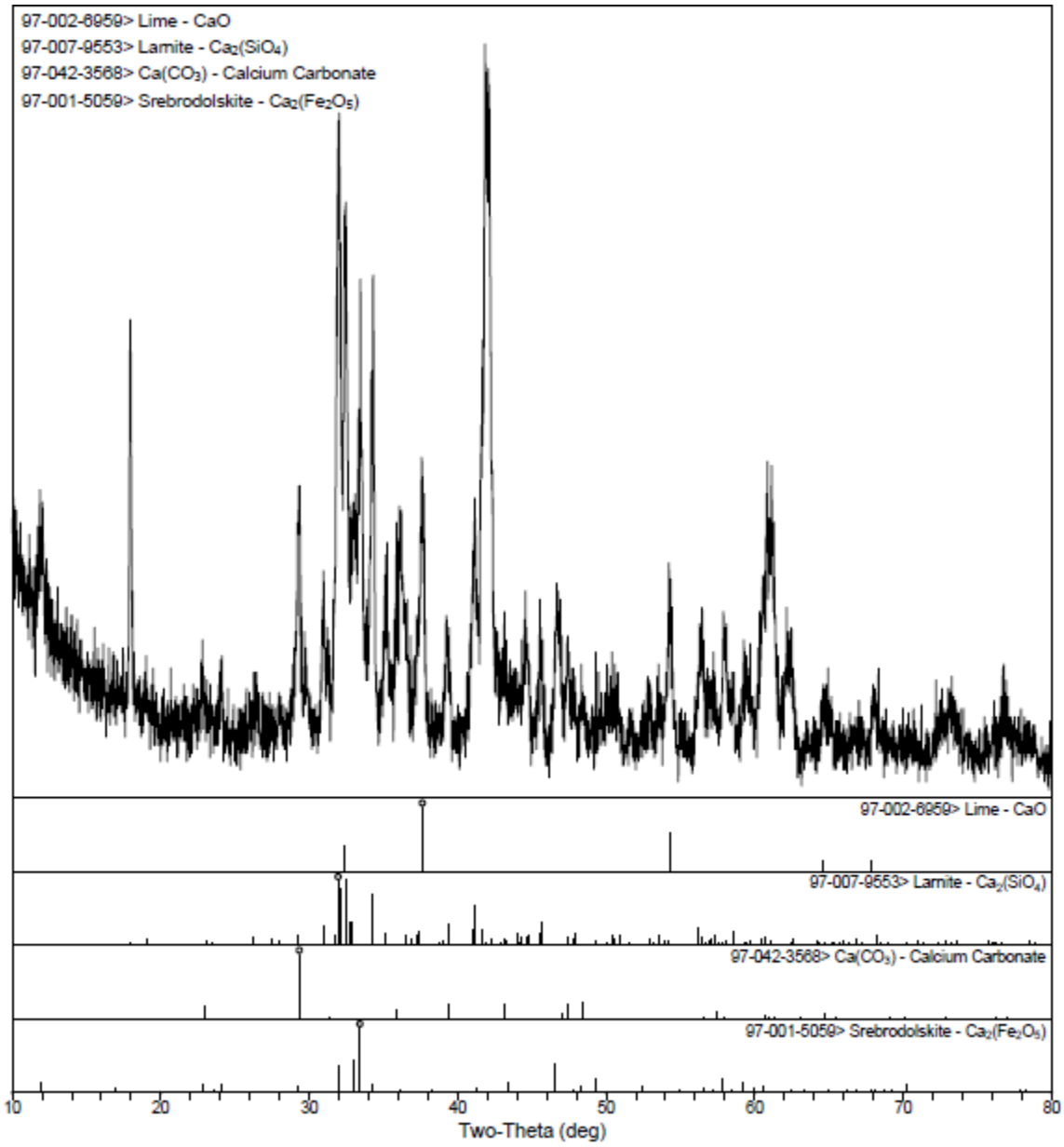

Figure 7. Second XRD scan and identified phases for Virgin SFS 1 (BOF), ≤150 µm particle size.

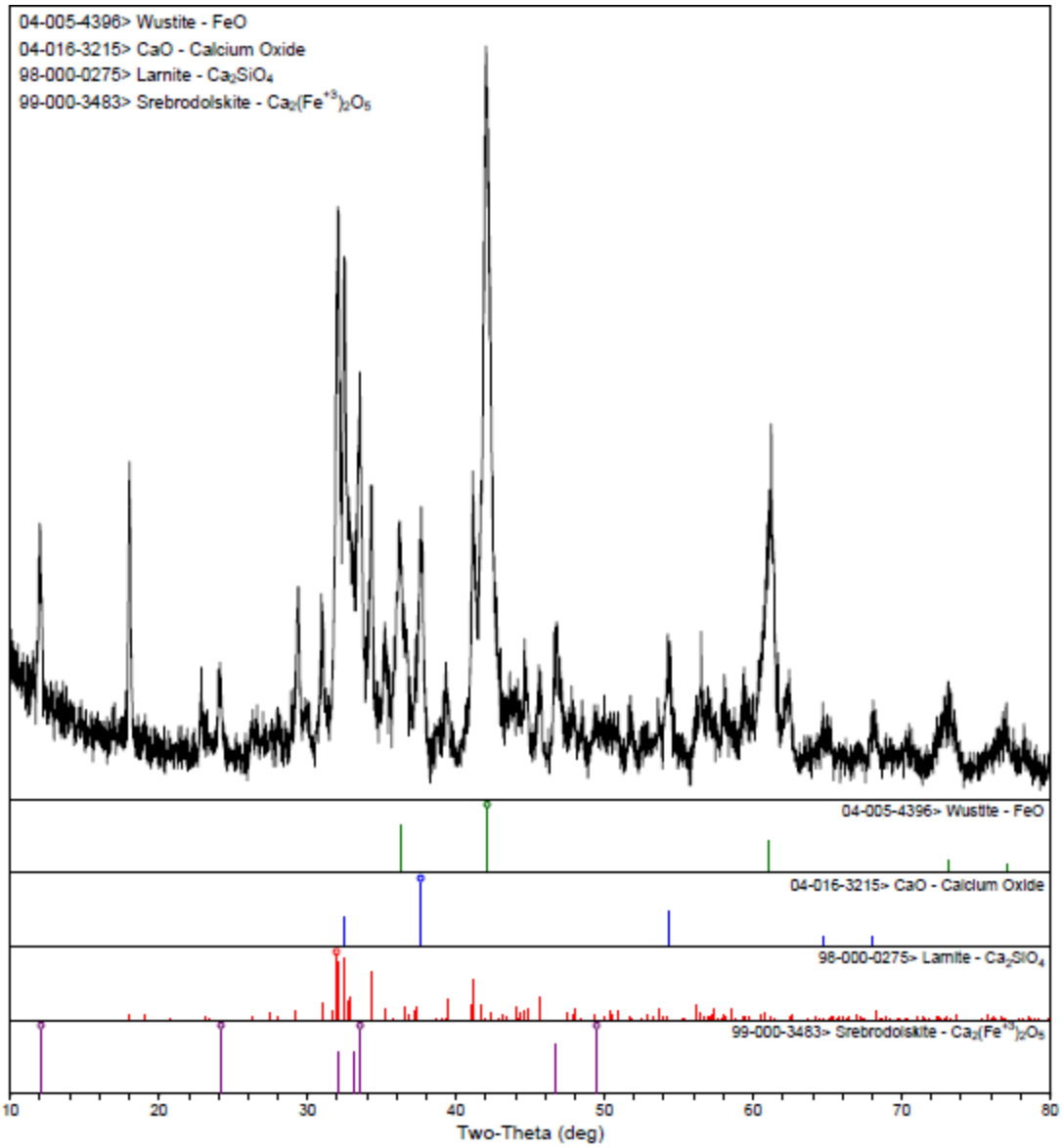

Figure 8. XRD scan and identified phases for Virgin SFS 1 (BOF), ≤44 µm particle size.

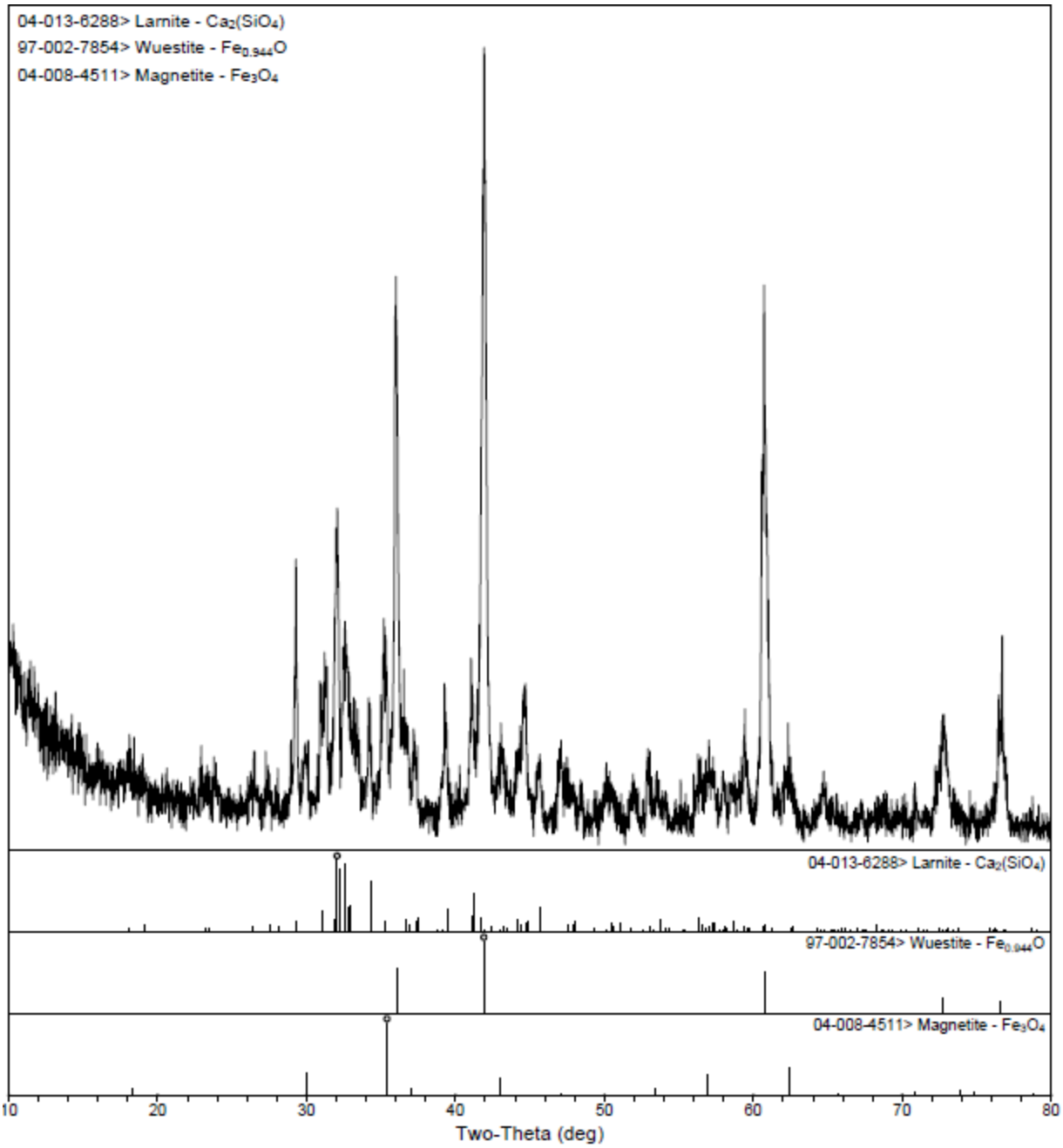

Figure 9. XRD scan and identified phases for Virgin SFS 2 (EAF), ≤150 µm particle size.

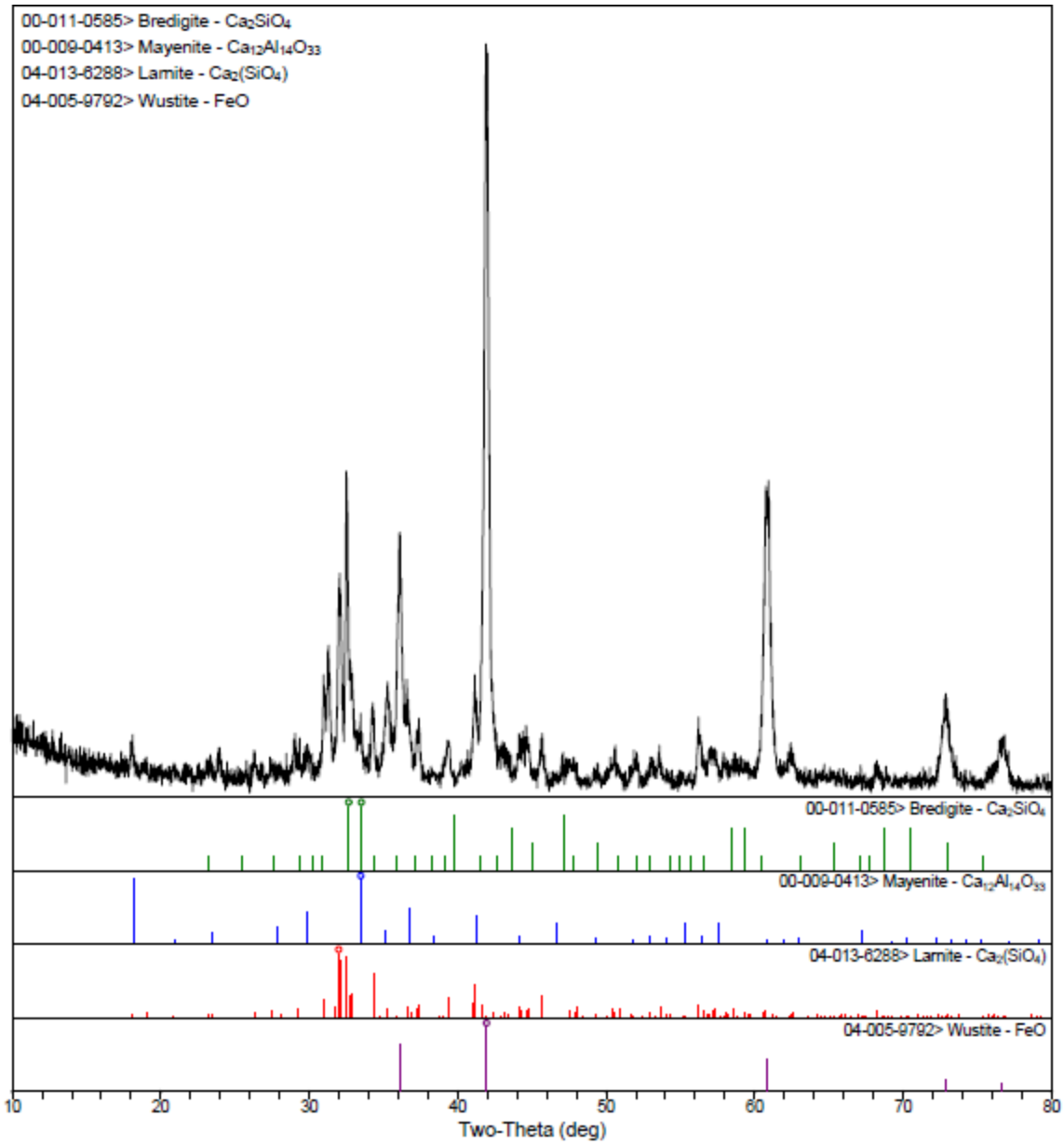

Figure 10. XRD scan and identified phases for Virgin SFS 2 (EAF), ≤44 µm particle size.

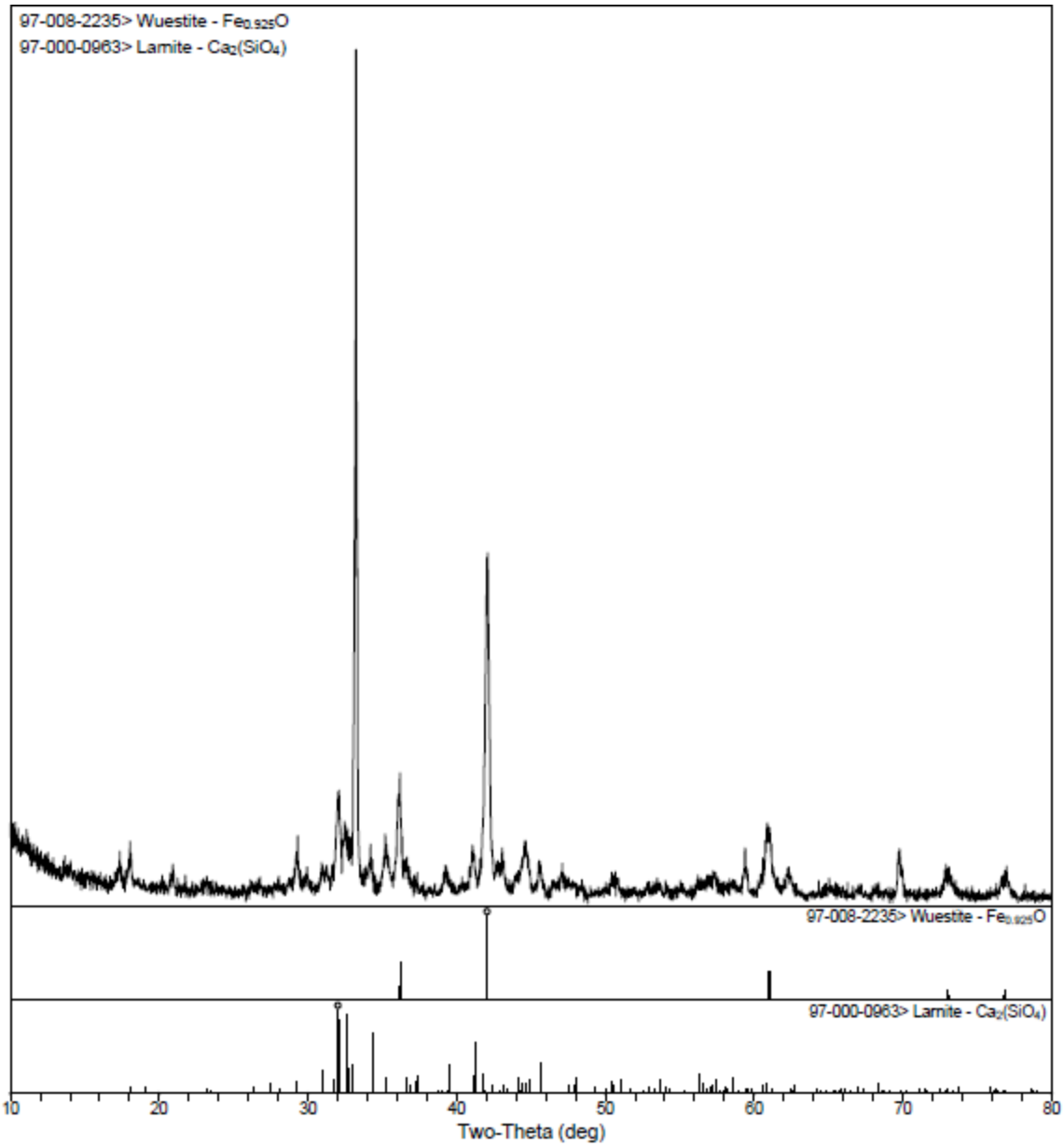

Figure 11. XRD scan and identified phases for Virgin SFS 3 (EAF/LMF), ≤150 µm particle size.

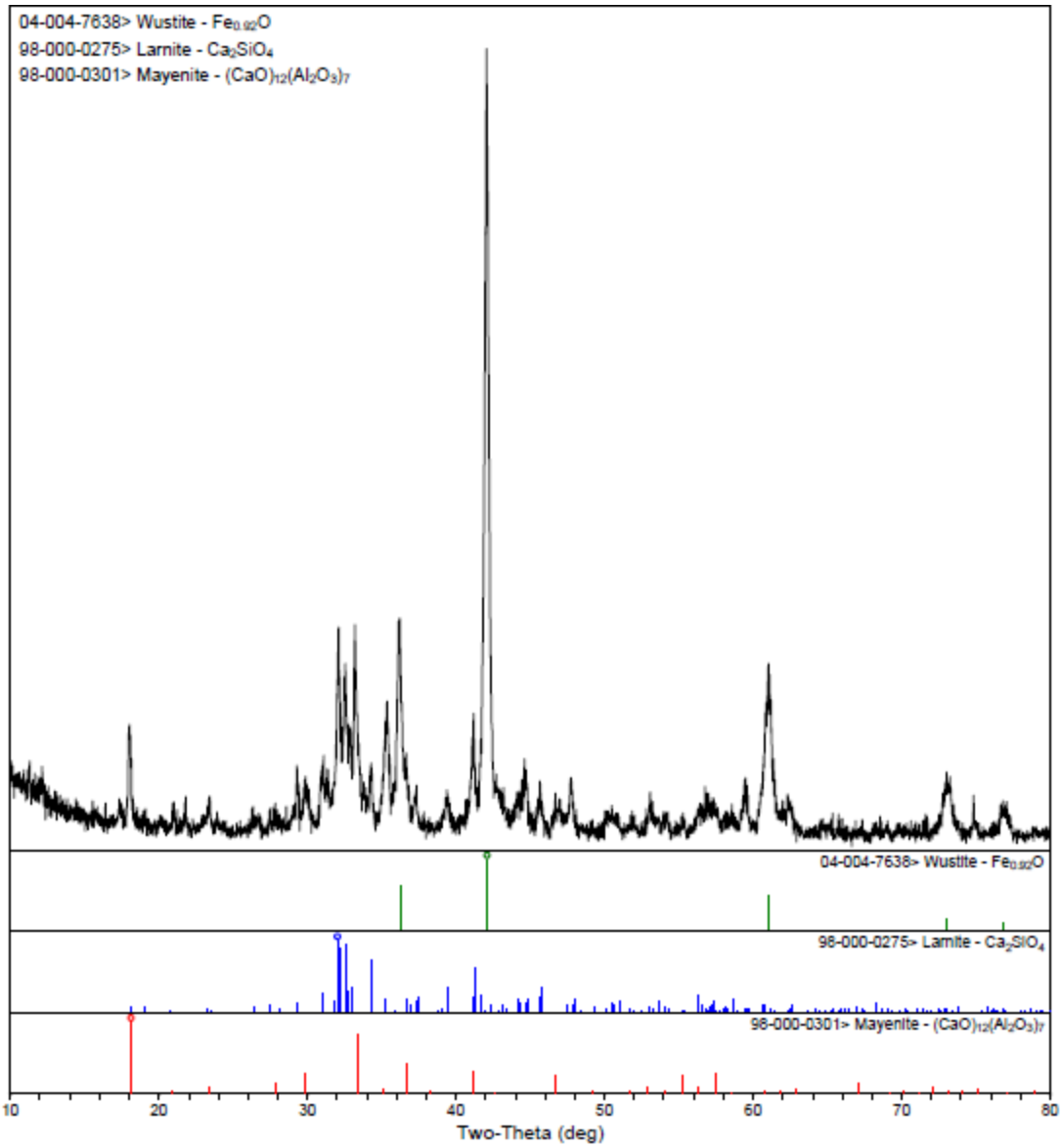

Figure 12. XRD scan and identified phases for Virgin SFS 3 (EAF/LMF), ≤44 µm particle size.

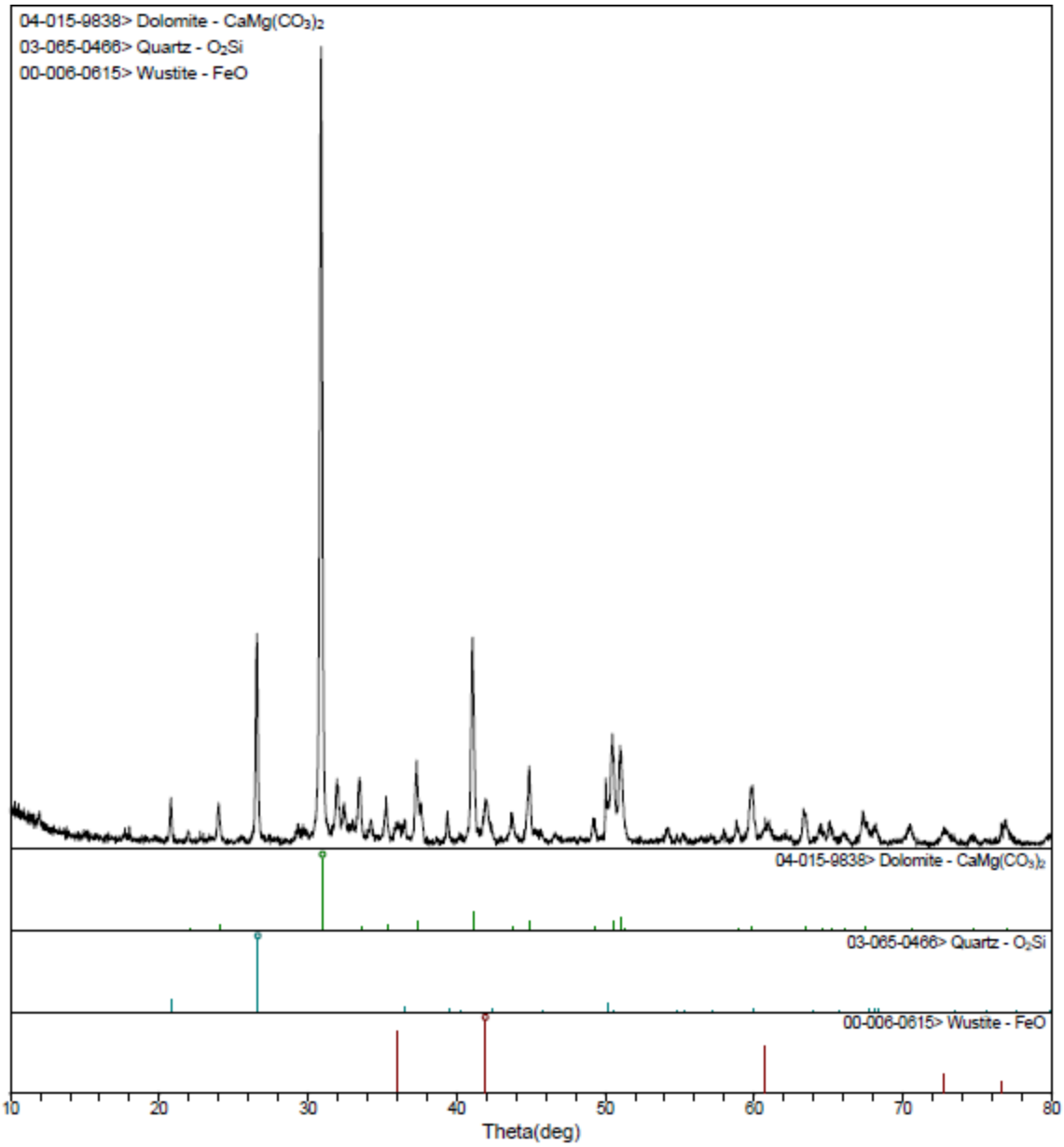

Figure 13. XRD scan and identified phases for SFS FRAP 1 (Curran) with asphalt binder removed, ≤150 µm particle size.

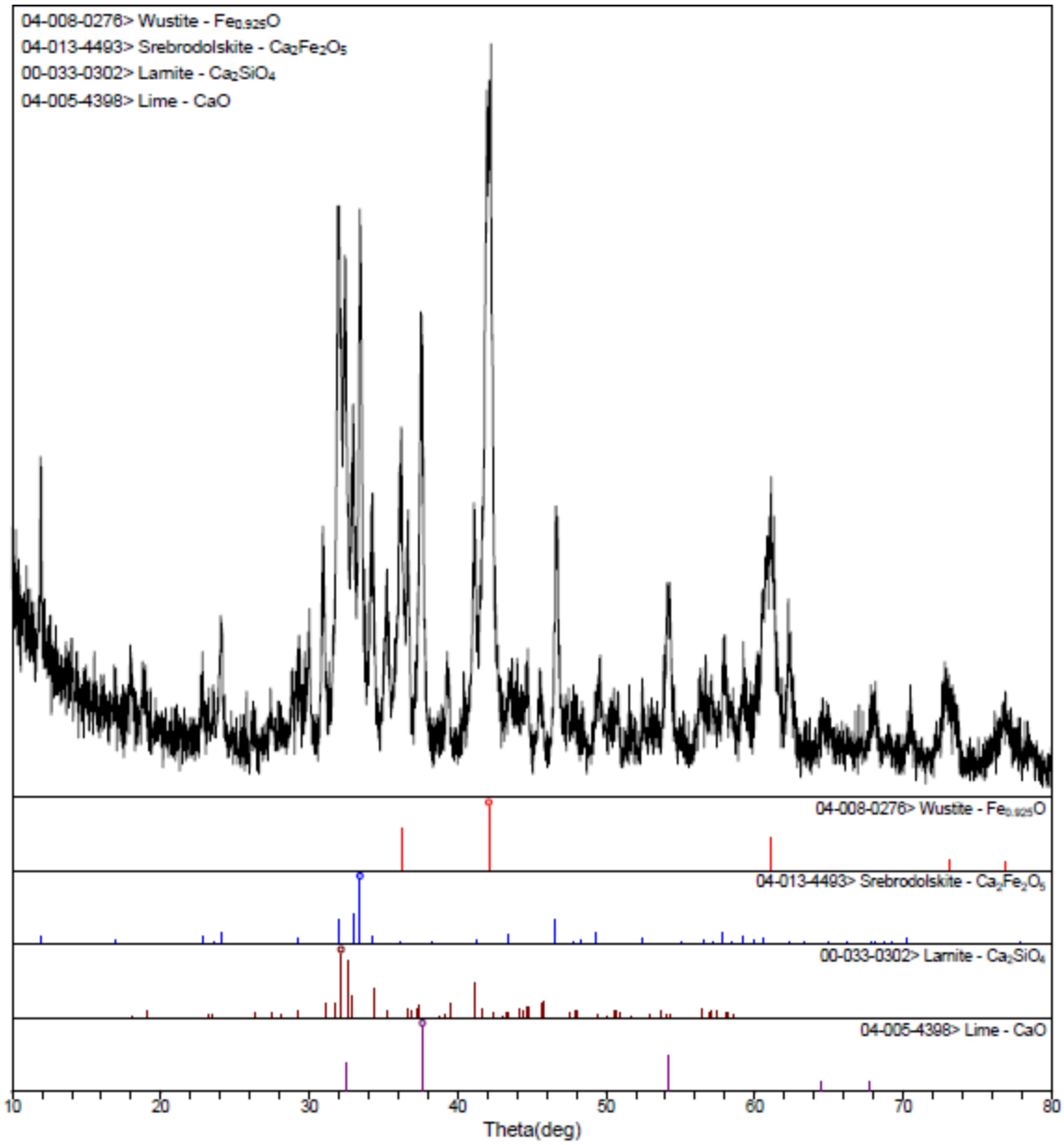

Figure 14. XRD scan and identified phases for the SFS from SFS FRAP 1 (Curran) with asphalt binder removed, ≤150 µm particle size.

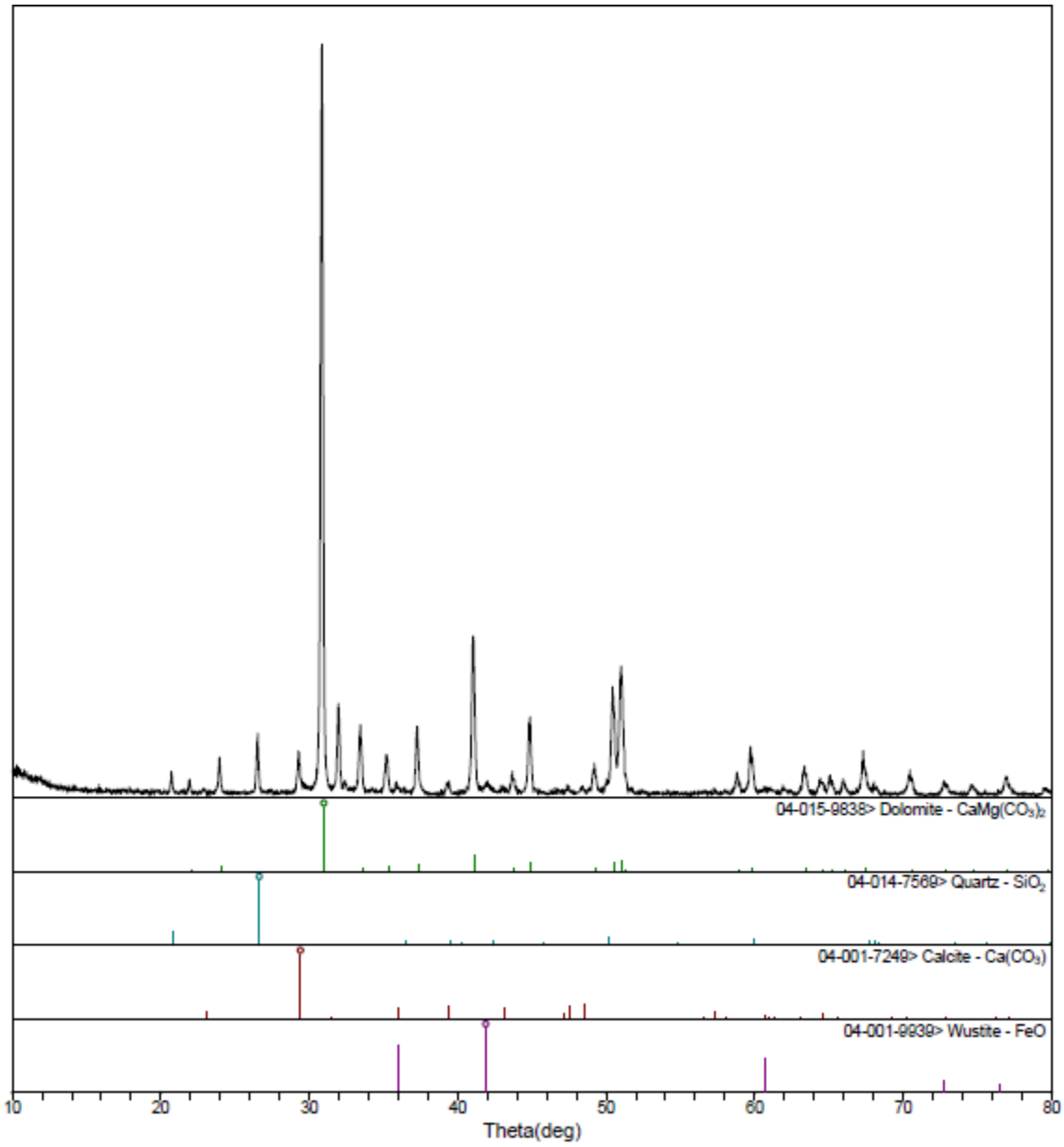

Figure 15. XRD scan and identified phases for SFS FRAP 2 (Geneva) with asphalt binder removed, ≤150 µm particle size.

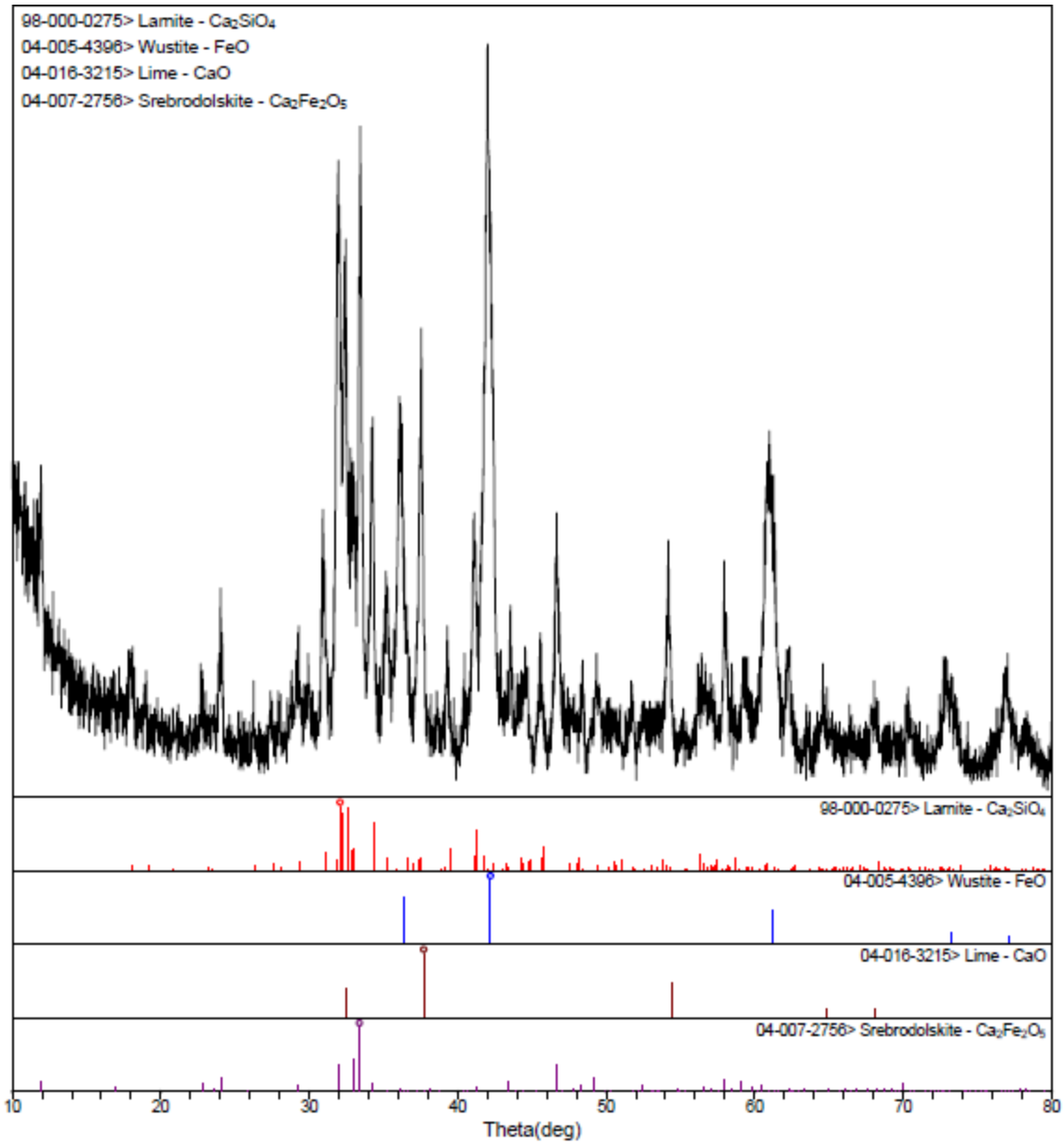

Figure 16. XRD scan and identified phases for the SFS from SFS FRAP 2 (Geneva) with asphalt binder removed, ≤150 µm particle size.

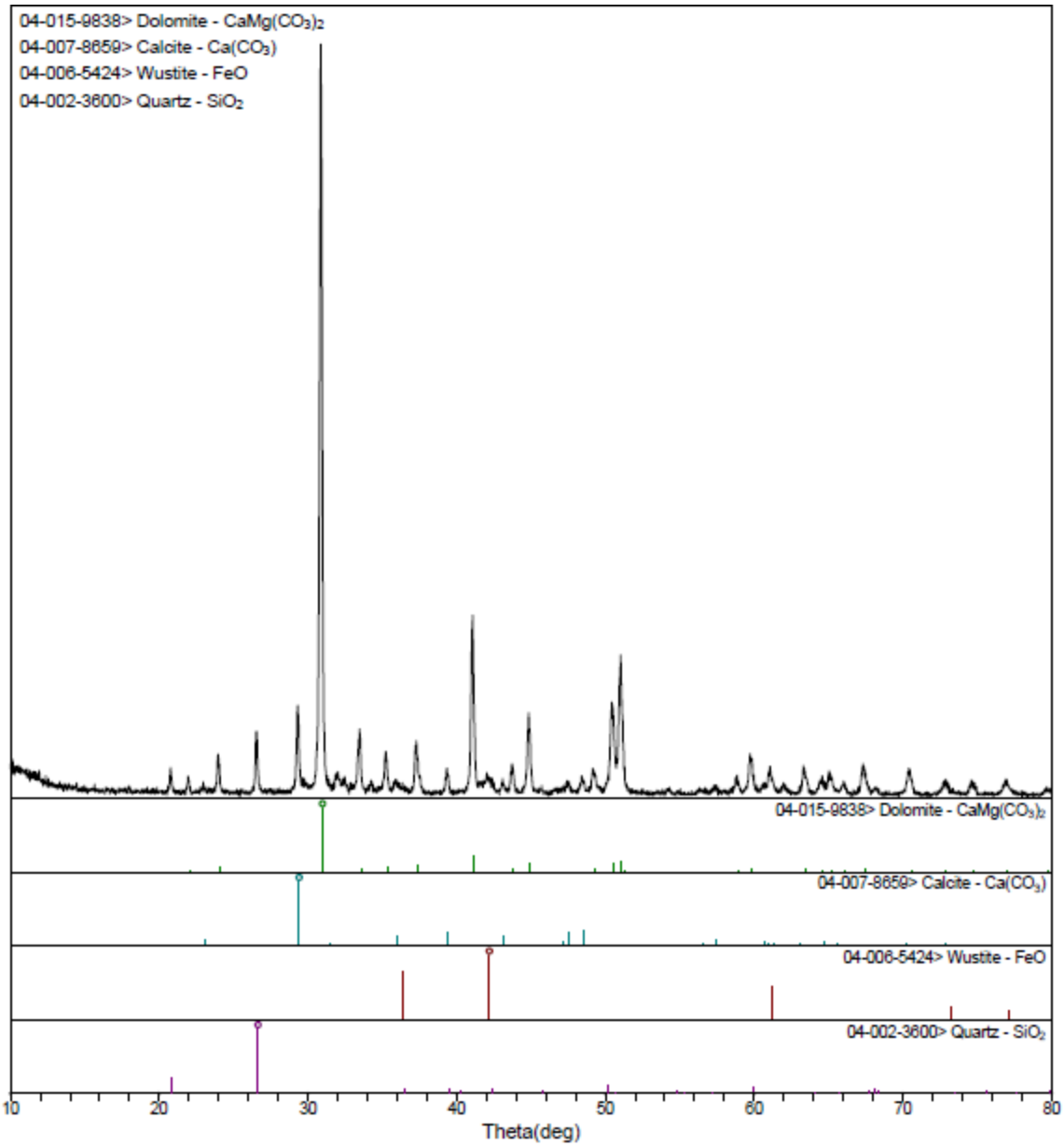

Figure 17. XRD scan and identified phases for SFS FRAP 3 (Central Blacktop) with asphalt binder removed, ≤150 µm particle size.

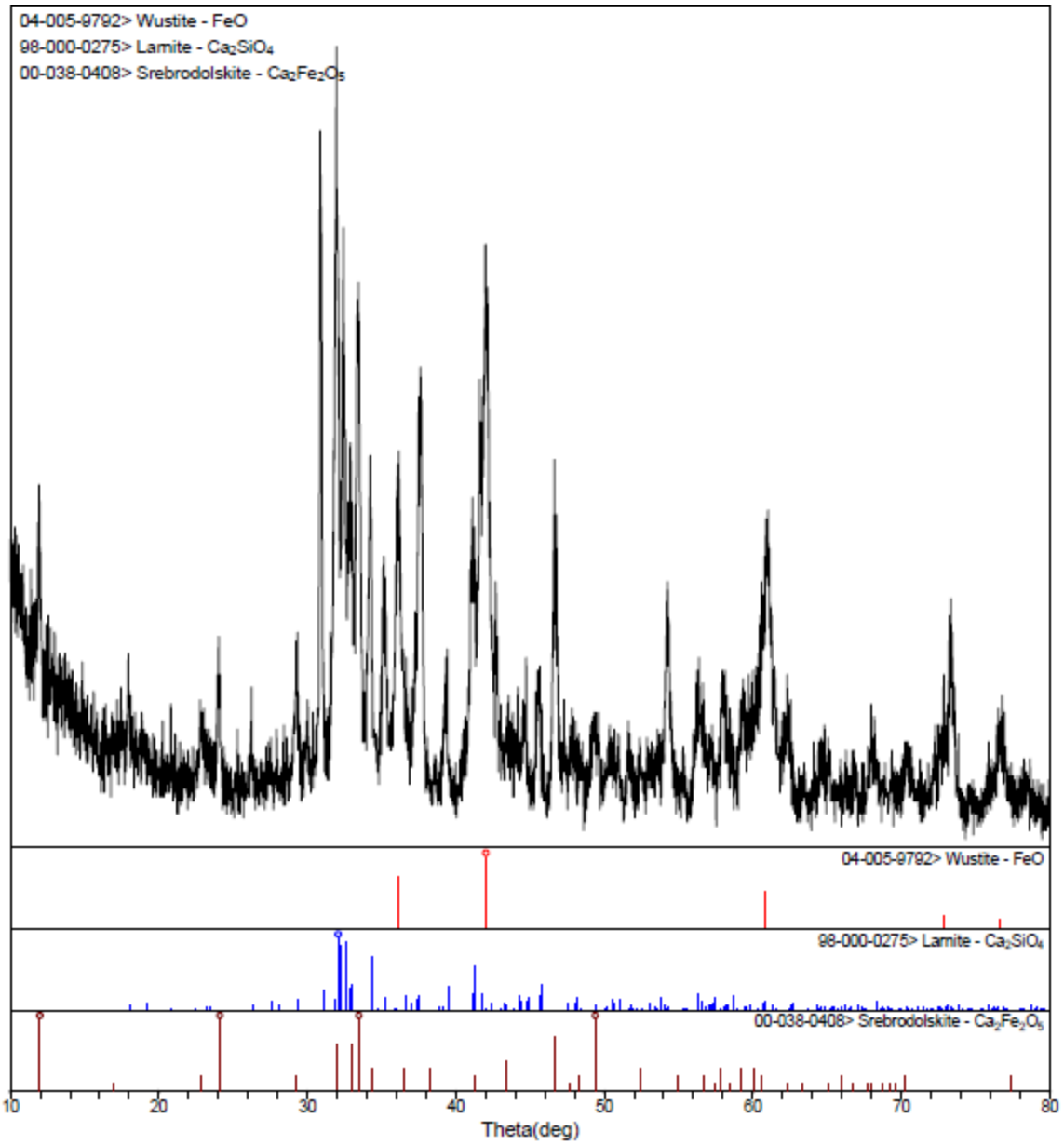

Figure 18. XRD scan and identified phases for the SFS from SFS FRAP 3 (Central Blacktop) with asphalt binder removed, ≤150 µm particle size.

3.4 CHEMICAL COMPOSITION

The chemical composition of the SFS samples was determined using inductively coupled plasma optical emission spectroscopy (ICP-OES). A PerkinElmer Optima 2000DV ICP-OES was used for the analysis. The particles of the tested sample were all passing the #100 sieve (≤150 µm); this ensured that a representative sample was obtained from the stockpile since all aggregate sizes were crushed. The composition detection was limited to only the main metallic elements in typical SFS samples, namely iron, calcium, silicon, magnesium, manganese, aluminum, titanium, sulfur, phosphorus, and chromium, as indicated previously by Table 1.

The samples were prepared for ICP-OES by acid digestion. A solution of nitric acid and hydrochloric acid was used with a microwave digester to prepare the sample to test for all of the aforementioned elements except for titanium and silicon. A solution of nitric acid, hydrochloric acid, and hydrofluoric acid was used with a microwave digester to prepare the sample to test for the titanium and silicon contents.

The ICP-OES analysis provides elemental composition (Table 20), but these values are commonly reported as the oxide contents. The oxide contents were determined stoichiometrically based on the elemental and oxide compound molecular weights. The calculated oxide contents for the virgin SFS samples are shown in Table 21, and, overall, the values agree with the literature. The CaO and SiO_2 contents appear to be lower than expected. In particular, the SiO_2 content was significantly lower for virgin SFS 3, which could perhaps be attributed to the LMF process. The composition of SFS is highly variable, depending on the location, process, and materials, so it is perhaps not surprising that the results reported here differ from the "typical" values reported in the literature. The oxide contents for the SFS FRAP samples (with asphalt removed) are shown in Table 22. Because of the presence of dolomite coarse aggregate, the MgO content is higher than a typical BOF slag composition and the CaO content is similar to typical BOF slag. The quartz present in the original HMA may have increased the SiO_2 content, particularly as noted in SFS FRAP 1. The overall contents of Cr, Fe, Mn, P, S, and Ti were all lower than typical BOF because these elements are not generally found in significant quantities in dolomite and quartz.

Table 20. Elemental Compositions Determined by ICP-OES

Element	Virgin SFS 1 (BOF)	Virgin SFS 2 (EAF)	Virgin SFS 3 (EAF/LMF)	SFS FRAP 1 (Curran)	SFS FRAP 2 (Geneva)	SFS FRAP 3 (Central Blacktop)
Al	1.24%	2.08%	3.74%	0.37%	0.43%	0.54%
Ca	7.86%	16.96%	19.38%	12.10%	19.30%	22.50%
Cr	0.12%	0.42%	0.37%	0.02%	0.04%	0.04%
Fe	26.20%	23.91%	25.68%	3.70%	7.24%	5.46%
Mg	7.66%	5.11%	5.74%	7.48%	11.21%	14.70%
Mn	1.82%	3.53%	1.90%	0.48%	0.63%	0.70%
P	0.25%	0.15%	0.22%	0.07%	0.14%	0.13%
S	0.11%	0.08%	0.15%	0.06%	0.09%	0.11%
Si	4.34%	4.50%	0.48%	5.96%	4.06%	3.73%
Ti	0.15%	0.27%	0.22%	0.10%	0.07%	0.06%

Table 21. Elemental and Oxide Compositions of Virgin SFS

Compound	Virgin SFS 1 (BOF)	Typical Values (BOF)	Virgin SFS 2 (EAF)	Virgin SFS 3 (EAF/LMF)	Typical Values (EAF)
Al_2O_3	2.3%	1-6%*	3.9%	7.1%	2-9%*
CaO	11.0%	30-55%*	18.8%	27.1%	35-60%*
Cr	0.1%	0.1-0.5%*	0.4%	0.4%	0.1-1%*
Total Fe	26.2%	14-22%**	23.9%	25.7%	20-30%**
MgO	12.7%	5-15%*	8.5%	9.5%	5-15%*
Total Mn	1.8%	1-5%**	3.5%	1.9%	2-8%**
P	0.3%	0.2-2%*	0.2%	0.2%	0.01-0.25%*
S	0.1%	0.05-0.15%*	0.1%	0.2%	0.08-0.2%*
SiO_2	9.3%	8-20%*	9.6%	1.0%	9-20%*
TiO_2	0.3%	0.4-2%*	0.5%	0.4%	0.3-1%***

References: *Shi (2004), **Balcázar et al. (1999), ***Gutt and Nixon (1979)

Table 22. Elemental and Oxide Compositions of SFS FRAP

Compound	SFS FRAP 1 (Curran)	SFS FRAP 2 (Geneva)	SFS FRAP 3 (Central Blacktop)	Typical Values (BOF Slag)
Al_2O_3	0.70%	0.81%	1.0%	1-6%*
CaO	16.9%	27.0%	31.5%	30-55%*
Cr	0.02%	0.04%	0.04%	0.1-0.5%*
Total Fe	3.7%	7.2%	5.5%	14-22%**
MgO	12.4%	18.6%	24.4%	5-15%*
Total Mn	0.48%	0.63%	0.70%	1-5%**
P	0.07%	0.14%	0.13%	0.2-2%*
S	0.06%	0.09%	0.11%	0.05-0.15%*
SiO_2	12.7%	8.7%	8.0%	8-20%*
TiO_2	0.16%	0.12%	0.10%	0.4-2%*

References: *Shi (2004), **Balcázar et al. (1999), ***Gutt and Nixon (1979)

3.5 FREE CALCIUM OXIDE AND MAGNESIUM OXIDE CONTENTS

3.5.1 Free CaO Contents

Based on the literature, the free CaO content of SFS is commonly determined by a complexometric titration technique using an ethylene glycol extraction with an acid titration and a pH indicator. For the existing documentation on determining the free CaO specifically of SFS, EN 1744-1:2009+A1 (2013) details extracting the calcium ions in ethylene glycol for 30 minutes in a 70°C water bath, while the Ministry of Transportation of Ontario specifies an extraction in a solution of 2/3 ethylene glycol and 1/3 methyl alcohol for 30 minutes in a boiling water bath (MTO 1996). Gupta et al. (1994) also used heated ethylene glycol (60 to 70°C) but did not specify the total time of extraction. Therefore, for this study, the extraction temperature would be at 100°C with hot ethylene glycol.

The extraction procedure followed was that about one gram of sample was weighted out. The material was all passing the #100 sieve (≤150 μm). The sample was added to a flask with 50 mL of ethylene glycol, which was stirred continuously (via magnetic stirrer) in a 95±5°C water bath on a hot plate for 30 minutes (Figure 19). The solution was then filtered under vacuum suction through filter paper that had been wetted with ethylene glycol. The flask was rinsed twice with 10 mL of ethylene glycol, which was then also filtered. Ten drops of phenolphthalein solution were added to the filtrate, which was then titrated with 0.05 N hydrochloric acid (HCl).

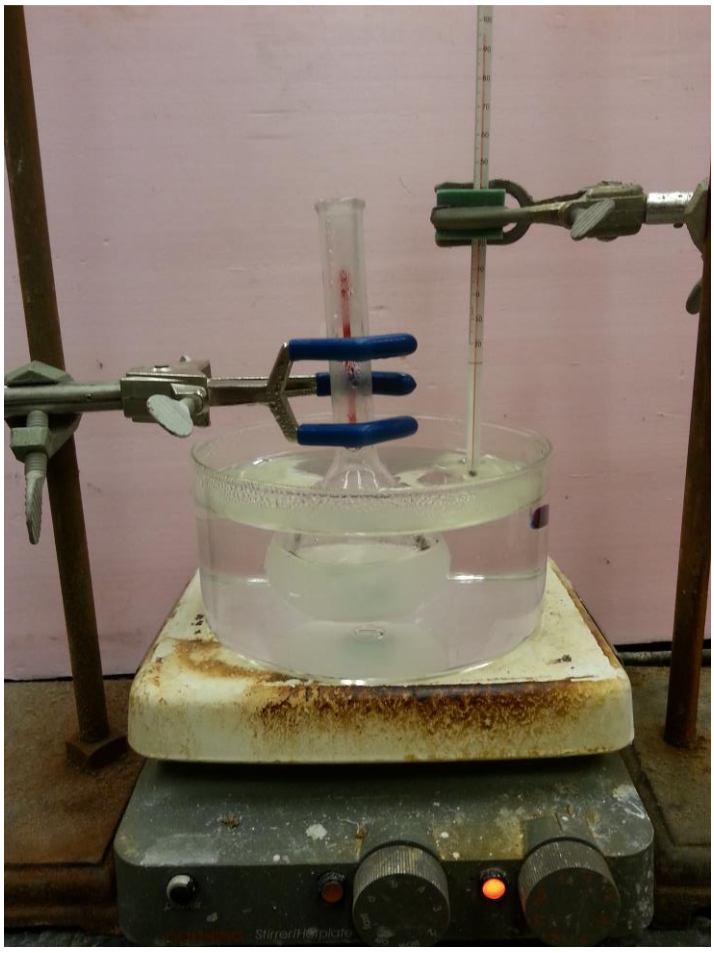

Figure 19. Hot water bath arrangement for ethylene glycol extraction.

Studies of SFS have suggested that ethylene glycol will dissolve both CaO and $Ca(OH)_2$ (Thomas 1983; Motz and Geiseler 2000; Lun et al. 2008; Belhadj et al. 2012), which is not necessarily correct. Rather, ethylene glycol will dissolve, or, more precisely, form a complex with, the calcium ions from the free CaO but not necessarily all of the free $Ca(OH)_2$. MacPherson and Forbrich (1937) were the first to recognize that ethylene glycol may not dissolve all of the available $Ca(OH)_2$, possibly as a result of the large crystal sizes. Therefore, the complexometric titration test was used to determine an ethylene glycol number (EGN), which represents the total free CaO and anywhere from all to none of the available $Ca(OH)_2$ in the sample. The EGN is determined based on the initial mass in grams

of the SFS sample (m), the normality of the HCl (N_{HCl}), the volume in mL of HCl titrated (V_{HCl}), a correction for the volume in mL of HCl titrated in a blank ethylene glycol sample (V_{blank}), and an equivalency factor (F):

$$EGN = F\left[\frac{N_{HCl}(V_{HCl} - V_{blank})}{10\ m}\right] \quad (1)$$

The equivalency factor *F* for this method and equation formulation is 28 (Javellana and Jawed 1982; MTO 1996). The correction V_{blank} is specified in other standards (EN 1744-1:2009+A1 2013) to account for the amount of HCl needed to titrate a plain solvent sample (i.e., plain ethylene glycol). To determine V_{blank}, 70 mL of 70°C ethylene glycol was titrated with 0.05 N HCl and a phenolphthalein indicator, which resulted in V_{blank} = 0 mL; this is a reasonable result because the pH of ethylene glycol is close to neutral.

To test the validity of this test procedure, samples of CaO, $Ca(OH)_2$, $CaCO_3$, and $CaMg(CO_3)_2$ were also tested using particle sizes ≤ 44 µm. The pure CaO was created by heating a sample of reagent grade CaO in an oven at 1000°C to effectively remove all $Ca(OH)_2$ and $CaCO_3$ present. The results in Table 23 indicate that both CaO and $Ca(OH)_2$ are dissolved by ethylene glycol while $CaCO_3$ and $CaMg(CO_3)_2$ are not. The pure CaO sample created by heating $CaCO_3$ did not yield a 100% free CaO content like the pure CaO sample derived from heating reagent grade CaO, which can be possibly because not all of the $CaCO_3$ decomposed into CaO or some of the sample re-carbonated as the sample cooled.

As can be noted, the free calcium ion content from the $Ca(OH)_2$ is less than 100%, which is expected because the ethylene glycol forms a complex with the CaO from the $Ca(OH)_2$. Stoichiometrically, the estimated $Ca(OH)_2$ content is 96.8% for the EGN value of 73.3%, which is reasonable considering that the reagent purity of the sample was ≥95%. This suggests that ethylene glycol will dissolve the available free $Ca(OH)_2$.

The filtrate of the EAF SFS and EAF/LMF SFS samples was clear, so it was relatively easy to see the final titration point when the pink color from phenolphthalein disappeared. However, the filtrate of the BOF SFS was orange-red in color, so to determine the final titration point, two samples of filtrate were placed side-by-side, and the phenolphthalein was added to one of the samples and then titrated with HCl until the color returned to the initial orange-red. The average EGN values were found to be: 4.4% for the virgin BOF SFS, 0.06% for the virgin EAF SFS, and 0.5% for the virgin EAF/LMF SFS. These values are not surprising considering that the free CaO content can be 1-10% for BOF slag and 0-4% for EAF (Balcázar et al. 1999). It is not unexpected that the free CaO content of the BOF slag was high, given that, when crushed, particles of unassimilated CaO could be clearly seen (Figure 20).

The SFS from the SFS FRAP samples also contained relatively high EGN values (Table 23), which is consistent with the SFS sources coming from BOF slags. However, the high EGN value is somewhat unexpected given that the samples were taken from existing pavements, and it was assumed a significant amount of weathering had occurred. Therefore, it appears that the asphalt coating in the field prevented the SFS from significantly hydrating the CaO and assumedly MgO.

Table 23. Ethylene Glycol Numbers as Determined by Complexometric Titration

Sample	Test Replicate	Sample weight (g)	Molarity of HCl	Amount HCl Titrated (mL)	Ethylene Glycol Number (EGN)
Pure CaO*	1	0.3315	0.05	239.0	100.9
Pure CaO**	1	0.4985	0.05	325.0	91.3
$Ca(OH)_2$	1	0.6592	0.05	345.0	73.3
$CaCO_3$	1	0.9102	0.05	0	0.0
$CaMg(CO_3)_2$	1	1.0278	0.05	0	0.0
SFS Tested “As Is”					
Virgin SFS 1 (BOF)	1	1.0575	0.05	33.6	4.45
	2	1.0760	0.05	33.4	4.35
Virgin SFS 2 (EAF)	1	0.9899	0.05	0.4	0.06
	2	1.0067	0.05	0.4	0.06
Virgin SFS 3 (EAF/LMF)	1	0.9757	0.05	3.6	0.52
	2	1.0529	0.05	3.8	0.51
SFS from SFS FRAP 1 (Curran)	1	1.0050	0.05	29.0	4.04
	2	1.0226	0.05	28.8	3.94
SFS from SFS FRAP 2 (Geneva)	1	1.0070	0.05	27.2	3.78
	2	0.9794	0.05	25.4	3.63
SFS from SFS FRAP 3 (Central Blacktop)	1	1.0486	0.05	39.2	5.23
	2	1.0244	0.05	36.1	4.93

Created by heating reagent grade CaO*, $CaCO_3$**

Figure 20. Particles of unassimilated CaO (white particles) could be seen in the Virgin SFS 1 (BOF) sample after crushing.

Because $Ca(OH)_2$ is not necessarily fully dissolved by ethylene glycol (MacPherson and Forbrich 1937), another method was devised to determine the total free CaO content. In this method, the powdered SFS sample was heated in an oven to 1000°C to convert the samples $Ca(OH)_2$ and $CaCO_3$ to CaO and then cooled to room temperature in the oven. The idea was to test the heat-treated SFS using the ethylene glycol extraction technique to determine the existing free CaO content (Table 24), and then adjust the value based on the $Ca(OH)_2$ and $CaCO_3$ contents from TGA. Because it was assumed in this case that all of the $Ca(OH)_2$ and $CaCO_3$ in the sample was converted to CaO after heating, the computed EGN was simply assumed to be the total free CaO. This idea was only applied to Virgin SFS 2 and 3 because it was evident that, while the percent free CaO content determined increased (compare Table 24 to Table 23), adjusting the measured free CaO content based on the CaO contents predicted by TGA would result in a negative free CaO content. For the Virgin SFS 3 example, the $Ca(OH)_2$ and $CaCO_3$ contents from TGA were 0.87% and 2.33%, respectively, which would estimate CaO contents, based on the molar mass ratios, of 0.66% and 1.31% from $Ca(OH)_2$ and $CaCO_3$, respectively. However, only 1.07% free CaO was directly measured. Therefore, upon cooling, some of the CaO could be carbonating, preventing the CaO from being dissolved by the ethylene glycol. The temperature affects the carbonation kinetics of CaO. In a study by Rouchon et al. (2013), $CaCO_3$ was calcined in an inert atmosphere and then the temperature was reduced to various levels (650, 600, 550, 500, and 450°C) before introducing CO_2, and it was found that the lower temperatures resulted in less formation of $CaCO_3$ at a given exposure time.

Table 24. Free CaO Content of Heated Samples (Cooled in the Oven) as Determined by Ethylene Glycol Extraction

Sample	Test Replicate	Sample weight (g)	Molarity of HCl	Amount HCl Titrated (mL)	Percent Free CaO
Virgin SFS 2 (EAF)	1	1.0216	0.05	0.7	0.10
	2	1.0052	0.05	1.0	0.14
Virgin SFS 3 (EAF/LMF)	1	1.0350	0.05	7.9	1.07
	2	0.9856	0.05	7.6	1.08

One final heating scheme was devised and tested in which the sample was heated to 1000°C and then immediately placed under vacuum so that, upon cooling, the sample could not carbonate. A similar method could also be tested in which the sample is heated and cooled in an inert environment (such as nitrogen) to prevent carbonation, but because such equipment was not available, the previously described heating and cooling scheme was tested. Again, it was assumed that the computed EGN only represented the total free CaO. However, as is indicated in Table 25, this test did not prove to be successful. It is suspected that the sample re-carbonated while cooling as the sample was moved from the oven to the vacuum, as Virgin SFS 2 (EAF) did not even indicate the presence of any CaO.

Table 25. Free CaO Content of Heated Samples (Cooled Under Vacuum) as Determined by Ethylene Glycol Extraction

Sample	Test Replicate	Sample Weight (g)	Molarity of HCl	Amount HCl Titrated (mL)	Percent Free CaO
Virgin SFS 2 (EAF)	1	1.0074	0.05	0.0	0.00
Virgin SFS 3 (EAF/LMF)	1	1.0091	0.05	4.2	0.58
	2	1.0401	0.05	3.6	0.48
	3	1.0181	0.05	3.8	0.52

Based on the findings, the EGN values reported in Table 23 were deemed to be the most acceptable. Because a sample of pure $Ca(OH)_2$ was found to be entirely complexed by ethylene glycol, it is assumed that, at least in this testing scenario, the ethylene glycol is complexing with all of the available $Ca(OH)_2$ in the SFS and SFS FRAP samples. Therefore, TGA testing was performed to determine the $Ca(OH)_2$ contents of the SFS samples in order to estimate (or backcalculate) a total free CaO content of the sample.

3.5.2 MgO Content

The European Standard EN 1744-1:2009+A1 (2013) states: "The total MgO content is used as a measure of free MgO, in the absence, at present of a reliable method of determining the content of free MgO." The standard then references using EN 196-2 to determine the MgO content of the SFS, which is a specified standard method to use x-ray fluorescence to determine the chemical composition of cement. Therefore, it is assumed that the Mg content determined from the ICP-OES method (Table 26) is a suitable representation of the total MgO content of the SFS sample. However, because MgO was not identified by XRD (see Section 3.3) – which suggests that the free MgO content is not high enough to be detected by XRD (unlike the free CaO detected for Virgin SFS 1 (BOF), which had a high enough content) – it is unclear whether or not these samples actually contain any free MgO available for reaction. In addition, the MgO content from ICP-OES for the SFS FRAP does not represent the content from the SFS aggregate alone; it is from both the SFS and the dolomite aggregate. However, one possible method for backcalculating the initial free MgO content is by TGA after autoclaving the SFS sample, as will be discussed in Section 3.6.1.

Table 26. MgO Content Determined by ICP-OES

Sample	MgO Content
Virgin SFS 1 (BOF)	12.7%
Virgin SFS 2 (EAF)	8.5%
Virgin SFS 3 (EAF/LMF)	9.5%
SFS FRAP 1 (Curran)	12.4%
SFS FRAP 2 (Geneva)	18.6%
SFS FRAP 3 (Central Blacktop)	24.4%

3.5.3 Hydroxide and Carbonate Contents

Knowing that ethylene glycol will complex with the free CaO and the free $Ca(OH)_2$, thermogravimetric analysis (TGA) was used to estimate the $Ca(OH)_2$ content in order to refine the total free CaO measurement, as has been conducted in other studies of SFS (Thomas 1983; Kneller et al. 1994; Gumieri et al. 2004; Lun et al. 2008; Waligora et al. 2010; Papayianni and Anastasiou 2011; Belhadj et al. 2012). TGA was selected as the appropriate thermal analysis technique because other studies have found the results to be more reliable compared with differential thermal analysis (Thomas 1983). The percent free CaO content (CaO_{free}) can thus be determined from a combination of the complexometric titration and TGA methods by subtracting the TGA-estimated $Ca(OH)_2$ (CH_{TGA}) content from the EGN value. A correction factor *f* can be included in the equation to account for the estimated amount of $Ca(OH)_2$ that was dissolved by the ethylene glycol. In this situation, *f* can vary from 0% to 100%. Because it could not be definitively concluded what the factor *f* actually is and because the sample of ≥95% reagent grade $Ca(OH)_2$ indicated that all of the $Ca(OH)_2$ complexed with ethylene glycol, it is assumed for this study that *f* is 100%.

$$CaO_{free} = EGN - f(CH_{TGA}) \quad (2)$$

For the thermal analysis, a TA Instruments Q50 TGA was used in this analysis, which heated the sample to 1000°C at a heating rate of 10°C per minute. To avoid any potential hydration or carbonation of the free oxides in the powdered sample, nitrogen was used as the purge gas at flow rates of 60 mL/min for the sample purge and 40 mL/min for the balance purge.

The content of $Ca(OH)_2$ – or any phase, for that matter, identified by TGA, such as $Mg(OH)_2$, $CaCO_3$, and $MgCO_3$, etc. – is determined stoichiometrically. In the case of the hydroxide phases ($Ca(OH)_2$, $Mg(OH)_2$), the TGA mass loss is due to dehydration and the loss of H_2O, while in the case of the carbonate phases ($CaCO_3$, $MgCO_3$, $CaMg(CO_3)_2$), the TGA mass loss is due to decarbonation and the loss of CO_2. The molar masses of the various phases are summarized in Table 27, which are used to stoichiometrically determine the contents of the various phases.

Table 27. Molar Masses of Identified Phases by TGA

Phase	Molar Mass (g/mol)
Calcium Hydroxide $Ca(OH)_2$	74.093
Magnesium Hydroxide $Mg(OH)_2$	58.320
Water H_2O	18.015
Calcium Carbonate $CaCO_3$	100.088
Magnesium Carbonate $MgCO_3$	84.314
Dolomite $CaMg(CO_3)_2$	184.402
Carbon Dioxide CO_2	44.010
Calcium Oxide CaO	56.078
Magnesium Oxide MgO	40.304

To confirm the decomposition temperatures for the phases to be examined by TGA, control samples of $CaCO_3$ (Figure 21), $MgCO_3$ (Figure 22), $CaMg(CO_3)_2$ (Figure 23), $Ca(OH)_2$ (Figure 24), and $Mg(OH)_2$ (Figure 25) were tested:

- Halikia et al. (2001) found that, in a nitrogen atmosphere, $CaCO_3$ decomposes over a range of temperatures from 635 to 865°C. The onset of decomposition of reagent grade $CaCO_3$ begins around 560°C and be completed around 750°C with the peak at about 730°C (Figure 21), indicating a $CaCO_3$ content of 99.5%.
- $MgCO_3$ typically exists as a compound of $MgCO_3$-$Mg(OH)_2$-H_2O, which decomposes in stages in a nitrogen atmosphere: any adsorbed water is lost around 100°C, chemically-bound water (water of crystallization) is lost between 130 and 350°C, and the hydroxide and carbonate phases decompose between 305 and 520°C (Khan et al. 2001). Two thermal events were identified (Figure 22), indicating the loss of water of crystallization from 185 to 310°C (peak at about 235°C) and the decomposition of the hydroxide and carbonate phases from 310 to 470°C (peak at about 430°C).
- In a nitrogen atmosphere at a heating rate of 10°C/minute, the decarbonation of dolomite occurs between 600 and 850°C (Gunasekaran and Anbalagan 2007). The decomposition appeared to start around 400°C, but the majority of the mass loss started at around 600°C, and finished at about 765°C with a peak at 740°C (Figure 21), indicating a dolomite content of 92.5%.
- At a heating rate of 10°C/minute in a nitrogen atmosphere, the peak decomposition of $Ca(OH)_2$ occurs around 400-410°C (Chen et al. 1993). The onset of decomposition of ≥95% reagent grade $Ca(OH)_2$ began around 295°C and completed around 435°C with the peak at about 418°C (Figure 24), indicating a $Ca(OH)_2$ content of 90.4%, which is reasonable considering that some of the sample could have been carbonated.
- The decomposition of $Mg(OH)_2$ starts around 350°C in a nitrogen atmosphere (Halikia and Economacou 1993). Decomposition of ≥95% reagent grade $Mg(OH)_2$ began around 275°C and completed around 440°C with a peak at around 380°C (Figure 25), indicating a $Mg(OH)_2$ content of 88.8%, which is reasonable considering that some of the sample could have been carbonated.

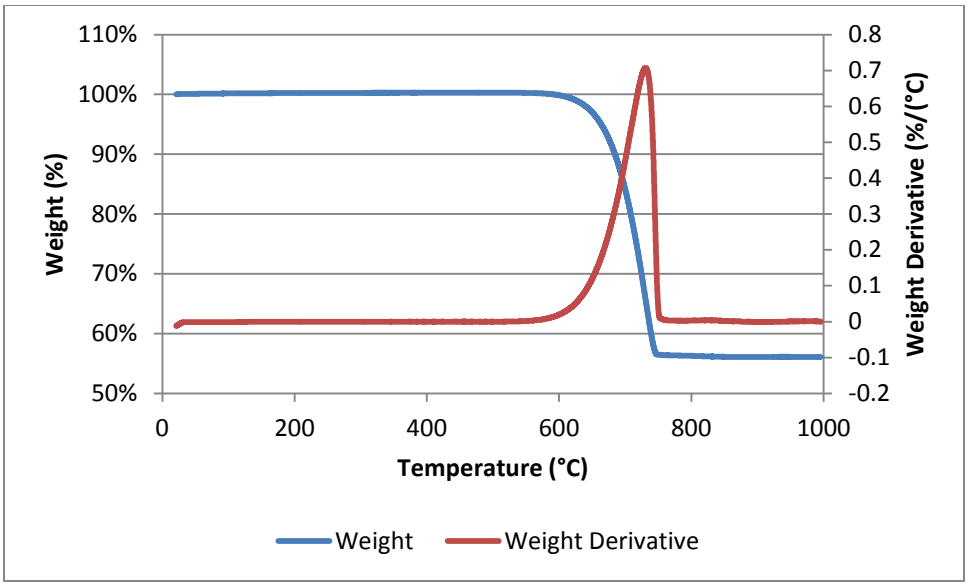

Figure 21. TGA mass loss for reagent grade calcium carbonate ($CaCO_3$) heated to 1000°C in nitrogen at 10°C/minute.

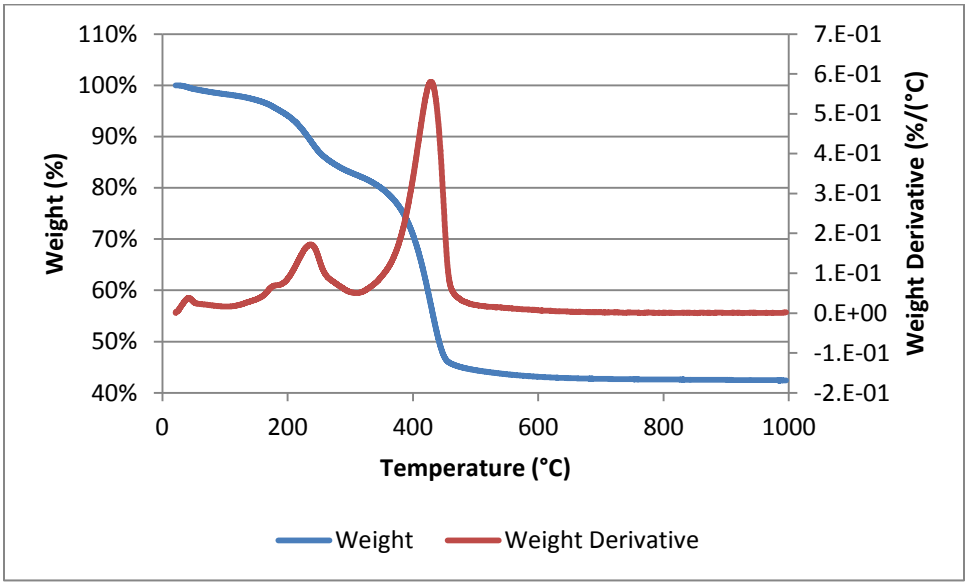

Figure 22. TGA mass loss for reagent grade magnesium carbonate ($MgCO_3$) heated to 1000°C in nitrogen at 10°C/minute.

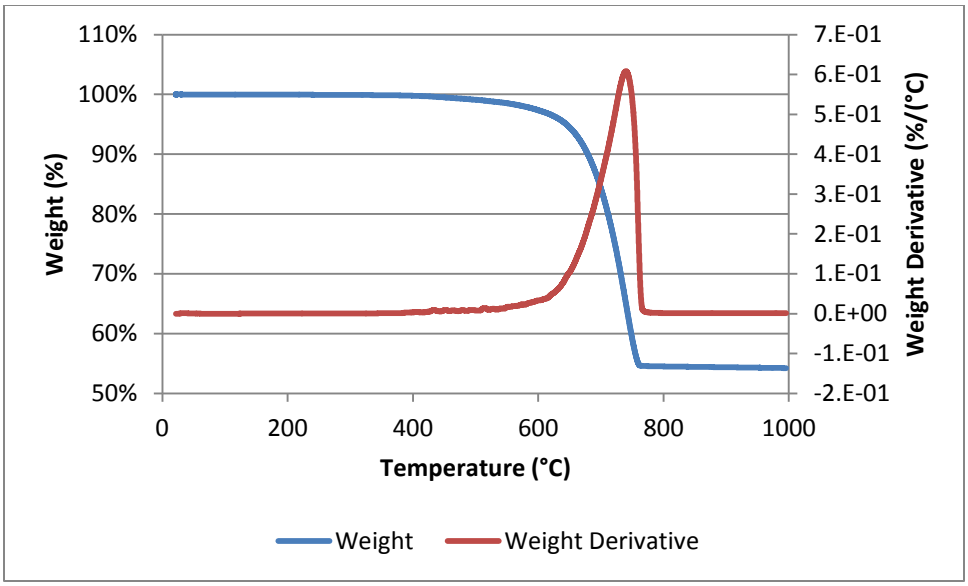

Figure 23. TGA mass loss for dolomite ($CaMg(CO_3)_2$) heated to 1000°C in nitrogen at 10°C/minute.

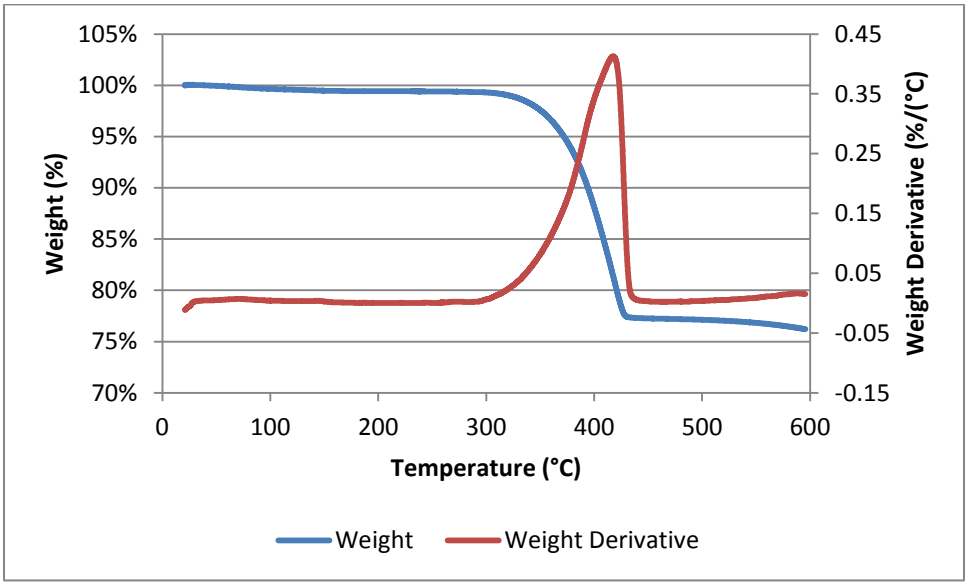

Figure 24. TGA mass loss for ≥95% reagent grade calcium hydroxide ($Ca(OH)_2$) heated to 600°C in nitrogen at 10°C/minute.

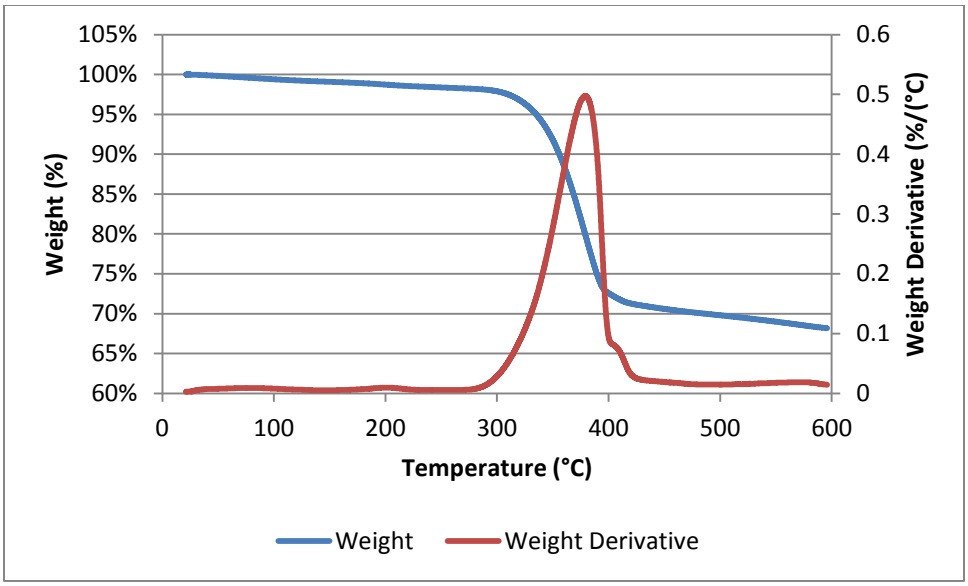

Figure 25. TGA mass loss for ≥95% reagent grade magnesium hydroxide ($Mg(OH)_2$) heated to 600°C in nitrogen at 10°C/minute.

The TGA data is shown in Figure 26 to Figure 28 for the virgin SFS samples. As can be seen, there are two clear peaks at around 400°C and 650°C, which are the decomposition peaks for $Ca(OH)_2$ and $CaCO_3$, respectively. The peaks do not occur over as broad of a temperature range as the pure samples, but the peak decomposition temperature is similar. The derivative of the weight loss clearly provides that start and end of the mass loss for $Ca(OH)_2$, so the mass loss for $Ca(OH)_2$ was assumed to occur between 360 to 420°C. For Virgin SFS 2 (EAF), if $Ca(OH)_2$ was present, the amount of it undetectably small (Figure 27), which is reasonable considering that the EGN was only 0.06%, so it is assumed that no $Ca(OH)_2$ is present. For Virgin SFS 3 (EAF/LMF), there are other peaks in addition to $Ca(OH)_2$ and $CaCO_3$ (Figure 28), which may correspond to the loss of free water around 100°C and perhaps the loss of chemically bound water around 250°C. A summary of the resultant $Ca(OH)_2$ and $CaCO_3$ contents for the virgin SFS samples are reported in Table 28.

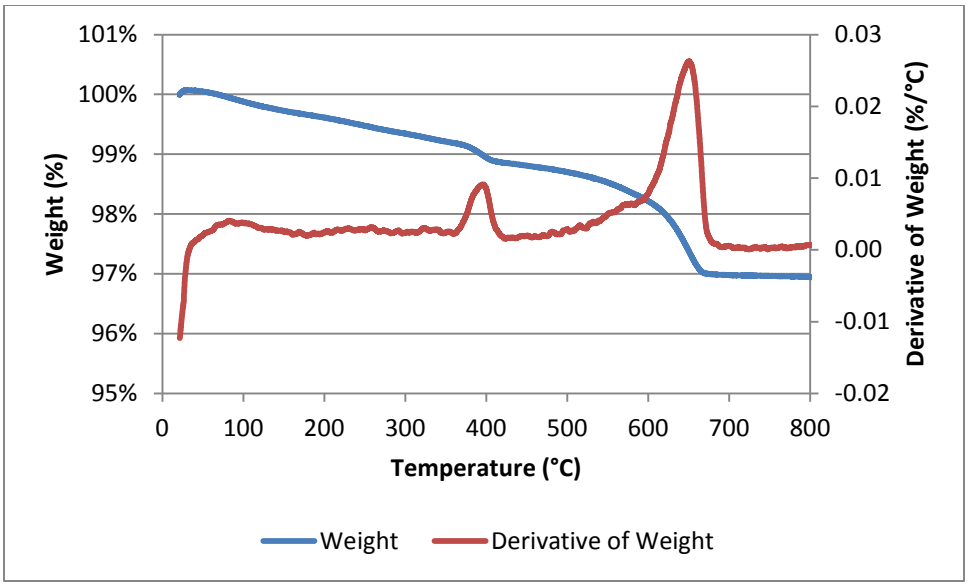

Figure 26. TGA mass loss for Virgin SFS 1 (BOF). The mass percent of $Ca(OH)_2$ was determined from 360 to 420°C (peak at 397°C). The mass percent of $CaCO_3$ was determined from 585 to 690°C (peak at 650°C).

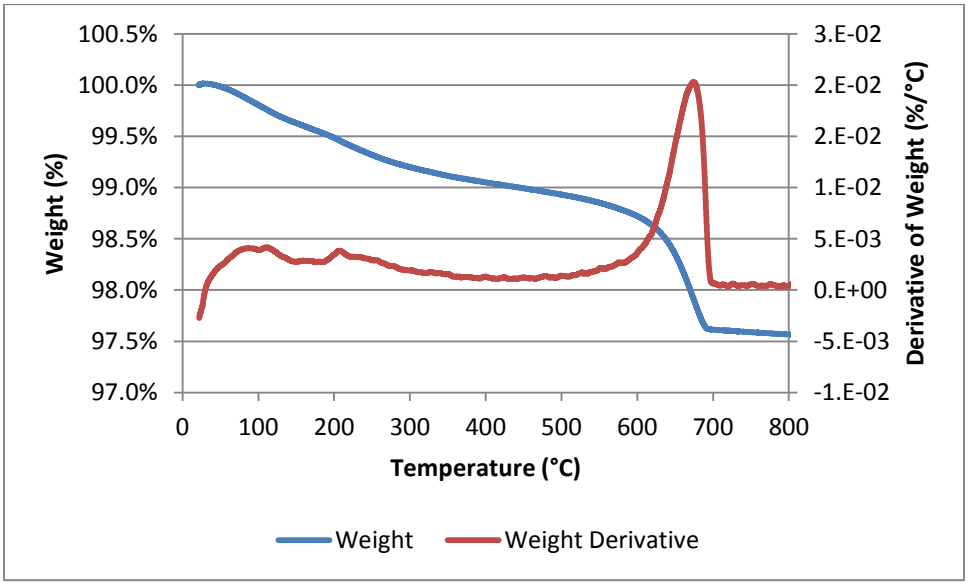

Figure 27. TGA mass loss for Virgin SFS 2 (EAF). It is assumed that no $Ca(OH)_2$ is present. The mass percent of $CaCO_3$ was determined from 585 to 690°C (peak at 675°C).

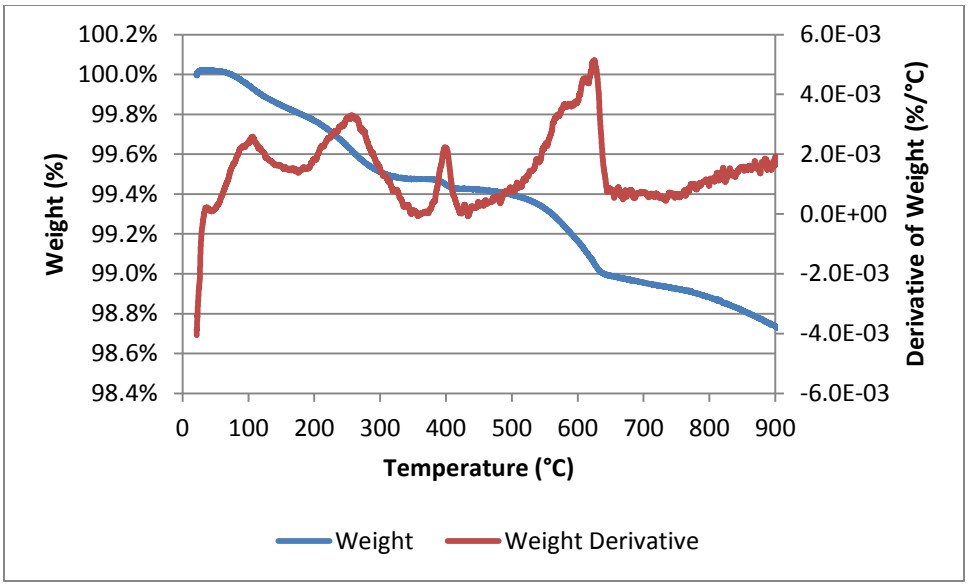

Figure 28. TGA mass loss for Virgin SFS 3 (EAF/LMF). The mass percent of $Ca(OH)_2$ was determined from 372 to 423°C (peak at 398°C). The mass percent of $CaCO_3$ was determined from 505 to 645°C (peak at 626°C).

Table 28. $Ca(OH)_2$ and $CaCO_3$ Contents for the Virgin SFS as Determined by TGA

Sample	$Ca(OH)_2$ Content	$CaCO_3$ Content
Virgin SFS 1 (BOF)	1.34%	3.04%
Virgin SFS 2 (EAF)	0.00%	2.57%
Virgin SFS 3 (EAF/LMF)	0.20%	0.91%

The refinement of the total free CaO content from ethylene glycol extraction was estimated based on the $Ca(OH)_2$ content determined by TGA. Assuming that the ethylene glycol complexed with 100% of the free $Ca(OH)_2$, the estimated total free CaO contents are shown in Table 29.

Table 29. Total Estimated Free CaO Content Determined for the Virgin SFS

Sample	Ethylene Glycol Number (EGN)	$Ca(OH)_2$ Content from TGA	Stoichiometric CaO Content in $Ca(OH)_2$	Estimated Total Free CaO Content*
Virgin SFS 1 (BOF)	4.40%	1.34%	1.01%	3.39%
Virgin SFS 2 (EAF)	0.06%	0.00%	0.00%	0.06%
Virgin SFS 3 (EAF/LMF)	0.51%	0.20%	0.11%	0.40%

*Assuming that ethylene glycol complexed with 100% of the free $Ca(OH)_2$

For the SFS FRAP samples (with binder removed), TGA was used to determine both the $Ca(OH)_2$ and the dolomite ($CaMg(CO_3)_2$) contents. The dolomite content is important to know so that the amount of SFS in the FRAP sample can be estimated. All of the SFS FRAP samples only revealed the presence of dolomite. For the SFS present in the samples, the

contents of any hydroxide phases were likely too little to show as a peak in the TGA. However, any $CaCO_3$ present in the SFS could have contributed to the dolomite peak, although the content was likely low enough to be relatively insignificant. As XRD had revealed, all three of the SFS FRAP samples contained quartz, which was likely from any virgin fine aggregate in the original HMA mixture. Assuming that the original virgin fine aggregate contained both silica (quartz) and carbonate mineral aggregates, the remaining material may not all be SFS. The thermal analyses of SFS FRAP 1 (Figure 29), SFS FRAP 2 (Figure 30), and SFS FRAP 3 (Figure 31) suggested that the dolomite contents were 54.2%, 59.0%, and 68.6%, respectively. These analyses grossly agree with the original construction information (Table 7, shown previously), which stated that all three SFS FRAP samples were comprised approximately of one-third SFS and two-thirds virgin aggregate.

Tests were also conducted with the SFS removed from the SFS FRAP samples (Figure 32, Figure 33, and Figure 34). The findings are similar to the virgin SFS tests in that the phases present are $Ca(OH)_2$ and $CaCO_3$, the amounts of which are summarized in Table 30. A very small mass loss was also noted for the SFS from SFS FRAP 3 (Figure 34) at around 540°C, which corresponded to an unknown and unidentifiable phase.

Considering that the peaks for dolomite and calcite overlap, the previously-determined dolomite contents of 54.2%, 59.0%, and 68.6% for SFS FRAP 1, SFS FRAP 2, and SFS FRAP 3, respectively, can be adjusted based on the $CaCO_3$ contents determined for the SFS from the SFS FRAP. Assuming the SFS contents of 33%, 33%, and 35% for SFS FRAP 1, SFS FRAP 2, and SFS FRAP 3, respectively, and using the $CaCO_3$ contents from Table 30, the dolomite contents for the SFS FRAP sources were determined to be 53.9%, 58.6%, and 67.8% for SFS FRAP 1, SFS FRAP 2, and SFS FRAP 3, respectively.

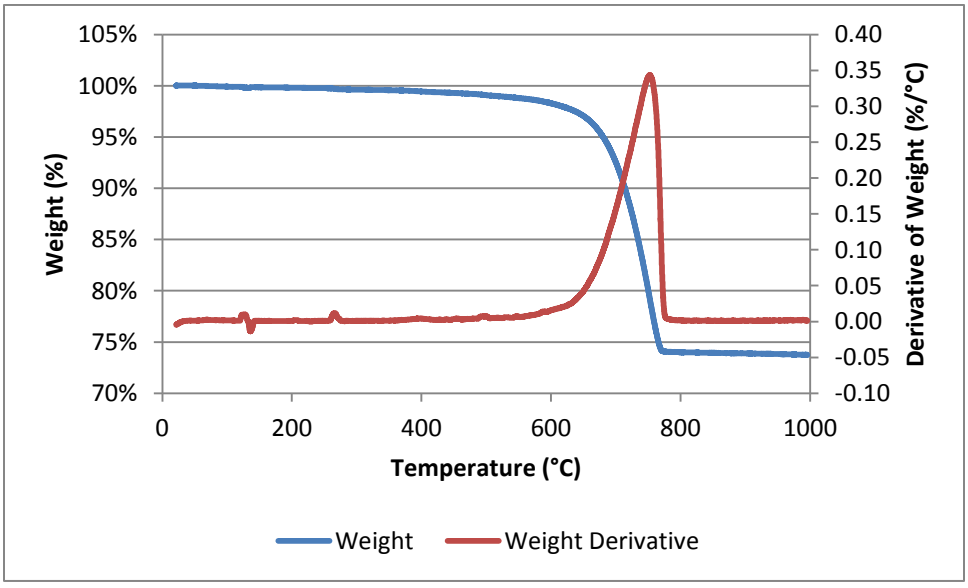

Figure 29. TGA mass loss for SFS FRAP 1 (Curran). The mass percent of dolomite was determined from 595 to 775°C. The event around 125°C appears to be irrelevant, perhaps a slight error with the scale in the TGA. A second event around 260°C could possibly be due to the loss of water of crystallization; the temperature range of the event is too low for it to be $Ca(OH)_2$.

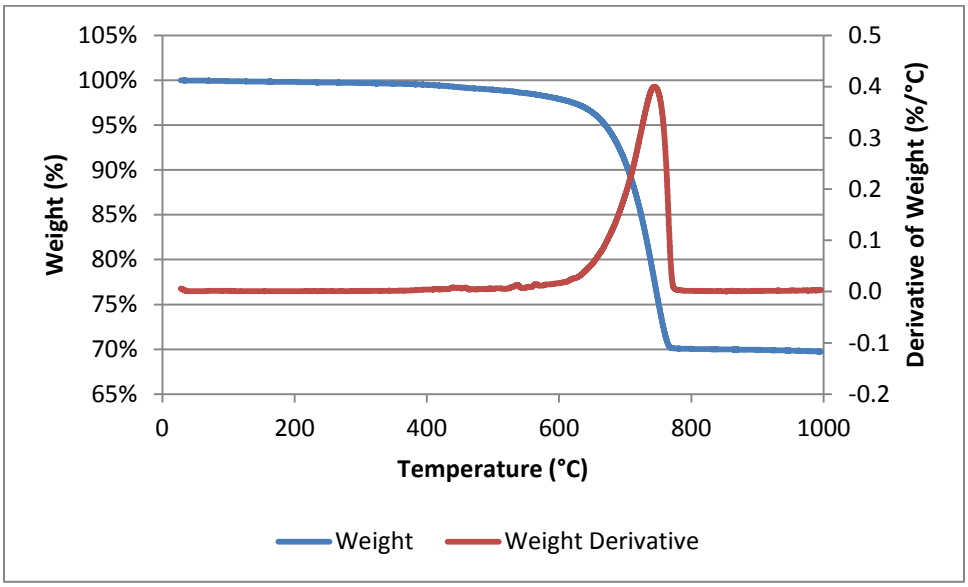

Figure 30. TGA mass loss for SFS FRAP 2 (Geneva). The mass percent of dolomite was determined from 575 to 775°C.

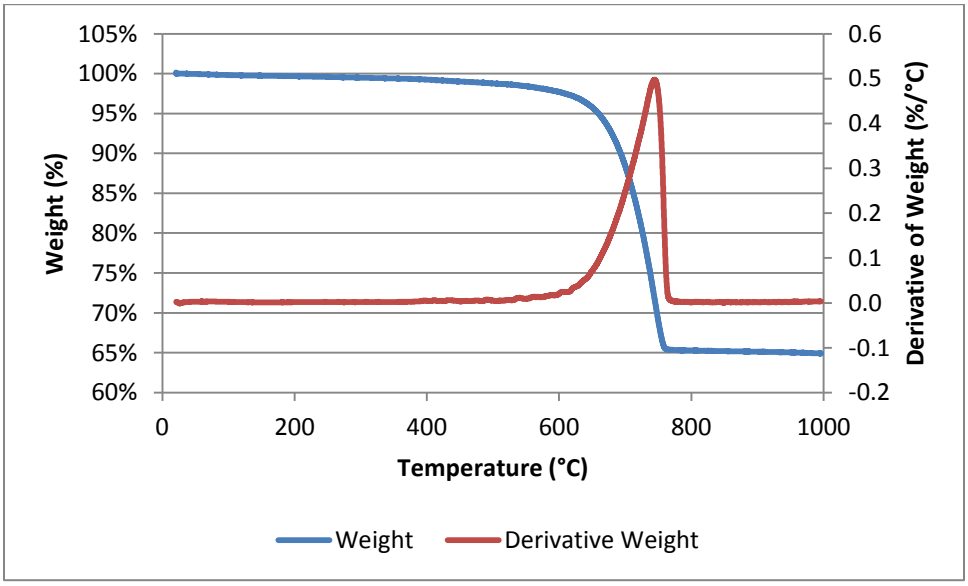

Figure 31. TGA mass loss for SFS FRAP 3 (Central Blacktop). The mass percent of dolomite was determined from 575 to 765°C.

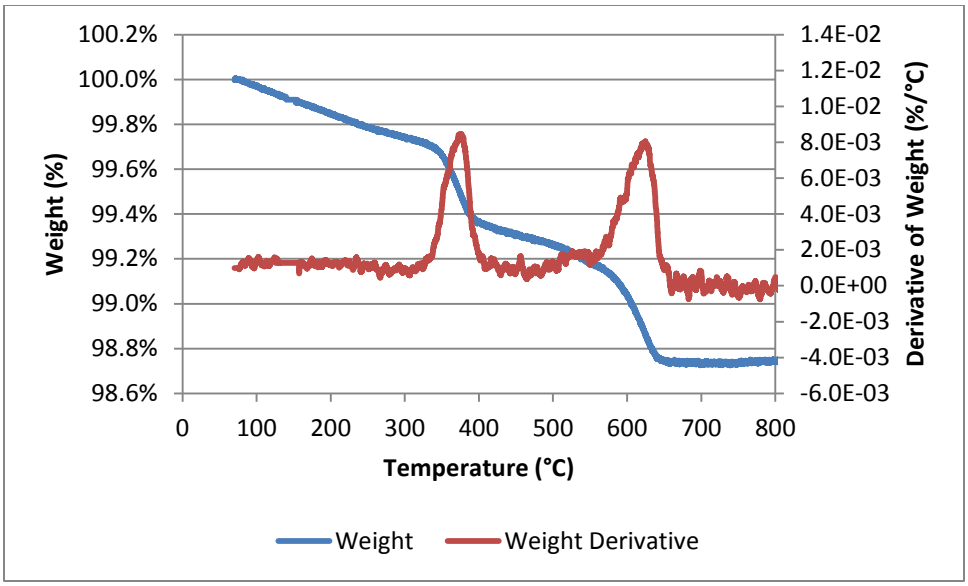

Figure 32. TGA mass loss for the SFS from SFS FRAP 1 (Curran). The mass percent of $Ca(OH)_2$ was determined from 340 to 405°C (peak at 376°C). The mass percent of $CaCO_3$ was determined from 555 to 650°C (peak at 625°C).

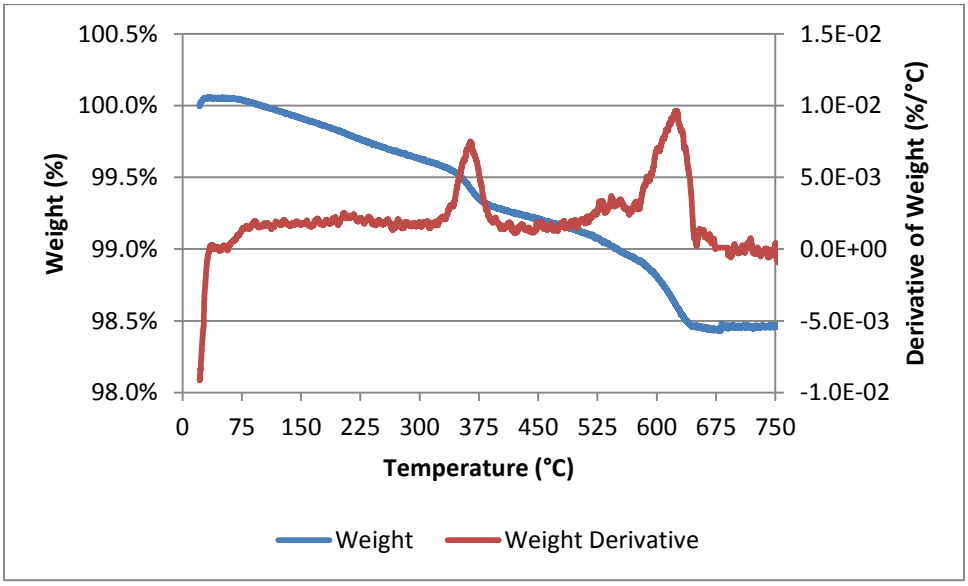

Figure 33. TGA mass loss for the SFS from SFS FRAP 2 (Geneva). The mass percent of $Ca(OH)_2$ was determined from 335 to 390°C (peak at 364°C). The mass percent of $CaCO_3$ was determined from 575 to 645°C (peak at 625°C).

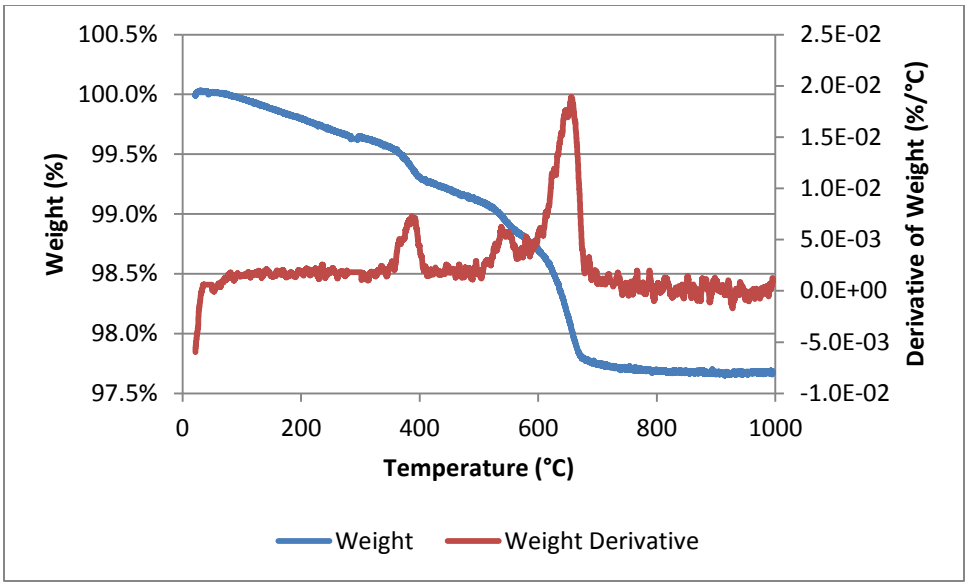

Figure 34. TGA mass loss for the SFS from SFS FRAP 3 (Central Blacktop). The mass percent of $Ca(OH)_2$ was determined from 355 to 415°C (peak at 387°C). The mass percent of $CaCO_3$ was determined from 585 to 680°C (peak at 655°C). An additional peak was found to correspond to the decomposition of some unknown phase from 520 to 565°C (peak at 538°C).

Table 30. $Ca(OH)_2$ and $CaCO_3$ Contents for the Virgin SFS as Determined by TGA

Sample	$Ca(OH)_2$ Content	$CaCO_3$ Content
SFS from SFS FRAP 1 (Curran)	1.39%	0.98%
SFS from SFS FRAP 2 (Geneva)	1.09%	1.05%
SFS from SFS FRAP 3 (Central Blacktop)	1.13%	2.24%

Based on the TGA data for the $Ca(OH)_2$ contents and the EGN values for the SFS from the SFS FRAP samples, the total free CaO content of the SFS from the SFS FRAP was estimated, as shown in Table 31, assuming that the ethylene glycol complexed with 100% of the free $Ca(OH)_2$. Based on this assumption and knowing the initial SFS contents in the SFS FRAP, the total free CaO content of the SFS FRAP was estimated, as shown in Table 32. The estimated total free CaO contents are 1.0% for SFS FRAP 1 and SFS FRAP 2 and 1.5% for SFS FRAP 3.

Table 31. Estimated Total Free CaO Contents for the SFS from the SFS FRAP Samples

Sample	Ethylene Glycol Number (EGN)	$Ca(OH)_2$ Content from TGA	Stoichiometric CaO Content in $Ca(OH)_2$	Estimated Total Free CaO Content*
SFS from SFS FRAP 1 (Curran)	3.99%	1.39%	1.05%	2.94%
SFS from SFS FRAP 2 (Geneva)	3.71%	1.09%	0.82%	2.89%
SFS from SFS FRAP 3 (Central Blacktop)	5.08%	1.13%	0.86%	4.22%

*Assuming that ethylene glycol complexed with 100% of the free $Ca(OH)_2$

Table 32. Estimated Total Free CaO Contents for the SFS FRAP Samples

Sample	Estimated Total Free CaO Content in the SFS*	Estimated SFS Content in the SFS FRAP	Estimated Total Free CaO Content of the SFS FRAP
SFS FRAP 1 (Curran)	2.94%	33%	1.0%
SFS FRAP 2 (Geneva)	2.89%	33%	1.0%
SFS FRAP 3 (Central Blacktop)	4.22%	35%	1.5%

*Assuming that ethylene glycol complexed with 100% of the free $Ca(OH)_2$

3.6 AUTOCLAVE EXPANSION TEST

An autoclave expansion test has been developed by the Edw. C. Levy Co. to quickly and effectively quantify the expansion potential of SFS aggregates. This test is particularly aggressive because it accelerates the hydration of both the free CaO and the free MgO compounds. The test specifies that a sample be subjected to 295±10 psi and 420±5°F for three hours. This test purposely follows the autoclave expansion test used to test for expansion in cement (ASTM C151).

The mold assembly consists of a specimen mold affixed to a base plate. An extension collar is connected to the specimen mold, where a stem and surcharge are placed on top of a compacted sample (Figure 35). The specimen mold measured 3.1 inches (7.9 cm) in diameter by 2.3 inches (5.8 cm) in height. The weight of the stem plus the surcharge was 3.22 pounds (1460 g). The stem was perforated to allow water to enter the sample. The compaction of the sample is similar to ASTM D698, where a 5.50-pound hammer is dropped from a height of 12 inches to compact the aggregate in three lifts with 25 blows per lift. The virgin aggregates were oven dried prior to compaction while the FRAP aggregates were air-dried in a room at 23°C and 50% relative humidity.

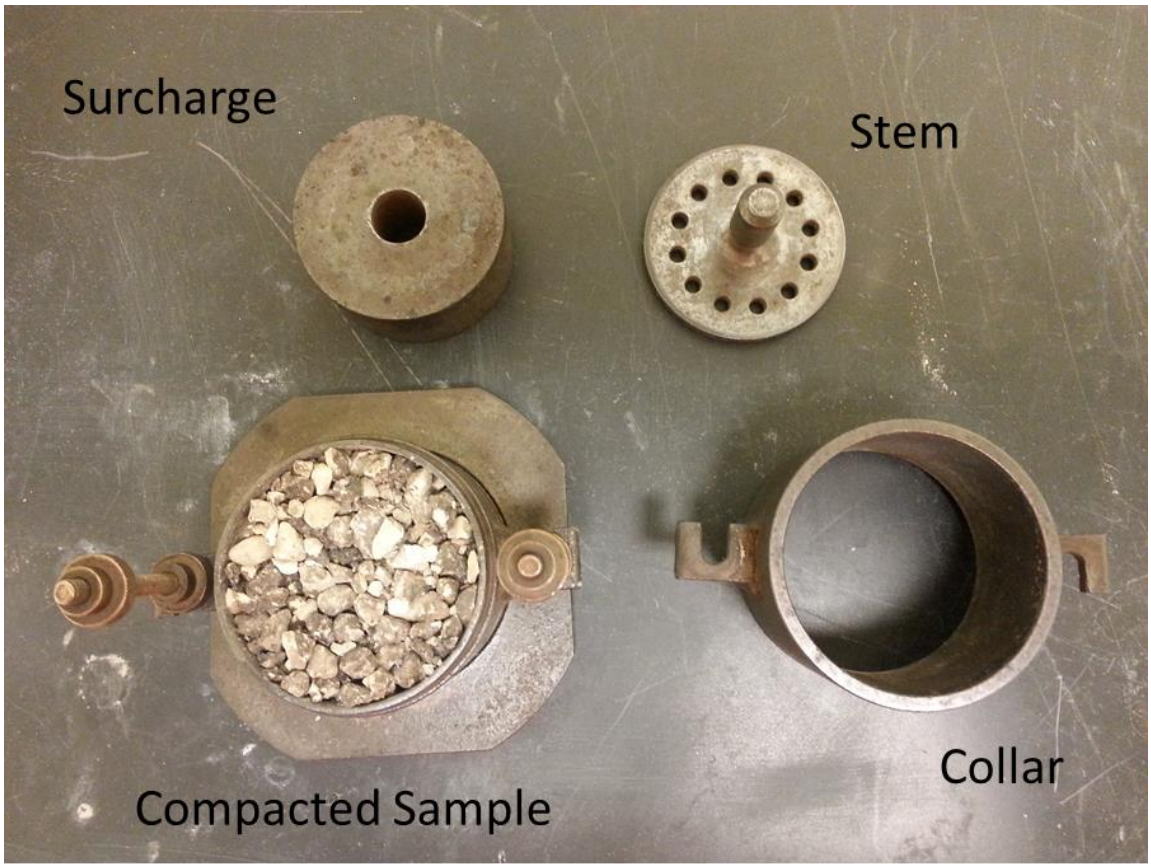

(a)

(b)

Figure 35. Components (a) and completed assembly (b) of the autoclave expansion mold.

One consideration for this test is its effectiveness in hydrating free CaO that has some degree of carbonation in the sample. It has been found that carbonation of CaO particles is on the surface, creating a layer of $CaCO_3$ around an unreacted CaO particle. Song and Kim (1990) found that this layer of $CaCO_3$ delays further CaO hydration, which is dependent on the diffusion of water through the $CaCO_3$ layer and the thickness of the $CaCO_3$ layer. Diffusion is strongly influenced by temperature – by the Arrhenius equation, the diffusion coefficient is a function of *exp(-1/T)* – and is minimally affected by pressure, with slight decreases in the diffusion coefficient as the pressure increases (Mehrer 2007). Therefore, it is expected that the elevated temperatures of the autoclave will not deter diffusion of water through the layer of $CaCO_3$ and to the free CaO particles.

The test procedure stipulated that 600 mL of distilled water be added to the bottom of the autoclave, after which the mold with sample and surcharge added. The temperature and pressure in the autoclave was then brought up to 295±10 psi and 420±5°F, per the manufacturer's instructions, and then held constant for three hours. The autoclave took about 45 minutes to reach the constant 295±10 psi and 420±5°F and around 1.5 hours to cool sufficiently. Once removed from the autoclave, the mold assembly was allowed to cool to room temperature prior to measuring the final height.

The height of the sample was measured before (h_i) and after (h_f) autoclaving, always relative to a reference, which was also measured before (ref_i) and after (ref_f) the sample was autoclaved. A dial gauge attached to a stationary stand was used to determine the specimen height (Figure 36). The percent expansion (e) was then determined relative to the gauge length of the specimen (G, 2.3 inches), which is the height of the compacted aggregate in the mold.

$$e = \frac{\left(h_f - ref_f\right) - \left(h_i - ref_i\right)}{G}\ 100\% \tag{3}$$

Figure 36. Measurement of the height of autoclave expansion mold.

Given that previous studies have shown that gradation can have a significant effect on the expansion results of SFS (Emery 1974, 1977), the gradation was controlled for each of the initial tests so that results from all samples could be directly compared. The maximum packing density gradation was selected for the study, as shown in Table 33, which was based on a 0.45-power curve. The virgin SFS aggregates were oven-dried and then sieved to match this specified gradation.

Table 33. Target Dense Gradation for Autoclave Study

Passing	Retained on	Mass Percent
1/2 in (12.5mm)	3/8 in (9.5mm)	14%
3/8 in (9.5mm)	1/4 in (6.35mm)	17%
1/4 in (6.35mm)	#4 (4.75mm)	10%
#4 (4.75mm)	#8 (2.36mm)	21%
#8 (2.36mm)	#16 (1.18mm)	14%
#16 (1.18mm)	#30 (0.6mm)	9%
#30 (0.6mm)	#50 (0.3mm)	8%
#50 (0.3mm)	#100 (0.15mm)	4%
#100 (0.15mm)	#200 (0.075mm)	3%

The samples with the matched dense gradation (Table 33) were run through the autoclave expansion test. As can be seen in Table 34, the expansion was related to the free CaO content: Virgin SFS 1 (BOF), which had the highest free CaO content, expanded the most, while Virgin SFS 2 (EAF), which had the lowest free CaO content, resulted in virtually no expansion. However, the results of this matched gradation study had significant variability and was not sufficiently repeatable.

Table 34. Autoclave Expansion of Samples with Matched Gradation

Sample	Test No.	Expansion
Virgin SFS 1 (BOF)	1	11.77%
	2	8.26%
Virgin SFS 2 (EAF)	1	-0.20%
	2	0.09%
Virgin SFS 3 (EAF/LMF)	1	3.48%
	2	3.87%

Given that there was some variation in the expansion results of the matched gradation, autoclave tests were conducted with a “monoparticle” size gradation. In these tests, only particles passing the 1/4 inch (6.35 mm) sieve and retained on the #4 (4.75 mm) sieve were used for the uncoated aggregate tests. For the tests with FRAP, only particles passing the 3/8 inch (9.5 mm) sieve and retained on the #4 (4.75 mm) sieve were used. Prior to the testing, all samples were washed to remove dust and finer particles before oven drying (virgin samples) or air drying (FRAP samples). Table 35 shows that the expansion results with the “monoparticle” size gradation were more repeatable than the previous tests. The expansions also related to the free CaO content – the samples with high free CaO content expanded the most. As validation of the autoclave results, dolomite aggregates underwent no expansion with this temperature and pressure.

The “monoparticle” size gradation was also applied to the SFS FRAP samples. Initially the asphalt binder was removed from the FRAP using methylene chloride because of potential hazards of asphalt at elevated temperatures (420°F is near the asphalt ignition temperature, and numerous compounds in the asphalt may vaporize at temperatures below 420°F). The expansions of the SFS FRAP (with binder removed) are shown in Table 35. The results indicate that SFS contained within the FRAP could have potentially deleterious expansive properties if water eventually makes it to the free CaO.

Initial trial tests with SFS FRAP indicated that the FRAP did not compromise the safety of safety of the autoclave, so expansion tests were then carried out with the “monoparticle” size SFS FRAP samples, as shown in

Table 36[*]. The results clearly indicate that the asphalt coating plays a significant role in mitigating the potential expansion of the SFS in the FRAP. The expansion that is measured could be due to the phase transition of β-dicalcium silicate (larnite) to γ-dicalcium silicate (calcio-olivine)[†], as evidenced by the powdery residue of some of the SFS particles noted after autoclaving (see Figure 37). In addition, the high temperature of the autoclave melted some of the asphalt, which appeared to mostly settle at the base of the mold (Figure 38). These two mechanisms likely resulted in the negative expansion (or contraction) that was noted for the SFS FRAP and dolomite FRAP samples. In general, the expansion was minimal for most SFS FRAP samples (Figure 39), resulting in net negative expansions in particular for SFS FRAP 2 (Geneva). Relative to dolomite FRAP, the SFS FRAP expansion (

[*] One note on the performance of FRAP in the autoclave. The asphalt on the FRAP does not fully melt and expose the aggregate; perhaps this is because of the rapid temperature increase, high pressure, and steam. However, the asphalt on the FRAP in the part of the mold that is submerged in the water does melt and accumulate at the base of the mold. Therefore, all of the FRAP expansion tests were conducted by using a spacer to elevate the mold with the FRAP above the water in the bottom of the autoclave. This way, none of the asphalt melted to expose the aggregate.

[†] This phase transition is discussed in further detail in Section 3.6.1.

Table 36) was similar for some cases and greater for others. The dolomite FRAP sources were the “clean” and “dirty” dolomite FRAP with 2.1% and 3.3% asphalt, respectively, from Brand et al. (2012). The other dolomite FRAP with 3.8% asphalt was from Brand et al. (2013).

Table 35. Autoclave Expansion of Uncoated Samples with Monoparticle Size Gradation

Sample	Estimated Free CaO Content	Test No.	Expansion	Average Expansion
Virgin SFS 1 (BOF)	3.4%	1	8.76%	8.8%
		2	8.74%	
Virgin SFS 2 (EAF)	0.1%	1	0.09%	0.1%
		2	0.07%	
		3	0.13%	
Virgin SFS 3 (EAF/LMF)	0.4%	1	0.85%	0.8%
		2	0.83%	
Dolomite	0.0%	1	-0.04%	0.0%
		2	-0.02%	
SFS FRAP 1 (Curran)*	1.0%	1	6.52%	6.6%
		2	6.61%	
SFS FRAP 2 (Geneva)*	1.0%	1	2.22%	2.1%
		2	2.00%	
SFS FRAP 3 (Central Blacktop)*	1.5%	1	4.20%	4.2%
		2	4.28%	

*With asphalt binder removed

Table 36. Autoclave Expansion of FRAP Samples with Monoparticle Size Gradation

Sample*	Test No	Expansion	Average Expansion
SFS FRAP 1 (Curran)	1	-0.83%	-0.8%
	2	-0.39%	
	3	-0.57%	
	4	-1.26%	
SFS FRAP 2 (Geneva)	1	-1.74%	-1.6%
	2	-1.30%	
	3	-1.70%	
	4	-1.78%	
SFS FRAP 3 (Central Blacktop)	1	0.43%	-0.1%
	2	0.35%	
	3	-0.52%	
	4	0.04%	
	5	-0.83%	
“Clean” Dolomite FRAP (2.1% Asphalt)	1	-0.43%	-0.7%
	2	-0.74%	
	3	-0.65%	
	4	-0.70%	
	5	-1.04%	
“Dirty” Dolomite FRAP (3.3% Asphalt)	1	-1.22%	-1.0%
	2	-0.87%	
	3	-1.00%	
	4	-1.09%	
Dolomite FRAP (3.8% Asphalt)	1	-1.57%	-1.6%
	2	-1.26%	
	3	-1.57%	
	4	-1.87%	

*With asphalt binder coating

Figure 37. The SFS particles in the FRAP that disintegrated are circled, which is evidence of the β-dicalcium silicate (larnite) to γ-dicalcium silicate (calcio-olivine) phase transformation.

Figure 38. The base of the mold after autoclaving contains a significant amount of agglomerated asphalt.

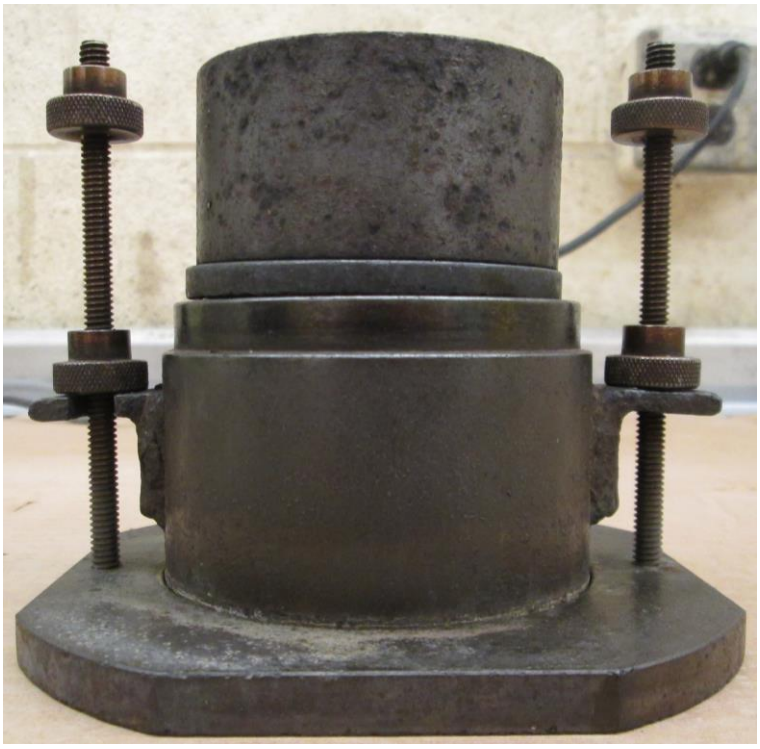

Figure 39. SFS FRAP 3 (Central Blacktop) exhibited little to no expansion after autoclaving.

Table 37 compares the autoclave expansion of the various FRAP samples to the asphalt content and free CaO content of the FRAP. There is small correlation between the average expansion and the approximate free CaO content determined from ethylene glycol extraction. Therefore, it is possible that there is some expansion as a result of the hydration of the free CaO and MgO in the SFS FRAP, but the net expansion is offset by the decrease in volume as the asphalt melts and fills voids and as some of the SFS particles disintegrate because of phase transitions. SFS FRAP 3, which had the highest free CaO content of the three SFS FRAP sources, experienced the least amount of contraction, which suggests some expansion from the free CaO and/or MgO along with contraction because of the asphalt melting and the SFS particle disintegration. SFS FRAP 1 and SFS FRAP 2, which had similarly low free CaO contents, contracted about as much as the “dirty” dolomite FRAP, which indicates that, for these two sources, there was little to no expansion from the hydration of the free CaO and/or free MgO.

Table 37. Comparison Between the Autoclave Expansion and Asphalt Content

FRAP Type	Average Autoclave Expansion	Asphalt Content	Total Estimated Free CaO Content
SFS FRAP 1 (Curran)	-0.8%	3.6%	1.0%
SFS FRAP 2 (Geneva)	-1.6%	3.8%	1.0%
SFS FRAP 3 (Central Blacktop)	-0.1%	3.9%	1.5%
“Clean” Dolomite FRAP	-0.7%	2.1%	0.0%
“Dirty” Dolomite FRAP	-1.0%	3.3%	0.0%
Dolomite FRAP	-1.6%	3.8%	0.0%

Figure 40 demonstrates that the presence of the asphalt coating on the SFS FRAP greatly hindered the expansion. The expansion with asphalt coated particles was less repeatable between replicate tests (i.e. higher standard deviation) compared with samples without the asphalt coating. The higher variability and lack of expansion between tests is because of the differences in the amount of asphalt that melted and filled voids and/or the amount of SFS particles that disintegrated. Without the asphalt coating, the SFS FRAP expansion was significantly greater, as the free CaO and free MgO were allowed to hydrate, although the magnitude of the expansion was not directly proportional to the estimated total free CaO content, which is likely related to the free MgO as well. Therefore, it is suspected that the asphalt coating prevents significant moisture ingress to react with the free CaO and MgO and cause expansion.

SFS FRAP 2 was stockpiled in 2008 after milling (compared with SFS FRAP 1 and 3, which were stockpiled in 2012 after milling). The stockpile weathering may have reduced the expansion of the SFS in the FRAP; compare the expansion of SFS FRAP 2 in Figure 40 with the dolomite FRAP with 3.8% asphalt. Because these two sources experienced similar expansions and had similar asphalt contents, it can be concluded that the SFS in SFS FRAP 2 perhaps did not significantly expand. It is possible that, while stockpiled, the accessible free CaO and/or free MgO hydrated; this would be the CaO and MgO near exposed particle faces (i.e., where there is a lack of asphalt coating). Then, during autoclaving, the remaining free CaO (which is about 1.0%) does not hydrate as it is perhaps hidden by the asphalt coating.

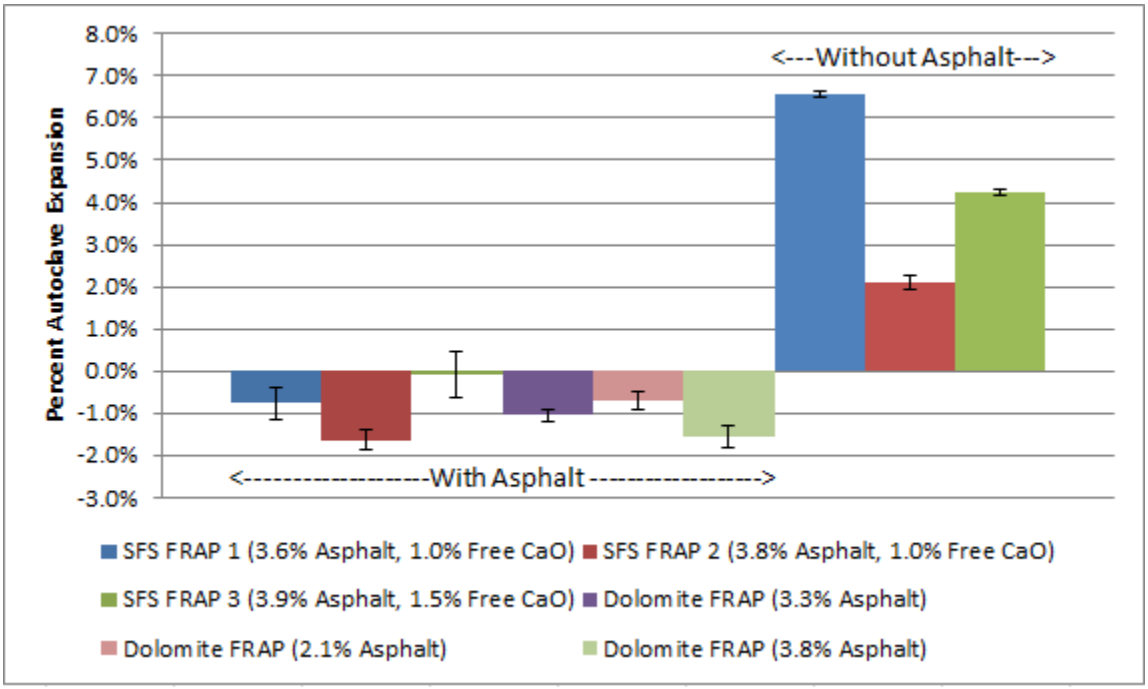

Figure 40. Comparison of the autoclave expansion for the various FRAP sources with and without asphalt coating. Uncoated dolomite aggregates were found to experience zero expansion and is not included. The error bars indicate one standard deviation.

Comparing the autoclave expansion of the six SFS sources (uncoated) to the estimated total free CaO content, there is an increasing expansion amount with increasing free CaO content (Figure 41). There is insufficient data to conclude whether the trend is linearly or quadratically increasing. The MgO content should be considered, as the formation of $Mg(OH)_2$ also causes expansion, but without a test available to estimate the free MgO content, it is not considered in Figure 41. Further testing is required over a range of SFS to further define the relationships in Figure 41 and to potentially include the free MgO content.

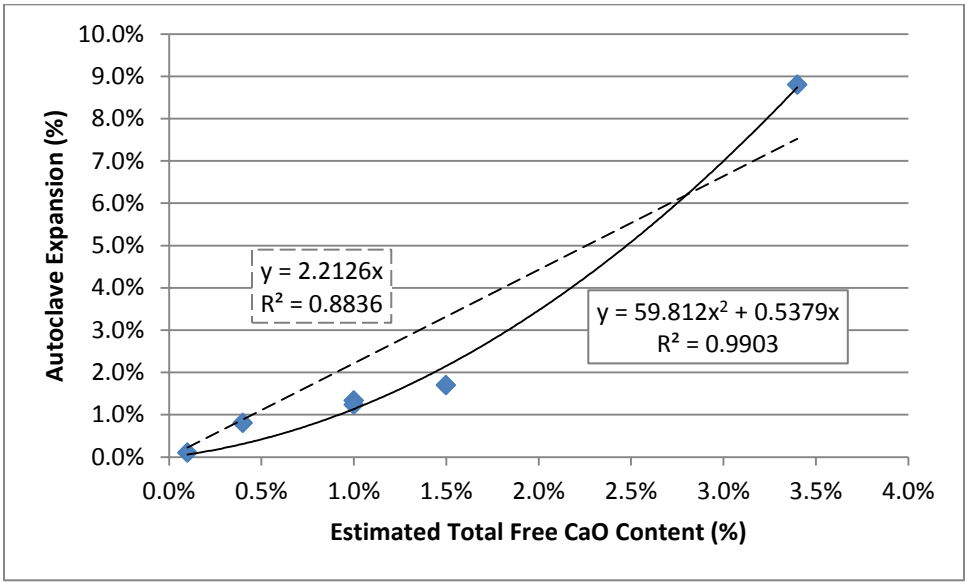

Figure 41. Autoclave expansion for uncoated aggregates versus the free CaO content.

3.6.1 Mineralogy and $Ca(OH)_2$ Content After Autoclaving

After autoclaving, one of the replicate samples of each of the virgin SFS was oven dried, crushed, sieved, and then tested to determine if the mineralogy and $Ca(OH)_2$ contents had changed. The SFS FRAP samples were not tested because the presence of the dolomite would dominate the results of XRD and TGA. In general, the previously identified phases by XRD (such as larnite, wüstite, mayanite) were also identified after autoclaving. However, the newly identified phase in all three virgin SFS samples was a phase transition in the dicalcium silicate from the β (larnite) to the γ (calcio-olivine) form. Typically, β-dicalcium silicate that is the form present in SFS, which is potentially metastable, although in SFS it is relatively nonreactive (Emery 1982). The γ polymorph is less dense than the β form (Taylor 1997), with a volume expansion from the β to the γ form on the order of 12%, based on the unit cell dimensions presented in Taylor (1997). The γ polymorph is the low temperature form of dicalcium silicate, transitioning from the β to the γ form at less than 500°C, but the γ polymorph does not typically occur in portland cement because of the presence of stabilizing ions that prevent the β form from transforming (Taylor 1997). However, γ-dicalcium silicate has been identified by XRD in BOF slags (Gupta et al. 1994; Poh et al. 2006), and in a study of synthetic stainless steel slags, Kriskova et al. (2013) found that a slow cooling rate after heating can result in a phase transition from β- to γ-dicalcium silicate. Chan et al. (1992) found that, in a powder, 10 μm was the critical particle

size below which the transformation from β- to γ-dicalcium silicate will not occur. The cooling of the SFS samples was slow after the autoclaving was finished and it is likely that the particle sizes of dicalcium silicate were larger than 10 μm, so a transition from β- to γ-dicalcium silicate could occur, but it may have only happened upon cooling. The actual expansion from autoclaving will be a combination of the hydration of the free CaO and MgO and, potentially, the dicalcium silicate phase transformation, but if the β- to γ-dicalcium silicate phase transition resulted in the disintegration of a SFS particle, then the net expansion could have been lessened.

By XRD, the mineralogy of virgin SFS 1 (BOF) after autoclaving was similar to the initial material, with the exception of the γ-dicalcium silicate phase (see Figure 42). Both free CaO and calcite ($CaCO_3$) were identified, which suggests that: 1) not all of the free CaO reacted (which is to be expected because the reaction is topochemical, so the CaO at the interior of a particle does not necessarily react), and 2) the $Ca(OH)_2$ that did form from autoclaving may have been carbonated, which is why $CaCO_3$ was identified in the sample and not $Ca(OH)_2$. The TGA analysis produced three distinct main decompositions: $Mg(OH)_2$, $Ca(OH)_2$, and $CaCO_3$ (Figure 43). The amounts of $Mg(OH)_2$ and $Ca(OH)_2$ present after autoclaving were 3.2% and 4.6%, respectively.

Given the very low free CaO content of virgin SFS 2 (EAF), it is likely that the expansion after autoclaving the EAF slag was partly caused by the phase transition of β- to γ-dicalcium silicate (Figure 44). From the TGA plot, evidence of $Mg(OH)_2$, $Ca(OH)_2$, and $CaCO_3$ in the virgin SFS 2 (EAF) after autoclaving (Figure 45) is seen.

Evidence of the β- to γ-dicalcium silicate transition was also noticed in virgin SFS 3 (EAF/LMF), seen in Figure 46, but the expansion was primarily hydration of the free CaO and free MgO in the sample, as seen in the TGA results in Figure 47. In an attempt to deconvolute the peaks between 200 and 400°C, a second TGA test was conducted at 3°C/minute to 500°C (Figure 48), but as can be seen, the peaks were the same. The TGA plot clearly displays the presence of $CaCO_3$ (peak at 635°C in Figure 47). In addition, based on the pure samples of $Ca(OH)_2$ and $Mg(OH)_2$ tested previously, the peaks at 420°C and 375°C were identified as $Ca(OH)_2$ and $Mg(OH)_2$, respectively. The peak at 245°C resembles the peak for the loss of water of crystallization from the $MgCO_3$ sample, so it is assumed that this is what this peak indicates.

A summary of the $Mg(OH)_2$, $Ca(OH)_2$, and $CaCO_3$ contents of the virgin SFS samples after autoclaving is shown in Table 38. Compared with the contents before autoclaving (Figure 49), it is evident that the $Mg(OH)_2$, $Ca(OH)_2$, and $CaCO_3$ contents all increase after autoclaving with the exception of the $CaCO_3$ content for Virgin SFS 2 (EAF). Considering the initial EGN values – which were 4.4%, 0.1%, and 0.5% for Virgin SFS 1 (BOF), 2 (EAF), and 3 (EAF/LMF), respectively, a significant portion (if not all of the free CaO) has hydrated, as the stoichiometric CaO contents from the $Ca(OH)_2$ contents are 3.5%, 0.2%, and 0.5% for Virgin SFS 1 (BOF), 2 (EAF), and 3 (EAF/LMF), respectively.

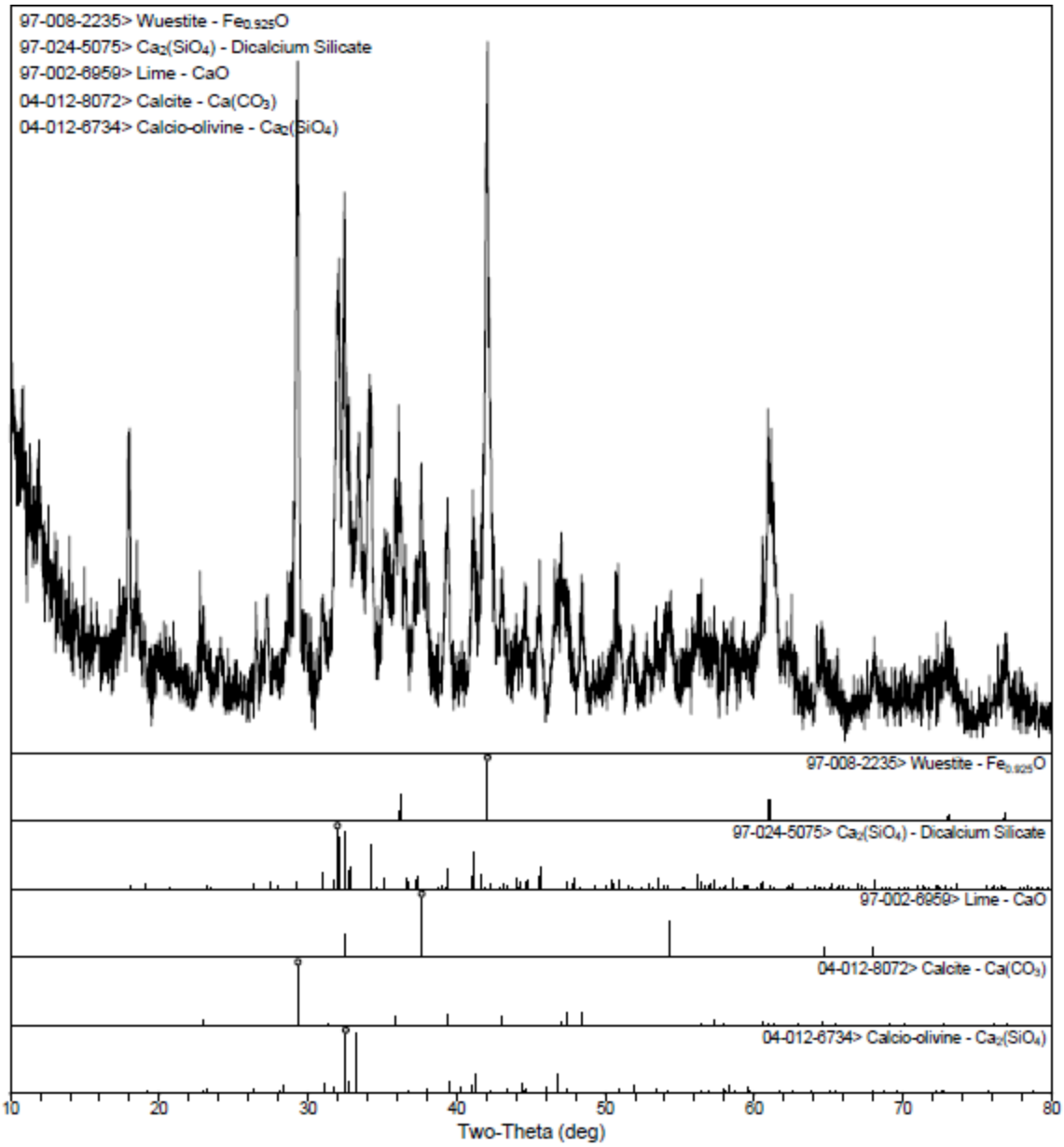

Figure 42. XRD scan and identified phases for Virgin SFS 1 (BOF), ≤150 µm particle size, after autoclaving.

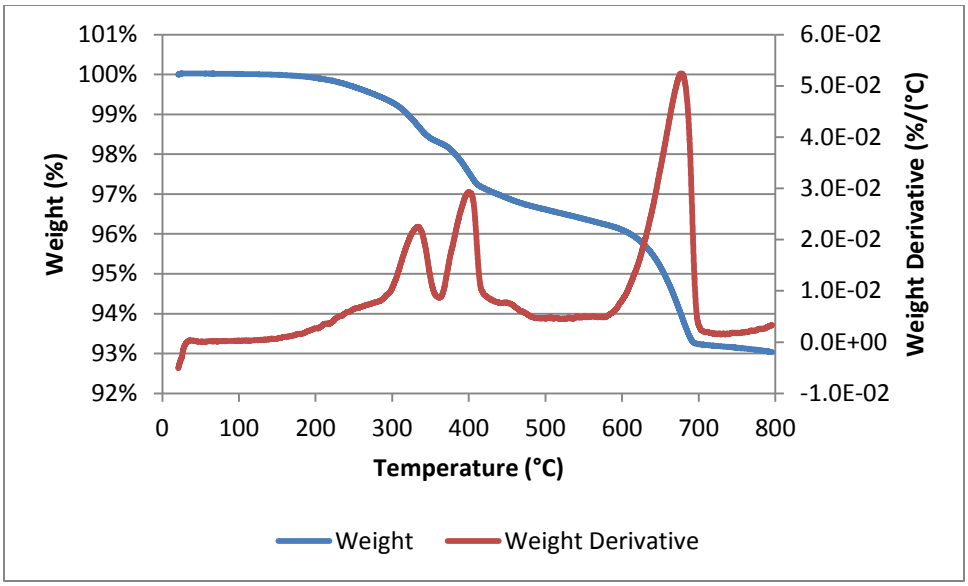

Figure 43. TGA mass loss for Virgin SFS 1 (BOF) after autoclaving. The mass percentages of $Mg(OH)_2$, $Ca(OH)_2$, and $CaCO_3$ were determined from 300 to 360°C (peak at 334°C), 365 to 420°C (peak at 399°C), and 580 to 700°C (peak at 678°C), respectively.

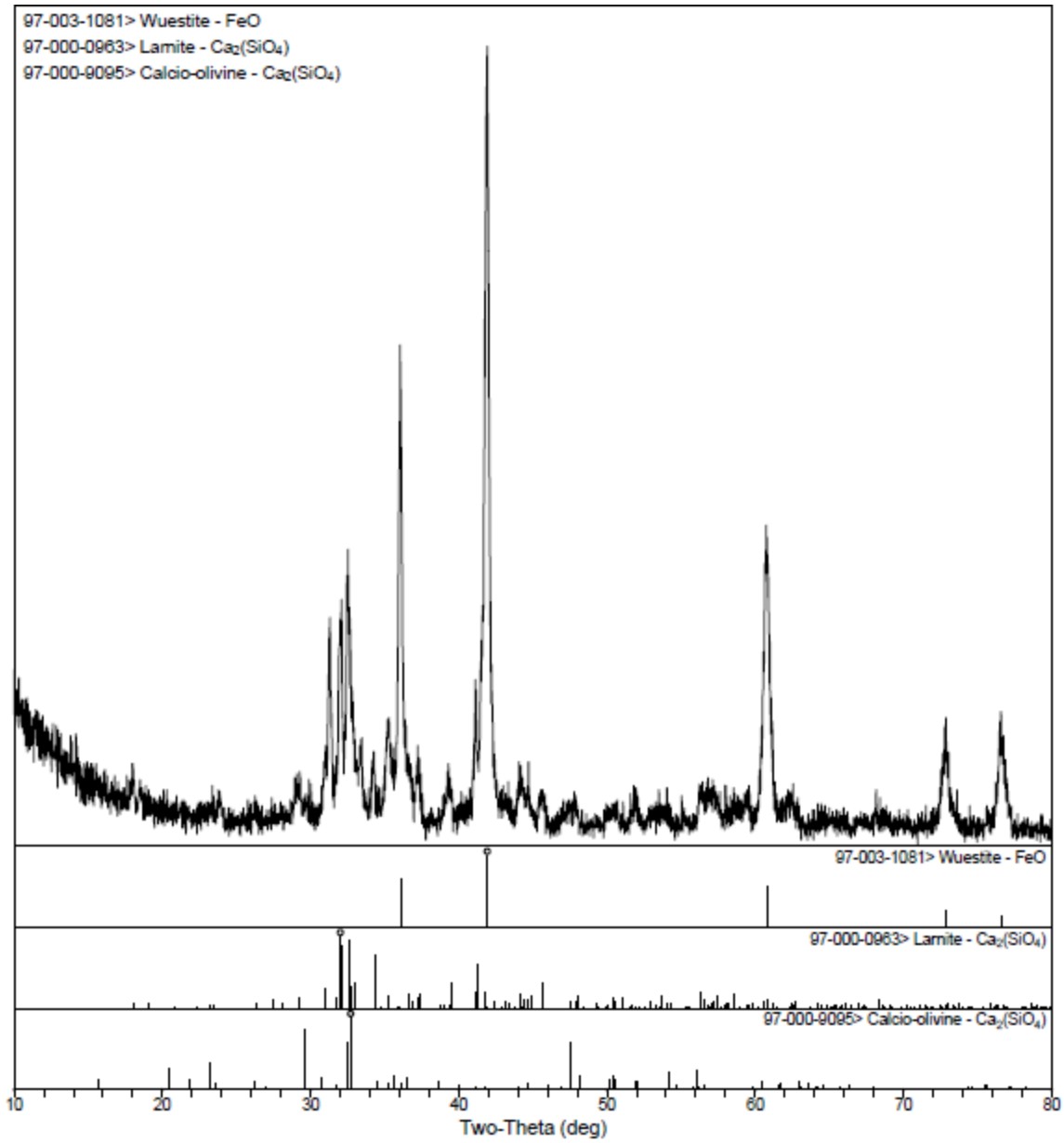

Figure 44. XRD scan and identified phases for Virgin SFS 2 (EAF), ≤150 µm particle size, after autoclaving.

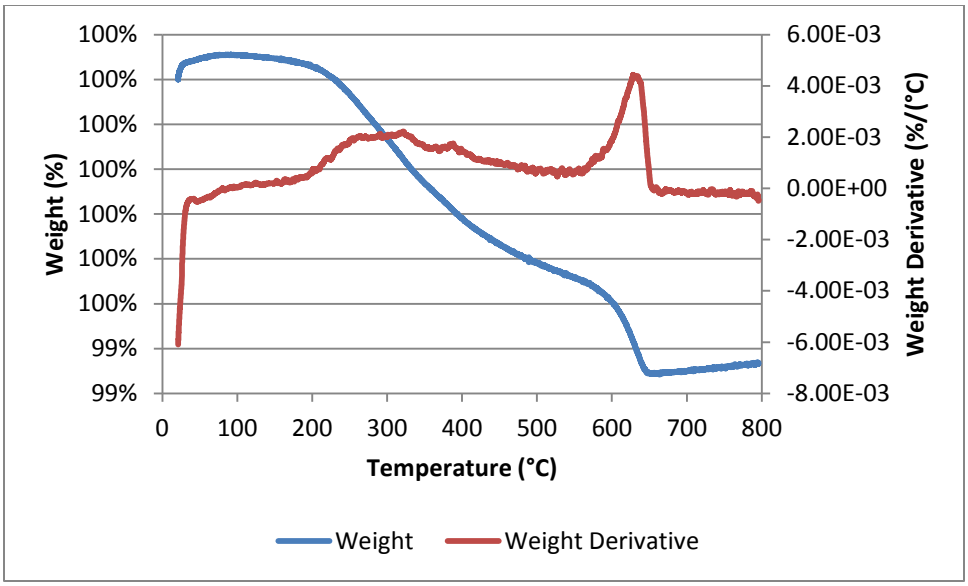

Figure 45. TGA mass loss for Virgin SFS 2 (EAF) after autoclaving. The mass percentages of $Mg(OH)_2$, $Ca(OH)_2$, and $CaCO_3$ were determined from 300 to 340°C (peak at 321°C), 370 to 415°C (peak at 388°C), and 560 to 655°C (peak at 628°C), respectively.

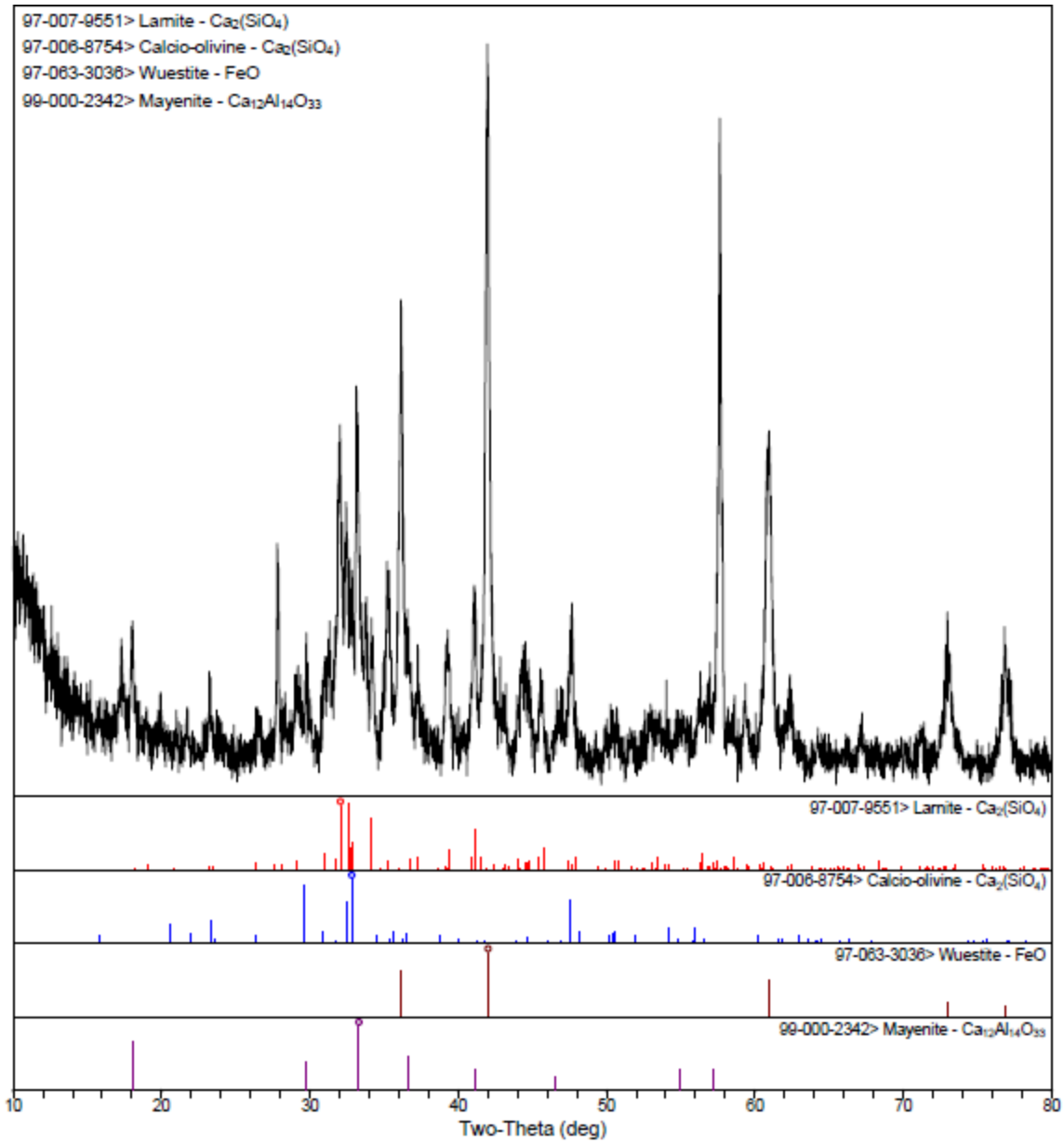

Figure 46. XRD scan and identified phases for Virgin SFS 3 (EAF/LMF), ≤150 µm particle size, after autoclaving.

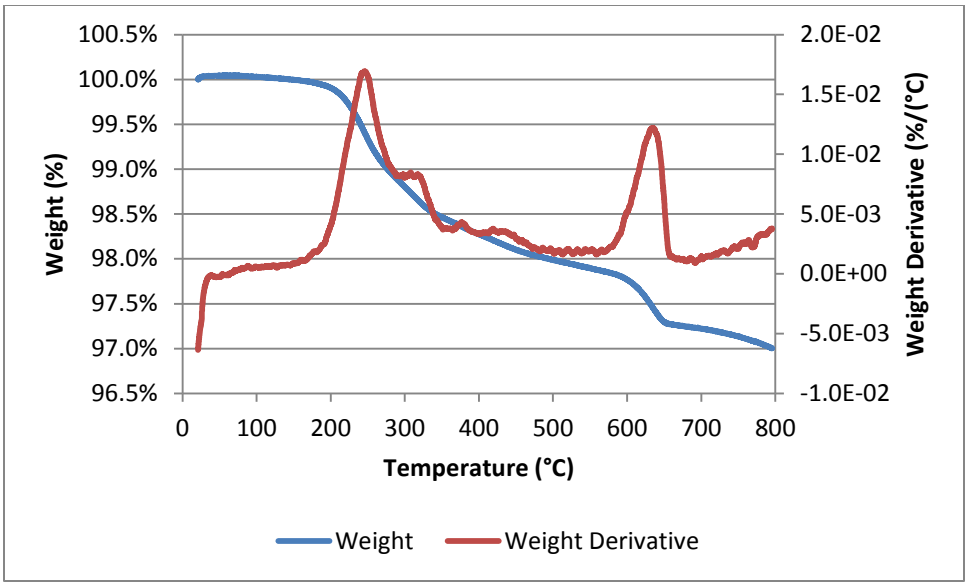

Figure 47. TGA mass loss for Virgin SFS 3 (EAF/LMF) after autoclaving for a heating rate of 10°C/minute. The mass percentages of $Ca(OH)_2$ and $CaCO_3$ were determined from 400 to 445°C (peak at 420°C) and 570 to 660°C (peak at 635°C), respectively. The mass percentage of the $Mg(OH)_2$ was determined from 365 to 400°C (peak at 375°C). The loss of water of crystallization was assumed to be from 180 to 350°C (peak at 245°C).

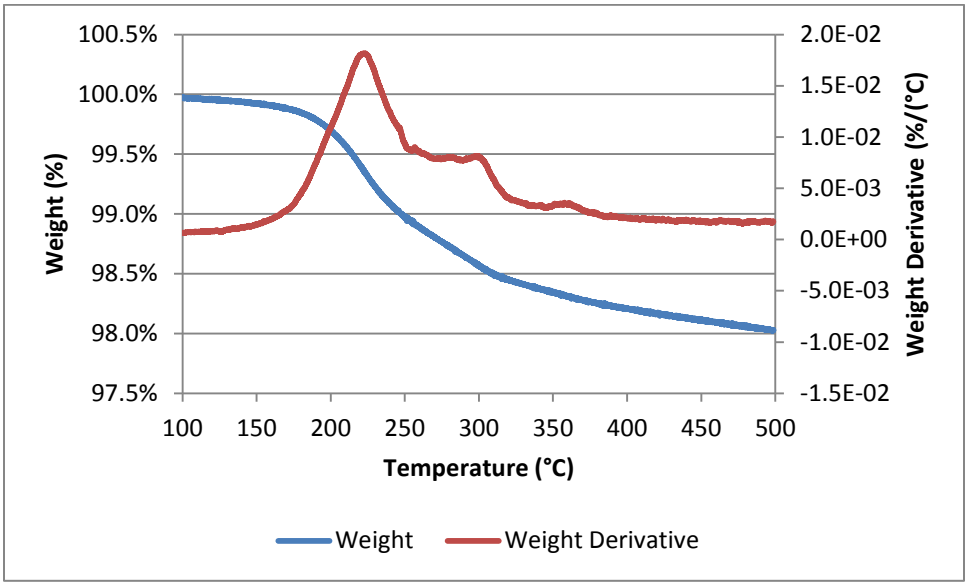

Figure 48. TGA mass loss for Virgin SFS 3 (EAF/LMF) after autoclaving for a heating rate of 3°C/minute.

Table 38. Post-Autoclave Hydroxide and Carbonate Contents Determined by TGA

Sample	$Mg(OH)_2$ Content	$Ca(OH)_2$ Content	$CaCO_3$ Content
Virgin SFS 1 (BOF)	3.23%	4.59%	6.80%
Virgin SFS 2 (EAF)	0.27%	0.28%	0.47%
Virgin SFS 3 (EAF/LMF)	0.43%	0.65%	1.33%

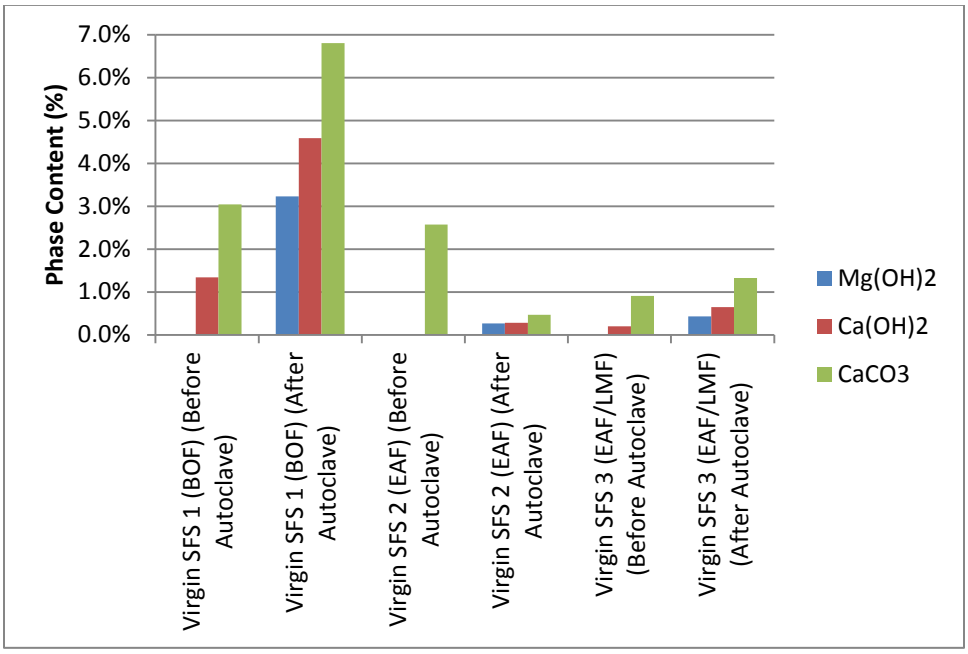

Figure 49. Contents of $Mg(OH)_2$, $Ca(OH)_2$, and $CaCO_3$ before and after autoclaving for the virgin SFS samples.

One final consideration from this post-autoclave analysis is the backcalculation of the initial free MgO content based on the $Mg(OH)_2$ content after autoclaving. As has been previously discussed, there is presently no proposed chemical method to accurately determine the free MgO content of SFS. Assuming that all of the available free MgO in the SFS sample actually hydrated, then the original free MgO content can be estimated, as shown in Table 39, by stoichiometrically converting from $Mg(OH)_2$ to MgO. At the current temperature, pressure, and duration of the autoclaving, it is uncertain if all of the available free MgO did actually hydrate. Further testing and analysis is required for validation, but the concept provides a simple and effective method for the estimation of the free MgO content.

Table 39. Estimated Free MgO Contents of the Virgin SFS Samples

Sample	$Mg(OH)_2$ Content	Estimated Original Free MgO Content*
Virgin SFS 1 (BOF)	3.23%	2.2%
Virgin SFS 2 (EAF)	0.27%	0.2%
Virgin SFS 3 (EAF/LMF)	0.43%	0.3%

*Assuming that all of the available free MgO hydrated from autoclaving

CHAPTER 4 CONCRETE MIX DESIGN

The mix design for the SFS FRAP aggregate followed the same proportions as the previous study with dolomite FRAP aggregates (Brand et al. 2012; Brand and Roesler 2014), which used the IDOT Portland Cement Concrete Technician Level III (IDOT PCC Level III) guide (IDOT 2009). This was done so that the concrete results with SFS FRAP could be compared with the known acceptable performance results with dolomite FRAP. A ternary cementitious blend, which contained 65% Type I portland cement, 25% Grade 100 ground granulated blast furnace slag (GGBFS), and 10% Class C fly ash, was used. The total cementitious content was 630 lb/yd^3 with a water-to-cementitious (w/cm) ratio of 0.37, which is within the IDOT limits of 565 to 705 lb/yd^3 and 0.32 to 0.42, respectively (IDOT 2012). The selected target air content was 6.5%, which is within the allowable range of 5 to 8%, and the mortar factor was selected to be 0.85, which was the middle of the allowable range of 0.70 to 0.90 (IDOT 2012). The other parameters in the mix design formulation are included in Table 40.

Table 40. Parameters for IDOT PCC Level III Mix Design

Cement Factor	6.3 cwt/yd^3
Fine Aggregate Water Requirement	5.3 gal/cwt cement
Coarse Aggregate Water Requirement	0.2 gal/cwt cement
Total Water Requirement	5.5 gal/cwt cement
Water Reduction	-20%
Adjusted Total Water Requirement	4.4 gal/cwt cement
Air Requirement	6.5%
Mortar Factor	0.85
Coarse Aggregate Solids	0.60
Volume Fraction Mortar	0.59

The blended aggregate specific gravity (SG_b) was determined based on the specific gravities of the SFS FRAP (SG_{SF}) and virgin coarse aggregate (SG_v) and the percentage replacements of the virgin coarse aggregate with SFS FRAP (P_{SF}):

$$SG_b = \frac{100}{\frac{P_{SF}}{SG_{SF}} + \frac{1 - P_{SF}}{SG_v}} \quad (4)$$

The blended specific gravity was then used to determine the total coarse aggregate content in the concrete mix design (Table 41). The percent replacement of virgin coarse aggregate by SFS FRAP was then done by weight. These properties were determined using SFS FRAP 3 (Central Blacktop), which was the only SFS FRAP source that was planned for use in multiple concrete property tests (the other SFS FRAP sources were tested for the effect on the concrete strength properties only). While the virgin coarse aggregate meets a CA11 gradation, the blended gradations did not meet the CA11 requirements. The mix with 20%

SFS FRAP does meet the CA11 limits, but the mix with 50% SFS FRAP does not and rather meets the CA9 gradation limits. This failure to meet the CA11 gradation limits is because of the high amount of material passing the #4 sieve (4.75 mm) for SFS FRAP 3, which is nearly 40% (see Table 12). Therefore, for the concrete study, the SFS FRAP 3 was sieved to reduce the amount of material passing the #4 sieve in order to ensure that only coarse SFS FRAP was being added in the concrete. After sieving, the material passing the #4 sieve was less than 10%.

Table 41. Blended Aggregate Specific Gravity and Total Coarse Aggregate Contents

SFS FRAP Amount	0%*	20%	50%
Blended Specific Gravity	2.72	2.72	2.71
Total Coarse Aggregate (lb/yd^3)	1895.4	1892.4	1888.0
SFS FRAP (lb/yd^3)	0.0	378.5	944.0
Virgin Coarse Aggregate (lb/yd^3)	1895.4	1513.9	944.0

*From Brand et al. (2012)

The final mix designs are shown in Table 42. Relative to the previous research (Brand et al. 2012; Brand and Roesler 2014), the mix design is the same except for the total fine aggregate content, which was 1129.6 lb/yd^3 in the previous study. This discrepancy is caused by the slightly different specific gravities of the cementitious materials. For the majority of the concrete tests in this study, the control (0% SFS FRAP) mix results will be from the previous study, but in the tests that were not previously conducted, the concrete will be produced following the mix design in Table 42. Based on the previous study, the chemical admixture dosages were selected to be 1 fluid ounce per 100 pounds of cement for the air-entraining admixture (Grace Daravair 1400) and ranged from 4.0 to 4.5 fluid ounces per 100 pounds of cement for the mid-range water reducing admixture (Grace WRDA 82). The water reducing admixture dosage varied since the previous study (Brand et al. 2012; Brand and Roesler 2014) found that the concrete slump increased with increasing FRAP content, possibly because of the hydrophobicity of the asphalt on the FRAP. Therefore, the water reducing admixture dosage was decreased as the SFS FRAP content increased.

Concrete mixtures with 100% virgin SFS were also created to compare some of the concrete properties with SFS FRAP. The highest potential for deleteriously expansive and the least potential for deleteriously expansive virgin SFS sources were selected for comparison, which were Virgin SFS 1 (BOF) and Virgin SFS 2 (EAF), respectively. As with the other mixtures, the volume of coarse aggregate was constant; the amount of virgin SFS added to the concrete varied, based on the specific gravity. The mix designs can be found in Table 42.

Table 42. Concrete Mix Design Proportions (in lb/yd^3)

	0% SFS FRAP	20% SFS FRAP	50% SFS FRAP	100% Virgin SFS 1 (BOF)	100% Virgin SFS 2 (EAF)
Cement	409.5				
GGBFS	157.5				
Fly Ash	63.0				
Total Coarse Aggregate (SSD)	1895.4	1892.4	1888.0	2322.5	2581.0
Virgin Coarse Aggregate (SSD)	1895.4	378.5	944.0	0.0	0.0
Coarse SFS FRAP (SSD)	0.0	1513.9	944.0	0.0	0.0
Virgin SFS Aggregate (SSD)	0.0	0.0	0.0	2322.5	2581.0
Virgin Fine Aggregate (SSD)	1167.7				
Water	230.9				
Air-Entraining Admixture*	1.0				
Mid-Range Water Reducer*	4.5	4.25	4.0	4.5	4.5

*In fl. oz. per 100 lbs cementitious

The concrete was mixed with a laboratory pan mixer following ASTM C192 (2007). The concrete mix water was adjusted for the moisture content of each aggregate type. The mix water was dosed with the air-entraining admixture while the water reducing admixture was added slowly at the start of the final 3 minutes of mixing. The fresh concrete slump, unit weight, and air content were determined immediately after mixing, after which the concrete molds were filled, covered with plastic, and left to cure at laboratory temperature for 24±4 hours. After the samples were demolded, they were either placed in a moist curing room or dealt with in accordance with the standard for a given testing procedure.

CHAPTER 5 CONCRETE TESTING RESULTS

A number of tests were performed to determine the effect of the SFS FRAP on the fresh and hardened concrete properties. A summary of the tests performed, concrete ages of the tests, and corresponding test standard or method is shown in Table 43.

Table 43. Concrete Tests Performed and Corresponding Standards or Methods

Concrete Test	Age(s) Tested (days)	Standard or Method
Fresh Concrete		
Slump	--	ASTM C143 (2012)
Air Content	--	ASTM C231 (2010)
Unit Weight	--	ASTM C138 (2013)
Hardened Concrete		
Compressive Strength	3, 7, 14, 28, and 90	AASHTO T22 (2007)
Split Tensile Strength	3, 7, 14, 28, and 90	AASHTO T198 (2009)
Flexural Strength	28	AASHTO T97 (2003)
Modulus of Elasticity	28	ASTM C469 (2010)
Fracture Properties	28	Jenq and Shah (1985); RILEM TC89-FMT (1990); Hillerborg (1985)
Drying Shrinkage	1 to 150	AASHTO T160 (2009)
Freeze/Thaw Durability	14 (Started)	AASHTO T161 (2008)

5.1 CONCRETE FRESH PROPERTIES

Because a large number of samples were created, several pans of concrete needed to be mixed per mixture. Thus, the fresh properties of each concrete mix produced are summarized in Table 44. As can be seen, the unit weight of the concretes with 20% and 50% SFS FRAP was often similar, which is expected because the specific gravity of the SFS FRAP and the virgin coarse aggregate were about the same. The air content and slump did not appear to be greatly affected by the SFS FRAP. As expected, the mixtures with virgin SFS had relatively high unit weights, because of the high specific gravity of the aggregate, and the slump and air content did not appear to be significantly influenced by the SFS.

Table 44. Concrete Fresh Properties for Each Mix Produced

Concrete Mix	SFS FRAP Content	Slump (in)	Air Content (%)	Unit Weight (lb/ft^3)
Trial Compression	20%	2-1/2	6.1	145.4
	50%	2	6.0	144.4
Compressive and Split Tensile Strength	20%	1-1/4	5.4	146.8
	50%	1-1/4	5.2	148.0
Flexural Strength and Free Shrinkage	20%	1	5.5	150.4
	50%	1	5.4	149.8
Flexural Strength #2	20%	2	7.5	145.4
	50%	2-1/2	7.0	145.0
Fracture	20%	2	6.6	146.8
	50%	2-1/2	6.8	147.0
Freeze/Thaw and Modulus	20%	1-1/2	5.6	149.4
	50%	1-1/4	5.5	150.2
Freeze/Thaw, Split Tension, Compression	100% BOF	1/2	5.5	164.8
	100% EAF	1	5.5	173.8
Fracture and Free Shrinkage	0%	3-1/4	6.8	140.0
	100% BOF	3	6.4	157.8
	100% EAF	1-1/4	6.3	168.2

5.2 TRIAL STUDY

An initial trial study was conducted to see the effects of the SFS FRAP on the compressive strength. This initial mix was created with the as-received SFS FRAP 3 material, so it contained the significant amount of material passing the #4 sieve. The average of three tests is reported in Table 45 and Figure 50, also indicating the standard deviation and coefficient of variation (COV). The results with 20 and 50% SFS FRAP are compared with the previous study with virgin aggregates and dolomite FRAP (Brand et al. 2012; Brand and Roesler 2014). As can be seen, the SFS FRAP results are similar to the dolomite FRAP results.

Table 45. Compressive Strength Results of the Trial Study Relative to Dolomite FRAP

Mix	Age	1	2	3	Average	COV
Control (0% FRAP)*	7	3807	4221	4074	**4034**	5.2%
	14	5583	5201	5596	**5460**	4.1%
	28	6814	6776	6449	**6680**	3.0%
20% SFS FRAP	7	3597	3574	3569	**3580**	0.4%
	14	4307	4526	4680	**4504**	4.2%
	28	5073	5217	5335	**5208**	2.5%
20% Dolomite FRAP*	7	3519	3311	3193	**3341**	4.9%
	14	4656	4730	4483	**4623**	2.7%
	28	5357	5363	5455	**5391**	1.0%
50% SFS FRAP	7	2938	2919	2933	**2930**	0.3%
	14	3589	3649	3640	**3626**	0.9%
	28	4172	4107	4224	**4168**	1.4%
50% Dolomite FRAP*	7	3018	3050	2842	**2970**	3.8%
	14	3624	3448	3396	**3489**	3.4%
	28	3977	3885	4304	**4055**	5.4%

*Results from Brand et al. (2012)

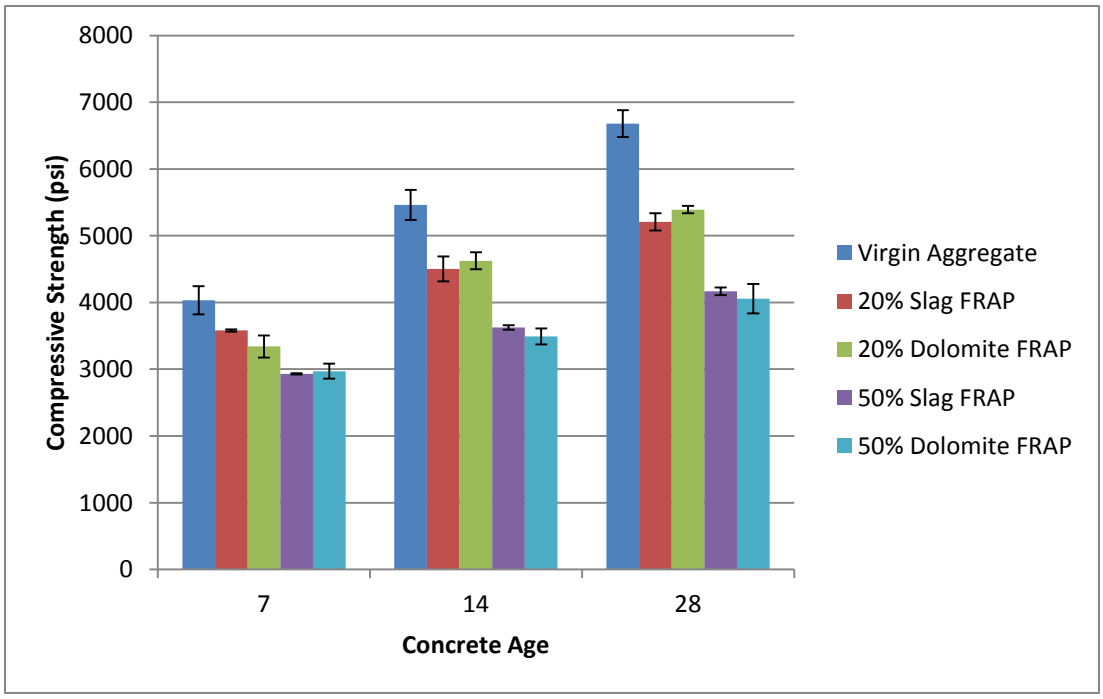

Figure 50. Compressive strength of trial study cylinders compared with virgin aggregate and dolomite FRAP results. Note: error bars indicate one standard deviation.

5.3 COMPRESSIVE STRENGTH

The compressive strength was evaluated at 3, 7, 14, 28, and 90 days with an average of three specimens. The specimens were tested for the peak load (*P*), which was converted to the compressive strength (σ_c), where *D* is the diameter of the specimen (4 inches):

$$\sigma_c = \frac{P}{\frac{\pi}{4} D^2} \tag{5}$$

As can be seen in Figure 51 and Table 46, the compressive strength of concrete with SFS FRAP is similar to concrete with dolomite FRAP. A similar trend is followed with decreasing compressive strength with increasing SFS FRAP content. Comparing concrete with virgin SFS and SFS FRAP (Figure 52), concrete with EAF slag aggregate can attain a higher compressive strength than dolomite aggregate, possibly because of the finer gradation, while the concrete with 100% BOF slag aggregate reached a compressive strength that was similar to the mix with 20% SFS FRAP. This behavior of concrete with virgin SFS aggregates agrees with the literature review (Table 4).

A t-test for statistical significance (Table 47) revealed that at early ages (3, 7, and 14 days), the compressive strengths of SFS FRAP were mostly statistically greater than the dolomite FRAP, but at later ages (28 and 90 days) the mixes were not statistically different. Therefore, the long-term compressive strength of concrete containing FRAP was not affected by the SFS in the FRAP.

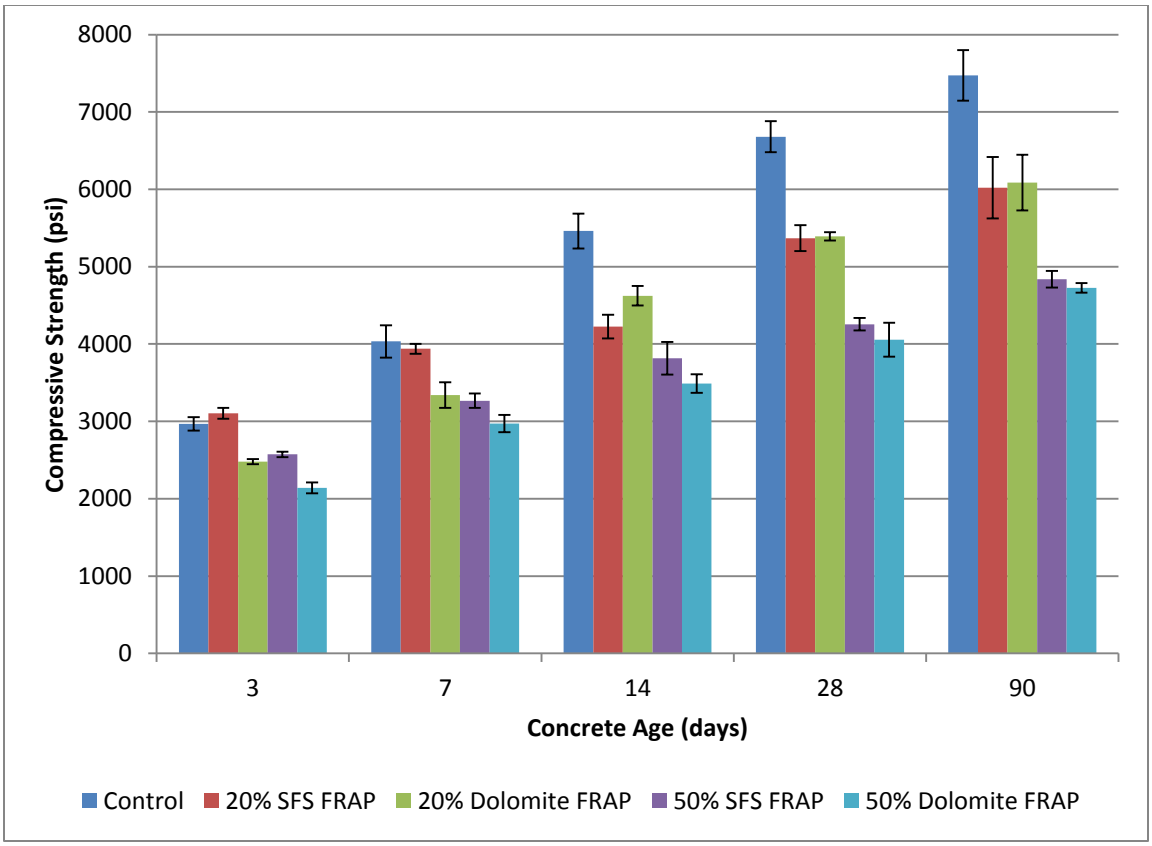

Figure 51. Average compressive strength of concrete with SFS FRAP relative to the control (0% FRAP) and dolomite FRAP concrete mixes. Error bars indicate one standard deviation.

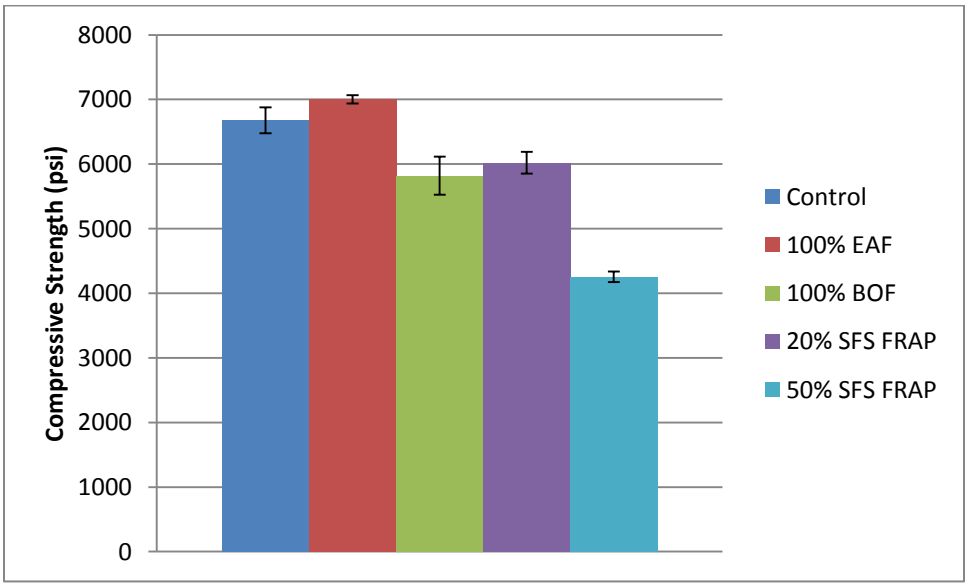

Figure 52. Average compressive strength at 28 days comparing concretes with 100% dolomite (control), 100% EAF, 100% BOF, and 20% and 50% SFS FRAP as coarse aggregate.

Table 46. Average Compressive Strength (psi) for SFS FRAP and Dolomite FRAP

Concrete Mix	Age (days)	SFS FRAP					Dolomite FRAP*	
		1	2	3	Average	COV	Average	COV
0% FRAP	3	--	--	--	--	--	2968	3.0%
	7	--	--	--	--	--	4034	5.2%
	14	--	--	--	--	--	5460	4.1%
	28	--	--	--	--	--	6680	3.0%
	90	--	--	--	--	--	7473	4.4%
20% FRAP	3	3169	3032	3110	3104	2.2%	2480	1.3%
	7	3868	3992	3955	3938	1.6%	3341	4.9%
	14	4049	4318	4312	4226	3.6%	4623	2.7%
	28	5531	5196	5377	5368	3.1%	5391	1.0%
	90	6329	6158	5572	6020	6.6%	6087	5.9%
50% FRAP	3	2600	2584	2535	2573	1.3%	2141	3.3%
	7	3350	3283	3166	3266	2.9%	2970	3.8%
	14	3933	3942	3572	3816	5.5%	3489	3.4%
	28	4350	4221	4197	4256	1.9%	4055	5.4%
	90	4741	4815	4954	4837	2.2%	4725	1.3%
100% Virgin SFS 1 (BOF)	28	6147	5750	5568	5822	5.1%	--	--
100% Virgin SFS 2 (EAF)	28	7078	6968	6962	7003	0.9%	--	--

*Source: Brand et al. (2012)

Table 47. Statistical Significance Testing for Concrete Compressive Strength with SFS FRAP and Dolomite FRAP

Mix	Age (days)	Compressive Strength (psi)					Pooled Standard Deviation	t-test	p-value
		1	2	3	Average	Standard Deviation			
20% SFS FRAP	3	3169	3032	3110	3104	68.62	--	--	--
20% D-FRAP	3	2456	2516	2466	2480	32.12	2870	14.27	0.00014
20% SFS FRAP	7	3868	3992	3955	3938	63.76	--	--	--
20% D-FRAP	7	3519	3311	3193	3341	164.90	15629	5.85	0.00425
20% SFS FRAP	14	4049	4318	4312	4226	153.55	--	--	--
20% D-FRAP	14	4656	4730	4483	4623	126.78	19826	-3.45	0.0260
20% SFS FRAP	28	5531	5196	5377	5368	167.77	--	--	--
20% D-FRAP	28	5357	5363	5455	5391	54.79	15574	-0.23	0.831
20% SFS FRAP	90	6329	6158	5572	6020	396.89	--	--	--
20% D-FRAP	90	5857	6502	5900	6087	360.63	143788	-0.22	0.840
Mix	Age (days)	Compressive Strength (psi)					Pooled Standard Deviation	t-test	p-value
		1	2	3	Average	Standard Deviation			
50% SFS FRAP	3	2600	2584	2535	2573	33.62	--	--	--
50% D-FRAP	3	2091	2110	2222	2141	70.58	3056	9.57	0.00067
50% SFS FRAP	7	3350	3283	3166	3266	93.10	--	--	--
50% D-FRAP	7	3018	3050	2842	2970	111.95	10600	3.53	0.0243
50% SFS FRAP	14	3933	3942	3572	3816	210.82	--	--	--
50% D-FRAP	14	3624	3448	3396	3489	119.59	29374	2.33	0.0801
50% SFS FRAP	28	4350	4221	4197	4256	82.20	--	--	--
50% D-FRAP	28	3977	3885	4304	4055	220.10	27600	1.48	0.214
50% SFS FRAP	90	4741	4815	4954	4837	107.82	--	--	--
50% D-FRAP	90	4795	4685	4696	4725	60.67	7653	1.56	0.193

D-FRAP = Dolomite FRAP

5.3 SPLIT TENSILE STRENGTH

The split tensile strength was evaluated at 3, 7, 14, 28, and 90 days with an average of three specimens. The peak load was measured and converted to the split tensile strength (σ_{sp}), where L is the length of the specimen (8 inches):

$$\sigma_{sp} = \frac{2P}{\pi LD} \tag{6}$$

The concrete split tensile strength also showed similar behavior between the SFS FRAP and dolomite FRAP concretes, as shown in Figure 53 and Table 48. A decreasing trend in the split tensile strength was observed with increasing SFS FRAP content. Concrete with virgin SFS had lower split tensile strengths than the control mix with dolomite coarse aggregate (Figure 54).

A t-test for statistical significance (Table 49) showed that the split tensile strengths were not statistically different between the SFS FRAP and dolomite FRAP mixes, with the exception of the early age (3 and 7 days) results for the 50% FRAP mixes. Images of the fracture surfaces can be seen in Figure 55 and Figure 56. These findings suggest that the presence of SFS in the FRAP does not affect the bonding between the asphalt on the FRAP and the cementitious matrix of the concrete. However, there is some evidence that the bonding is stronger between dolomite and the cementitious matrix compared with between the virgin SFS types (BOF and EAF) and the cementitious matrix, but these sources had different gradations, porosities, and particle angularities, which could also affect the strength.

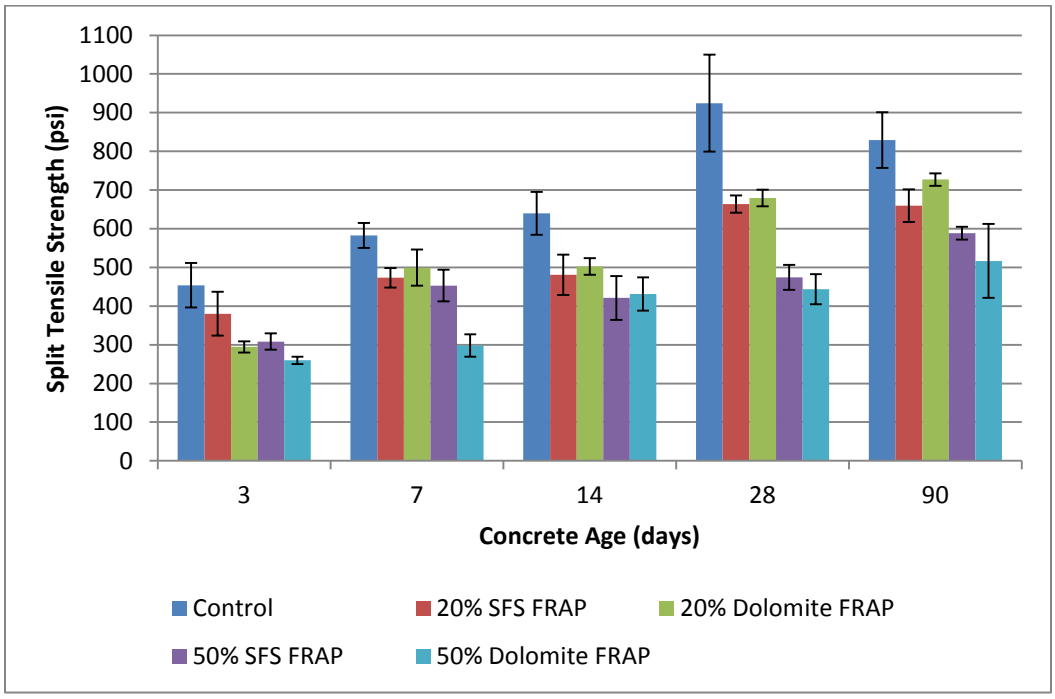

Figure 53. Average split tensile strength of concrete with SFS FRAP relative to the control (0% FRAP) and dolomite FRAP concrete mixes. Error bars indicate one standard deviation.

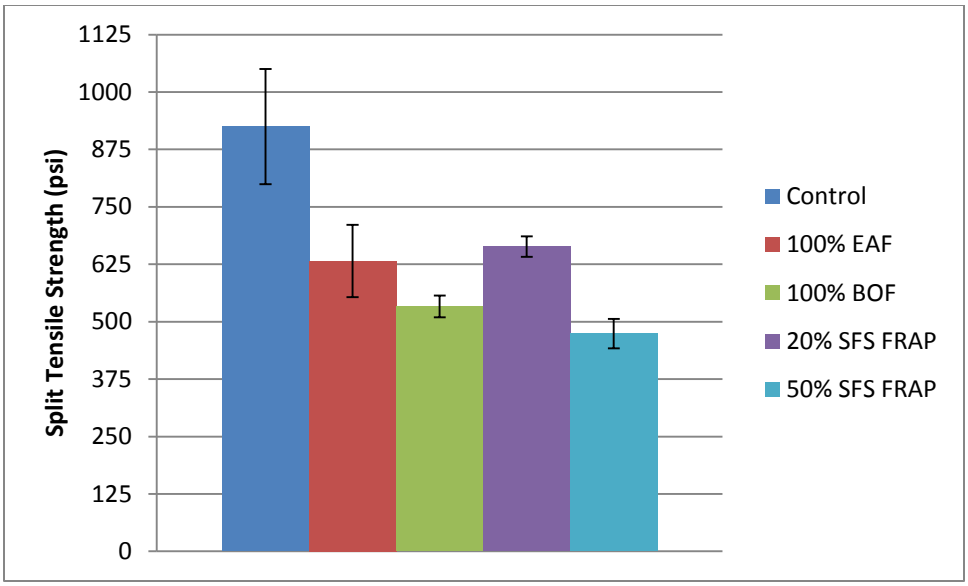

Figure 54. Average split tensile strength at 28 days comparing concretes with 100% dolomite (control), 100% EAF, 100% BOF, and 20% and 50% SFS FRAP as coarse aggregate.

Table 48. Average Split Tensile Strength (psi) for SFS FRAP and Dolomite FRAP

Concrete Mix	Age (days)	SFS FRAP					Dolomite FRAP*	
		1	2	3	Average	COV	Average	COV
0% FRAP (Control)	3	--	--	--	--	--	454	12.7%
	7	--	--	--	--	--	583	5.6%
	14	--	--	--	--	--	640	8.7%
	28	--	--	--	--	--	925	13.6%
	90	--	--	--	--	--	829	8.7%
20% FRAP	3	321	434	385	380	14.9%	295	4.9%
	7	463	502	454	473	5.3%	499	9.4%
	14	526	493	424	481	10.8%	502	4.3%
	28	662	642	687	664	3.4%	679	3.2%
	90	644	707	627	659	6.4%	727	2.2%
50% FRAP	3	331	305	289	308	6.7%	260	3.8%
	7	498	418	443	453	9.0%	298	9.7%
	14	486	398	380	421	13.5%	432	10.0%
	28	504	478	440	474	6.8%	443	8.7%
	90	570	596	600	589	2.8%	517	18.4%
100% Virgin SFS 1 (BOF)	28	560	524	516	533	4.4%	--	--
100% Virgin SFS 2 (EAF)	28	594	723	580	632	12.5%	--	--

*Source: Brand et al. (2012)

Table 49. Statistical Significance Testing for Concrete Split Tensile Strength with SFS FRAP and Dolomite FRAP

Mix	Age (days)	Split Tensile Strength (psi)					Pooled Standard Deviation	t-test	p-value
		1	2	3	Average	Standard Deviation			
20% SFS FRAP	3	321	434	385	380	56.7	--	--	--
20% D-FRAP	3	305	284	-	295	14.5	2210	1.99	0.140
20% SFS FRAP	7	463	502	454	473	25.1	--	--	--
20% D-FRAP	7	528	524	445	499	46.7	1406	-0.86	0.440
20% SFS FRAP	14	526	493	424	481	52.1	--	--	--
20% D-FRAP	14	526	497	483	502	21.5	1586	-0.64	0.555
20% SFS FRAP	28	662	642	687	664	22.3	--	--	--
20% D-FRAP	28	704	669	664	679	21.7	484	-0.87	0.434
20% SFS FRAP	90	644	707	627	659	42.3	--	--	--
20% D-FRAP	90	719	746	717	727	16.0	1023	-2.59	0.061

Mix	Age (days)	Split Tensile Strength (psi)					Pooled Standard Deviation	t-test	p-value
		1	2	3	Average	Standard Deviation			
50% SFS FRAP	3	331	305	289	308	20.8	--	--	--
50% D-FRAP	3	258	251	270	260	9.8	264	3.67	0.0214
50% SFS FRAP	7	498	418	443	453	41.0	--	--	--
50% D-FRAP	7	265	315	315	298	28.9	1255	5.35	0.00588
50% SFS FRAP	14	486	398	380	421	56.8	--	--	--
50% D-FRAP	14	462	450	382	432	43.0	2539	-0.25	0.812
50% SFS FRAP	28	504	478	440	474	32.3	--	--	--
50% D-FRAP	28	401	477	452	443	38.7	1270	1.05	0.352
50% SFS FRAP	90	570	596	600	589	16.5	--	--	--
50% D-FRAP	90	584	559	408	517	95.3	4680	1.29	0.267

D-FRAP = Dolomite FRAP

(a) 20% SFS FRAP

(b) 50% SFS FRAP

Figure 55. Images of the split tension fracture surfaces for concrete with (a) 20% SFS FRAP and (b) 50% SFS FRAP.

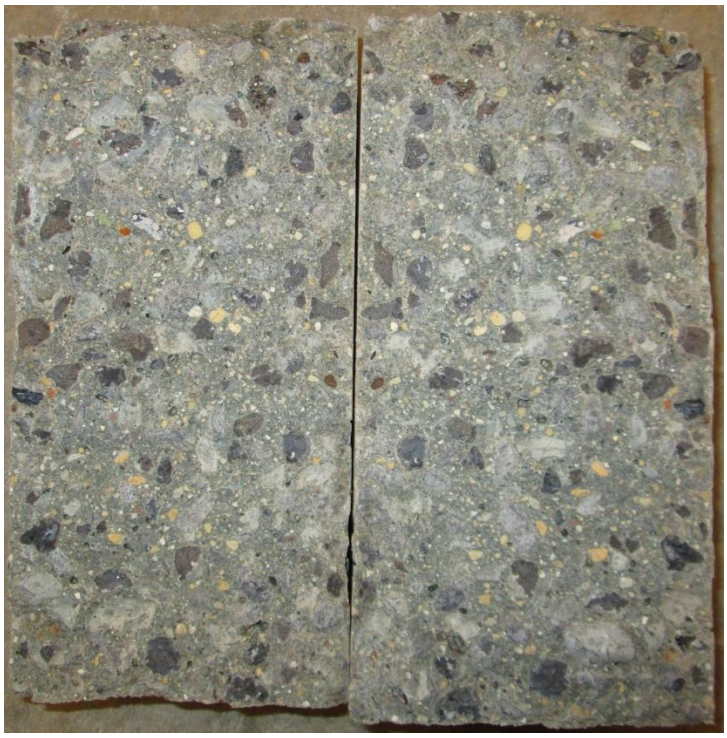

(a) 100% Virgin SFS 1 (BOF)

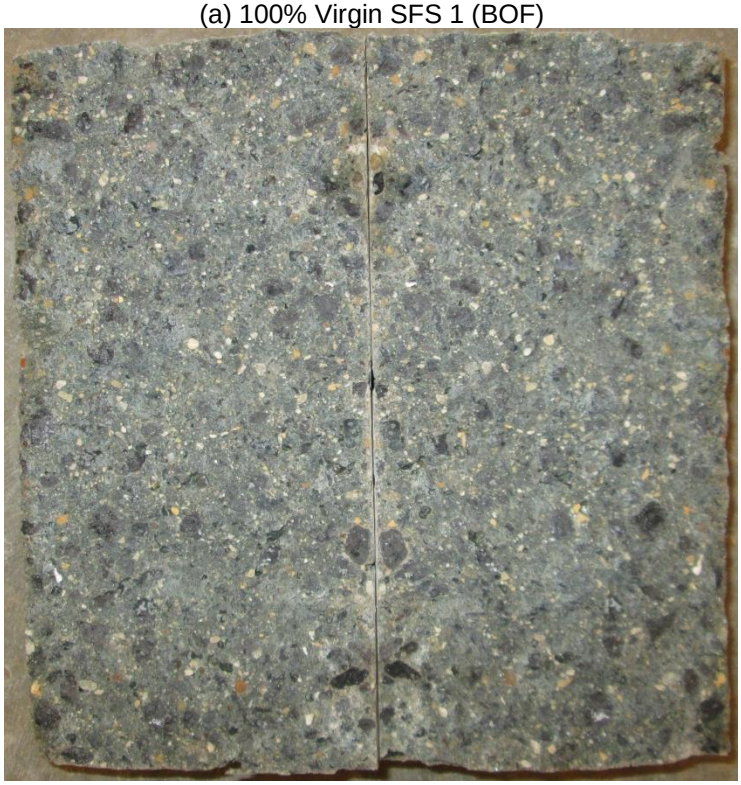

(b) 100% Virgin SFS 2 (EAF)

Figure 56. Images of the split tension fracture surfaces for concrete with 100% virgin SFS: (a) BOF and (b) EAF.

5.5 FLEXURAL STRENGTH

The flexural strength was evaluated at an age of 28 days with the average of three replicate specimens. The beams had a nominal 6 inches square cross section and were 21 inches long. The tested span length was 18 inches, and the strength was calculated for third-point (four-point) loading, where the loading was applied at one-third the span length (6 inches). The flexural strength, or modulus of rupture (MOR), is measured from the peak load (*P*), the span length (*l*, 18 inches), the beam width (*b*), and the beam depth (*d*). After the beam fractured, the cross-sectional area of the fracture surface was measured to obtain the dimensions of *b* and *d*.

$$MOR = \frac{Pl}{bd^2} \quad (7)$$

The flexural strength results are shown in Table 50. The flexural strength for concrete with SFS FRAP was higher than the control and concrete with dolomite FRAP. Images of the fracture surfaces for the concrete with SFS FRAP can be seen in Figure 57. A large agglomerated FRAP particle appeared to influence the failure crack path in one of the flexural strength beams with 50% SFS FRAP, as shown in Figure 58.

Because the flexural strengths were unexpectedly high, a second batch of concrete was mixed, the results of which are shown in Table 50. As can be seen in Table 50 and Figure 59, there is a trend of decreasing flexural strength with increasing FRAP content for SFS FRAP compared with dolomite FRAP. The concrete with SFS FRAP was found to result in higher flexural strengths than concrete with dolomite FRAP, which can possibly be the result of the SFS in the FRAP and/or the finer gradation of the SFS FRAP compared with tested dolomite FRAP. Statistically, with 95% confidence, a t-test revealed that the flexural strength of concrete with SFS FRAP was higher than concrete with dolomite FRAP (Table 51). Images of the fracture surfaces for the concrete with SFS FRAP (Test 2) can be seen in Figure 60.

Table 50. 28-Day Flexural Strengths (psi) for Concrete with SFS FRAP and Dolomite FRAP

Concrete Mix	SFS FRAP					Dolomite FRAP*	
	1	2	3	Average	COV	Average	COV
0% FRAP (Control)	--	--	--	--	--	857	12.2%
20% FRAP (Test 1)	1044	920	986	983	6.3%	735	2.0%
50% FRAP (Test 1)	849	919	883	884	3.9%	577	1.3%
20% FRAP (Test 2)	778	812	788	793	2.2%	735	2.0%
50% FRAP (Test 2)	762	770	771	768	0.6%	577	1.3%

*Source: Brand et al. (2012)

(a) 20% SFS FRAP

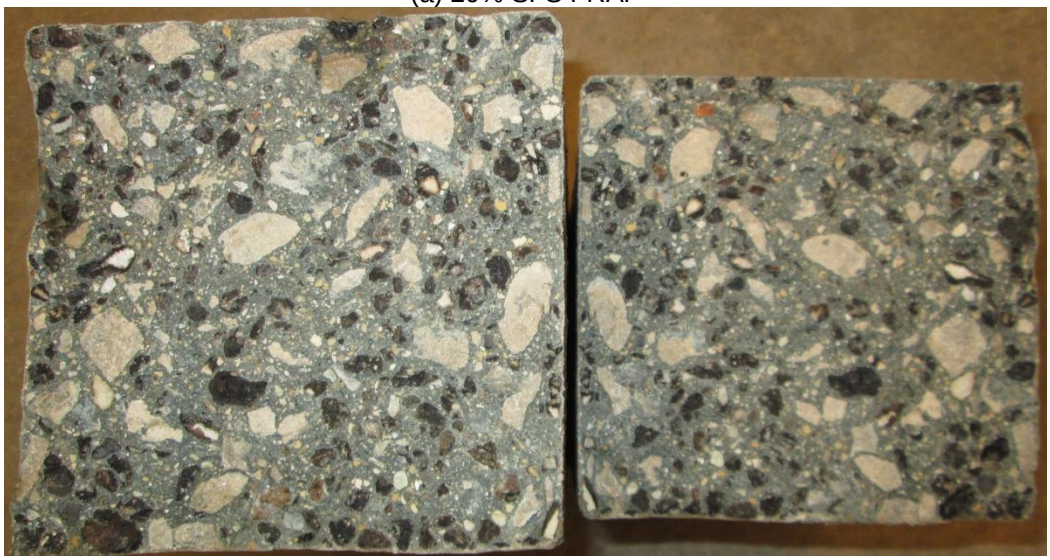

(b) 50% SFS FRAP

Figure 57. Images of the flexural fracture surfaces for concrete (Test 1) with (a) 20% SFS FRAP and (b) 50% SFS FRAP.

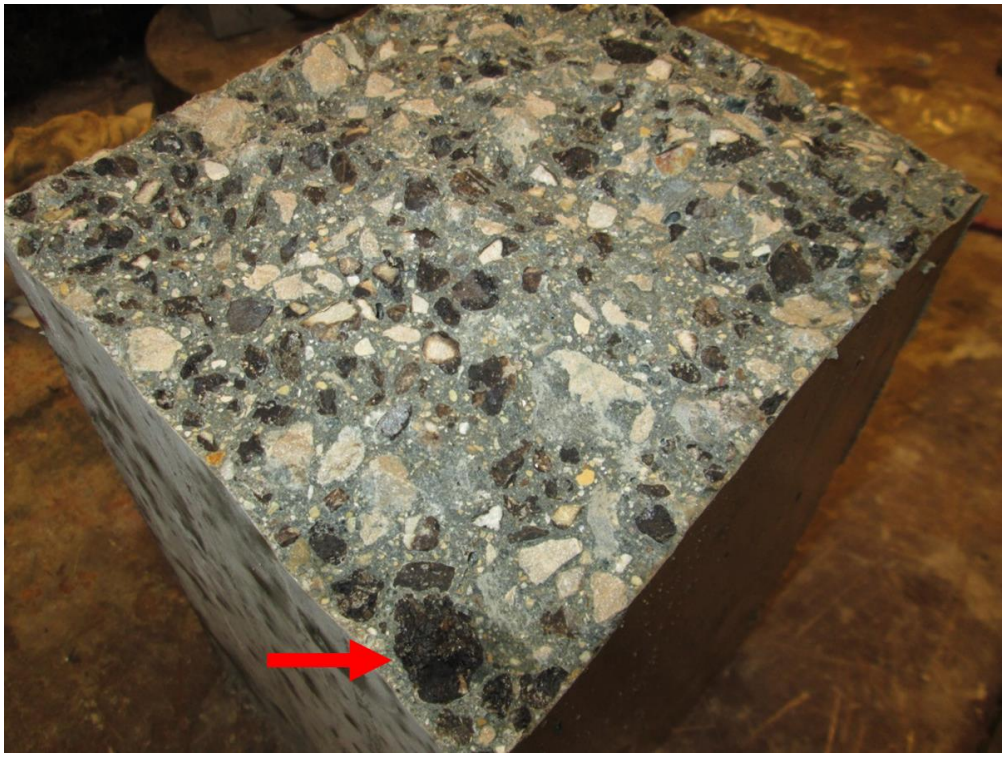

Figure 58. An image of one of the flexural strength beams where a large agglomerated FRAP particle appeared to affect the path of the crack.

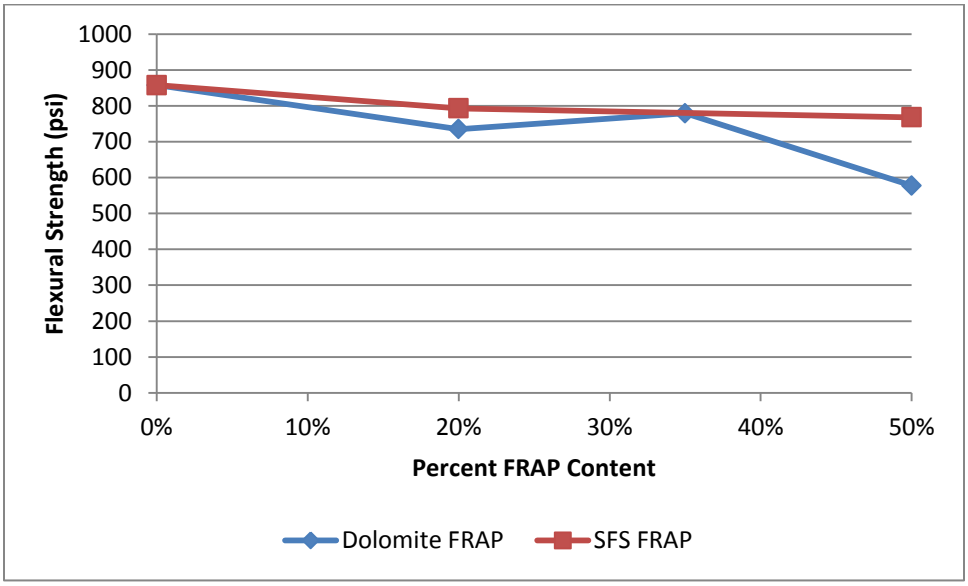

Figure 59. A plot of average 28-day flexural strength versus percent FRAP content for dolomite FRAP and SFS FRAP.

Table 51. Statistical Significance Testing for Concrete Flexural Strength with SFS FRAP and Dolomite FRAP

Mix	Flexural Strength (psi)					Pooled Standard Deviation	t-test	p-value
	1	2	3	Average	Standard Deviation			
20% SFS FRAP	778	812	788	793	17.3	--	--	--
20% D-FRAP	722	751	732	735	14.9	261	4.39	1.18E-02
50% SFS FRAP	762	770	771	768	4.9	--	--	--
50% D-FRAP	578	570	584	577	7.3	38	37.65	2.97E-06

D-FRAP = Dolomite FRAP

(a) 20% SFS FRAP

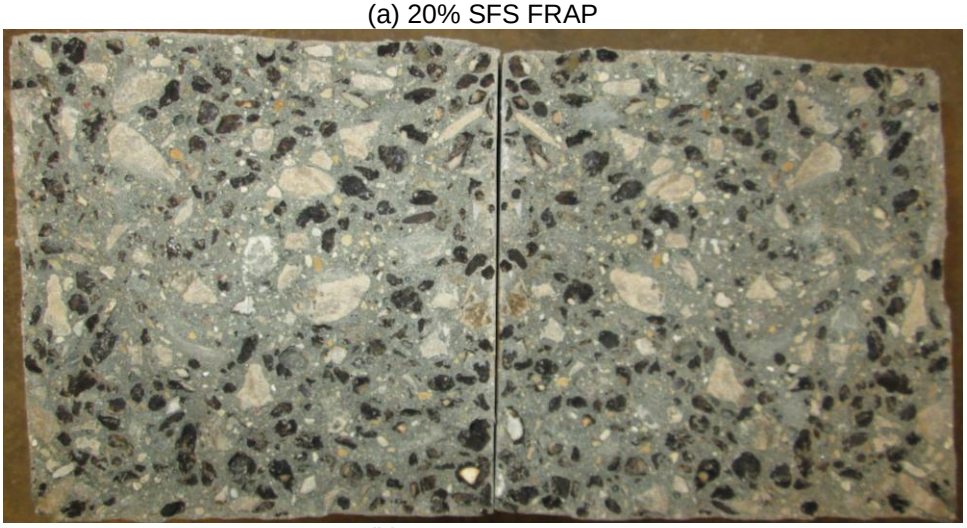

(b) 50% SFS FRAP

Figure 60. Images of the flexural fracture surfaces for concrete (Test 2) with (a) 20% SFS FRAP and (b) 50% SFS FRAP.

5.6 STRENGTH RATIOS

The typical ratio for split tensile strength to compressive strength ranges from 0.08 to 0.14, and the ratio for flexural strength to compressive strength ranges from 0.11 to 0.23 (Mindess et al. 2003). The ratios for SFS FRAP and dolomite FRAP can be found in Table 52. The strength ratios are within the expected typical ranges. The split tensile to compressive strength ratio is similar for the concretes with 0, 20, and 50% SFS FRAP or dolomite FRAP, which is around 0.11 to 0.12 at later ages; the ratio for concrete with virgin SFS is lower than the control concrete and concretes with FRAP, but is still within the typical range at 0.09. The flexural to compressive strength ratio is also within the expected range, although the ratio is slightly greater for the concretes with SFS FRAP because of the higher measured flexural strength.

Table 52. Strength Ratios for Concrete with SFS and Dolomite FRAP

Concrete Mix	Age (days)	SFS FRAP		Dolomite FRAP*	
		Split Tensile to Compressive Strength	Flexural to Compressive Strength	Split Tensile to Compressive Strength	Flexural to Compressive Strength
0% FRAP (Control)	3	--	--	0.15	--
	7	--	--	0.14	--
	14	--	--	0.12	--
	28	--	--	0.14	0.13
	90	--	--	0.11	--
20% FRAP	3	0.12	--	0.12	--
	7	0.12	--	0.15	--
	14	0.11	--	0.11	--
	28	0.12	0.15	0.13	0.14
	90	0.11	--	0.12	--
50% FRAP	3	0.12	--	0.12	--
	7	0.14	--	0.10	--
	14	0.11	--	0.12	--
	28	0.11	0.18	0.11	0.14
	90	0.12	--	0.11	--
100% Virgin SFS 1 (BOF)	28	0.09	--	--	--
100% Virgin SFS 2 (EAF)	28	0.09	--	--	--

*Source: Brand et al. (2012)

5.7 MODULUS OF ELASTICITY

The modulus of elasticity (MOE) was evaluated at an age of 28 days with the average of three replicate specimens (see Figure 61). The chord modulus of elasticity (E) was calculated as follows, where S_2 is the stress at approximately 40% of the compressive strength, S_1 is the stress at longitudinal strain ε_1, and ε_2 is the longitudinal strain at stress S_2. According to ASTM C469 (2010), ε_1 should be selected as 0.000050.

$$E = \frac{S_2 - S_1}{\varepsilon_2 - \varepsilon_1} = \frac{S_2 - S_1}{\varepsilon_2 - 0.000050} \quad (8)$$

The cylinder was loaded at least twice to confirm the data and to make sure that the strain gauges were recording acceptable data (these first two measurements were not used in the eventual MOE calculation). The cylinder was then loaded at least three more times to obtain the actual data from which the modulus of elasticity would be calculated. Once the cylinder was completely tested for modulus of elasticity data, it was loaded until failure to obtain the compressive strength.

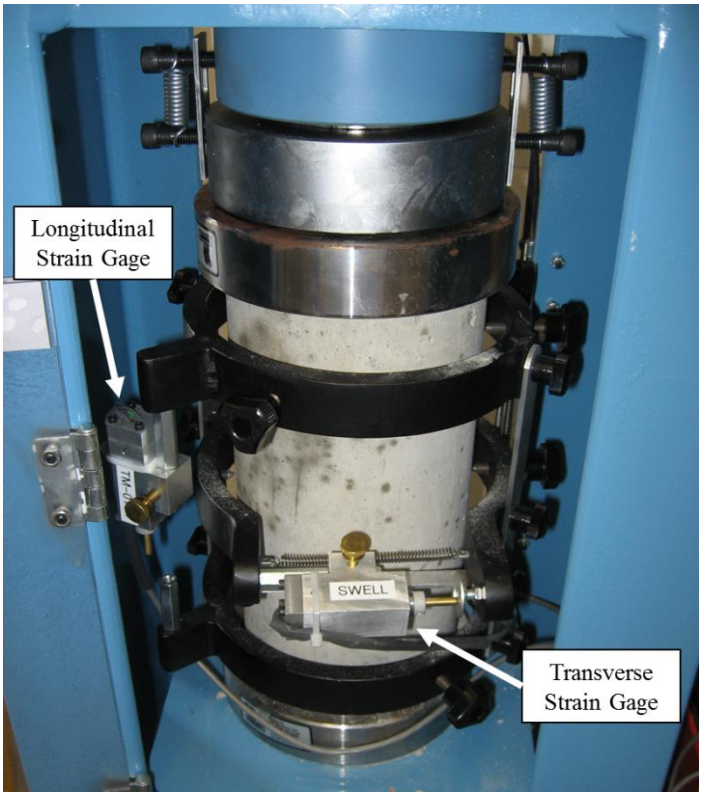

Figure 61. Configuration to determine the modulus of elasticity.

The average MOE values for concrete with SFS FRAP and dolomite FRAP are shown in Table 53 and Figure 62. As expected, the MOE for concrete with FRAP was lower than the control mix with dolomite. The concrete with SFS FRAP had a greater MOE than concrete with dolomite FRAP, because of the stiffer modulus of the SFS in the FRAP; the modulus with SFS FRAP was statistically greater than the dolomite FRAP with 95% confidence (Table 54). The compressive strength of the MOE cylinders is shown in Table 55, which indicates that the compressive strength of these cylinders was slightly greater than the strength of the cylinders tested in Table 46.

Table 53. Average Modulus of Elasticity (in psi) for Concrete with SFS and Dolomite FRAP

Concrete Mix	Sample	SFS FRAP						Dolomite FRAP*	
		Test 1	Test 2	Test 3	Average	Average	COV	Average	COV
0% FRAP (Control)	--	--	--	--	--	--		6.44E+06	4.6%
20% FRAP	1	5.82E+06	5.79E+06	5.58E+06	5.73E+06	6.02E+06	4.4%	5.42E+06	3.3%
	2	6.23E+06	6.24E+06	6.26E+06	6.25E+06				
	3	6.06E+06	6.15E+06	6.02E+06	6.08E+06				
50% FRAP	1	4.97E+06	4.94E+06	4.74E+06	4.88E+06	5.48E+06	9.5%	4.48E+06	3.1%
	2	5.68E+06	5.82E+06	5.91E+06	5.80E+06				
	3	5.90E+06	5.82E+06	5.56E+06	5.76E+06				

*Source: Brand et al. (2012)

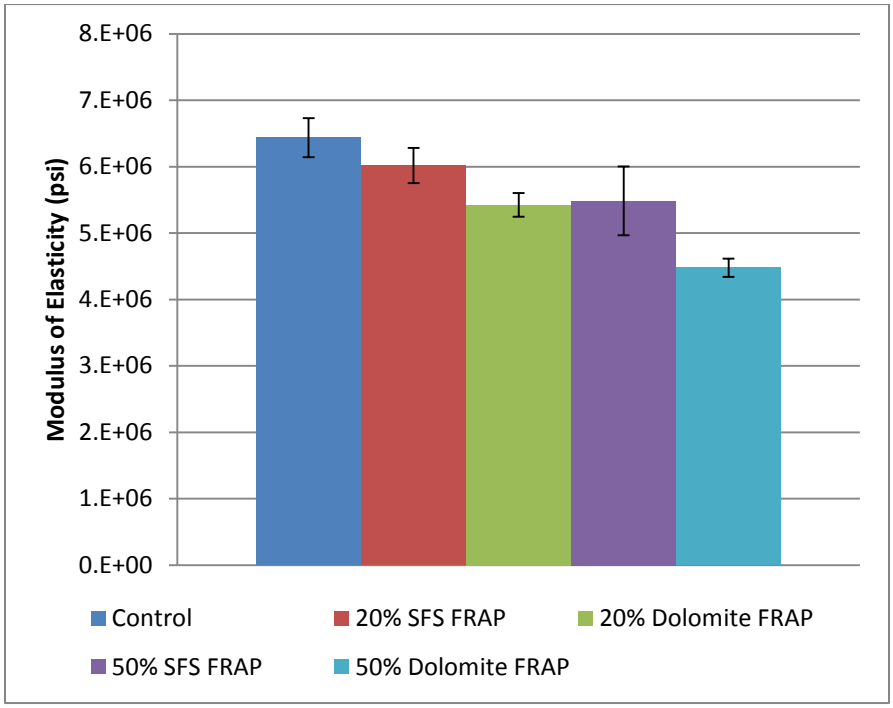

Figure 62. Modulus of elasticity for concrete with SFS and dolomite FRAP.

Table 54. Statistical Significance Testing for Concrete Modulus of Elasticity with SFS FRAP and Dolomite FRAP

Mix	Modulus of Elasticity (psi)					Pooled Standard Deviation	t-test	p-value
	1	2	3	Average	Standard Deviation			
20% SFS FRAP	5.73E+06	6.25E+06	6.08E+06	6.02E+06	2.64E+05			
20% D-FRAP	5.62E+06	5.39E+06	5.27E+06	5.42E+06	1.78E+05	5.07E+10	3.22	0.032
50% SFS FRAP	4.88E+06	5.80E+06	5.76E+06	5.48E+06	5.18E+05			
50% D-FRAP	4.32E+06	4.58E+06	4.54E+06	4.48E+06	1.38E+05	1.44E+11	3.24	0.032

D-FRAP = Dolomite FRAP

Table 55. Compressive Strength of the MOE Specimens

Mix	Sample	Peak Load (lb)	Compressive Strength (psi)
20% SFS FRAP	1	179735	6357
	2	176670	6248
	3	180335	6378
50% SFS FRAP	1	147030	5200
	2	140515	4970
	3	141715	5012

The MOE can be estimated based on the concrete unit weight (w_c) and the compressive strength (σ_c) (Mindess et al. 2003; ACI318 2008):

$$MOE = 33\, {w_c}^{1.5} {\sigma_c}^{0.5} \quad (9)$$

The predicted MOE is shown in Table 56 relative to the measured MOE for both SFS and dolomite FRAP. For all concretes, the MOE is underpredicted by the equation. By minimizing the error between the actual and predicted moduli, the MOE prediction equation was updated as follows (see Figure 63):

$$MOE = 121.6\, {w_c}^{1.44} {\sigma_c}^{0.41} \quad (10)$$

Table 56. Predicted versus Measured Modulus of Elasticity

Concrete Mix	Sample	Compressive Strength (psi)	Unit Weight (lb/ft^3)	Predicted MOE (psi) (ACI 318)	Predicted MOE (psi) (Updated)	Measured MOE (psi)
0% FRAP (Control)*	1	7006	145.2	4.83E+06	6.21E+06	6.66E+06
	2	6417	145.2	4.63E+06	5.99E+06	6.55E+06
	3	4727	145.2	3.97E+06	5.28E+06	6.10E+06
20% SFS FRAP	1	6357	149.4	4.80E+06	6.22E+06	5.73E+06
	2	6248	149.4	4.76E+06	6.17E+06	6.25E+06
	3	6378	149.4	4.81E+06	6.23E+06	6.08E+06
50% SFS FRAP	1	5200	150.2	4.38E+06	5.76E+06	4.88E+06
	2	4970	150.2	4.28E+06	5.66E+06	5.80E+06
	3	5012	150.2	4.30E+06	5.68E+06	5.76E+06
20% Dolomite FRAP*	1	3638	143.2	3.41E+06	4.64E+06	5.62E+06
	2	5419	143.2	4.16E+06	5.47E+06	5.39E+06
	3	5326	143.2	4.13E+06	5.43E+06	5.27E+06
35% Dolomite FRAP*	1	4349	140.8	3.64E+06	4.88E+06	4.48E+06
	2	4000	140.8	3.49E+06	4.71E+06	4.66E+06
	3	3835	140.8	3.41E+06	4.63E+06	4.76E+06
50% Dolomite FRAP*	1	4226	140.2	3.56E+06	4.79E+06	4.32E+06
	2	4112	140.2	3.51E+06	4.74E+06	4.58E+06
	3	4342	140.2	3.61E+06	4.84E+06	4.54E+06

*Source: Brand et al. (2012)

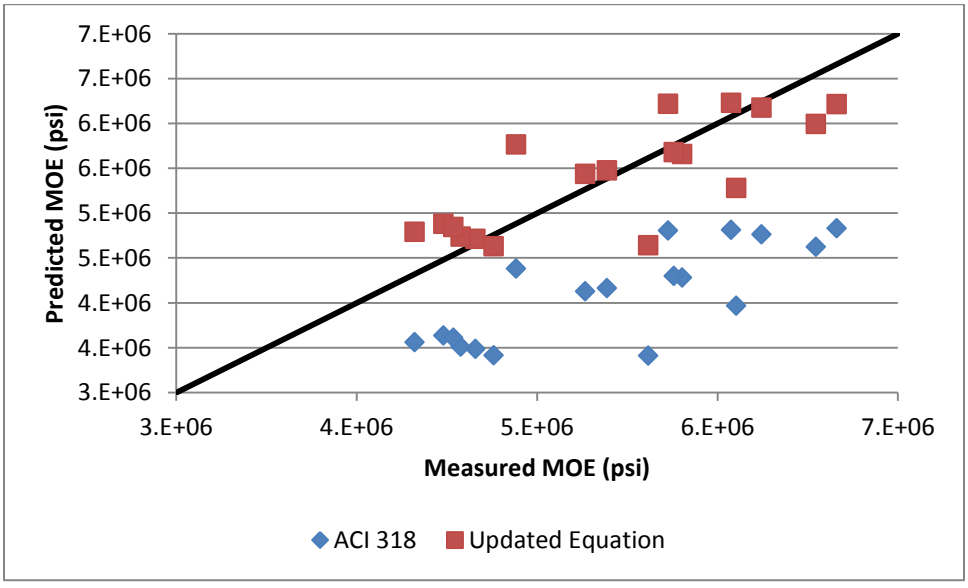

Figure 63. Predicted versus measured modulus of elasticity.

5.8 FRACTURE PROPERTIES

The fracture properties of the concrete was determined at an age of 28 days using the single edge notched beam (SENB) geometry following the two-parameter fracture model (Jenq and Shah 1985; RILEM TC89-FMT 1990) and the work of fracture method (Hillerborg 1985). Five concrete mixtures were tested: 0% SFS FRAP (control), 20% SFS FRAP, 50% SFS FRAP, 100% Virgin SFS 1 (BOF), and 100% Virgin SFS 2 (EAF). Five replicates were tested for the 20% and 50% SFS FRAP mixes and four replicates were tested for the 0% SFS FRAP (control), 100% Virgin SFS 1 (BOF), and 100% Virgin SFS 2 (EAF) mixes. The dimensions of the SENB specimens were 150 by 80 by 700 mm, and the specimens were tested with a span length of 600 mm. A notch depth of 50 mm was cut into the beam at the mid-span (350 mm). The specimen was loaded at a constant crack mouth opening displacement (CMOD) rate. The beam was monotonically loaded until peak and then unloaded after dropping to 95% of the peak load in order to obtain data for the unloading compliance. Subsequently, the beam was reloaded until the specimen failed.

The SENB test estimates the initial stiffness (E_i) of the concrete based on the loading-unloading (load-CMOD) curve as follows, where a_0 is the notch depth, S is the span length (600 mm), C_i is the initial compliance from the load-CMOD curve (20% to 50% of the peak load), b is the beam depth, t is the beam width, and H is the knife-edge thickness:

$$E_i = \frac{6Sa_0[g_2(\alpha_0)]}{C_i b^2 t} \tag{11}$$

$$g_2(\alpha) = 0.76 - 2.28\alpha + 3.87\alpha^2 - 2.04\alpha^3 + \frac{0.66}{(1-\alpha)^2} \tag{12}$$

$$\alpha_0 = \frac{a_0 + H}{b + H} \tag{13}$$

The unloading compliance (C_u) is similarly calculated from the unloading curve from 20% to 80% of the peak load and then used to compute the unloading stiffness (E_u):

$$E_u = \frac{6Sa_c[g_2(\alpha_c)]}{C_u b^2 t} \tag{14}$$

The critical effective crack length (a_c) at the peak load is then calculated by setting initial and unloading stiffnesses equal and solving for critical crack depth:

$$a_c = a_0 \frac{C_u}{C_i} \frac{g_2(\alpha_0)}{g_2(\alpha_c)} \tag{15}$$

The critical stress intensity factor (K_{Ic}) is then determined, where P_{max} is the maximum peak load and W_0 is the self-weight of the beam:

$$K_{Ic} = 3\left[P_{max} + 0.5\frac{W_0 S}{L}\right]\left[\frac{S(\pi a_c)^{1/2} g_1(a_c/b)}{2b^2 t}\right] \tag{16}$$

$$g_1\left(\frac{a_c}{b}\right) = \frac{1.99 - (a_c/b)(1 - a_c/b)(2.15 - 3.93(a_c/b) + 2.7(a_c/b)^2)}{\sqrt{\pi}(1 + 2(a_c/b))(1 - (a_c/b))^{3/2}} \tag{17}$$

The second fracture parameter, the critical crack tip opening displacement ($CTOD_c$), is also calculated from the critical crack depth as follows, where $\beta = a_c/a_0$:

$$CTOD_c = \frac{6Sa_c g_1(a_c/b)}{Eb^2 t}\left(P_{max} + 0.5\frac{W_0 S}{L}\right)[(1-\beta)^2 + (1.081 - 1.149(a_c/b))(\beta - \beta^2)]^{1/2} \quad (18)$$

The initial fracture energy (G_{Ic}), or strain energy release rate, is computed from the previously-derived stiffness (*E*):

$$G_{Ic} = \frac{(K_{Ic}^s)^2}{E} \quad (19)$$

The total fracture energy (G_F) is computed using the method by Hillerborg (1985), which normalizes the total work of fracture to the fracture area; *A* is the area under the load-CMOD curve (without the loop from unloading) and δ_f is the displacement at failure with zero load.

$$G_F = \frac{A + \frac{W_0 S}{L}\delta_f}{(b - a_0)t} \quad (20)$$

The fracture properties were determined at an age of 28 days for the mixes with 20% (Figure 64) and 50% (Figure 65) SFS FRAP as well as 0% SFS FRAP (Figure 66), 100% Virgin SFS 1 (BOF) (Figure 67), and 100% Virgin SFS 2 (EAF) (Figure 68). A total of four or five replicate beams were tested, the results of which are shown in Table 57. Relative to the control concrete with virgin aggregates, the other mixes with recycled aggregates all appeared to have an increased critical stress intensity factor and initial and total fracture energies.

A t-test with 95% confidence was used to compare the fracture properties of the concretes with SFS FRAP and virgin SFS to the concrete with virgin aggregates (Table 58). The t-test indicated that the concrete with 100% Virgin SFS 2 (EAF) resulted in fracture properties that were statistically greater than the control, which agrees with other studies. Papayianni and Anastasiou (2010a) found a 9% increase in the total fracture energy when coarse EAF slag aggregates were used, and Montgomery and Wang (1992) found an increase in K_{Ic} on the order of 10% when coarse instant-chilled SFS was added to concrete. The concrete with 100% Virgin SFS 1 (BOF) had statistically similar properties to the control, except for the modulus and K_{Ic}. For concrete with SFS FRAP, the fracture properties were statistically similar to the control, except for $CTOD_c$ and G_{Ic} for the 50% SFS FRAP mix. This finding agrees with previous studies that have shown the fracture properties of concrete with FRAP to be statistically similar to virgin aggregate concrete (Brand et al. 2012, 2013, 2014; Brand and Roesler 2014).

Comparing the 20% and 50% SFS FRAP mixes, the peak load and modulus decreased at higher SFS FRAP contents, as expected, but the K_{Ic}, $CTOD_c$, G_{Ic}, and G_F were similar between the two SFS FRAP contents. All of the fracture properties were not statistically different with 95% confidence (Table 59).

The fracture parameters for the various concretes are compared with the results from other studies in Table 60. As can be seen, the values for concrete with SFS FRAP are similar to concrete with dolomite FRAP, despite the differences in concrete age. However, the total fracture energy appears to be slightly greater for concrete with SFS FRAP relative

to dolomite FRAP, potentially because of the presence of the SFS and gradation differences.

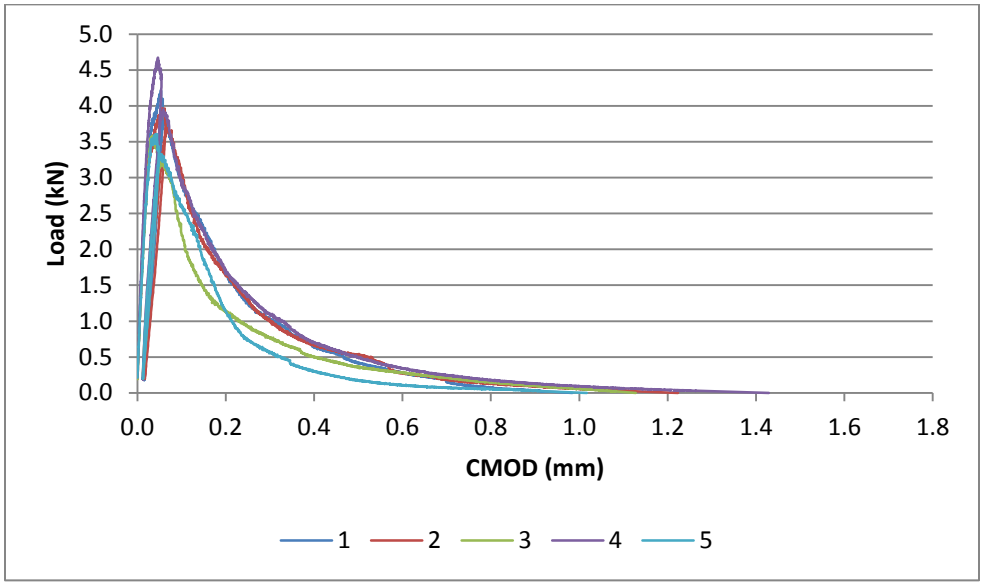

Figure 64. Load-CMOD curves for the replicate beams with 20% SFS FRAP.

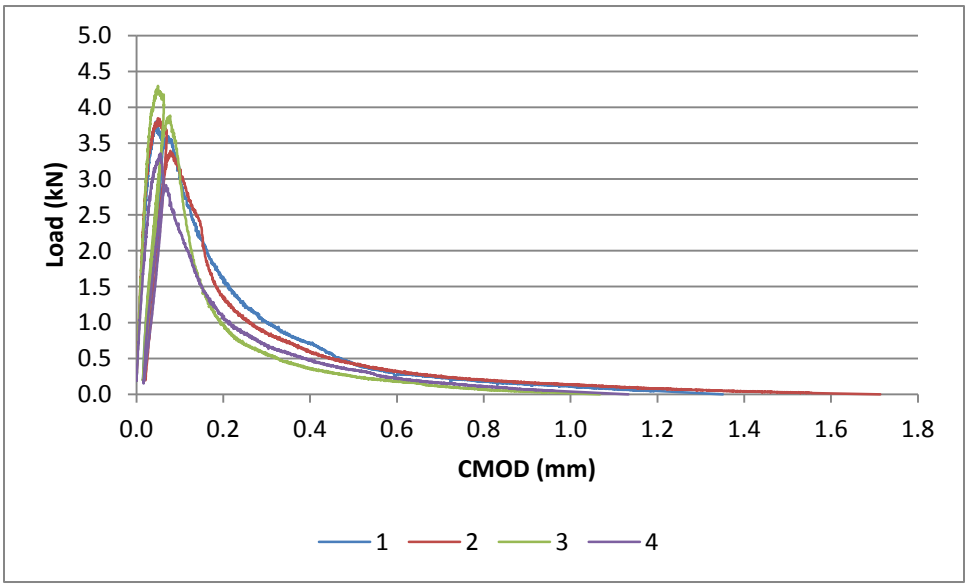

Figure 65. Load-CMOD curves for the replicate beams with 50% SFS FRAP.

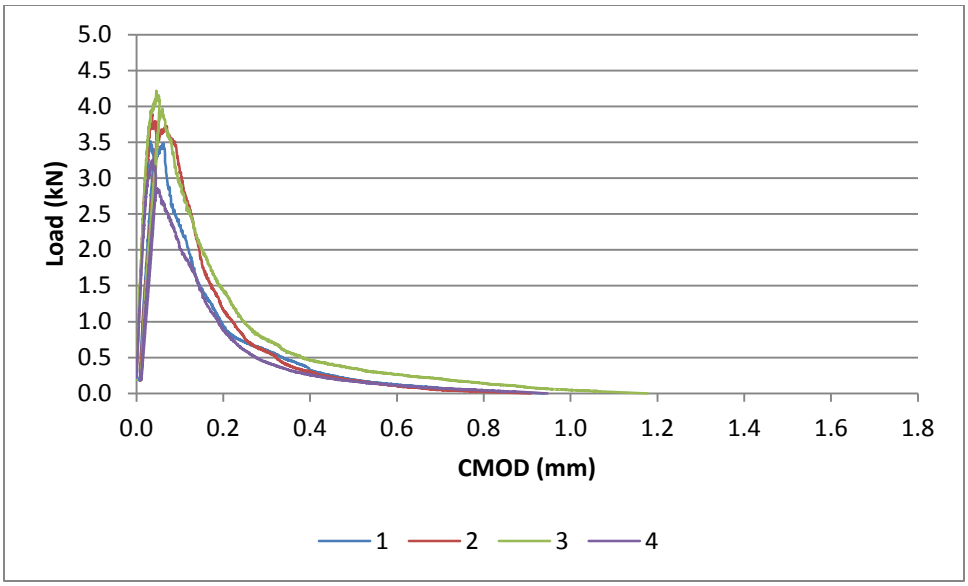

Figure 66. Load-CMOD curves for the replicate beams with 0% SFS FRAP.

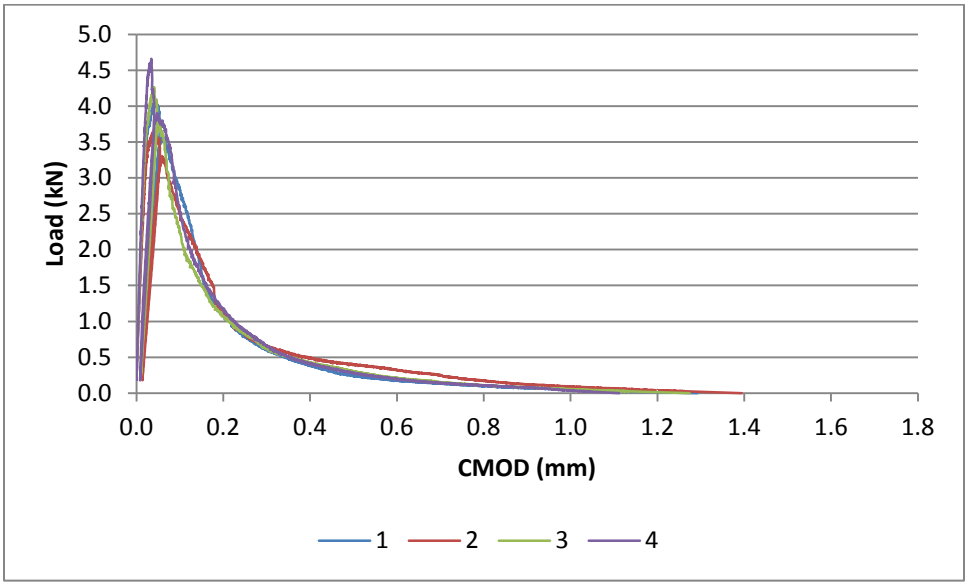

Figure 67. Load-CMOD curves for the replicate beams with 100% Virgin SFS 1 (BOF).

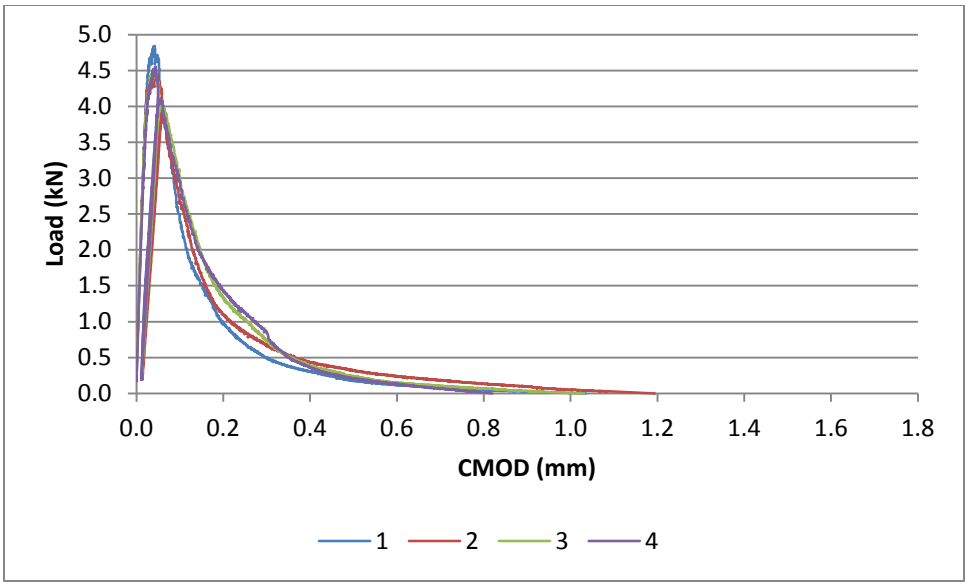

Figure 68. Load-CMOD curves for the replicate beams with 100% Virgin SFS 2 (EAF).

Table 57. Fracture Parameters at 28 Days

Mix	Beam No.	Peak Load, P_{max} (kN)	Modulus, E (MPa)	Critical Stress Intensity Factor, K_{Ic} (MPa-$m^{1/2}$)	Critical Crack Tip Opening Displacement $CTOD_c$ (mm)	Initial Fracture Energy, G_{Ic} (N/m)	Total Fracture Energy, G_F (N/m)
0% SFS FRAP	1	3.51	25.4	0.873	0.0117	30.04	92.4
	2	3.89	28.3	1.086	0.0159	41.62	104.4
	3	4.22	26.2	1.113	0.0180	47.19	122.8
	4	3.26	26.8	0.928	0.0142	32.16	86.8
	Average	**3.72**	**26.7**	**1.000**	**0.0149**	**37.75**	**101.6**
	COV	**11.3%**	**4.7%**	**11.8%**	**17.8%**	**21.3%**	**15.7%**
20% SFS FRAP	1	4.22	25.1	1.075	0.0179	46.04	124.2
	2	3.97	26.1	1.163	0.0222	51.79	135.0
	3	3.59	25.8	0.966	0.0147	36.12	113.3
	4	4.67	31.6	1.334	0.0190	56.24	152.7
	5	3.61	25.3	0.985	0.0152	38.30	102.2
	Average	**4.01**	**26.8**	**1.104**	**0.0178**	**45.70**	**125.5**
	COV	**11.3%**	**10.2%**	**13.6%**	**17.1%**	**18.8%**	**15.5%**
50% SFS FRAP	1	3.80	23.1	1.096	0.0209	51.98	143.2
	2	3.85	26.0	1.218	0.0261	57.15	146.8
	3	4.30	27.7	1.305	0.0216	61.51	111.8
	4	3.36	20.9	0.973	0.0190	45.38	108.8
	Average	**3.83**	**24.4**	**1.148**	**0.0219**	**54.00**	**127.6**
	COV	**10.0%**	**12.4%**	**12.6%**	**13.7%**	**12.9%**	**15.8%**
100% Virgin SFS 1 (BOF)	1	4.10	30.7	1.248	0.0218	50.67	117.0
	2	3.63	29.3	1.124	0.0200	43.07	128.0
	3	4.27	31.8	1.204	0.0178	45.59	114.6
	4	4.66	34.3	1.245	0.0158	45.16	114.3
	Average	**4.16**	**31.5**	**1.205**	**0.0189**	**46.12**	**118.5**
	COV	**10.2%**	**6.6%**	**4.8%**	**13.9%**	**7.0%**	**5.5%**
100% Virgin SFS 2 (EAF)	1	4.84	36.5	1.427	0.0199	55.82	134.6
	2	4.45	36.7	1.447	0.0228	56.96	124.5
	3	4.51	37.4	1.375	0.0193	50.58	121.7
	4	4.56	35.3	1.305	0.0167	48.32	115.1
	Average	**4.59**	**36.5**	**1.388**	**0.0197**	**52.92**	**124.0**
	COV	**3.8%**	**2.4%**	**4.5%**	**12.8%**	**7.8%**	**6.5%**

Table 58. t-test Results for the Mixes with SFS FRAP and Virgin SFS Relative to the Control

	20% SFS FRAP		50% SFS FRAP		100% Virgin SFS 1 (BOF)		100% Virgin SFS 2 (EAF)	
Fracture Parameter	p-value	Statistically Significant	p-value	Statistically Significant	p-value	Statistically Significant	p-value	Statistically Significant
P_{max}	0.359	No	0.727	No	0.190	No	0.009	Yes
E	0.940	No	0.214	No	0.007	Yes	1.4E-05	Yes
$CTOD_c$	0.179	No	0.013	Yes	0.080	No	4.1E-02	Yes
K_{Ic}	0.294	No	0.164	No	0.020	Yes	0.001	Yes
G_{Ic}	0.200	No	0.022	Yes	0.102	No	0.015	Yes
G_F	0.089	No	0.089	No	0.098	No	0.046	Yes

Table 59. Results of the t-test between the Mixes with 20% and 50% SFS FRAP

Fracture Parameter	p-value	Statistically Significant
P_{max}	0.537	No
E	0.253	No
K_{Ic}	0.674	No
$CTOD_c$	0.084	No
G_{Ic}	0.162	No
G_F	0.874	No

Table 60. Comparison of Fracture Parameters for Concrete with FRAP Aggregates

Mix	Age (days)	Peak Load, P_{max} (kN)	Critical Stress Intensity Factor, K_{Ic} (MPa-$m^{1/2}$)	Critical Crack Tip Opening Displacement $CTOD_c$ (mm)	Initial Fracture Energy, G_{Ic} (N/m)	Total Fracture Energy, G_F (N/m)
0% SFS FRAP	28	3.72	1.000	0.0149	37.8	101.6
20% SFS FRAP	28	4.01	1.104	0.0178	45.7	125.5
50% SFS FRAP	28	3.83	1.148	0.0219	54.0	127.6
100% BOF SFS	28	4.16	1.205	0.0189	46.1	118.5
100% EAF SFS	28	4.59	1.388	0.0197	52.9	124.0
Concrete Slab Mix (0% FRAP)*	39	3.57	1.146	0.0191	44.3	73.8
Concrete Slab Mix (45% FRAP)*	39	2.38	0.898	0.0205	36.6	75.7
Laboratory Supplement Mix (45% FRAP)*	39	3.85	1.043	0.0173	47.1	119.4
Tollway I-88 Top Lift (0% FRAP)*	140	4.93	1.349	0.0148	49.2	72.5
Tollway I-88 Bottom Lift (21% FRAP)*	140	4.61	1.311	0.0163	50.3	79.4
0% FRAP**	156	4.39	1.267	0.0157	44.7	100.4
20% FRAP**	156	4.16	1.140	0.0159	43.7	86.3
35% FRAP**	104	3.53	0.974	0.0137	35.8	106.5
50% FRAP**	104	3.54	1.054	0.0193	47.7	113.5

Source: *Brand et al. (2013); **Brand et al. (2012)

5.9 DRYING SHRINKAGE

The drying shrinkage was measured for specimens that had cured for 24 hours in order to examine the early age shrinkage behavior of the concrete. Three replicates were tested over the span of 150 days. Five concrete mixtures were tested: 0% SFS FRAP (control), 20% SFS FRAP, 50% SFS FRAP, 100% Virgin SFS 1 (BOF), and 100% Virgin SFS 2 (EAF). The virgin SFS aggregates were tested in order to evaluate how the SFS in the FRAP could affect the shrinkage. The specimens were also weighed in order to determine the mass loss as shrinkage progressed. All shrinkage specimens were kept in an environmentally controlled room with the relative humidity around 50% and the temperature at approximately 23°C. The free shrinkage prism specimens measured 3 inches in width and depth by 11.25 inches in length. Two gauge studs were inserted into the mold at the ends of the concrete specimens, resulting in a gauge length of 10 inches. The shrinkage was measured relative to a constant length reference bar. The shrinkage (*S*, in mircostrain) is

calculated as follows, where L_c is the length of the concrete specimen, L_{ref} is the length of the reference bar, and *GL* is the gauge length (10 inches):

$$S(\mu strain) = \frac{L_c - L_{ref}}{GL}(10^6) \quad (21)$$

The percent weight lost (WL) was computed as follows, where W_0 is the initial weight and W_i is the weight after *i* days:

$$WL = \frac{W_i - W_0}{W_0}(100\%) \quad (22)$$

Figure 69 shows the shrinkage behavior of each concrete mixture during the first 14 days. The shrinkage trends were relatively unclear until about 7 days. As can be seen at later ages as well (Figure 70), the general shrinkage trend is that the control (0% SFS FRAP) concrete experiences the least amount of shrinkage, followed by the concrete with 20% SFS FRAP, then 50% SFS FRAP, and finally the virgin SFS concrete mixes experience the highest amount of shrinkage. A t-test for statistical significance (Table 61) indicated that the shrinkage of the mix with 20% SFS FRAP was not statistically different from the shrinkage of the control mix (0% SFS FRAP) while, only at later ages, the shrinkage of the mixes with 50% SFS FRAP, 100% EAF, and 100% BOF was statistically greater than the shrinkage of the control mix (0% SFS FRAP).

It was observed in previous studies of concrete with virgin SFS aggregate that the shrinkage was greater than (Coppola et al. 2010), equal to (Netinger et al. 2011), or less than (Madej et al. 1996; Al-Negheimish et al. 1997; Liu et al. 2011) concrete with natural aggregates. Brand et al. (2012) found that the shrinkage of 28-day-cured concrete with 20, 35, and 50% dolomite FRAP was statistically similar to the shrinkage of the control concrete without FRAP (except for the 35% FRAP mixture at 56 and 90 days). The trends suggest that the SFS present in the FRAP may have an effect on shrinkage behavior of the concrete, but the gradation of each aggregate source was different so this may be a significant reason. The asphalt content of the FRAP may also be important, considering that the asphalt content (3.9%) of the SFS FRAP was higher than the asphalt content (2.1%) of the dolomite FRAP in the study by Brand et al. (2012).

The mass loss caused by shrinkage (Figure 71) indicated that that the control mix (0% SFS FRAP) experienced the greatest amount of mass loss and that the mixtures with SFS FRAP exhibited the lowest mass loss. This is not consistent with the findings by Brand et al. (2012), who found that concrete with higher FRAP contents (35 and 50%) exhibited greater mass loss.

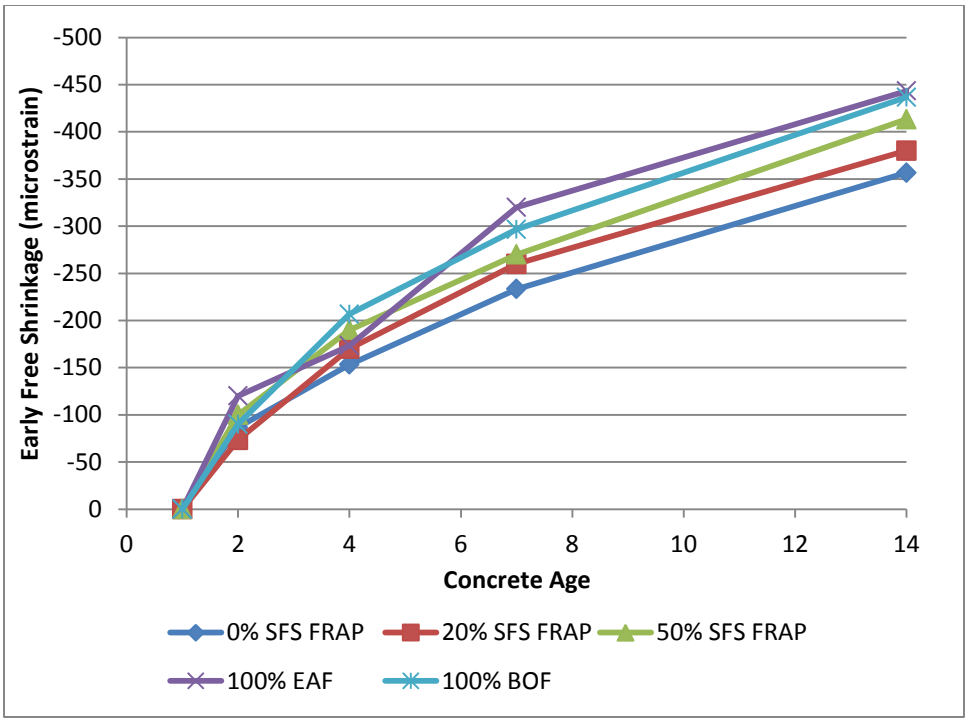

Figure 69. Free drying shrinkage up to 14 days of concrete with 0, 20, and 50% SFS FRAP and 100% virgin SFS (EAF and BOF).

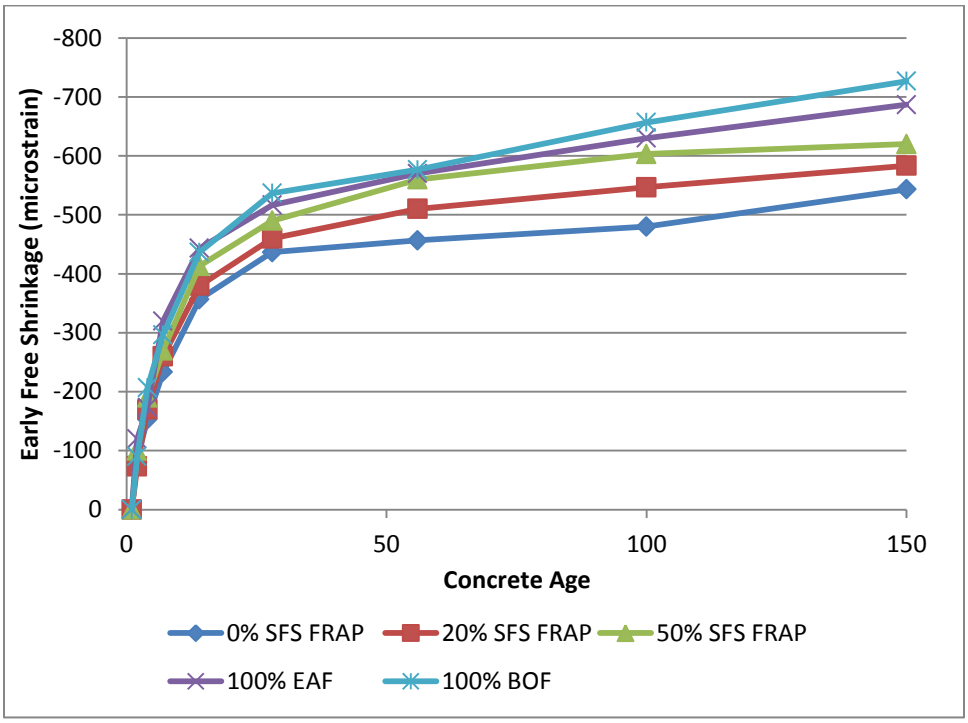

Figure 70. Free drying shrinkage up to 150 days of concrete with 0, 20, and 50% SFS FRAP and 100% virgin SFS (EAF and BOF).

Table 61. Statistical Significance of Concrete Shrinkage Relative to the Control

Mix	Concrete Age (days)	Average Shrinkage Strain (μstrain)	Pooled Standard Deviation (μstrain)	t-test	p-value	Statistically Different from Control?
20% SFS FRAP	2	-73	183.33	1.206	0.294	No
	4	-170	66.67	2.500	0.067	No
	7	-260	216.67	2.219	0.091	No
	14	-380	1066.67	0.875	0.431	No
	28	-460	266.67	1.750	0.155	No
	56	-510	1066.67	2.000	0.116	No
	100	-547	2966.67	1.499	0.208	No
	150	-583	233.33	3.207	0.0327	Yes
50% SFS FRAP	2	-100	166.67	1.265	0.275	No
	4	-190	116.67	4.158	0.014	Yes
	7	-270	66.67	5.500	0.005	Yes
	14	-413	683.33	2.655	0.057	No
	28	-490	416.67	3.200	0.033	Yes
	56	-560	1016.67	3.969	0.017	Yes
	100	-603	2866.67	2.821	0.048	Yes
	150	-620	266.67	5.750	0.0045	Yes
100% EAF	2	-120	1516.67	1.048	0.354	No
	4	-173	183.33	1.809	0.145	No
	7	-320	666.67	4.111	0.015	Yes
	14	-443	1483.33	2.756	0.051	No
	28	-517	1733.33	2.353	0.078	No
	56	-570	2416.67	2.824	0.048	Yes
	100	-630	3900.00	2.942	0.042	Yes
	150	-687	1333.33	4.808	0.0086	Yes
100% BOF	2	-90	316.67	0.229	0.830	No
	4	-207	883.33	2.198	0.093	No
	7	-297	533.33	3.359	0.028	Yes
	14	-437	1633.33	2.424	0.072	Yes
	28	-537	2033.33	2.716	0.053	Yes
	56	-577	2283.33	3.076	0.037	Yes
	100	-657	4966.67	3.070	0.037	Yes
	150	-727	1333.33	6.149	0.0035	Yes

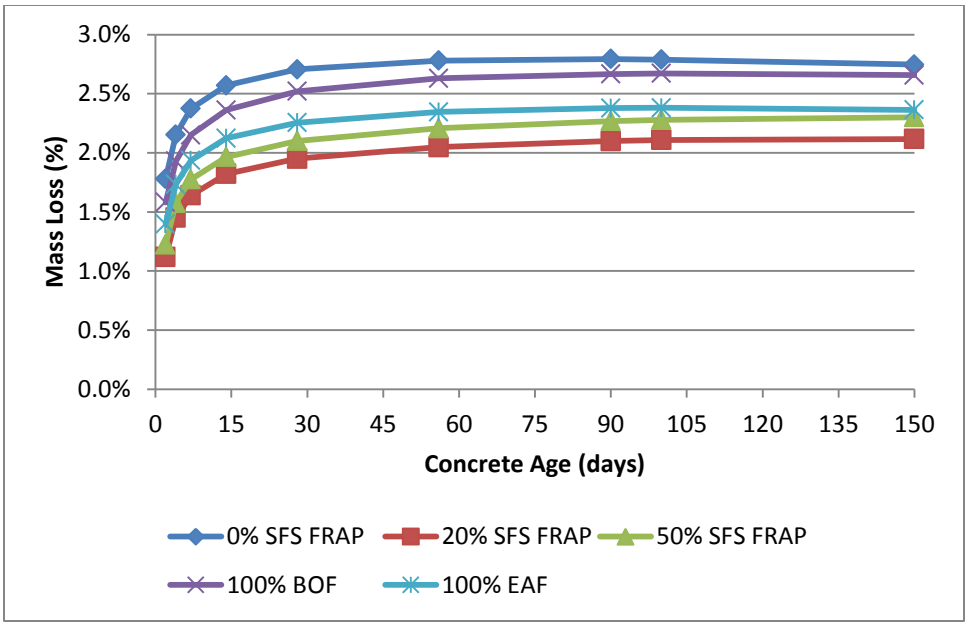

Figure 71. Mass loss caused by shrinkage up to 150 days for concrete with 0, 20, and 50% SFS FRAP and 100% virgin SFS (EAF and BOF).

5.10 FREEZE/THAW DURABILITY

The freeze/thaw testing was performed on four mixes: 20% SFS FRAP, 50% SFS FRAP, 100% Virgin SFS 1 (BOF), and 100% Virgin SFS 2 (EAF). The virgin SFS aggregates were tested in order to evaluate if and how the SFS in the FRAP could affect the freeze-thaw durability, particularly SFS with high expansion potential. Three replicates of each mix were tested. The temperature cycled between 40°F (4°C) and 0°F (-18°C) with the samples covered with 1/32 to 1/8 inch (1 to 3 mm) of water. At intervals of 36 freeze/thaw cycles or less, the fundamental transverse frequency and specimen weight were measured. The test was completed once 300 freeze/thaw cycles were achieved. The relative dynamic modulus of elasticity (P_i) after *i* number of freeze/thaw cycles is computed as follows, where n_0 is the initial fundamental transverse frequency and n_i is the fundamental transverse frequency after *i* number of freeze/thaw cycles:

$$P_i = \left(\frac{n_i}{n_0}\right)^2 (100\%) \quad (23)$$

The durability factor (DF) is then considered the P_i at the end of the freeze/thaw cycling. The weight lost after *i* number of freeze/thaw cycles can be computed using the same equation used for shrinkage (Equation 22), except that *i* instead refers to the *i* number of freeze/thaw cycles.

Initially, in the first 50 cycles, the freeze/thaw cycles were slower than the ASTM C666 specification, with about 2 cycles occurring per day. This resulted in an increase in the fundamental transverse frequency within the first 36 cycles, as the concrete prisms essentially gained strength from 14 days (when the test started) to 28 days (when the prisms were tested after 36 cycles), as can be seen in Figure 72. Because of a refrigerant leak, the freeze/thaw chamber frequently required a refrigerant recharge, but after each recharge, the chamber was able to complete at most about 4 cycles per day. Towards the

end of the freeze/thaw cycling (after about 270 freeze/thaw cycles), the machine was only able to perform about one cycle per day.

The durability factor did not significantly decrease for any of the mixtures after 300 cycles, as indicated in Table 62 and Table 63. Only the mixture with 50% SFS FRAP decreased significantly, while the other mixtures (20% SFS FRAP, 100% BOF, 100% EAF) were relatively constant throughout all freeze/thaw cycles.

Considering that there was an increase in the durability factor from 0 to 36 cycles, the durability factor could also be considered as a reduction from 36 cycles, essentially considering the overall net change in the durability factor from 36 to 300 cycles. As can be seen in Table 63, the durability factor from 36 to 300 cycles was reduced to 80% for the mix with 50% SFS FRAP while the other mixtures (20% SFS FRAP, 100% BOF, 100% EAF) remained at a factor of around 100%. Thus, it can be seen that all mixtures exhibited suitable freeze/thaw durability after 300 cycles, considering that a typical acceptable freeze/thaw durability factor is 70% (Marek 1991).

The weight loss throughout the freeze/thaw cycling is shown in Figure 73, Table 64, and Table 65. The mixes with SFS FRAP did not experience as much weight loss as the two virgin SFS mixes. The mix with 100% BOF, which had a high free CaO content, experienced the most weight loss as a result of surface scaling, possibly from the hydration expansion of the free CaO.

The prisms were tested after an additional 36 freeze/thaw cycles in order to determine the net change from 36 to 336 cycles (i.e. considering the “zero” point to be after 36 cycles). As can be seen in Figure 74, there was a significant decrease in the durability factors for the mixes with SFS FRAP, particularly for 50% SFS FRAP which decreased to 53%. After 336 cycles, as expected, all mixes experienced additional mass loss (Figure 75).The mixes with virgin SFS did not appear to be greatly affected by the additional freeze/thaw cycles.

It is concluded that the asphalt coating and not the SFS content was the main factor in the freeze/thaw durability of the concrete with SFS FRAP. Obratil et al. (2009) tested an unspecified type of SFS with an unknown free CaO content and found a durability factor of 87% after 300 freeze/thaw cycles. Papayianni and Anastasiou (2010a) tested the freeze/thaw scaling resistance in a sodium chloride solution of concrete with 100% low-expansion EAF and found relatively low mass losses when supplementary cementitious materials were not used. Brand et al. (2012) also found that higher FRAP contents reduce the freeze/thaw durability of concrete, although the dolomite FRAP tested in that study had a durability factor of 86% for 50% dolomite FRAP after 300 freeze/thaw cycles. For a mix with 100% coarse RAP and 50% fine RAP, Berry et al. (2013) found a durability factor of 94% after 300 freeze/thaw cycles.

In studies of HMA, freeze/thaw cycling has been found to strip the asphalt from an aggregate surface (Williams and Miknis 1998), effectively altering the chemical composition of the asphalt adsorbed at the asphalt-aggregate interface (S.-C. Huang et al. 2005), which reduces the HMA modulus (McCann and Sebaaly 2003; Ameri et al. 2013). This suggests that the freeze/thaw cycling of concrete with FRAP may separate the asphalt from the aggregate or the cement interfaces, thus reducing the overall dynamic modulus of the concrete.

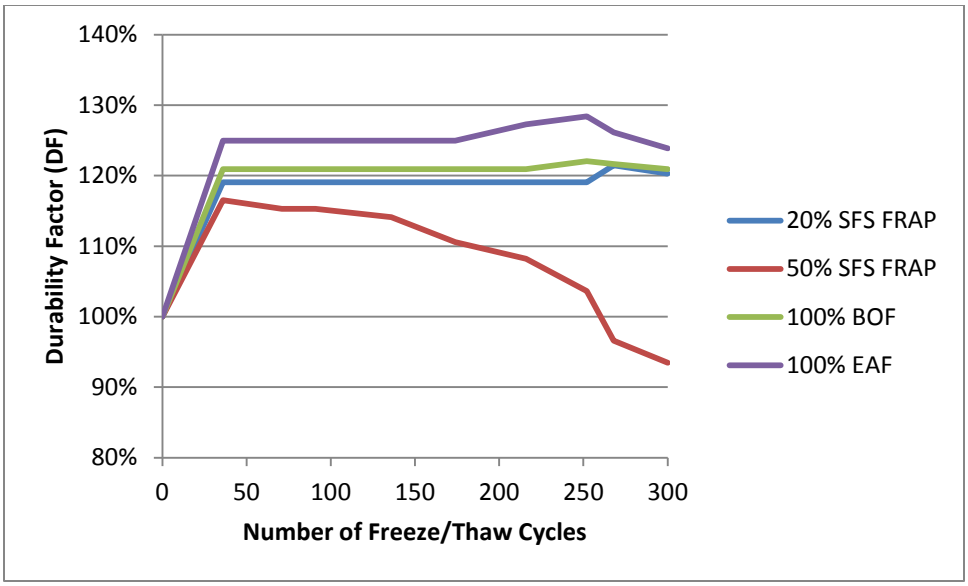

Figure 72. Freeze/thaw durability of mixtures with SFS FRAP and virgin SFS from 0 to 300 cycles.

Table 62. Durability Factors for Each Specimen from 0 to 300 Cycles

Mix	Prism No.	Durability Factor (After X Cycles) (%)									
		0	36	71	91	136	174	216	252	268	300
20% SFS FRAP	1	100	124	124	124	124	124	124	124	128	128
	2	100	116	116	116	116	116	116	116	116	116
	3	100	116	116	116	116	116	116	116	120	116
50% SFS FRAP	1	100	119	115	115	115	112	108	105	101	97
	2	100	114	114	114	114	107	107	101	90	85
	3	100	116	116	116	113	113	109	106	99	99
100% BOF	1	100	120	120	120	120	120	120	120	123	120
	2	100	120	120	120	120	120	120	124	120	120
	3	100	123	123	123	123	123	123	123	122	123
100% EAF	1	100	124	124	124	124	124	128	128	131	124
	2	100	125	125	125	125	125	125	128	125	125
	3	100	126	126	126	126	126	129	129	122	122

Table 63. Average Durability Factor after 300 Freeze/Thaw Cycles

Mixture	Average Durability Factor from 0 to 300 Cycles	Average Durability Factor from 36 to 300 Cycles	Average Durability Factor from 36 to 336 Cycles
20% SFS FRAP	120%	101%	88%
50% SFS FRAP	93%	80%	53%
100% BOF	121%	100%	100%
100% EAF	124%	99%	101%

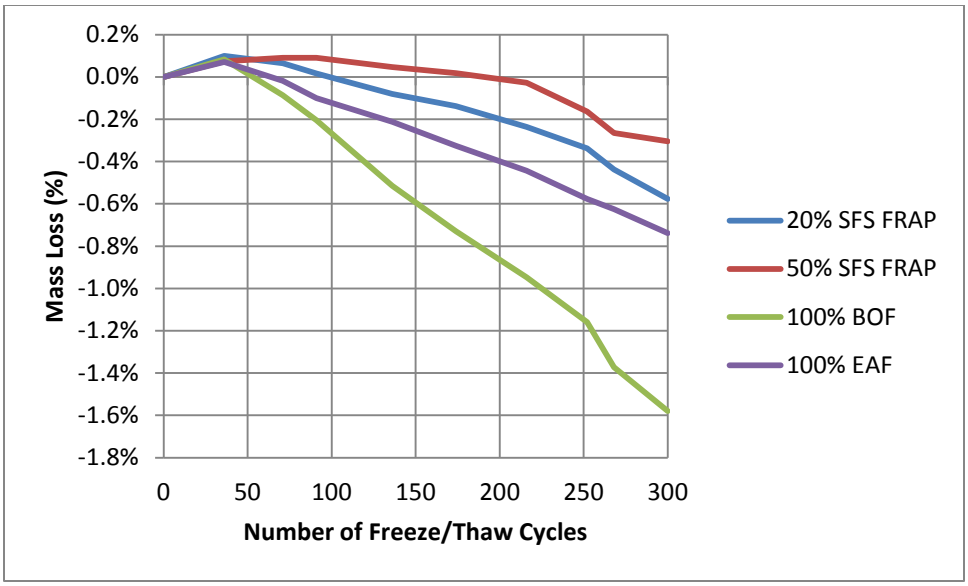

Figure 73. Weight loss during freeze/thaw cycling (0 to 300 cycles) for mixtures with SFS FRAP and virgin SFS.

Table 64. Mass Loss for Each Specimen from 0 to 300 Cycles

Mix	Prism No.	Mass Loss (After X Cycles) (%)									
		0	36	71	91	136	174	216	252	268	300
20% SFS FRAP	1	0.00	0.09	0.06	-0.04	-0.21	-0.35	-0.50	-0.61	-0.71	-0.82
	2	0.00	0.04	0.04	0.03	-0.06	-0.08	-0.18	-0.30	-0.48	-0.74
	3	0.00	0.16	0.10	0.06	0.03	0.02	-0.02	-0.11	-0.12	-0.16
50% SFS FRAP	1	0.00	0.04	0.09	0.08	0.02	0.02	-0.01	-0.29	-0.35	-0.18
	2	0.00	0.10	0.09	0.08	0.04	-0.05	-0.14	-0.23	-0.46	-0.65
	3	0.00	0.07	0.09	0.11	0.08	0.08	0.07	0.02	0.01	-0.08
100% BOF	1	0.00	0.06	-0.10	-0.25	-0.53	-0.72	-0.93	-1.13	-1.36	-1.59
	2	0.00	0.08	-0.08	-0.20	-0.56	-0.77	-1.03	-1.23	-1.46	-1.70
	3	0.00	0.10	-0.08	-0.17	-0.45	-0.70	-0.88	-1.11	-1.29	-1.44
100% EAF	1	0.00	0.07	-0.04	-0.09	-0.24	-0.33	-0.41	-0.54	-0.58	-0.71
	2	0.00	0.06	-0.03	-0.13	-0.20	-0.29	-0.42	-0.59	-0.63	-0.76
	3	0.00	0.08	0.02	-0.08	-0.20	-0.36	-0.50	-0.60	-0.66	-0.75

Table 65. Average Weight Loss after 300 Freeze/Thaw Cycles

Mixture	Average Weight Loss from 0 to 300 Cycles	Average Weight Loss from 36 to 300 Cycles	Average Weight Loss from 36 to 336 Cycles
20% SFS FRAP	-0.58%	-0.67%	-1.13%
50% SFS FRAP	-0.30%	-0.38%	-1.12%
100% BOF	-1.58%	-1.66%	-2.17%
100% EAF	-0.74%	-0.81%	-1.22%

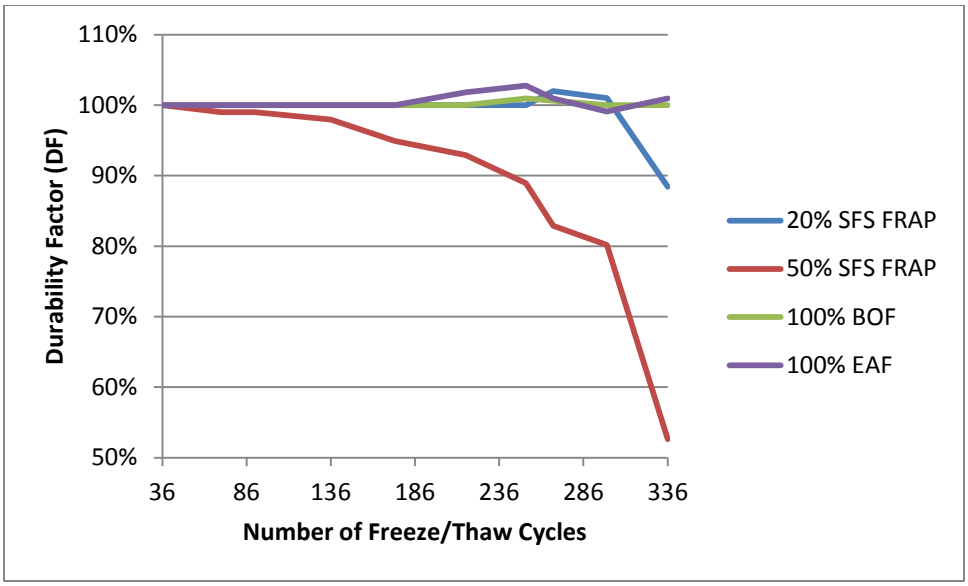

Figure 74. Freeze/thaw durability of mixtures with SFS FRAP and virgin SFS from 36 to 336 cycles.

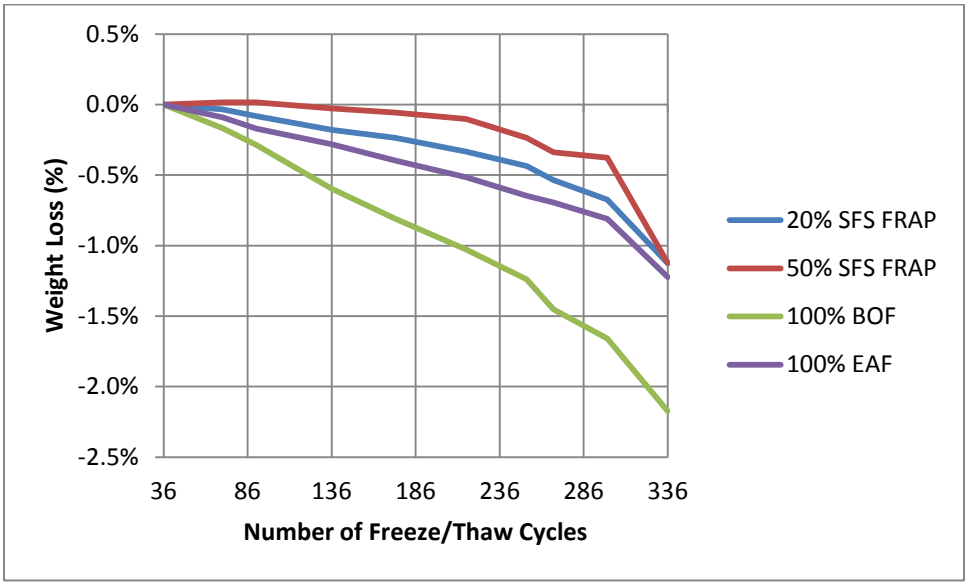

Figure 75. Weight loss during freeze/thaw cycling (0 to 336 cycles) for mixtures with SFS FRAP and virgin SFS.

Comparing the SFS FRAP freeze/thaw durability with the dolomite FRAP results (Table 66), the SFS FRAP performed similarly to dolomite FRAP, particularly at lower FRAP contents. The 50% SFS FRAP mix durability factor was lower than the 50% dolomite FRAP mix, but the durability was still suitable. The SFS FRAP had a higher asphalt content than the dolomite FRAP, which may have been the primary cause of the reduction in durability factor.

Table 66. Net Freeze/Thaw Durability after 300 Cycles Comparing Dolomite and SFS FRAP

Mix	Durability Factor		Mass Loss	
	Dolomite FRAP*	SFS FRAP	Dolomite FRAP*	SFS FRAP
0% FRAP	101%	--	-1.79%	--
20% FRAP	102%	101%	-1.79%	-0.67%
35% FRAP	90%	--	-2.72%	--
50% FRAP	86%	80%	-2.58%	-0.38%
100% BOF	--	100%	--	-1.66%
100% EAF	--	99%	--	-0.81%

*Source: Brand et al. (2012)

Images of the concrete specimens after 300 freeze/thaw cycles can be found in Figure 76, Figure 77, Figure 78, and Figure 79. The mixes SFS FRAP showed scaling particularly over the FRAP particles, but there also appeared to be pop-outs over the virgin aggregates in the concrete. The mixes with virgin SFS showed significant surface scaling, particularly the concrete with 100% BOF, which is to be expected considering that this mix had the greatest amount of mass loss. In one of the prisms with 100% EAF, an EAF slag aggregate near the surface appears to have undergone corrosion, as evidenced by the rust-colored stains on the surface of the concrete, as shown in Figure 78.

Prism 1

Prism 2

Prism 3

Figure 76. Images of the concrete prisms with 20% SFS FRAP after 300 freeze/thaw cycles.

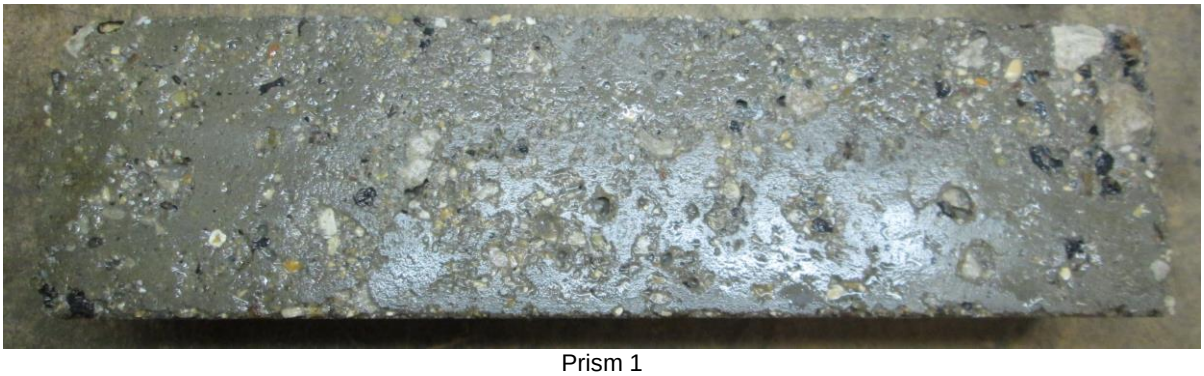

Prism 1

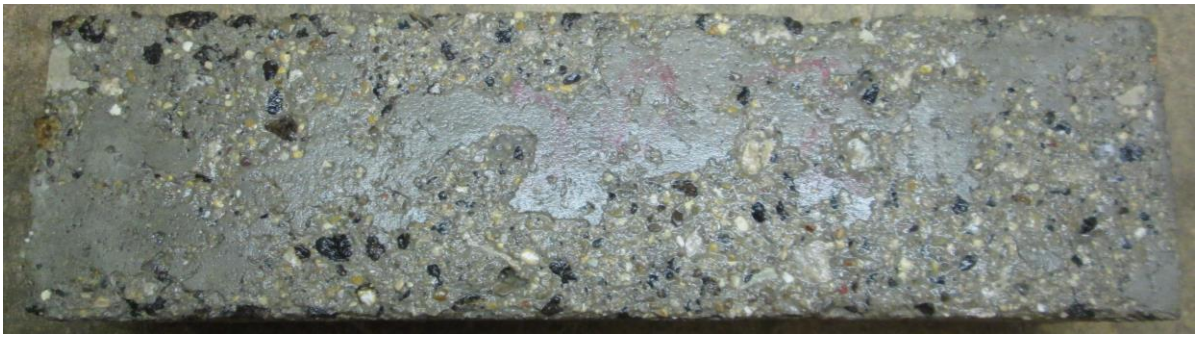

Prism 2

Prism 3

Figure 77. Images of the concrete prisms with 50% SFS FRAP after 300 freeze/thaw cycles.

Prism 1

Evidence of corrosion in and EAF slag particle in Prism 1

Prism 2

Prism 3

Figure 78. Images of the concrete prisms with 100% EAF after 300 freeze/thaw cycles.

Prism 1

Prism 2

Prism 3

Figure 79. Images of the concrete prisms with 100% BOF after 300 freeze/thaw cycles.

5.11 MATCHED GRADATION STUDY

The three SFS FRAP sources all had similar asphalt and SFS aggregate contents but different stockpiled ages. To best compare the three SFS FRAP sources and see if an older stockpiled (i.e. more oxidized) FRAP will improve the concrete strength, each source was sieved to match a single gradation (Table 67). This gradation was selected because it was similar to the base gradations of each SFS FRAP source.

Table 67. Matched Gradation to Compare the SFS FRAP Sources

Sieve Size		Cumulative Percent Passing	Percent Retained
5/8 inch	16mm	100.0%	0.0%
1/2 inch	12.5mm	99.5%	0.5%
3/8 inch	9.5mm	80.0%	19.5%
1/4 inch	6.35mm	40.0%	40.0%
#4	4.75mm	10.0%	30.0%
#8	2.36mm	0.0%	10.0%

Because of material availability, a different fine aggregate (natural sand) source was used (SSD Specific Gravity = 2.57, Absorption = 1.57%). Also, in order to avoid any potential chemical interactions, no chemical admixtures were used. The concrete mix design used for this matched gradation study is shown in Table 68. The water-to-cement ratio was 0.40. The coarse aggregate consisted entirely of SFS FRAP. The mixing procedure consisted of mixing the SFS FRAP and fine aggregate with about one-half of the water for 30 seconds, after which the cement and remaining water were added. The concrete was mixed for 3 minutes, rested for 3 minutes, and mixed a final 2 minutes.

Table 68. Concrete Mix Design for the Matched Gradation SFS FRAP Study

Constituent	Content (lb/yd^3)
Cement	600.0
SFS FRAP (SSD)	1806.4
Fine Aggregate (SSD)	1151.6
Water	239.2

The concrete fresh properties are shown in Table 69. As expected, the air content was relatively low because of the absence of an air-entrainment admixture. In addition, without a water reducing admixture, the slump was relatively low as well. The unit weights were similar between all three mixtures because the SFS FRAP sources all had similar specific gravities.

Table 69. Concrete Fresh Properties for the Matched Gradation Study

SFS FRAP Type	Slump (inch)	Air Content (%)	Unit Weight (lb/ft^3)
SFS FRAP 1 (Curran)	1/4	2.8	153.0
SFS FRAP 2 (Geneva)	1/4	2.5	150.8
SFS FRAP 3 (Central Blacktop)	1/4	3.0	151.6

Because 100% SFS FRAP was used as the coarse aggregate, the compressive strength was significantly less than at lower SFS FRAP contents (Figure 80). At all ages, SFS FRAP 2 was statistically different (with 95% confidence) from both SFS FRAP 1 and 3, while SFS FRAP 1 and 3 were statistically similar. The coefficient of variation for the compressive strengths was similar to the mixes with lower SFS FRAP contents.

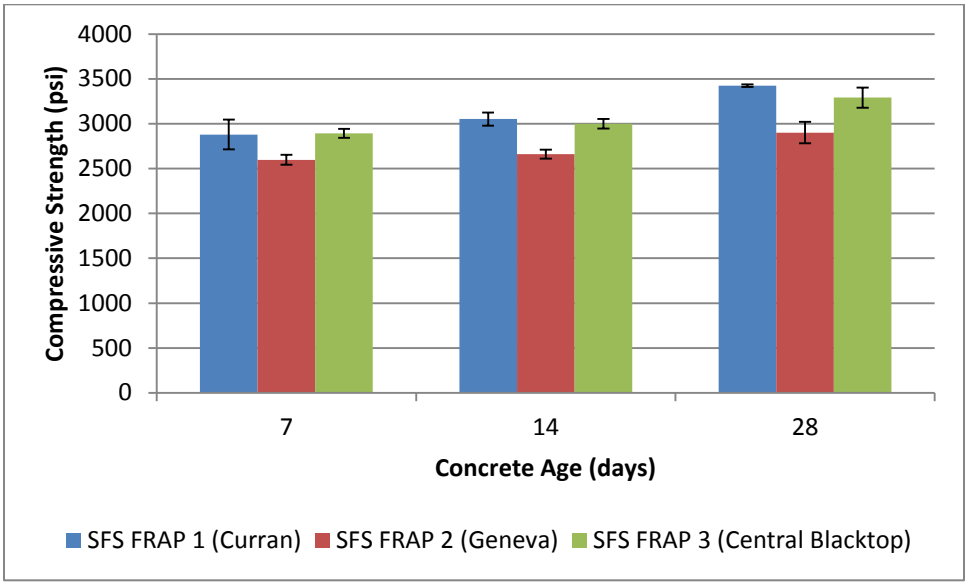

Figure 80. Compressive strength of the 100% SFS FRAP matched gradation study.

Similarly, the split tensile strengths were likewise significantly lower relative to mixes with lower SFS FRAP contents (Figure 81). At all ages, all three SFS FRAP mixes were statistically similar with 95% confidence, which was likely an artifact of the high standard deviations. The coefficient of variation was found to be consistently high (upwards of 20%) at all ages, relative to the values for mixes with lower SFS FRAP contents. This could be a result of using 100% SFS FRAP in the concrete mixture.

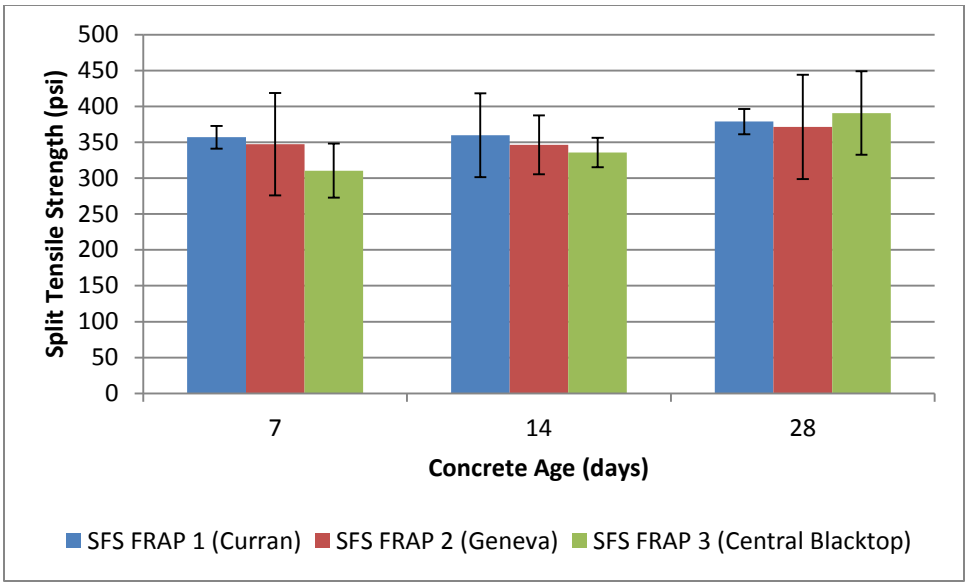

Figure 81. Split tensile strength of the 100% SFS FRAP matched gradation study.

The results of this matched gradation study suggest that concrete made with similar SFS FRAP sources (similar in asphalt content and SFS content) can have statistically similar properties. The magnitude of the findings does not represent the realistic strength performance of paving mixes, which would have a lower SFS FRAP content. Standard deviations were very high also because of the 100% SFS FRAP content.

RECOMMENDATIONS

Tests performed on the three SFS FRAP samples indicate that the SFS aggregates can retain residual free CaO despite years in service in an asphalt pavement and even after some weathering in stockpiles. The asphalt coating on the SFS aggregates prevents or hinders the complete hydration of the free CaO and/or free MgO in the SFS aggregates. Autoclave expansion testing, with and without the asphalt coating, suggested that the asphalt coating did hinder, but did not necessarily prevent, the CaO and MgO hydration reactions. This finding agrees with past studies that have found that SFS FRAP may not expand significantly (Senior et al. 1994; Deniz et al. 2010; Dayioglu et al. 2014), at least relative to the expansion of virgin SFS. Concrete strength, shrinkage, and fracture testing with up to 50% coarse SFS FRAP indicated suitable performance relative to conventional concrete with virgin aggregates and similar dolomite FRAP.

The SFS FRAP expansion appears to be dependent on the free CaO, free MgO, and asphalt contents, so prior to utilizing SFS FRAP as an aggregate in concrete, it is recommended that the material be tested to determine the residual free CaO, the free MgO, and asphalt contents, and autoclave expansion with the coated and uncoated SFS FRAP. It is recommended that SFS FRAP be potentially utilized as a coarse aggregate in concrete pavements only if the extracted SFS has a limited autoclave expansion and low free CaO and free MgO contents. Additional testing is required to establish these limits. A number of previous field studies in the United States have shown deleterious expansion of SFS concrete, likely with high free CaO and free MgO contents, but a number of projects in Europe have clearly demonstrated that SFS can be successfully utilized as an aggregate in concrete with appropriate material characterization and processing. Based on the limited SFS FRAP sources tested in this study, definitive limits on the free CaO and free MgO content, asphalt content, and permissible autoclave expansion cannot be established without a larger sample size of SFS sources.

From the concrete strength, durability, and fracture tests, it is clear that virgin SFS and SFS FRAP performs acceptably in the short-term pending expansion testing. Temporary roads, barriers, and concrete fill, for example, could all be suitable applications for the immediate utilization of SFS FRAP without further testing.

Additionally, SFS aggregates may be tested for new asphalt pavement surfaces in order to ensure that SFS aggregates could be used as SFS FRAP aggregates in concrete or other stabilized or unstabilized layers in the future. Ideally, SFS aggregate for this application would contain low free CaO and free MgO contents and be minimally expansive. Weathering the (virgin) SFS aggregates – such as by keeping the stockpile continuously moist and periodically turning the pile – could assist in mitigating the expansive characteristics of the SFS aggregates prior to use in asphalt pavements. Weathering has been shown to be effective for SFS aggregates use in concrete (Manso et al. 2004, 2006, 2011). Also, there may be other acceptable processes to reduce the free CaO and/or free MgO contents in the SFS aggregates, which would require further investigation.

SUMMARY AND CONCLUSIONS

Steel furnace slag (SFS), an industrial by-product, has typically seen little utilization in bound applications, such as in concrete as an aggregate, but has often been used a high-quality frictional aggregate in asphalt pavement surface courses. In recent years, roadway reconstruction and rehabilitation initiatives have produced significant amounts of reclaimed asphalt pavement (RAP) containing SFS aggregates, and there is presently few allowable applications for the use of SFS RAP in the United States.

This study primarily investigated the potential of using coarse fractionated reclaimed asphalt pavement (FRAP) with SFS aggregates as a partial replacement of the coarse aggregate in concrete. Initially, three SFS FRAP sources (the total aggregate of each roughly contained one-third SFS) and three virgin SFS sources were evaluated for chemical and mineralogical composition, free calcium oxide (CaO) content, and expansion potential. Of the SFS FRAP sources, only one was evaluated as 20% and 50% replacements of the virgin aggregate in concrete, and this concrete was evaluated for strength (compression, split tension, and flexural), modulus, drying shrinkage, freeze/thaw durability, and fracture. Additionally, for comparison, two of the virgin SFS sources (one with high free CaO and the other with very low free CaO) were evaluated as 100% replacements of the coarse aggregate in concrete to determine the effects on strength, drying shrinkage, freeze/thaw durability, and fracture.

Based on the chemical and mineralogical tests, it was concluded that the virgin SFS compositions were similar to other SFS materials documented in the literature. Mineralogical testing confirmed that the SFS FRAP was composed of dolomite, SFS, and quartz. Complexometric titration using an ethylene glycol extraction technique in conjunction with thermogravimetric analysis was utilized to estimate the total free CaO content of each of the samples. The virgin SFS sources had free CaO ranging from <0.1% to 3.4% while the estimated free CaO contents of the SFS FRAP sources were about 1.0% to 1.5%. Using the results of the thermogravimetric analysis of SFS aggregates after autoclaving and assuming that all of the available free magnesium oxide (MgO) in the SFS fully hydrated, the free MgO content was estimated to range from 0.2% to 2.2% for the virgin SFS sources.

Compacted aggregate samples were autoclaved with steam at 300 psi and 420°F for three hours. Additional SFS mineralogical testing confirmed that expansion was being caused by the hydration of the free CaO and free MgO. An additional mineralogical phase change was noted as the conversion from β-dicalcium silicate (larnite) to γ-dicalcium silicate (calcio-olivine), which in some instances resulted in the disintegration of the SFS particle as there is a slight increase in unit cell volume associated with this phase change. In particular, this phase change was visibly evident with the SFS FRAP. The virgin SFS and the SFS FRAP with the asphalt coating removed experienced significant expansion (1% to 9%), except for the virgin SFS source with only <0.1% free CaO, which expanded by only 0.1%. In comparison, all SFS FRAP sources with the asphalt intact experienced a contraction rather than an expansion, which was partially due to some of the asphalt binder filling the voids between aggregates as well as the some of the SFS particles disintegrating from the β- to γ-dicalcium silicate phase change. These findings suggest that, for two of the three SFS FRAP sources, the asphalt coating prevents or hinders the hydration of the free

expansive oxide phases (for one of these sources, stockpile weathering after milling may have resulted in minimal expansion), while for the third SFS FRAP source, the expansion of the free oxides was offset by the contraction as a result of the asphalt and dicalcium silicate phase conversion.

In concrete, the SFS FRAP as a partial coarse aggregate replacement performed comparably to dolomite FRAP. The strength (compressive, split tensile, and flexural) was similar to, and in some instances not statistically different from, the strength of concrete with the same content of dolomite FRAP. The concrete modulus of elasticity with SFS FRAP was slightly higher than dolomite FRAP because of the stiffer SFS aggregates. Concrete with SFS FRAP aggregates experienced slightly greater shrinkage than concrete with dolomite aggregates, resulting in statistically higher shrinkage strains at later ages, although the shrinkage magnitude was still acceptable for conventional paving concrete. Concrete with SFS FRAP had some statistically similar fracture properties to dolomite concrete, namely the total fracture energy and the critical stress intensity factor. The freeze/thaw durability showed acceptable performance after 300 freeze/thaw cycles, with net durability factors of 101% and 80% for the 20% and 50% SFS FRAP mixes, respectively, although continuing past 300 cycles to 336 cycles significantly reducing the net durability factors to 88% and 53% for the 20% and 50% SFS FRAP mixes, respectively. This reduction in freeze/thaw durability is suspected to be due to the asphalt coating on the FRAP and not the SFS aggregate in the FRAP.

Concrete mixtures were also tested with 100% coarse virgin SFS, evaluating the effects of the SFS with high (3.4%) and low (<0.1%) free CaO contents. The compressive and split tensile strengths were lower than dolomite concrete, with the exception of the low free CaO SFS concrete compressive strength. The drying shrinkage of the concrete with SFS was statistically greater than dolomite concrete possibly because of the porous nature of the SFS aggregates and different aggregate source gradations. Relative to the dolomite concrete, the concrete fracture properties were statistically greater for the low free CaO SFS, while only the critical stress intensity factor was greater for the concrete with high free CaO SFS,. The freeze/thaw durability was unaffected by the free CaO content of the SFS, resulting in a durability factor of around 100% after 300 freeze/thaw cycles.

The main conclusions drawn from this study are the following: (1) SFS FRAP can contain significant amounts of free expansive oxides (CaO and MgO) even after weathering; (2) despite residual free expansive oxide contents, the autoclave testing of SFS FRAP produces minimal expansion, which can be misleading; (3) concrete performance with up to 50% SFS FRAP is suitable and similar to concrete with dolomite FRAP, indicating that the presence of the SFS in the FRAP is not detrimental to the concrete strength and durability; (4) concrete strength and durability with 100% virgin SFS (up to 3.4% free CaO) is acceptable; (5) virgin SFS free oxide content and expansion tests should be run before accepting them to make sure they are being used in the correct application.

REFERENCES

AASHTO T22. (2007). “Compressive Strength of Cylindrical Concrete Specimens,” American Association of State Highway and Transportation Officials: Washington DC.

AASHTO T97. (2003). “Flexural Strength of Concrete (Using Simple Beam with Third-Point Loading),” American Association of State Highway and Transportation Officials: Washington DC.

AASHTO T160. (2009). “Length Change of Hardened Hydraulic Cement Mortar and Concrete,” American Association of State Highway and Transportation Officials: Washington DC.

AASHTO T161. (2008). “Resistance of Concrete to Rapid Freezing and Thawing,” American Association of State Highway and Transportation Officials: Washington DC, 10 p.

AASHTO T164. (2011). “Quantitative Extraction of Asphalt Binder from Hot Mix Asphalt (HMA),” American Association of State Highway and Transportation Officials: Washington DC.

AASHTO T198. (2009). “Splitting Tensile Strength of Cylindrical Concrete Specimens,” American Association of State Highway and Transportation Officials: Washington DC.

AASHTO T313. (2010). “Determining the Flexural Creep Stiffness of Asphalt Binder Using the Bending Beam Rheometer (BBR),” American Association of State Highway and Transportation Officials: Washington DC.

AASHTO T315. (2010). “Determining the Rheological Properties of Asphalt Binder Using a Dynamic Shear Rheometer (DSR),” American Association of State Highway and Transportation Officials: Washington DC.

Abu-Eishah, S.I., A.S. El-Dieb, and M.S. Bedir. (2012). “Performance of Concrete Mixtures Mad with Electric Arc Furnace (EAF) Steel Slag Aggregate Produced in the Arabian Gulf Region,” *Construction and Building Materials*, Volume 34, pp. 249-256.

ACI318. (2008). *Building Code Requirements for Structural Concrete*, American Concrete Institute: Farmington Hills.

Adégoloyé, G., A.-L. Beaucour, S. Ortola, and A. Noumowé. (2013). “High-Strength Concrete using EAF and AOD Slags and Aggregates,” *Proceedings of the Third International Slag Valorisation Symposium*, eds. A. Malfliet, P.T. Jones, K. Binnemans, Ö. Cizer, J. Fransaer, P. Yan, Y. Pontikes, M. Guo, and B. Blanpain, Leuven, Belgium, pp. 351-354.

Ahmed, I. (1991). *Use of Waste Materials in Highway Construction*, Report No. FHWA/IN/JHRP-91/03, Purdue University, Indiana Department of Transportation, Indianapolis.

Ahmed, I., and C.W. Lovell. (1991). “Use of Waste Materials in Highway Construction: State of the Practice and Evaluation of the Selected Waste Products,” *Transportation Research Record*, Issue 1345, pp. 1-9.

AHTD. (2014). “Standard Specification for Highway Construction,” Arkansas State Highway and Transportation Department, Little Rock, Arkansas.

Akinmusuru, J.O. (1991). “Potential Beneficial Uses of Steel Slag Wastes for Civil Engineering Purposes,” *Resources, Conservation and Recycling*, Volume 5, pp. 73-80.

Al-Negheimish, A.I., F.H. Al-Sugair, and R.Z. Al-Zaid. (1997). “Utilization of Local Steelmaking Slag in Concrete,” *Journal of King Saud University, Engineering Sciences*, Volume 9, Issue 1, pp. 39-55.

Al-Oraimi, S., H.F. Hassan, and A. Hago. (2009). “Recycling of Reclaimed Asphalt Pavement in Portland Cement Concrete,” *The Journal of Engineering Research*, Volume 6, Issue 1, pp. 37-45.

ALDOT. (2012). “Standard Specifications for Highway Construction,” Alabama Department of Transportation, Montgomery, Alabama.

Ali, S.I. (2003). *Effects of Aggregate Quality on Reinforcement Corrosion*, Master of Science Thesis, King Fahd University of Petroleum and Minerals, Dhahran, Saudi Arabia.

Ali, K.S., N.M. Ishak, and A.R.M. Ridzuan. (2011). “Performance of Concrete Containing Steel Slag Exposed to Sulphate Environment: A Comparison of Steel Slag and Natural Aggregate Use,” *Proceedings of the IEEE Symposium on Business, Engineering and Industrial Applications*, Langkawi, Malaysia, pp. 570-575.

Alizadeh, R., M. Chini, P. Ghods, M. Hoseini, Sh. Montazer, and M. Shekarchi. (2003). “Utilization of Electric Arc Furnace Slag as Aggregates in Concrete – Environmental Issue,” *Proceedings of the CANMET/ACI International Conference on Recent Advances in Concrete Technology*, Bucharest, Romania, pp. 451-464.

Almusallam, A.A., H. Beshr, M. Maslehuddin, and O.S.B. Al-Amoudi. (2004). “Effect of Silica Fume on the Mechanical Properties of Low Quality Coarse Aggregate Concrete,” *Cement and Concrete Composites*, Volume 26, pp. 891-900.

Ameri, M., H. Shahabishahmiri, and S. Kazemzadehazad. (2012). “Evaluation of the Use of Steel Slag in Concrete,” *Proceedings of the 25th ARRB Conference*, Perth, Australia, 9 p.

Ameri, M., S. Kouchaki, and H. Roshani. (2013). “Laboratory Evaluation of the Effect of Nano-Organosilane Anti-Stripping Additive on the Moisture Susceptibility of HMA Mixtures under Freeze-Thaw Cycles,” *Construction and Building Materials*, Volume 48, pp. 1009-1016.

Anastasiou, E., K. Georgiadis Filikas, and M. Stefanidou. (2014). “Utilization of Fine Recycled Aggregates in Concrete with Fly Ash and Steel Slag,” *Construction and Building Materials*, Volume 50, pp. 154-161.

Armaghani, J.M., T.J. Larsen, and L.L. Smith. (1988). “Design-Related Distress in Concrete Pavements,” *Concrete International*, Volume 10, Issue 8, pp. 43-49.

Arribas, I., J.T. San-José, I. Vegas, J.A. Hurtado, and J.A. Chica. (2010). “Application of Steel Slag Concrete in the Foundation Slab and Basement Wall of the TECNALIA Kubik Building,” in *Ferrous Slag – Resource Development for an Environmentally Sustainable World*, Proceedings of the 6th European Slag Conference, Madrid, Spain, EUROSLAG Publication No. 5, pp. 251-264.

Artioli, G. (2010). “Inorganic Compounds and Minerals Studied Using X-Ray Diffraction,” in *Encyclopedia of Spectroscopy and Spectrometry*, 2nd Edition, eds. J.C. Lindon, G.E. Tranter, and D. Koppenaal, Academic Press: Waltham, pp. 1048-1056.

ASTM C29. (2009). “Standard Test Method for Bulk Density (‘Unit Weight‘) and Voids in Aggregate,” ASTM International: West Conshohocken.

ASTM C127. (2007). “Standard Test Method for Density, Relative Density (Specific Gravity), and Absorption of Coarse Aggregate,” ASTM International: West Conshohocken.

ASTM C136. (2006). “Standard Test Method for Sieve Analysis of Fine and Coarse Aggregates,” ASTM International: West Conshohocken.

ASTM C138. (2013). “Standard Test Method for Density (Unit Weight), Yield, and Air Content (Gravimetric) of Concrete,” ASTM International: West Conshohocken.

ASTM C143. (2012). “Standard Test Method for Slump of Hydraulic-Cement Concrete,” ASTM International: West Conshohocken.

ASTM C192. (2007). “Standard Practice for Making and Curing Concrete Test Specimens in the Laboratory,” ASTM International: West Conshohocken.

ASTM C231. (2010). “Standard Test Method for Air Content of Freshly Mixed Concrete by Pressure Method,” ASTM International: West Conshohocken.

ASTM C469. (2010). “Standard Test Method for Static Modulus of Elasticity and Poisson’s Ratio of Concrete in Compression,” ASTM International: West Conshohocken.

ASTM D5106. (2013). “Standard Specification for Steel Slag Aggregates for Bituminous Paving Mixtures,” ASTM International: West Conshohocken.

ASTM D5404. (2011). “Standard Practice for Recovery of Asphalt from Solution Using the Rotary Evaporator,” ASTM International: West Conshohocken.

ASTM D6847. (2002). “Standard Test Method for Quantitative Extraction and Recovery of Asphalt Binder from Asphalt Mixtures,” ASTM International: West Conshohocken.

Bailey, J.J., and H.M. Reitz. (1970). “Discussion: ‘Building Damage from Expansive Steel Slag Backfill’ by C.B. Crawford and K.N. Burn,” *Journal of the Soil Mechanics and Foundations Division*, Proceedings of the American Society of Civil Engineers, Volume 96, Issue SM5, pp. 1810-1813.

Balcázar, N., M. Kühn, J.M. Baena, A. Formoso, and J. Piret. (1999). *Summary Report on RTD in Iron and Steel Slags: Development and Perspectives*, Proceedings No. EUR 19066 EN, European Commission, Luxembourg.

Barnes, T.M., and J.M. Strong. (1980). “Use of Lime Values in Steelmaking Slag Wastes,” *Proceedings of the Seventh Mineral Waste Utilization Symposium*, ed. M. Van Ness, Jr., Chicago, Illinois, pp. 135-144.

Bäverman, C., and F. Aran Aran. (1997). "A Study of the Potential of Utilising Electric Arc Furnace Slag as Filling Material in Concrete," in *Waste Materials in Construction: Putting Theory into Practice*, Studies in Environmental Science, Volume 71, eds. J.J.J.M. Goumans, G.J. Senden, and H.A. van der Sloot, pp. 373-376.

Belhadj, E., C. Diliberto, and A. Lecomte. (2012). "Characterization and Activation of Basic Oxygen Furnace Slag," *Cement and Concrete Composites*, Volume 34, pp. 34-40.

Bentsen, R.A., W.A. Vavrik, J.R. Roesler, and S.L. Gillen. (2013). "Ternary Blend Concrete with Reclaimed Asphalt Pavement as an Aggregate in Two-Lift Concrete Pavement," *Proceedings of the 2013 International Concrete Sustainability Conference*, National Ready Mixed Concrete Association, San Francisco, California.

Bergren, J. V., and R. A. Britson. (1977). *Portland Cement Concrete Utilizing Recycled Pavement*, Report MLR-7703, Iowa Department of Transportation.

Berry, M., J. Stephens, B. Bermel, A. Hagel, and D. Schroeder. (2013). *Feasibility of Reclaimed Asphalt Pavement as Aggregate in Portland Cement Concrete*, Report No. FHWA/MT-13-009/8207, Montana State University, Montana Department of Transportation.

Beshr, H., A.A. Almusallam, and M. Maslehuddin. (2003). "Effect of Coarse Aggregate Quality on the Mechanical Properties of High Strength Concrete," *Construction and Building Materials*, Volume 17, pp. 97-103.

Bilodeau, K., C. Sauzéat, H. Di Benedetto, F. Olard, and D. Bonneau. (2011). "Laboratory and In Situ Investigations of Steel Fiber Reinforced Compacted Concrete Containing Reclaimed Asphalt Pavement," *90th Annual Meeting of the Transportation Research Board*, Washington DC.

Bilodeau, K., C. Sauzéat, H. Di Benedetto, and F. Olard. (2012). "Roller Compacted Concrete for Road Base Layer with RAP and Steel Fibers: Viscous Properties and Description of Experimental Sites," *Proceedings from the 10th International Conference on Concrete Pavements*, Québec City, Canada, pp. 435-448.

Bly, P.G., and C.A. Weiss Jr. (2012). "Performance of Concrete Pavement Mixtures with Marginal Aggregates: Laboratory Investigation," *Proceedings of the 10th International Conference on Concrete Pavements*, Québec City, Canada.

Bonchin, S.L., G.K. Zoorob, and J.A. Caruso. (2010). "Atomic Emission, Methods and Instrumentation," in *Encyclopedia of Spectroscopy and Spectrometry*, 2nd Edition, eds. J.C. Lindon, G.E. Tranter, and D. Koppenaal, Academic Press: Waltham, pp. 70-77.

Bosela, P., N. Delatte, R. Obratil, and A. Patel. (2008). "Fresh and Hardened Properties of Paving Concrete with Steel Slag Aggregate," *Proceedings of the 9th International Conference on Concrete Pavements*, San Francisco, California, pp. 836-853.

Bosela, P.A., N.J. Delatte, and B. Fronek. (2012). *Freasibility of Expanding the Use of Steel Slag as a Concrete Pavement Aggregate*, Final Report, Cleveland State University, Federal Highway Administration, Washington DC.

Brand, A.S., J.R. Roesler, I.L. Al-Qadi, and P. Shangguan. (2012). *Fractionated Reclaimed Asphalt Pavement (FRAP) as a Coarse Aggregate Replacement in a Ternary Blended Concrete Pavement*, Report No. ICT-12-008, Illinois Center for Transportation, Illinois State Toll Highway Authority.

Brand, A.S., A.N. Amirkhanian, and J.R. Roesler. (2013). *Flexural Capacity of Rigid Pavement Concrete Slabs with Recycled Aggregates*, Report No. ICT-13-018, Illinois Center for Transportation, Illinois State Toll Highway Authority.

Brand, A.S., and J.R. Roesler. (2014). "Ternary Concrete with Fractionated Reclaimed Asphalt Pavement," *ACI Materials Journal*, in press.

Brand, A.S., A.N. Amirkhanian, and J.R. Roesler. (2014). "Flexural Capacity of Full-Depth and Two-Lift Concrete Slabs with Recycled Aggregates," *Transportation Research Record*, in press.

Caltrans. (2006). "Slag Aggregate," Standard Special Provision S8-M25, California Department of Transportation, Sacramento, California.

CCAA. (2008). *Use of Recycled Aggregates in Construction*, Report, Cement Concrete and Aggregates Australia, Sydney, Australia, 25 p.

CCAA. (2013). "Sustainable Use of Aggregates," Briefing 19, Cement Concrete and Aggregates Australia, Sydney, Australia, 11 p.

CDOT. (2011). "Standard Specifications for Road and Bridge Construction," Colorado Department of Transportation, Denver, Colorado.

Chan, C.J., W.M. Kriven, and J.F. Young. (1992). “Physical Stabilization of the β→γ Transformation in Dicalcium Silicate,” *Journal of the American Ceramic Society*, Volume 75, Issue 6, pp. 1621-1627.

Chaurand, P., J. Rose, V. Briois, L. Olivi, J.-L. Hazemann, O. Proux, J. Domas, and J.-Y. Bottero. (2007). “Environmental Impacts of Steel Slag Reused in Road Construction: A Crystallographic and Molecular (XANES) Approach,” *Journal of Hazardous Materials*, Volume 139, Issue 3, pp. 537-542.

Chen, D., X. Gao, and D. Dollimore. (1993). “The Application of Non-Isothermal Methods of Kinetic Analysis to the Decomposition of Calcium Hydroxide,” *Thermochimica Acta*, Volume 215, Issue C, pp. 65-82.

Collins, R.J. (1976). “Waste Products as a Potential Replacement for Aggregates,” in *Ash Utilization*, Proceedings of the Forth International Ash Utilization Symposium, St. Louis, Missouri, pp. 93-113.

Collins, R.J., and S.K. Ciesielski. (1994). *Recycling and Use of Waste Materials and By-Products in Highway Construction*, NCHRP Synthesis 199, Transportation Research Board, Washington DC.

Collins, R.J., and P.T. Sherwood. (1995). *Use of Waste and Recycled Materials as Aggregates: Standards and Specifications*, Final Report, Building Research Establishment, Department of the Environment, HMSO: London.

Coomarasamy, A., and T.L. Walzak. (1995). “Effects of Moisture on Surface Chemistry of Steel Slags and Steel Slag-Asphalt Paving Mixes,” *Transportation Research Record*, Issue 1492, pp. 85-95.

Coppola, L., S. Lorenzi, and A. Buoso. (2010). “Electric Arc Furnace Granulated Slag as a Partial Replacement of Natural Aggregates for Concrete Production,” *Proceedings of the Second International Conference on Sustainable Construction Materials and Technologies*, Ancona, Italy, 9 p.

Crawford, C.B., and K.N. Burn. (1969). “Building Damage from Expansive Steel Slag Backfill,” *Journal of the Soil Mechanics and Foundations Division*, Proceedings of the American Society of Civil Engineers, Volume 95, Issue SM6, pp. 1325-1334.

Crawford, C.B., and K.N. Burn. (1971). “Closure: Building Damage from Expansive Steel Slag Backfill,” *Journal of the Soil Mechanics and Foundations Division*, Proceedings of the American Society of Civil Engineers, Volume 97, Issue SM7, pp. 1027-1029.

da Silveira, N.O., M.V.A.M. e Silva, E.J. Agrizzi, M.F. de Lana, and R.L. de Mendonça. (2005). “ACERITA – Steel Slag with Reduced Expansion Potential,” in *Slags – Providing Solutions for Global Construction and Other Markets*, Proceedings of the 4th European Slag Conference, Oulu, Finland, EUROSLAG Publication No. 3, pp. 145-157.

Dayioglu, A.Y., A.H. Aydilek, and B. Cetin. (2014). “Preventing Swelling and Decreasing Alkalinity of Steel Slags Used in Highway Infrastructures,” *Transportation Research Record*, Issue 2401, pp. 52-57.

De Bock, L.P., and H. Van den Bergh. (2004). “Stainless Steel Slags in Hydraulic Bound Mixtures for Road Construction, Two Case Studies in Belgium,” in *International RILEM Conference on the Use of Recycled Materials in Buildings and Structures*, Volume 2, eds. E. Vázquez, Ch.F. Hendriks, and G.M.T. Janssen, RILEM Publications: Bagneux, pp. 1095-1104.

De Schutter, G., K. Audenaert, and J. De Rouck. (2002). “Full-Scale Static Loading Tests on Concrete Armour Units with the Incorporation of LD-Slag,” *Structural Concrete*, Volume 3, Issue 2, pp. 99-105.

Delwar, M., M. Fahmy, and R. Taha. (1997). “Use of Reclaimed Asphalt Pavement as an Aggregate in Portland Cement Concrete,” *ACI Materials Journal*, Volume 94, Issue 3, pp. 251-256.

Deniz, D., E. Tutumluer, and J.S. Popovics. (2010). “Evaluation of Expansive Characteristics of Reclaimed Asphalt Pavement and Virgin Aggregate Used as Base Materials,” *Transportation Research Record*, Issue 2167, pp. 10-17.

Deshpande, Y.S., and J.E. Hiller. (2012). “Pore Characterization of Manufactured Aggregates: Recycled Concrete Aggregates and Lightweight Aggregates,” *Materials and Structures*, Volume 45, pp. 67-79.

Diener, S. (2006). *Mineral Phases of Steel Industry Slags Used in a Landfill Cover Construction*, Master Thesis, Technische Universität Dresden, Dresden, Germany.

Ducman, V., and A. Mladenovič. (2011). “The Potential Use of Steel Slag in Refractory Concrete,” *Materials Characterization*, Volume 62, pp. 716-723.

Dumitru, I., G. Smorchevsky, and V. Caprar. (1999). “Trends in the Utilisation of Recycled Materials and By-Products in the Concrete Industry in Australia,” *Concrete 99: Our Concrete Environment*, Sydney, Australia, pp. 289-301.

Dunster, A.M. (2002). “Blast Furnace Slag and Steel Slag as Aggregates: A Review of Their Uses and Applications in UK Construction,” in *Manufacturing and Processing of Iron and Steel Slags*, Proceedings of the 3rd European Slag Conference, Keyworth, United Kingdom, EUROSLAG Publication No. 2, pp. 21-29.

Emery, J.J. (1974). “A Simple Test Procedure for Evaluating the Potential Expansion of Steel Slag,” *Proceedings of the 1974 Annual Conference of the Roads and Transportation Association of Canada*, Toronto, Canada, pp. 90-103.

Emery, J.J. (1977). “Steel Slag Applications in Highway Construction,” *Silicates Industriels*, Volume 42, Issue 4-5, pp. 209-218.

Emery, J.J. (1982). “Slag Utilization in Pavement Construction,” in *Extending Aggregate Resources*, ASTM Special Technical Publication 774, American Society for Testing and Materials, Philadelphia, pp. 95-118.

EN 1744-1:2009+A1. (2013). “Tests for Chemical Properties of Aggregates – Part 1: Chemical Analysis,” European Committee for Standardization: Brussels, 65 p.

Erdem, S., and M.A. Blankson. (2014). “Environmental Performance and Mechanical Analysis of Concrete Containing Recycled Asphalt Pavement (RAP) and Waste Precast Concrete as Aggregate,” *Journal of Hazardous Materials*, Volume 264, pp. 403-410.

Erlin, B., and D. Jana. (2003). “Forces of Hydration that Can Cause Havoc in Concrete,” *Concrete International*, Volume 25, Issue 11, pp. 51-57.

Etxeberria, M., C. Pacheco, J.M. Meneses, and I. Berridi. (2010). “Properties of Concrete Using Metallurgical Industrial By-Products as Aggregates,” *Construction and Building Materials*, Volume 24, pp. 1594-1600.

Faraone, N., G. Tonello, E. Furlani, and S. Maschio. (2009). “Steelmaking Slag as Aggregate for Mortars: Effects of Particle Dimension on Compression Strength,” *Chemosphere*, Volume 77, pp. 1152-1156.

Farrand, B., and J. Emery. (1995). “Recent Improvements in the Quality of Steel Slag Aggregate,” *Transportation Research Record*, Issue 1486, pp. 137-141.

Ferrebee, E.C., A.S. Brand, A.S. Kachwalla, J.R. Roesler, D.J. Gancarz, and J.E. Pforr. (2014). “Fracture Properties of Roller-Compacted Concrete with Virgin and Recycled Aggregates,” *Transportation Research Record*, accepted for publication.

FHWA. (1998). *User Guidelines for Waste and Byproduct Materials in Pavement Construction*, Publication No. FHWA-RD-97-148, Federal Highway Administration, Washington DC.

Fronek, B., P. Bosela, and N. Delatte. (2012). “Steel Slag Aggregate Used in Portland Cement Concrete: U.S. and International Perspectives,” *Transportation Research Record*, Issue 2267, pp. 37-42.

Fujii, T., T. Ayano, and K. Sakata. (2007). “Freezing and Thawing Resistance of Steel-Making Slag Concrete,” *Journal of Environmental Science for Sustainable Society*, Volume 1, pp. 1-10.

Gebhardt, R.F., Ed. (1988). *Rapid Methods for Chemical Analysis of Hydraulic Cement*, Special Technical Publication 985, American Society for Testing and Materials: Philadelphia.

Geiseler, J. (1995). “Composition and Structure of Slags,” in *Slag Atlas*, 2nd Edition, ed. Verein Deutscher Eisenhüttenleute, Verlag Stahleisen: Düsseldorf, pp. 215-224.

Geiseler, J. (1996). “Use of Steelworks Slag in Europe,” *Waste Management*, Volume 16, Issue 1-3, pp. 59-63.

George, C.M., and F.P. Sorrentino. (1982). “New Concrete Based on Oxygen Steel Slag Containing Alumina,” *Silicates Industriels*, Volume 47, Issue 3, pp. 77-83.

Gillen, S.L., A.S. Brand, J.R. Roesler, and W.R. Vavrik. (2012). “Sustainable Long-Lift Composite Concrete Pavement for Illinois Tollway,” *Proceedings of the International Conference on Long-Lift Concrete Pavements*, Seattle, Washington.

Glass, C. (2003). “Steel Slag Expansion – A Professional Experience,” Document No. MF 203-10, National Slag Association.

Gnaedinger, J.P. (1987). “Open Hearth Slag—A Problem Waiting to Happen,” *Journal of Performance of Constructed Facilities*, Volume 1, Issue 2, pp. 78-83.

Gnaedinger, J.P., and R.J. Gnaedinger, Jr. (1970). “Discussion: ‘Building Damage from Expansive Steel Slag Backfill’ by C.B. Crawford and K.N. Burn,” *Journal of the Soil Mechanics and Foundations Division*, Proceedings of the American Society of Civil Engineers, Volume 96, Issue SM6, pp. 2131-2132.

Goldring, D.C., and L.M. Juckes. (1980). “Petrology and Stability of Steel Slags,” *Ironmaking and Steelmaking*, Volume 24, Issue 6, pp. 447-456.

González-Ortega, M.A., I. Segura, S.H.P. Cavalaro, B. Toralles-Cabonari, A. Aguado, and A.C. Andrello. (2014). “Radiological Protection and Mechanical Properties of Concretes with EAF Steel Slags,” *Construction and Building Materials*, Volume 51, pp. 432-438.

Gray, R.E., and H.A. Salver. (1970). “Discussion: ‘Building Damage from Expansive Steel Slag Backfill’ by C.B. Crawford and K.N. Burn,” *Journal of the Soil Mechanics and Foundations Division*, Proceedings of the American Society of Civil Engineers, Volume 96, Issue SM5, pp. 1814-1817.

Gumieri, A.G., D.C.C. Dal Molin, and A.C.F. Vilela. (2004). “Characteristics of Steel Slag Granulated in a Steel Plant – Valuation of the Microstructure Through Electron Probe Micro Analysis,” in *International RILEM Conference on the Use of Recycled Materials in Building and Structures*, Volume 2, eds. E. Vázquez, Ch.F. Hendriks and G.M.T. Janssen, pp. 1067-1075.

Gunasekaran, S., and G. Anbalagan. (2007). “Thermal Decomposition of Natural Dolomite,” *Bulletin of Materials Science*, Volume 30, Issue 4, pp. 339-344.

Gupta, J.D., W.A. Kneller, R. Tamirisa, and E. Skrzypczak-Jankun. (1994). “Characterization of Base and Subbase Iron and Steel Slag Aggregates Causing Deposition of Calcareous Tufa in Drains,” *Transportation Research Record*, Issue 1434, pp. 8-16.

Gutt, W., and P.J. Nixon. (1979). “Use of Waste Materials in the Construction Industry,” *Materials and Structures*, Volume 12, Issue 70, pp. 255-306.

Halikia, I., and A. Economacou. (1993). “Application of Various Methods of Nonisothermal Kinetic Analysis to Magnesium Hydroxide Decomposition,” *International Journal of Chemical Kinetics*, Volume 28, Issue 8, pp. 609-631.

Halikia, I., L. Zoumpoulakis, E. Christodoulou, and D. Prattis. (2001). “Kinetic Study of the Thermal Decomposition of Calcium Carbonate by Isothermal Methods of Analysis,” *The European Journal of Mineral Processing and Environmental Protection*, Volume 1, Issue 2, pp. 89-102.

Hassan, K.E., J.J. Brooks, and M. Erdman. (2000). “The Use of Reclaimed Asphalt Pavement (RAP) Aggregates in Concrete,” *Waste Materials in Construction*, Waste Management Series, Volume 1, Elsevier Science: Oxford, pp. 121-128.

Heaton, B.S. (1989). “Steelworks Slag Road Pavement Test Sections,” *Australian Road Research*, Volume 19, Issue 2, pp. 145-154.

Heaton, B.S. (1993). “Steel Plant Slag in Road Pavements,” *Australian Civil Engineering Transactions*, Volume CE35, Issue 1, pp. 49-58.

Heaton, B.S. (1996). “Developments in the Uses of Slags from Iron and Steel Plants in Road Pavements,” *Proceedings of the National Symposium on the Use of Recycled Materials in Engineering Construction*, Sydney, Australia, pp. 157-164.

Heaton, B.S., C.L. Francis, W. James, and T. Cao. (1996). “The Use of BOS Steel Slags in Road Pavements,” *Roads 96*, Proceedings of the Combined 18th ARRB Transport Research Conference and Transit New Zealand Land Transport Symposium, Christchurch, New Zealand, Part 3, pp. 49-62.

Hill, S.J., and A.S. Fisher. (2010). “Atomic Absorption, Methods and Instrumentation,” in *Encyclopedia of Spectroscopy and Spectrometry*, 2nd Edition, eds. J.C. Lindon, G.E. Tranter, and D. Koppenaal, Academic Press: Waltham, pp. 46-53.

Hillerborg, A. (1985). “The Theoretical Basis of a Method to Determine the Fracture Energy G_F of Concrete,” *Materials and Structures*, Volume 18, Issue 4, pp. 291-296.

Hossiney, N., G. Wang, M. Tia, and M.J. Bergin. (2008). “Evaluation of Concrete Containing RAP for Use in Concrete Pavement,” *87th Annual Meeting of the Transportation Research Board*, Washington DC.

Hossiney, N., M. Tia, and M.J. Bergin. (2010). “Concrete Containing RAP for Use in Concrete Pavement,” *Proceedings of the International Conference on Sustainable Concrete Pavements*, Sacramento, California.

Huang, B., X. Shu, and G. Li. (2005). “Laboratory Investigation of Portland Cement Concrete Containing Recycled Asphalt Pavements,” *Cement and Concrete Research*, Volume 35, Issue 10, pp. 2008-2013.

Huang, B., X. Shu, and E.G. Burdette. (2006). “Mechanical Properties of Concrete Containing Recycled Asphalt Pavements,” *Magazine of Concrete Research*, Volume 58, Issue 5, pp. 313-320.

Huang, S.-C., R.E. Robertson, J.F. Branthaver, and J.C. Petersen. (2005). “Impact of Lime Modification of Asphalt and Freeze-Thaw Cycling on the Asphalt-Aggregate Interaction and Moisture Resistance to Moisture Damage,” *Journal of Materials in Civil Engineering*, Volume 17, Issue 6, pp. 711-718.

Iacobescu, R.I., D. Koumpouri, Y. Pontikes, R. Saban, and G.N. Angelopoulos. (2011). “Valorisation of Electric Arc Furnace Steel Slag as Raw Material for Low Energy Belite Cements,” *Journal of Hazardous Materials*, Volume 196, pp. 287-294.

Ibrahim, A., E. Mahmoud, Y. Khodair, and V. C. Patibandla. (2014). “Fresh, Mechanical, and Durability Characteristics of Self-Consolidating Concrete Incorporating Recycled Asphalt Pavements,” *Journal of Materials in Civil Engineering*, Volume 26, Issue 4, pp. 668-675.

IDOT. (2009). “Portland Cement Concrete Level III Technician Manual,” Illinois Department of Transportation, Springfield, Illinois.

IDOT. (2012). “Standard Specifications for Road and Bridge Construction,” Illinois Department of Transportation, Springfield, Illinois.

INDOT. (2014). “Standard Specifications,” Indiana Department of Transportation, Indianapolis, Indiana.

ITM 219. (2008). “Acceptance Procedures of Steel Furnace Slag for Deleterious Materials,” Indiana Department of Transportation, Office of Materials Management, Indianapolis, Indiana.

Javellana, M.P., and I. Jawed. (1982). “Extraction of Free Lime in Portland Cement and Clinker by Ethylene Glycol,” *Cement and Concrete Research*, Volume 12, Issue 3, pp. 399-403.

Jenq, Y., and S.P. Shah. (1985). “Two Parameter Fracture Model for Concrete,” *Journal of Engineering Mechanics*, Volume 111, Issue 10, pp. 1227-1241.

Jones, D.E. (1982). “Application of Steel Plant By-Products to Roadworks,” *Proceedings of the Eleventh ARRB Conference*, Australian Road Research Board, Melbourne, Australia, Volume 11, Part 3, p. 106-119.

Kandhal, P.S., and G.L. Hoffman. (1997). “Evaluation of Steel Slag Fine Aggregate in Hot-Mix Asphalt Mixtures,” *Transportation Research Record*, Issue 1583, pp. 28-36.

Katsakou, M., and S. Kolias. (2007). “Mechanical Properties of Cement-Bound Recycled Pavements,” *Proceedings of the Institution of Civil Engineers - Construction Materials*, Volume 160, Issue 4, pp. 171-179.

Kawamura, M., K. Torii, S. Hasaba, N. Nicho, and K. Oda. (1983). “Applicability of Basic Oxygen Furnace Slag as a Concrete Aggregate,” in *Fly Ash, Silica Fume, Slag and Other Mineral By-Products in Concrete*, ACI Special Publication 79, ed. V.M. Malhotra, American Concrete Institute, Detroit, pp. 1123-1141.

KDOT. (2007). “Standard Specifications for State Road and Bridge Construction,” Kansas Department of Transportation, Topeka, Kansas.

Khan, N., D. Dollimore, K. Alexander, and F.W. Wilburn. (2001). “The Origin of the Exothermic Peak in the Thermal Decomposition of Basic Magnesium Carbonate,” *Thermochimica Acta*, Volume 367-368, pp. 321-333.

Khan, R., and S.B. Shinde. (2013). “Effect of Unprocessed Steel Slag on the Strength of Concrete When Used as Fine Aggregate,” *International Journal of Civil Engineering and Technology*, Volume 4, Issue 2, pp. 231-239.

Kim, J.-M., S.-H. Cho, and E.-G. Kwak. (2014). “Experimental Evaluation of Volume Stability of Rapidly-Cooled Steel Slag [RCSS] as Fine Aggregate for Concrete,” *KSCE Journal of Civil Engineering*, in press.

Kim, S.-W., Y.-J. Lee, and K.-H. Kim. (2012). “Flexural Behavior of Reinforced Concrete Beams with Electric Arc Furnace Slag Aggregates,” *Journal of Asian Architecture and Building Engineering*, Volume 138, pp. 133-138.

Kim, S.-W., Y.-S. Kim, J.-Mi, Lee, and K.-H. Kim. (2013). “Structural Performance of Spirally Confined Concrete with EAF Oxidising Slag Aggregate,” *European Journal of Environmental and Civil Engineering*, Volume 17, Issue 8, pp. 654-674.

Kneller, W.A., J. Gupta, M.L. Borkowski, and D. Dollimore. (1994). “Determination of Original Free Lime Content of Weathered Iron and Steel Slags by Thermogravimetric Analysis,” *Transportation Research Record*, Issue 1434, pp. 17-22.

Kolias, S. (1996a). “Mechanical Properties of Cement-Treated Mixtures of Milled Bituminous Concrete and Crushed Aggregates,” *Materials and Structures*, Volume 29, pp. 411-417.

Kolias, S. (1996b). “The Influence of the Type of Loading and Temperature on the Modulus of Elasticity of Cement-Bound Mixes of Milled Bituminous Concrete and Crushed Aggregates,” *Materials and Structures*, Volume 29, pp. 543-551.

Kramar, U. (2010). “X-Ray Fluorescence Spectrometers,” in *Encyclopedia of Spectroscopy and Spectrometry*, 2nd Edition, eds. J.C. Lindon, G.E. Tranter, and D. Koppenaal, Academic Press: Waltham, pp. 2989-2999.

Kriskova, L., Y. Pontikes, L. Pandelaers, Ö. Cizer, P.T. Jones, K. Van Balen, and B. Blanpain. (2013). “Effect of High Cooling Rates on the Mineralogy and Hydraulic Properties of Stainless Steel Slags,” *Metallurgical and Materials Transactions B*, Volume 44, Issue 5, pp. 1173-1184.

Kvick, Å. (2010). “Materials Science Applications of X-Ray Diffraction,” in *Encyclopedia of Spectroscopy and Spectrometry*, 2nd Edition, eds. J.C. Lindon, G.E. Tranter, and D. Koppenaal, Academic Press: Waltham, pp. 1470-1478.

Lee, M.-H., and J.-C. Lee. (2009). “Study on the Cause of Pop-Out Defects on the Concrete Wall and Repair Method,” *Construction and Building Materials*, Volume 23, pp. 482-490.

Legret, M., P. Chaurand, A. Bénard, Y. Capowiez, D. Deneele, J. Reynard, L. Lassabatére, D. Yilmaz, J. Rose, J. Domas, B. Béchet, D. Richard, and J.-Y. Bottero. (2010). “A Multidisciplinary Approach for the Assessment of the Environmental Behavior of Basic Oxygen Furnace Slag Used in Road Construction,” in *Ferrous Slag – Resource Development for an Environmentally Sustainable World*, Proceedings of the 6th European Slag Conference, Madrid, Spain, EUROSLAG Publication No. 5, pp. 77-88.

Li, G., Y. Zhao, S.-S. Pang, and W. Huang. (1998). “Experimental Study of Cement-Asphalt Emulsion Composite,” *Cement and Concrete Research*, Volume 28, Issue 5, pp. 635-641.

Lifshin, E. (2001). “Electron Microprobe Analysis,” in *Encyclopedia of Materials: Science and Technology*, eds. K.H. Jürgen Buschow, R.W. Cahn, M.C. Flemings, B. Ilschner, E.J. Kramer, S. Mahajan, and P. Veyssière, Pergamon: Oxford, pp. 2563-2569.

Liu, C., K. Zha, and D. Chen. (2011). “Possibility of Concrete Prepared with Steel Slag as Fine and Coarse Aggregates: A Preliminary Study,” *Procedia Engineering*, Volume 24, pp. 412-416.

Lun, Y., M. Zhou, X. Cai, and F. Xu. (2008). “Methods for Improving Volume Stability of Steel Slag as Fine Aggregate,” *Journal of Wuhan University of Technology - Material Science Edition*, Volume 23, Issue 5, pp. 737-742.

Luo, S. (1980). “Effect of MgO in Steel Slag on Soundness of Cement,” *Proceedings of the 7th International Congress on the Chemistry of Cement*, Paris, France, Volume 3, pp. 25-30.

Luxán, M.P., R. Sotolongo, F. Dorrego, and E. Herrero. (2000). “Characteristics of the Slags Produced in the Fusion of Scrap Steel by Electric Arc Furnace,” *Cement and Concrete Research*, Volume 30, pp. 517-519.

Lykoudis, S., and I. Liapis. (2010). “Egnatia Odos, the 670 km Project and EAF Slag,” in *Ferrous Slag – Resource Development for an Environmentally Sustainable World*, Proceedings of the 6th European Slag Conference, Madrid, Spain, EUROSLAG Publication No. 5, pp. 335-346.

MacPherson, D.R., and L.R. Forbrich. (1937). “Determination of Uncombined Lime in Portland Cement: the Ethylene Glycol Method,” *Industrial and Engineering Chemistry Analytical Edition*, Volume 9, Issue 10, pp. 451-453.

Madej, J., L. Ševula, and K. Slovák. (1996). “Investigation of Industrial By-Products Considered for Use as Concrete Aggregates,” in *Concrete for Environment Enhancement and Protection*, eds. R.K. Dhir and T.D. Dyer, E&FN Spon: London, pp. 99-108.

Mahieux, P.-Y., J.-E. Aubert, and G. Escadeillas. (2009). “Utilization of Weathered Basic Oxygen Furnace Slag in the Production of Hydraulic Road Binders,” *Construction and Building Materials*, Volume 23, pp. 742-747.

Mahieux, P.Y., J.E. Aubert, G. Escadeillas, and M. Measson. (2014). “Quantification of Hydraulic Phase Contained in a Basic Oxygen Furnace Slag,” *Journal of Materials in Civil Engineering*, Volume 26, Issue 4, pp. 593-598.

Manso, J.M., J.J. Gonzalez, and J.A. Polanco. (2004). “Electric Arc Furnace Slag in Concrete,” *Journal of Materials in Civil Engineering*, Volume 16, Issue 6, pp. 639-645.

Manso, J.M., J.A. Polanco, M. Losañez, and J.J. González. (2006). “Durability of Concrete Made with EAF Slag as Aggregate,” *Cement and Concrete Composites*, Volume 28, pp. 528-534.

Manso, J.M., D. Hernández, M.M. Losáñez, and J.J. González. (2011). “Design and Elaboration of Concrete Mixtures Using Steelmaking Slags,” *ACI Materials Journal*, Volume 108, Issue 6, pp. 673-681.

Marek, C.R. (1991). “Basic Properties of Aggregate,” in *The Aggregate Handbook*, ed. R.D. Barksdale, National Stone Association: Washington DC.

Maslehuddin, M., M. Shameem, M. Ibrahim, and N.U. Khan. (1999). “Performance of Steel Slag Aggregate Concretes,” in *Exploiting Wastes in Concrete*, eds. R.K. Dhir and T.G. Jappy, Thomas Telford: London, pp. 109-119.

Maslehuddin, M., A.M. Sharif, M. Shameem, M. Ibrahim, and M.S. Barry. (2003). “Comparison of Properties of Steel Slag and Crushed Limestone Aggregate Concretes,” *Construction and Building Materials*, Volume 17, pp. 105-112.

Mathew, P., L. Stephen, and J. George. (2013). “Steel Slag Ingredient for Concrete Pavement,” *International Journal of Innovative Research in Science, Engineering and Technology*, Volume 2, Issue 3, pp. 710-714.

Mathias, V., T. Sedran, F. de Larrard. (2004). “Recycling Reclaimed Asphalt Pavement in Concrete Roads,” *International RILEM Conference on the Use of Recycled Materials in Buildings and Structures*, Barcelona, Spain.

Mathur, S., S.K. Soni, and A. Murty. (1999). “Utilization of Industrial Wastes in Low-Volume Roads,” *Transportation Research Record*, Issue 1652, pp. 246-256.

Matsunaga, H., F. Kogiku, M. Takagi, K. Tanishiki, and M. Nakagawa. (2004). "Environment-Friendly Block Made from Steel Slag," in *Eighth CANMET/ACI International Conference on Fly Ash, Silica Fume, Slag and Natural Pozzolans in Concrete*, ed. V.M. Malhotra, Special Publication 221, American Concrete Institute: Farmington Hills, pp. 457- 470.

Maw, K.J. (1991). “Steel Slag: Its Use and Development in the United Kingdom by the Slag Reduction Co. Ltd,” Slag: the Material of Choice, Papers Presented to an International Seminar, Australasian Slag Association, pp. 27-49.

McCann, M., and P.E. Sebaaly. (2003). “Evaluation of Moisture Sensitivity and Performance of Lime in Hot-Mix Asphalt: Resilient Modulus, Tensile Strength, and Simple Shear Tests,” *Transportation Research Record*, Issue 1832, pp. 9-16.

Mehrer, H. (2007). *Diffusion in Solids: Fundamentals, Methods, Materials, Diffusion-Controlled Processes*, Springer: Berlin.

Miller, R.H., and R.J. Collins. (1976). *Waste Materials as Potential Replacements for Highway Aggregates*, NCHRP Report 166, National Cooperative Highway Research Program, Transportation Research Board, Washington DC.

Mindess, S., J.F. Young, and D. Darwin. (2003). *Concrete*, 2nd edition, Pearson Education: Upper Saddle River.

Mn/DOT. (2014). “Materials Lab Supplemental Specifications for Construction,” Minnesota Department of Transportation, St. Paul, Minnesota.

MoDOT. (2011). “Standard Specifications for Highway Construction,” Missouri Department of Transportation, Jefferson City, Missouri.

Mohammed, K.J., F.O. Abbas, and M.O. Abbas. (2009). “Using of Steel Slag in Modification of Concrete Properties,” *Engineering and Technology Journal*, Iraq Academic Scientific Journals, Volume 27, Issue 9, pp. 1711-1720.

Moosberg-Bustnes, H. (2004). “Steel-Slag as Filler Material in Concrete,” *VII International Conference on Molten Slags, Fluxes and Salts*, The South African Institute of Mining and Mineralogy, Symposium Series S36, pp. 385-391.

Montgomery, D.G., and G. Wang. (1991). “Instant-Chilled Steel Slag Aggregate in Concrete – Strength Related Properties,” *Cement and Concrete Research*, Volume 21, pp. 1083-1091.
Montgomery, D.G., and G. Wang. (1992). “Instant-Chilled Steel Slag Aggregate in Concrete – Fracture Related Properties,” *Cement and Concrete Research*, Volume 22, pp. 755-760.
Moon, H.Y., J.H. Yoo, and S.S. Kim. (2002). “A Fundamental Study on the Steel Slag Aggregate for Concrete,” *Geosystem Engineering*, Volume 5, Issue 2, pp. 38-45.
Motz, H., and J. Geiseler. (2000). “Products of Steels Slags: An Opportunity to Save Natural Resources,” in *Waste Materials in Construction*, eds. G.R. Woolley, J.J.J.M. Goumans, and P.J. Wainwright, Elsevier Science: Oxford, pp. 207-220.
MTO. (1996). “Method of Test for Determination of Free Lime Content of Steel Slag Aggregates,” Test Method LS-622 Revision 16, Ministry of Transportation of Ontario, Toronto, Ontario.
MTO. (2013). *Ontario Provincial Standards for Roads and Public Works*, Ontario Provincial Standard Specification, Ministry of Transportation of Ontario, Toronto, Ontario.
Nakagawa, M., N. Tsutsumi, T. Kato, and E. Kiso. (2010). “Technology of Constructing Seaweed Beds by Steel-Making Slag,” in *Ferrous Slag – Resource Development for an Environmentally Sustainable World*, Proceedings of the 6th European Slag Conference, Madrid, Spain, EUROSLAG Publication No. 5, pp. 89-102.
Navarro, C., M. Díaz, and M.A. Villa-García. (2010). “Physico-Chemical Characterization of Steel Slag: Study of its Behavior under Simulated Environmental Conditions,” *Environmental Science and Technology*, Volume 44, pp. 5383-5388.
NCHRP. (2013). *Recycled Materials and Byproducts in Highway Applications*, NCHRP Synthesis 435, National Cooperative Highway Research Program, Transportation Research Board, Washington DC.
Netinger, I., D. Bjegović, and A. Mladenovič. (2010). “Fire Resistance of Steel Slag Aggregates Concrete,” *High Temperature Materials and Processes*, Volume 29, Issue 1-2, pp. 77-87.
Netinger, I., D. Bjegović, and G. Vrhovac. (2011). “Utilisation of Steel Slag as an Aggregate in Concrete,” *Materials and Structures*, Volume 44, pp. 1565-1575.
Netinger, I., M. Jelčić Rukavina, D. Bjegović, and A. Mladenovič. (2012). “Concrete Containing Steel Slag Aggregate: Performance After High Temperature Exposure,” in *Concrete Repair, Rehabilitation and Retrofitting III: 3rd International Conference on Concrete Repair*, eds. M.G. Alexander, H.-D. Beushausen, F. Dehn, and P. Moyo, pp. 1347-1352.
Nicolae, M., I. Vîlciu, and F. Zăman. (2007). “X-Ray Diffraction Analysis of Steel Slag and Blast Furnace Slag Viewing Their Use for Road Construction,” *UPB Scientific Bulletin Series B*, Volume 69, Issue 2, pp. 99-108.
Nguyen, M.L., J.M. Balay, C. Sauzéat, H. Di Benedetto, K. Bilodeau, F. Olard, and B. Ficheroulle. (2012). “Accelerated Pavement Testing Experiment of Pavement Made of Fiber-Reinforced Roller-Compacted Concrete,” *Advances in Pavement Design through Full-Scale Accelerated Pavement Testing*, ed. D. Jones, J. Harvey, I.L. Al-Qadi, and A. Mateos, CRC Press: Boca Raton, pp. 299-311.
NJDOT. (2007). “Standard Specifications for Road and Bridge Construction,” New Jersey Department of Transportation, Trenton, New Jersey.
Obratil, R.S., A.B. Patel, P.A. Bosela, and N.J. Delatte, Jr. (2008). “Effect of Steel Slag Replacement on Fresh and Hardened Properties of Concrete,” *Presented at the 87th Annual Meeting of the Transportation Research Board*, Washington DC.
Obratil, R.S., M.A. Pastorelle, P.A. Bosela, and N.J. Delatte, Jr. (2009). “Examination of Steel Slag as a Replacement for Natural Aggregates in Concrete Paving Mixtures,” *Presented at the 88th Annual Meeting of the Transportation Research Board*, Washington DC.
ODOT. (2013). “Construction and Material Specifications,” Ohio Department of Transportation, Columbus, Ohio.
ODOT Supplement 1071. (2008). “Quality Control Requirements for Steel Slag Aggregate Producer/ Processors,” Ohio Department of Transportation, Columbus, Ohio.
Okafor, F.O. (2010). “Performance of Recycled Asphalt Pavement as Coarse Aggregate in Concrete,” *Leonardo Electronic Journal of Practices and Technologies*, Issue 17, pp. 47-58.
Okamoto, A., E. Futamura, and K. Kawamura. (1981). “Hydration Behavior of LD Slag at Autoclave Test,” *Transactions of the Iron and Steel Institute of Japan*, Volume 21, Issue 1, pp. 16-24.

Ozeki, S. (1997). “Properties and Usage of Steel Plant Slag,” *Proceedings of ENCOSTEEL*, International Iron and Steel Institute, Stockholm, Sweden, pp. 135-139.

Ozkul, M.H. (1996). “Properties of Slag Aggregate Concrete,” in *Concrete for Environment Enhancement and Protection*, eds. R.K. Dhir and T.D. Dyer, E&FN Spon: London, pp. 553-558.

Pacheco, M.C., M. Etxeberria, J.M. Meneses, I. Berridi, and J.M. Ávila. (2010). “Physical-Mechanical Properties and Durability of Concrete Made with Blast Furnace and Electric Arc Furnace Slag As Aggregate,” in *Ferrous Slag – Resource Development for an Environmentally Sustainable World*, Proceedings of the 6th European Slag Conference, Madrid, Spain, EUROSLAG Publication No. 5, pp. 265-277.

Papayianni, I., and E. Anastasiou. (2003). “Concrete Incorporating High Volumes of Industrial by-Products,” in *Role of Concrete in Sustainable Development*, eds. R.K. Dhir, M.D. Newlands, and K.A. Paine, Thomas Telford: London, pp. 595-604.

Papayianni, I., and E. Anastasiou. (2005). “Heavyweight Concrete with Steel Slag Aggregates,” in *Role of Concrete in Nuclear Facilities*, eds. R.K. Dhir, K.A. Paine, and M.C. Tang, Thomas Telford: London, pp. 25-31.

Papayianni, I., and E. Anastasiou. (2010a). “Production of High-Strength Concrete using High Volume of Industrial By-Products,” *Construction and Building Materials*, Volume 24, pp. 1412-1417.

Papayianni, I., and E. Anastasiou. (2010b). “Utilization of Electric Arc Furnace Steel Slags in Concrete Products,” in *Ferrous Slag – Resource Development for an Environmentally Sustainable World*, Proceedings of the 6th European Slag Conference, Madrid, Spain, EUROSLAG Publication No. 5, pp. 319-334.

Papayianni, I., and E. Anastasiou. (2011). “Concrete Incorporating High-Calcium Fly Ash and EAF Slag Aggregates,” *Magazine of Concrete Research*, Volume 63, Issue 8, pp. 597-604.

Patankar, V.D., and R.I.T. Williams. (1970). “Bitumen in Dry Lean Concrete,” *Highways and Traffic Engineering*, Volume 38, Issue 1721, pp. 32-35.

Pellegrino, C., and V. Gaddo. (2009). “Mechanical and Durability Characteristics of Concrete Containing EAF Slag as Aggregate,” *Cement and Concrete Composites*, Volume 31, pp. 663-671.

Pellegrino, C., P. Cavagnis, F. Faleschini, and K. Brunelli. (2013). “Properties of Concretes with Black/Oxidizing Electric Arc Furnace Slag Aggregate,” *Cement and Concrete Composites*, Volume 37, pp. 232-240.

Pellegrino, C., and F. Faleschini. (2013). “Experimental Behavior of Reinforced Concrete Beams with Electric Arc Furnace Slag as Recycled Aggregate,” *ACI Materials Journal*, Volume 110, Issue 2, pp. 197-206.

PennDOT. (2011a). “Publication 408 Construction Specifications,” Pennsylvania Department of Transportation, Harrisburg, Pennsylvania.

PennDOT. (2011b). “PennDOT Benchmark Study: Current Practices and Future Trends for the Use of Recycled Materials in Highway Construction,” Pennsylvania Department of Transportation, Environmental Quality Assurance Division, Harrisburg, Pennsylvania.

Piché, M. (2003). “Long Term Properties for Steel Slag in Hot Mix Asphalt in Canada,” *Proceedings of the 31st Annual Conference of the Canadian Society for Civil Engineering*, Moncton, New Brunswick.

Poh, H.Y., G.S. Ghataora, and N. Ghazireh. (2006). “Soil Stabilization Using Basic Oxygen Steel Slag Fines,” *Journal of Materials in Civil Engineering*, Volume 18, Issue 2, pp. 229-240.

Polanco, J.A., J.M. Manso, J. Setién, and J.J. González. (2011). “Strength and Durability of Concrete Made with Electric Steelmaking Slag,” *ACI Materials Journal*, Volume 108, Issue 2, pp. 196-203.

Qasrawi, H., F. Shalabi, and I. Asi. (2009). “Use of Low CaO Unprocessed Steel Slag in Concrete as Fine Aggregate,” *Construction and Building Materials*, Volume 23, pp. 1118-1125.

Qasrawi, H. (2012). “Use of Relatively High Fe_2O_3 Steel Slag as Coarse Aggregate in Concrete,” *ACI Materials Journal*, Volume 109, Issue 4, pp. 471-478.

Qasrawi, H. (2014). “The Use of Steel Slag Aggregate to Enhance the Mechanical Properties of Recycled Aggregate Concrete and Retain the Environment,” *Construction and Building Materials*, Volume 54, pp. 298-304.

Qian, G.R., D.D. Sun, J.H. Tay, and Z.Y. Lai. (2002). "Hydrothermal Reaction and Autocalve Stability of Mg Bearing RO Phase in Steel Slag," *British Ceramic Transactions*, Volume 101, Issue 4, pp. 159-164.

Rainová, A., K. Šeps, and V. Vytlacilova. (2012). "Possible Use of the Slag Aggregate in Fibre Reinforced Concrete," *Proceedings of Metal 2012 (21st International Conference on Metallurgy and Materials)*, Brno, Czech Republic.

RILEM TC89-FMT. (1990). "Determination of the Fracture Parameters (K^S_{Ic} and $CTOD_c$) of Plain Concrete Using Three-Point Bend Tests," *Materials and Structures*, Volume 23, pp. 457-460.

Ritchie, L.R. (1970). "Discussion: 'Building Damage from Expansive Steel Slag Backfill' by C.B. Crawford and K.N. Burn," *Journal of the Soil Mechanics and Foundations Division*, Proceedings of the American Society of Civil Engineers, Volume 96, Issue SM5, pp. 1813-1814.

Robinson, H.L. (2002). "The Utilization of Blastfurnace and Steel Making Slags as Aggregates for Construction," in *Industrial Minerals and Extractive Industry Geology*, eds. P.W. Scott and C.M. Bristow, Geological Society: London, pp. 327-330.

Rojas, M.F., and M.I.S. de Rojas. (2004). "Chemical Assessment of the Electric Arc Furnace Slag as Construction Material: Expansive Compounds," *Cement and Concrete Research*, Volume 34, pp. 1881-1888.

Rouchon, L., L. Favergeon, and M. Pijolat. (2013). "Analysis of the Kinetic Slowing Down During Carbonation of CaO by CO_2," *Journal of Thermal Analysis and Calorimetry*, Volume 113, Issue 3, pp. 1145-1155.

Sachet, T., M.C.F. Albuquerque, J.T. Balbo, and C.E. Sansone. (2011). "Investigation of Resistance and Fracture Parameters for Compacted Concrete with Incorporation of Reclaimed Asphalt Pavement," *International Journal of Pavements*, Volume 10, Issue 1-2-3, pp. 83-93.

San-José, J.T., I. Vegas, I. Arribas, and I. Marcos. (2014). "The Performance of Steel-Making Slag Concretes in the Hardened State," *Materials and Design*, Volume 60, pp. 612-619.

Sánchez Fransesch, C., and J. Soria Tonda. (2010). "Recovery of Electric Furnace Slag as Aggregate," in *Ferrous Slag – Resource Development for an Environmentally Sustainable World*, Proceedings of the 6th European Slag Conference, Madrid, Spain, EUROSLAG Publication No. 5, pp. 63-76.

SCDOT. (2007). "Standard Specifications for Highway Construction," South Carolina Department of Transportation, Columbia, South Carolina.

Senior, S.A., S.I. Szoke, and C.A. Rogers. (1994). "Ontario's Experience with Reclaimed Materials for Use as Aggregates," *Roads to the 21st Century*, Proceedings of the 1994 International Road Federation Conference, Calgary, Canada, pp. A31-A55.

Sersale, R., V. Amicarelli, G. Frigione, and P. Ubbriaco. (1986a). "A Study on the Utilization of an Italian Steel Slag," in *Proceedings of the 8th International Congress on the Chemistry of Cement*, Rio de Janeiro, Brazil, Theme 1, Volume 2, pp. 194-198.

Sersale, R., V. Amicarelli, G. Frigione, and P. Ubbriaco. (1986b). "Characterization and Potential Uses of a Steel Slag," *Silicates Industriels*, Volume 51, Issue 11-12, pp. 163-170.

Shen, D.-H., C.-M. Wu, and J.-C. Du. (2009). "Laboratory Investigation of Basic Oxygen Furnace Slag for Substitution of Aggregate in Porous Asphalt Mixture," *Construction and Building Materials*, Volume 23, Issue 1, pp. 453-461.

Shi, C. (2004). "Steel Slag – Its Production, Processing, Characteristics, and Cementitious Properties," *Journal of Materials in Civil Engineering*, Volume 16, Issue 3, pp. 230-236.

Smith, M.R., and L. Collis (eds). (2001). *Aggregates: Sand, Gravel and Crushed Rock Aggregates for Construction Purposes*, 3rd Edition, Engineering Geology Special Publication No. 17, Geological Society: London.

Sommer, H. (1994). "Recycling of Concrete for the Reconstruction of the Concrete Pavement of the Motorway Vienna-Salzburg," *Proceedings of the 7th International Concrete Roads Symposium*, Vienna, Austria.

Sommer, H., and J. Bohrn. (1998). "Beton mit Asphalt als Zuschlag," Bundesministerium für wirtschaftliche Angelegenheiten, Schriftenreihe Straßenforschung, Heft 476, 29 p. (in German)

Song, H.S., and C.H. Kim. (1990). "The Effect of Surface Carbonation on the Hydration of CaO," *Cement and Concrete Research*, Volume 20, Issue 5, pp. 815-823.

Spanovich, M., and R. Fewell. (1970). “Discussion: ‘Building Damage from Expansive Steel Slag Backfill’ by C.B. Crawford and K.N. Burn,” *Journal of the Soil Mechanics and Foundations Division*, Proceedings of the American Society of Civil Engineers, Volume 96, Issue SM5, pp. 1808-1810.

Su, Y.-M., N. Hossiney, M. Tia, and M. Bergin. (2014). “Mechanical Properties Assessment of Concrete Containing Reclaimed Asphalt Pavement Using the Superpave Indirect Tensile Strength Test,” *Journal of Testing and Evaluation*, Volume 42, Issue 4, pp. 1-9.

Suer, P., J.-E. Lindqvist, M. Arm, and P. Frogner-Kockum. (2009). “Reproducing Ten Years of Road Ageing – Accelerated Carbonation and Leaching of EAF Steel Slag,” *Science of the Total Environment*, Volume 407, Issue 18, pp. 5110-5118.

Tarawneh, S.A., E.S. Gharaibeh, and F.M. Saraireh. (2014). “Effect of Using Steel Slag Aggregate on Mechanical Properties of Concrete,” *American Journal of Applied Sciences*, Volume 11, Issue 5, pp. 700-706.

Taylor, H.F.W. (1997). *Cement Chemistry*, 2nd edition, Thomas Telford: London.

Thomas, G.H. (1983). *Investigations on LD Slag with Particular Reference to Its Use for Road Construction*, Report EUR 8622 EN, Commission of the European Communities, Luxembourg.

Tomasiello, S., and M. Felitti. (2010). “EAF Slag in Self-Compacting Concretes,” *Facta Universitatis, Architecture and Civil Engineering*, Volume 8, Issue 1, pp. 13-21.

Tsakiridis, P.E., G.D. Papadimitriou, S. Tsivilis, and C. Koroneos. (2008). “Utilization of Steel Slag for Portland Cement Clinker Production,” *Journal of Hazardous Materials*, Volume 152, Issue 2, pp. 805-811.

TxDOT. (1999). “Year of the Recycled Roadway: Materials – September: Slags,” Texas Department of Transportation. Available online at http://ftp.dot.state.tx.us/pub/txdot-info/gsd/pdf/yrr_sept.pdf

van Oss, H.G. (2011). “Slag – Iron and Steel,” *2011 Minerals Yearbook*, U.S. Geological Survey: Reston.

van Oss, H.G. (2013). “Iron and Steel Slag,” *Mineral Commodity Summaries 2013*, U.S. Geological Survey: Reston.

Vázquez, E., M. Barra, F. Perez, P. Alavedra, E. Scheibmeir, and M. Bou. (2010). “Experimental Assessment of Electric Arc Furnace Slag for Road Construction Purposes in Catalonia,” in *Ferrous Slag – Resource Development for an Environmentally Sustainable World*, Proceedings of the 6th European Slag Conference, Madrid, Spain, EUROSLAG Publication No. 5, pp. 347-358.

Vázquezramonich, E., and M. Barra. (2001). “Reactivity and Expansion of Electric Arc Furnace Slag in Their Application in Construction,” *Materiales de Construcción*, Volume 51, Issue 263-264, pp. 137-148.

Verhasselt, A., and F. Choquet. (1989). “Steel Slags as Unbound Aggregate in Road Construction: Problems and Recommendations,” in *Unbound Aggregates in Roads*, eds. R.H. Jones and A.R. Dawson, Butterworths: London, pp. 204-211.

Vlcek, J., V. Tomkova, H. Ovcacikova, F. Ovcacik, M. Topinkova, and V. Matejka. (2013). “Slags from Steel Production: Properties and Their Utilization,” *Metalurgija*, Volume 52, Issue 1, pp. 329-333.

Wachsmuth, F., J. Geiseler, W. Fix, K. Koch, and K. Schwerdtfeger. (1981). “Contribution to the Structure of BOF-Slags and Its Influence on Their Volume Stability,” *Canadian Metallurgical Quarterly*, Volume 20, Issue 3, pp. 279-284.

Waligora, J., D. Bulteel, P. Degrugilliers, D. Damidot, J.L. Potdevin, and M. Measson. (2010). “Chemical and Mineralogical Characterizations of LD Converter Steel Slags: A Multi-Analytical Approach,” *Materials Characterization*, Volume 61, pp. 39-48.

Wang, G. (1992). *Properties and Utilization of Steel Slag in Engineering Applications*. PhD Dissertation, University of Wollongong, Wollongong, Australia.

Wang, G. (2010). “Determination of the Expansion Force of Coarse Steel Slag Aggregate,” *Construction and Building Materials*, Volume 24, pp. 1961-1966.

Wang, G., Y. Wang, and Z. Gao. (2010). “Use of Steel Slag as a Granular Materials: Volume Expansion Prediction and Usability Criteria,” *Journal of Hazardous Materials*, Volume 184, pp. 555-560.

Wang, Y. (1988). “The Effect of Bond Characteristics between Steel Slag Fine Aggregate and Cement Paste on Mechanical Properties of Concrete and Mortar,” *Materials Research Society Symposium Proceedings*, Volume 113, pp. 301-306.

Williams, T., and F. Miknis. (1998). “Use of Environmental SEM to Study Asphalt-Water Interactions,” *Journal of Materials in Civil Engineering*, Volume 10, Issue 2, pp. 121-124.

Winslow, D. (1994). “The Pore System of Coarse Aggregates,” in *Significance of Tests and Properties of Concrete and Concrete Making Materials*, Special Technical Publication 169C, eds. P. Klieger and J.F. Lamond, American Society for Testing and Materials: Philadelphia, pp. 429-437.

Wojakowski, J. (1998). *High Performance Concrete Pavement*, Report FHWA-KS-98/2, Kansas Department of Transportation.

Wu, S., Y. Xue, Q. Ye, and Y. Chen. (2007). “Utilization of Steel Slag as Aggregate for Stone Mastic Asphalt (SMA) Mixtures,” *Building and Environment*, Volume 42, pp. 2580-2585.

WVDOH. (2010). “Standard Specifications Roads and Bridges,” West Virginia Division of Highways, Charleston, West Virginia.

Xue, Y., S. Wu, H. Hou, and J. Zha. (2006). “Experimental Investigation of Basic Oxygen Furnace Slag Used as Aggregate in Asphalt Mixture,” *Journal of Hazardous Materials*, Volume 138, Issue 2, pp. 261-268.

Yildirim, I.Z., and M. Prezzi. (2011). “Chemical, Mineralogical, and Morphological Properties of Steel Slag,” *Advances in Civil Engineering*, Volume 2011.